

Physikalische Chemie

**CONTROLLING THE RELEASE OF THE DRUGS PROPRANOLOL  
AND PERSANTIN FROM SOL-GEL MATERIALS BY  
MOLECULAR INTERACTIONS AND PARTICLE ENGINEERING**

INAUGURAL-DISSERTATION

zur Erlangung des Doktorgrades  
der Naturwissenschaften  
in der NRW Graduate School of Chemistry  
im Fachbereich Chemie und Pharmazie  
der Mathematisch-Naturwissenschaftlichen Fakultät  
der Westfälischen Wilhelms-Universität Münster

vorgelegt von  
Geo Paul  
aus Thrissur-Kerala, Indien

-March 2007-

*Dekan:*

*Prof. Dr. F. E. Hahn*

*Erster Gutachter:*

*PD Dr. H. Koller*

*Zweiter Gutachter:*

*Prof. Dr. H. -D. Wiemhöfer*

*Tag der Disputation:*

*...25/04/2007.....*

*Tag der Promotion:*

*...25/04/2007.....*

*Für Jijo*



## *Acknowledgements*

*I would like to thank all the people who have helped me in any respect for the realisation of this thesis.*

*First and foremost, I wish to thank my principal mentor, PD Dr. H. Koller, for giving me the opportunity to undertake this project. His advice and guidance over the last three and half years have been highly appreciated. I would like to thank him for sending me overseas and within Germany on a number of occasions to present my work at conferences and to collaborate with other scientists, where I gained a great deal of valuable experience. I am thankful to him for the freedom and moral support he gave me throughout the PhD period. I truly think, look at and act in the world differently due to Hubert's influence. Hubert has been so much more than just the PhD advisor that he is beyond categorization. He has been the best friend, mentor, teacher and companion. Thanks, Hubert.*

*I wish to thank Prof. Wiemhöfer for being my co-mentor and reviewing the thesis in a tight time schedule. I also thank Prof. Schönhoff for being my co-mentor and for valuable discussions.*

*I would like to acknowledge the international NRW Graduate School of Chemistry and the department of physical chemistry for the financial support. I would like to express my additional thanks to GSC and Dr. Koller, Dr. Elbers and Uta for many scientific and cultural opportunities provided during my studies.*

*Thanks also must go to Prof. Eckert for fruitful discussions and providing resources. I also wish to thank PD Dr. van Wüllen for suggesting the HETCOR experiment.*

*I am grateful to the following people for their assistance to characterize my gels. DRT measurements were done with the help of Mr. Scherges at Landesinstitut für den Öffentlichen Gesundheitsdienst NRW (lögD), Münster. SEM measurements were done by Herr Göcke, Falko and Frau Lammers.*

*I owe a huge debt of thanks to Dr. Steuernagel of Bruker Biospin, whose advice on my 2D NMR data has proven invaluable. I would also like to thank him for the time he spend in Münster to set up the HETCOR experiment and for allowing me to use the facilities at Bruker, Karlsruhe.*

*Thanks to all members, present and past, of AK Koller, AK Eckert, AK van Wüllen and AK Schönhoff for assistance and helpful chats on NMR and also for their friendliness and cooperation.*

*I want to thank Dr. Bögershausen for introducing me to sol-gel science and experimental NMR, Jakob Kopp for providing hardware support, Dr. Meise-Gresch and Wilma for scientific support, Sebastian Wegner and Hendrik Feldhues for IT support.*

*I owe my deepest thanks to Huong, Nina, Simone and Jan for their support, interesting discussions and nice moments. I also wish to thank my student co-workers, Thomas, Jan, Melanie, Daniel, Michael and Martin, for sharing nice time in the lab. I have benefited from the work of Ansgar, Jan, Simone, Nina and my student co-workers.*

*I express my sincere thanks to all my friends especially batchmates Sebastian, Gawas, Panda, Jana and Raje for the precious moments, Carla, Roland, Loli, Maryam, Liyi, Matthias, Yunus, and Svenja for a friendly atmosphere in Münster. Special thanks to Sreeraj and Sebastian for providing a mallu atmosphere in Münster.*

*I wish to thank Münster Indian community, former and present, especially Dr. Banhatti, Arijit, Sanju, Nitin, Ajay, Devidas, Rashmi, Srinidhi, Joyram, Rudra, Sabu, Nirupam, Sonia, Barun, Chandan, Anil, Saleem, Abbas, Ashuthosh, Diptangshu, Sunil, Modhu.....*

*I would like to express my gratitude to David Laughman, Dr. Ralf van Bühren, Hartwig Bouillon for their support and wonderful moments.*

*I wish to express my deepest thanks to Pattery uncle, aunty, Santhosh, Cyna, Bijosh, Manjaly family, Caleb family, Mampilly family and Kizhakepaliam family for providing a family atmosphere in Germany.*

*This thesis certainly would not have been possible without the love, support and constant encouragement of my dad, mom and Jijo. I always remain indebted for everything they have done for me. Above all I thank Him for everything.....*

# Table of Contents

---

<i>Acknowledgements</i> .....	<i>VII</i>
<i>Table of Contents</i> .....	<i>IX</i>
<i>List of Abbreviations</i> .....	<i>XIII</i>
1. Introduction.....	1
1.1 Objectives of the thesis .....	1
1.2 Review of literature .....	3
1.2.1 Introduction to sol-gel science.....	3
1.2.2 Evaporation induced self assembly (EISA).....	4
1.2.3 Spray Drying.....	5
1.2.4 Controlled release .....	6
1.2.5 Organic-inorganic hybrid materials.....	8
1.2.6 2D HETCOR NMR spectroscopy .....	8
2. Theoretical Background.....	11
2.1 Sol-gel processing .....	11
2.2 Physisorption .....	15
2.2.1 Classification of pore sizes .....	16
2.2.2 Types of adsorption isotherms.....	16
2.2.3 The BET Model .....	17
2.3 Semi-empirical equation for describing drug release .....	18
2.4 Nuclear magnetic resonance.....	19
2.4.1 Introduction.....	19
2.4.2 Boltzmann distribution .....	20
2.5 NMR of solids .....	21
2.5.1 Line broadening by Dipole-Dipole interactions .....	21
2.5.2 Chemical shift interactions .....	22
2.5.3 Long spin lattice relaxation times.....	24
2.5.4 Highly resolved solid state NMR spectra .....	25
2.5.5 2D NMR spectroscopy .....	32

2.5.6 2D FSLG HETCOR NMR .....	33
2.6 Spray Drying: A theoretical investigation .....	34
<b>3. Methods and Materials .....</b>	<b>40</b>
3.1 Silica precursors.....	40
3.2 Model Drugs and their physicochemical characteristics .....	41
3.2.1 Persantin.....	41
3.2.2 Propranolol .....	42
3.3 Preparation of Hybrid silica gels .....	43
3.3.1 Evaporation Induced Self Assembled (EISA) gels .....	43
3.3.2 Spray dried (SD) gels .....	44
3.3.3 Gel notations .....	45
3.4 Characterization techniques .....	45
3.4.1 Drug release studies <i>in vitro</i> .....	46
3.4.2 Nitrogen sorption technique .....	48
3.4.3 Scanning Electron Microscopy (SEM) .....	49
3.4.4 Solid state NMR spectroscopy .....	49
3.5 Pre-characterization techniques .....	55
3.5.1 Differential Scanning Calorimetry (DSC).....	55
3.5.2 X-Ray powder diffraction (XRD) .....	57
<b>4. Evaporation Induced Self Assembled Gels .....</b>	<b>59</b>
4.1 EISA silica gel formulations from a single precursor .....	59
4.1.1 Preparation .....	59
4.1.2 Dissolution rate test.....	60
4.1.3 Surface studies by SEM .....	61
4.1.4 N <sub>2</sub> Sorption studies.....	62
4.1.5 <sup>29</sup> Si MAS NMR studies .....	63
4.1.6 <sup>1</sup> H MAS NMR studies.....	65
4.1.7 <sup>13</sup> C { <sup>1</sup> H} CPMAS NMR studies.....	70
4.1.8 Discussion .....	71
4.2 EISA gel formulations from two precursors.....	74
4.2.1 Hydrophobic Precursors.....	74
4.2.2 Hydrophilic Precursor - ATS .....	93



4.2.3 Aromatic precursors.....	99
4.2.4 Discussion.....	103
<b>5. Spray Dried Gels with Persantin.....</b>	<b>109</b>
5.1 Spray dried gel formulations from a single precursor.....	109
5.1.1 Preparation.....	109
5.1.2 Surface studies by SEM.....	111
5.1.3 N <sub>2</sub> Sorption studies .....	112
5.1.4 <sup>1</sup> H MAS NMR studies .....	113
5.1.5 <sup>29</sup> Si MAS NMR studies .....	113
5.2 Spray dried gel formulations from two precursors .....	115
5.2.1 Hydrophobic Precursors .....	115
5.2.2 Hydrophilic Precursor - ATS.....	119
5.2.3 Aromatic Precursors .....	123
5.2.4 Discussion.....	131
<b>6. Spray Dried Gels with Propranolol.....</b>	<b>134</b>
6.1 Spray dried gel formulations from a single precursor.....	134
6.1.1 Preparation.....	134
6.1.2 Drug release studies .....	135
6.1.3 Surface studies by SEM.....	136
6.1.4 N <sub>2</sub> Sorption studies .....	137
6.1.5 <sup>1</sup> H MAS NMR studies .....	138
6.1.6 <sup>13</sup> C { <sup>1</sup> H} CPMAS NMR studies .....	139
6.2 Spray dried gel formulations from two precursors .....	141
6.2.1 Hydrophobic Precursors .....	141
6.2.2 Hydrophilic Precursor - ATS.....	146
6.2.3 Aromatic Precursors .....	149
6.2.4 Discussion.....	154
<b>7. High resolution solid state NMR spectroscopy.....</b>	<b>156</b>
7.1 2D <sup>1</sup> H- <sup>13</sup> C FSLG HETCOR NMR - Propranolol Hydrochloride .....	156
7.2 Methyl Substituted Hybrid EISA Gel – Gel 37 .....	158
7.2.1 <sup>1</sup> H High Field High Speed MAS NMR .....	158

7.2.2 2D $^1\text{H}$ - $^{29}\text{Si}$ FSLG HETCOR NMR.....	160
7.2.3 2D $^1\text{H}$ - $^{13}\text{C}$ FSLG HETCOR NMR.....	164
7.3 Methyl Substituted Hybrid EISA Gel – Gel 177.....	168
7.3.1 2D $^1\text{H}$ - $^{29}\text{Si}$ FSLG HETCOR NMR.....	168
7.3.2 2D $^1\text{H}$ - $^{13}\text{C}$ FSLG HETCOR NMR.....	169
7.4 Benzyl Substituted Hybrid EISA Gel – Gel 191.....	173
7.4.1 2D $^1\text{H}$ - $^{29}\text{Si}$ FSLG HETCOR NMR.....	173
7.4.2 2D $^1\text{H}$ - $^{13}\text{C}$ FSLG HETCOR NMR.....	174
7.5 Acetoxypropyl substituted Hybrid EISA Gel – Gel 182.....	177
7.5.1 2D $^1\text{H}$ - $^{29}\text{Si}$ FSLG HETCOR NMR.....	177
7.5.2 2D $^1\text{H}$ - $^{13}\text{C}$ FSLG HETCOR NMR.....	178
7.6 Acetoxypropyl Substituted Spray Dried Gel – Gel 148.....	181
7.6.1 2D $^1\text{H}$ - $^{29}\text{Si}$ FSLG HETCOR NMR.....	181
7.7 Discussion.....	185
8. Conclusions and final remarks.....	195
9. Appendix.....	197
9.1 $^1\text{H}$ MAS NMR spectra of various EISA hybrid gels.....	197
9.2 $^1\text{H}$ MAS NMR spectra of various SD gels.....	200
9.3 $^{29}\text{Si}$ MAS NMR spectra of various EISA hybrid gels.....	208
9.4 $^{29}\text{Si}$ MAS NMR spectra of various SD hybrid gels.....	211
9.5 $^{13}\text{C}\{^1\text{H}\}$ CPMAS NMR spectra of various hybrid EISA gels.....	216
9.6 $^{13}\text{C}\{^1\text{H}\}$ CPMAS NMR spectra of various hybrid SD gels.....	219
9.7 $\text{N}_2$ sorption isotherms of various aromatic hybrid EISA gels.....	224
10. Bibliography.....	225

---

## List of Abbreviations

1D/2D	One dimensional/two dimensional
ATS	Acetoxypropyltrimethoxysilane
BET	Brunauer Emmet Teller
BTS	Benzyltriethoxysilane
CP	Cross Polarization
CW	Continues Wave
DRT	Dissolution Rate Test
DSC	Differential Scanning Calorimetry
DPhDS	Diphenyldiethoxysilane
ETS	Ethyltriethoxysilane
EISA	Evaporation Induced Self-Assembly
FSLG	Frequency Switched Lee-Goldburg
FT	Fourier Transformation
HETCOR	Heteronuclear Correlation
MAS	Magic Angle Spinning
NMR	Nuclear Magnetic Resonance
PS	Persantin
PP	Propranolol Hydrochloride
PTS	n-Propyltriethoxysilane
PhTS	Phenyltriethoxysilane
RF	Radio Frequency
SD	Spray drying
SEM	Scanning Electron Microscopy
SS	Solid State
TEOS	Tetraethoxysilane
TMOS	Tetramethoxysilane
TMS	Tetramethylsilane
UV/VIS	Ultra-Violet/Visible



# 1. Introduction

---

## 1.1 Objectives of the thesis

The general objective of this thesis was to develop new silica based drug carriers by sol-gel technique for the controlled release of drugs. Two drugs, Persantin and Propranolol were used as model substances to evaluate the possibilities to control the drug release rate from evaporation induced self assembled (EISA) gels and spray dried (SD) gels. Persantin is a coronary vasodilator and is also used to prevent platelet aggregation after heart valve disease, whereas, Propranolol is a beta-blocker used extensively in the treatment of cardiovascular disorders.

Controlled release over an extended duration is highly beneficial for drugs that are rapidly metabolized and eliminated from the body after administration. All controlled release systems aim to improve the effectiveness of drug therapy. This improvement can take the form of increasing therapeutic activity compared to the intensity of side effects and reducing the number of administrations required during the treatment. One of the aims of this thesis was to develop a controlled release system for Propranolol by imprinting the drug into a sol-gel derived silica network. In addition, the surface interactions of the drug as well as the diffusion barriers of the matrix are probed for tailoring the controlled release of Propranolol.

The enhancement of oral bioavailability of sparingly water soluble drug remains one of the most challenging aspects of drug development. Although salt formation, solubilization and particle size reduction have commonly been used to increase dissolution rate and thereby oral absorption and bioavailability of such drugs, there are practical limitations for these techniques. Another aim of this thesis was to develop a practical method to overcome the limitations. In this thesis, the investigations are made on the encapsulation of the drug molecules in silica sols followed by spray drying, for the accelerated release of sparingly soluble drug Persantin. Drug dissolution enhancements

upon enrichment of the molecularly dispersed drug molecules on the surface of spray dried microparticles are also examined.

An understanding of the molecular level interactions between the drug and the drug-incorporated system has a great fundamental interest. The release of the active pharmaceutical agent from silica gels was controlled by the different gel synthesis parameters and the physicochemical properties of the agent. To fine tune the bioavailability of the drug from the silica gel, one need to know the interactions at the molecular level. The local molecular interaction between the drug and the host matrix has been investigated by employing high-resolution two-dimensional heteronuclear magnetic resonance correlation spectroscopy.

The relationship between drug release and matrix porosity development upon synthesis parameters were also investigated in detail with the help of nitrogen sorption technique. The molecular imprinting capabilities of the drug molecules and their stability in the storage system were also probed.

## 1.2 Review of literature

### 1.2.1 Introduction to sol-gel science

Interest in the sol-gel process of inorganic ceramic and glass materials began as early as the mid-1800's with Ebelman and Graham's studies on silica gels.<sup>1</sup> These early investigators observed that hydrolysis of tetraethyl orthosilicate (TEOS), under acidic conditions yielded SiO<sub>2</sub> in the form of a "glass like material". Roy and coworkers<sup>2</sup> recognized the potential for achieving very high levels of chemical homogeneity in colloidal gels and used the sol-gel method in the 1950's and 1960's to synthesize large number of novel ceramic oxide compositions, involving Al, Si, Ti, Zr etc. During the same time Iler's pioneering works in silica chemistry<sup>3</sup> led to the commercial development of colloidal silica powders. Stober et al.<sup>4</sup> extended Iler's findings to show that using ammonia as a catalyst for the TEOS hydrolysis reaction could control both the morphology and size of the silica powders. The final size of the spherical silica powder is a function of the initial concentration of water and ammonia, the type of silicon alkoxide and alcohol mixture used and the reactant temperature.

The motivation for sol-gel processing is primarily the potentially higher purity and homogeneity and the lower processing temperature associated with sol-gels compared with traditional glass melting or ceramic powder methods. Mackenzie<sup>5</sup> summarizes a number of potential advantages and disadvantages and the relative economics of sol-gel methods in general. During the past decades there has been an enormous growth in the interest in the sol-gel process. This growth has been stimulated by several factors. On the basis of Kistler's work,<sup>6</sup> several teams have produced very low density silica monoliths, called aerogels, by hypercritical point drying.<sup>7</sup> Zarzycki, Prassas and Phalippou<sup>8</sup> demonstrated that hypercritical point drying of silica gels could yield large fully dense silica glass monoliths.

Molecular recognition is one of the basic processes in nature.<sup>9</sup> It can be envisaged as the preferential binding of a molecule to a receptor with high selectivity over its close structural analogue. The first approach to synthesizing molecular imprinted materials was based on silica gels and traces back to the early 1930's. Polyakov<sup>10</sup> first reported that the silica pore structure was influenced by the presence of benzene, toluene and xylene during the drying process. In 1942 Pauling and Canpell<sup>11</sup> reported the preparation of

artificial antibodies using antigen molecules as templates. In the 1970's imprinted sol-gel materials have been produced and applied as adsorbents, separation media, catalysts and more recently as sensing phases.<sup>12</sup>

The engineering of porosity in common materials such as silica is emerging as a new area of technological and scientific interest.<sup>13</sup> The development of porous materials with large specific surface area is currently an area of extensive research, particularly with regard to potential applications in areas such as adsorption, chromatography, catalysis, sensor technology and gas storage.<sup>14</sup> Microporous cavities of zeolites and other engineered porous materials have been used as nanosized reaction vessels<sup>15</sup> or hosts in which to assemble semiconductor clusters,<sup>16</sup> organic molecules,<sup>17</sup> and even molecular wires.<sup>18</sup> Brinker et al. have done some pioneering works on the synthesis of porous amorphous silicas using sol-gel approach.<sup>19</sup> They have found that in organic template derived amorphous silicas, the nature of template-matrix interactions and the subsequent processing dictates the final pore morphology. The pore structure in silica gel is an important factor especially in controlling the function as a drug release system.<sup>20</sup>

### 1.2.2 Evaporation induced self assembly (EISA)

Self assembly can be defined as the spontaneous organization of materials (e.g., drug molecules and silica oligomer/polymer) through noncovalent interactions such as hydrogen bonding, van der Waals forces, electrostatic forces,  $\pi$ - $\pi$  interactions etc.<sup>21</sup> Self assembly typically employs asymmetric molecules that are pre-programmed to organize into well-defined supramolecular assemblies. In EISA gels, self assembly is driven by the evaporation of solvents such as water or ethanol resulting in a semi-solid. Subsequent aging by temperature treatment solidifies the silicon skeleton, thereby locking the drug molecules inside the pores.

In 1983 Unger and co-workers introduced the idea using sol-gel derived EISA silica gel in drug delivery applications.<sup>22</sup> Unger found that the physicochemical characteristics of the drug molecule significantly control the release rate. In addition, sol-gel based materials are bioactive i.e. they bind to bone and can be used in biomedical and dental applications.<sup>23</sup> In recent years, the sol-gel method has attracted many researchers.<sup>24</sup> Entrapment of organic molecules is done through chemical routes. The introduction of guest molecules is done by adding its solution to the polymerizing mixture.<sup>25</sup> When the polymerization is completed, the dopant molecules are entangled in the inorganic



polymeric network. The entrapped molecules are accessible to external reagents through the pore network. Some of the advantages of sol-gel matrix include the chemical, photochemical, electrochemical inertness as well as the thermal stability of the matrix and the enhanced stability of the entrapped molecules.

### 1.2.3 Spray Drying

Spray drying is a useful method for powder generation.<sup>26</sup> The process involves the evaporation of moisture from an atomized feed by mixing the spray and drying medium to form the powder product. Several features distinguish spray drying from both solid state and liquid phase chemical reaction routes. In earlier drug delivery studies, silica xerogel was used as monoliths or crushed particles.<sup>27</sup> Crushed silica gel particles are irregular in shape and release the active agent quickly.<sup>28</sup> Spray drying is a promising way to produce spherical silica gel particles with a narrow particle size range for controlled delivery of drugs.<sup>29</sup> Spray drying provides the ability to control and maintain uniform chemical composition from particle to particle for multicomponent materials and to obtain submicron and high purity particles directly without milling.<sup>30</sup> Spray drying has been used in pharmaceutical technology studies for the purpose of drying heat sensitive materials, improving flow properties, preparing free flowing granules for tablet production and increasing the solubility of poorly water soluble substances.<sup>31</sup> Spray drying was evaluated as a potential method to prepare inclusions of various hydrophobic drugs in complexes with  $\beta$ -cyclodextrin (nicardipine hydrochloride,<sup>32</sup> progesterone<sup>33</sup> and carbamazepine<sup>34</sup>) in order to improve their aqueous solubility and consequently their bioavailability.<sup>35</sup> Korteso et al. have studied sol-gel derived spray dried silica gel microspheres as carrier material for dexmedetomidine HCl and toremifene citrate.<sup>36</sup> Vanbever et al. suggested that large porous particles produced by spray drying have advantages for the delivery of drugs to the lungs.<sup>37</sup> Takeuchi et al. reported the solid dispersion particles with colloidal silica or porous silica prepared by spray drying method could improve the dissolution property of tolbutamide and indomethacin.<sup>38</sup> Palmieri et al. have prepared paracetamol/polymer and paracetamol/ethylcellulose microspheres by spray drying method and verified their use in controlled release solid dosage forms.<sup>39</sup> Ibuprofen and naproxen encapsulated microspheres produced by spray drying were evaluated for controlled drug delivery.<sup>40</sup> Czuryzkiewicz et al. reported the use of spray dried silica particles as a drug carrier matrix providing a long-term release of

biphosphonates and other highly water soluble drugs.<sup>41</sup> Other reports in the literature include the formulation of large hollow nanoparticles aggregates as potential carriers in inhaled delivery of nanoparticulate drugs.<sup>42</sup> Alonso et al. have reported spray drying as a new route to mesoporous silica based spheres with functionalized surfaces.<sup>43</sup> Lind et al. have prepared spherical silica agglomerated by spray drying of MCM-41 and MCM-48 nanospheres.<sup>44</sup>

### 1.2.4 Controlled release

Controlled drug release technology represents one of the most rapidly advancing areas of science in which chemists and chemical engineers are contributing to human health care.<sup>45</sup> Controlled release formulations were first used in the agricultural industries for low molecular weight fertilizers, pesticides and antifoulants in the 1950's.<sup>46</sup> In the 1960's these approaches were extended into the medical field.<sup>47</sup> By the mid-1970's controlled release formulations for large molecular weight drugs were designed.<sup>48</sup> In a controlled release system a drug or other bioactive agent is incorporated into a carrier, generally a polymeric material. Controlled release systems are capable of delivering substances slowly and continuously for up to several years.<sup>49</sup> An important consideration in developing a drug release matrix is the knowledge of long-term stability of the form of the drug and matrix after formulation and any changes that might occur to the drug throughout the release process.<sup>50</sup> These controlled release systems represent a relatively new development that evolved out of a continuing need to prolong and better control drug administration. The significance of such systems can be appreciated by considering typical drug level resulting from conventional drug formulations (tablets, sprays, injections). In most cases, drug levels reach a maximum and then fall to a minimum, at which point repeated administration becomes necessary. However, if the maximum and minimum drug concentrations fall above or below the toxic level or minimum effective level, respectively, alternating periods of toxicity or inefficiency can result. A controlled release system should release drug continuously in a fixed, predetermined pattern for a desired time period. Ideally, this should result in a uniform drug concentration as a function of time, require smaller dosages and cause fewer side effects (Figure 1.1).<sup>51</sup> Alternative approaches to polymeric systems involve embedding the drug molecule in ordered mesoporous systems, for example mesoporous silica, MCM-41,<sup>52</sup> or intercalation of the drug in layered aluminosilicates such as double-layer hydroxides and clays.<sup>53</sup> A

recent study by Chang et al.<sup>54</sup> uses swollen, thermoresponsive nanocomposites. Several sol-gel derived silicon oxide based materials have been investigated as alternative controlled drug release systems.<sup>55</sup> These materials are potentially multifunctional, since another possible application area for these types of silica ceramics is as bioactive bone-generating implants or bone-filling materials.<sup>56</sup> Introducing a pharmaceutical to such a matrix could therefore make it possible to combine bone-generating ability with controlled release properties.<sup>57</sup> Bögershausen et al. have recently reported the drug release from self-assembled inorganic-organic hybrid silica gels.<sup>58</sup> Silica xerogel as an implantable carrier for controlled drug delivery has been proposed by Korteso et al.<sup>59</sup>

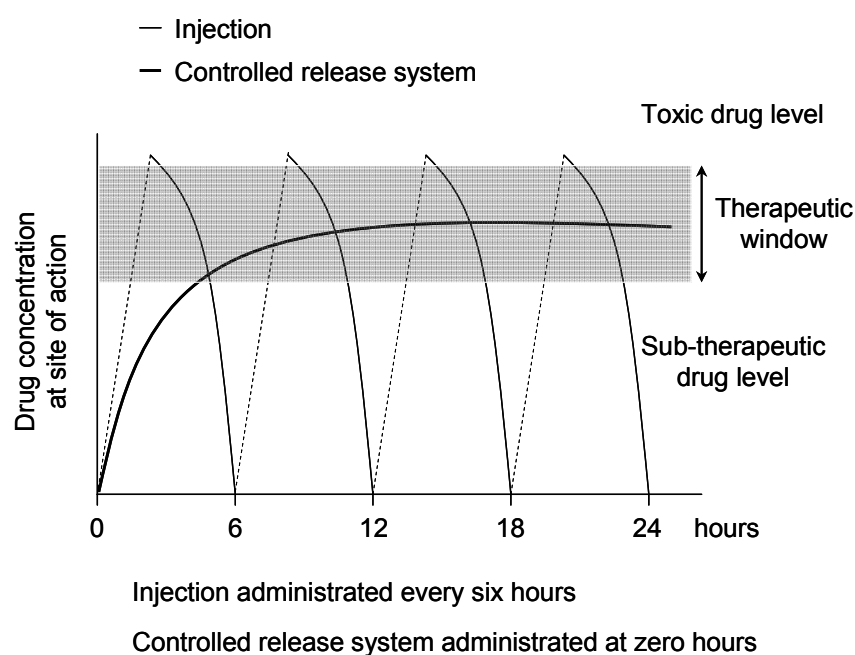


**Figure 1.1:** Drug concentration at site of therapeutic action after delivery as a conventional injection (thin line) and as a temporal controlled release system (bold line).

Sol-gel derived silica xerogel has been studied as a carrier material for various drugs, peptides and proteins.<sup>60</sup> Bioactive agents can be incorporated into silica xerogel either by adsorbing drug onto the surface of the heat-treated silica xerogel<sup>61</sup> or by adding the drug during the sol-gel manufacturing process. The solubility of the drug may limit the amount of drug added during the sol-gel phase. The self assembly of organized nanoscopic structures is of great interest in both colloidal and material science.<sup>62</sup> Smirnova et al. have shown that the dissolution rate of poorly soluble drugs can be significantly accelerated through adsorption on silica gel.<sup>63</sup>

### 1.2.5 Organic-inorganic hybrid materials

Hybrid materials lie at the interface of the organic and inorganic realms.<sup>64,65</sup> Their synthesis offers exceptional opportunities not only to combine the important properties from both the worlds, but also to create entirely new compositions with truly unique properties. The size of the organic-inorganic domains can range from traditional composites prepared from physical mixtures of relatively large, micrometer size particles to nanophase materials that include substances with organic and inorganic domains that are dispersed homogeneously at the molecular level. A hybrid organic-inorganic material can be prepared by the hydrolysis and condensation of monomers containing a variable organic side groups with two or more trifunctional silyl groups.<sup>66</sup> The organic group, covalently attached to the trialkoxysilyl groups through Si-C bonds, can be varied in length, rigidity, geometry of substitution, functionality and hydrophobicity. This variability provides an opportunity to explore how the organic structural unit contributes to bulk properties such as porosity, thermal stability, optical clarity, chemical resistance and dielectric constant. Sol-gel polymerization of these hybrid monomers involve a series of hydrolysis reactions forming silanol-functionalized intermediates and subsequent condensation reactions that produce oligomeric siloxanes. These species react further to produce higher molecular weight polymers that eventually form a 3D infinite network which spans the dimensions of the reaction vessel. At this point, the solution loses fluidity and has reached the gel point. The wet gel is then dried to afford a xerogel. During the drying process the gel undergoes significant shrinkage, resulting in partial collapse of pore structure. These materials are considered as innovative advanced materials and promising applications are expected in many fields: Optics, electronics, mechanics, membranes, protective coatings, catalysis, sensors, biology etc.<sup>67</sup>

### 1.2.6 2D HETCOR NMR spectroscopy

Based on magnetization transfer between abundant and rare spins ( $^1\text{H}$  and  $^{13}\text{C}$  or  $^{29}\text{Si}$ , respectively), CP technique has often been combined with MAS and high power proton decoupling to increase the sensitivity of dilute nuclei. However, the main difficulty encountered in the 1D CPMAS experiment is the uncertain nature of the protons that are actual sources of the magnetization that is transferred, which interferes with conclusions concerning the spatial proximities between  $^1\text{H}$  and  $^{13}\text{C}/^{29}\text{Si}$  nuclei. The use of 2D

HETCOR<sup>68</sup> NMR experiment can circumvent this problem. Detailed information about the structure, topology and dynamics of complex molecular systems may be best provided by multidimensional heteronuclear correlation NMR, which offers improved resolution by separating the resonance in two or more dimensions and reveal through space connectivities between spins.<sup>69</sup> This technique was first introduced to characterize surface species on silica and zeolites<sup>70</sup> and has also been applied to two siloxane-silica systems prepared from MTES and TEOS<sup>71</sup> and PhTES and TEOS.<sup>72</sup> Recently Babonneau et al. used the technique to evaluate the chemical homogeneity in hybrid silica gels.<sup>73</sup> The major experimental challenge associated with application of 2D  $^1\text{H}$ -X (X =  $^{13}\text{C}$ ,  $^{29}\text{Si}$ , ...) correlation experiments under MAS involves suppressing  $^1\text{H}$ - $^1\text{H}$  homonuclear dipolar interactions during the evolution period, such as the isotropic chemical shift and resonance offsets dominate the behavior of  $^1\text{H}$  magnetization in the indirect dimension. Lee-Goldburg schemes proved effective in  $^1\text{H}$ - $^{13}\text{C}$  HETCOR experiments performed under fast MAS.<sup>74</sup>  $^1\text{H}$ - $^{29}\text{Si}$  and  $^1\text{H}$ - $^{13}\text{C}$  HETCOR NMR was used to study the surface and interfacial species on silica,<sup>75</sup> mesoporous aluminosilicates<sup>76</sup> and organic-inorganic nanocomposites.<sup>77</sup> Recently it has been shown that the Lee-Goldburg (LG) homonuclear decoupling technique can be combined with CP to achieve polarization transfer with efficient suppression of  $^1\text{H}$ - $^1\text{H}$  spin diffusion.<sup>78</sup> Luliucci et al. have probed the polymer-filler interface by using  $^1\text{H}$ - $^{29}\text{Si}$  2D HETCOR NMR experiment.<sup>79</sup> More recently, Trebosc et al. explored the HETCOR technique in the study of MCM-41 type mesoporous silica nanoparticles.<sup>80</sup> Geppi et al. investigated the conformational and molecular dynamic properties of drugs and their solid dispersions with polymer Eudragit RL100.<sup>81</sup> NMR spectroscopy has also been used to characterize proteins encapsulated in a sol-gel matrix.<sup>82</sup> It has been shown by Wilhelm et al.<sup>83</sup> and Massiot et al.<sup>84</sup> that proton spin diffusion could be used to characterize domain sizes and spatial proximity at length scale of up to 200 nm. Bose et al. have employed HETCOR NMR spectroscopy for the characterization of physisorbed siloxane polymer on silica.<sup>85</sup> There are also reports of investigations by HETCOR NMR of silica interfaces in mesostructured materials.<sup>86</sup> Sozzani et al. have probed the nanoporosity of an organo-clay by xenon and 2D HETCOR NMR spectroscopy.<sup>87</sup> The solid state 2D HETCOR technique has been successfully used to obtain detailed structural information and to probe the nature of intermolecular interactions in polymers.<sup>88</sup> Epping and Chmelka have reviewed nucleation and growth of mesoporous solids with molecular insights from NMR.<sup>89</sup> Wiench et al.

have used SPAM-MQ-HETCOR NMR spectroscopy for the high resolution solid state correlation between Al and Si in zeolites.<sup>90</sup>

## 2. Theoretical Background

---

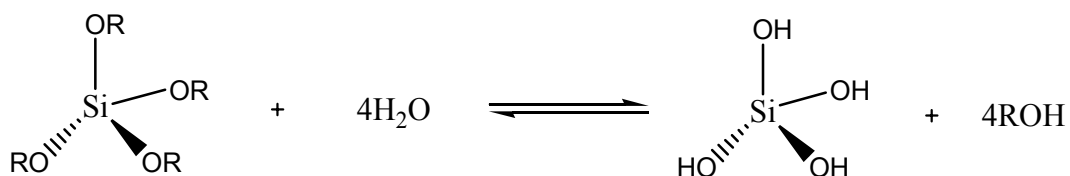
### 2.1 Sol-gel processing<sup>91</sup>

Silicon is the most abundant metal in the earth's crust, and evidence of silicate hydrolysis and condensation to form polysilicate gels and particles is seen in many natural systems. A colloid is a suspension in which the dispersed phase is so small (~1-1000 nm) that gravitational forces are negligible and interactions are dominated by short-range forces, such as van der Waals attraction and surface charges. A sol is a colloidal suspension of solid particles in a liquid.

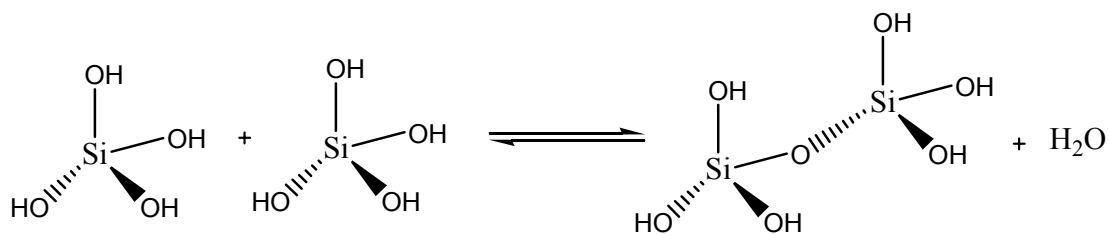
Sol-gel process can be described as the creation of an oxide network by progressive polycondensation reactions of molecular precursors in a liquid medium. It generally starts with alcoholic or other low molecular weight organic solutions of monomeric, metal or semi-metal alkoxide precursors  $M(OR)_n$ , where M represents a network-forming element such as Si, Ti, Al etc., and R is typically an alkyl group and water. Generally hydrolysis and condensation reactions occur simultaneously once the hydrolysis reaction has been initiated. During the sol-gel transformation, the viscosity of the solution gradually increases as the sol becomes interconnected to form a rigid, porous network-the gel. As seen in Figure, both the hydrolysis and condensation steps generate low molecular weight by-products such as alcohol and water. These small molecules must be removed from the system, thus resulting in a tetrahedral  $SiO_2$  (if the species is silicon) network. During drying alcohol and water evaporate from the pores causing the gel to shrink. Xerogels are significantly less porous than their hydrated counterparts. The chemical reactions that take place during the formation of the sol, gel and xerogel strongly influence the properties and composition of the final material. Also, the physical properties such as average pore size, pore size distribution, pore shape, surface area etc. of the dried gel depend on the sol-gel process parameters and the methods used to prepare the material. Sol-gel process involves the manufacture of inorganic matrices through the formation of a colloidal suspension (sol) and the gelation of the sol to form a wet gel, which after drying, forms dry gel called xerogel. Most sol-gel techniques use water and low molecular weight alkoxysilanes, such as tetraethoxysilane (TEOS) or tetramethoxysilane (TMOS), as silica precursors. The alkoxide hydrolysis with water to

form silanols, with either acid or base as catalyst. The reactions of alkoxy silanes can be summarized in terms of three steps: hydrolysis of the alkoxy, silanol-silanol condensation and silanol-ester condensation.

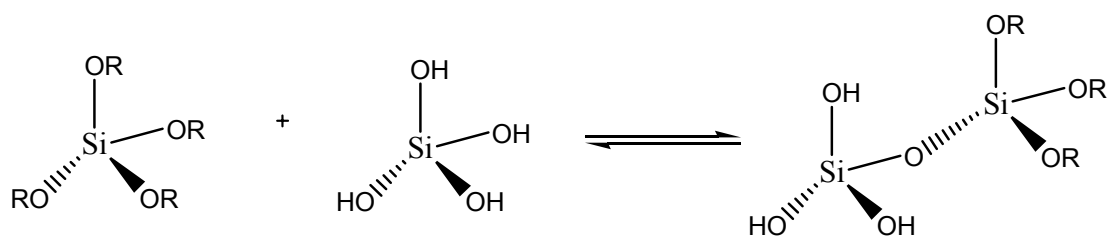
### Hydrolysis



### Silanol-silanol condensation

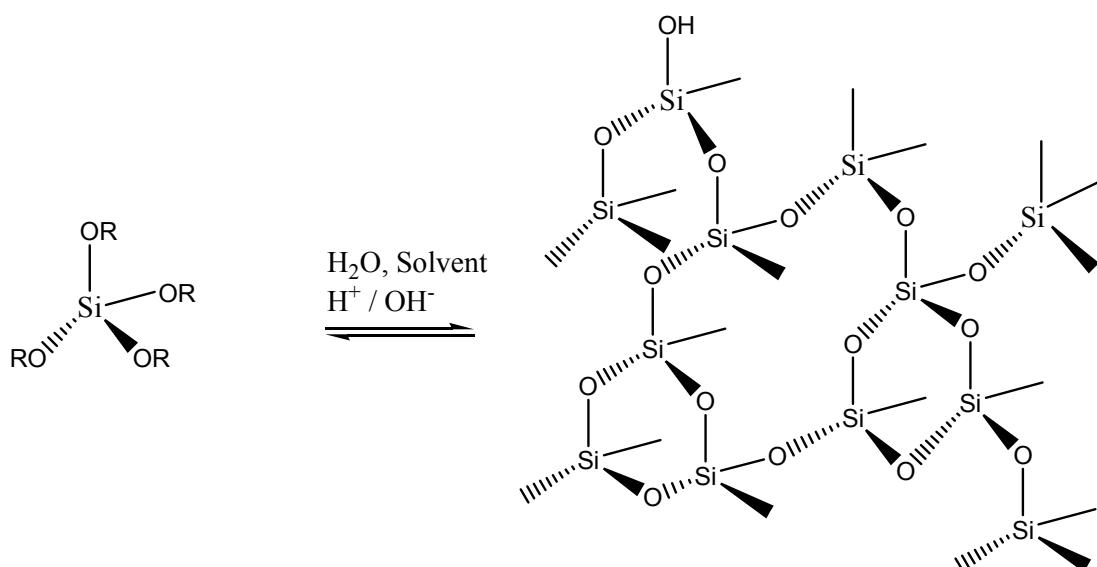


### Silanol-ester condensation





## Overall reaction



Monomers  $\rightarrow$  Polymers  $\rightarrow$  Particles  $\rightarrow$  Sol  $\rightarrow$  Gel

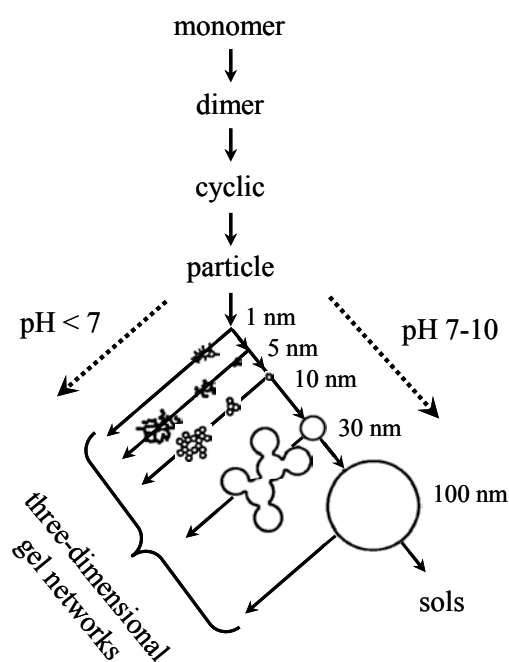


**Figure 2.1:** Polymerization behaviour of aqueous silica. In basic solution, particles grow in size with decrease in number and in acid solution, particles aggregates into 3D networks and form gels.<sup>91</sup>

Hydrolysis occurs by the nucleophilic attack of the oxygen contained in water in the silicon atom. Subsequent condensation reactions take place producing siloxane bonds. The polymerization stages may be described as, (i) polymerization of monomers to

polymers, (ii) condensation of polymers to primary particles, (iii) growth or agglomeration of primary particles and (iv) linking of particles into chains and to three dimensional network.<sup>92</sup> Networks of the chains extend throughout the liquid medium, thickening the network into a gel. In the last stage water and alcohol are evacuated from the network structure causing gradual shrinkage and even cracking of the monolithic gel. Spray drying has been used in pharmaceutical technology since the early 1940's. It is a useful method because it offers a means to predetermine properties such as particle size, flow ability, porosity and retention of activity of heat sensitive pharmaceuticals.<sup>93</sup> The particles formed are in micrometer size range. From a manufacturing viewpoint, spray drying offers the advantage of being a single step process which can be readily scaled up. It is already widely used for preparation of microparticles from biodegradable polyester polymers.<sup>94</sup>

### **Factors affecting the structure of sol-gel processed silica xerogel**

A porous and amorphous structure is one of the most characteristic features of sol-gel derived silica xerogel. Reactivity of the matrix, due to free hydroxyl groups, is the other typical property of silica xerogel. The microstructure of silica xerogel can be controlled by changing the water/alkoxide molar ratio, the catalyst type or concentration or by using alkyl-substituted alkoxides or other additives.

### **Water/alkoxide molar ratio**

The water/alkoxide molar ratio ( $r$ ) has significant effect on the silica xerogel microstructure.<sup>91</sup> When the water/alkoxide molar ratio is low, alcohol condensation is dominating and gelation time is longer, leading to more micro porous materials. Gels made from higher water content sol ( $r > 4$ ) have shown more coarse microstructure than gels made from lower water content sols ( $r < 4$ ).<sup>95</sup>

### **Catalyst**

The effect of pH on the pore structure and morphology has been extensively studied.<sup>96</sup> Changes in solution pH alter the relative rates of hydrolysis and condensation, yielding products ranging from weakly branched to particulate silica sols. Iler divides the

polymerization process into three approximate pH domains:  $\text{pH} < 2$ ,  $\text{pH} 2\text{-}7$  and  $\text{pH} > 7$ .<sup>3</sup>  $\text{pH} = 7$  appears as a boundary because the silica solubility and dissolution rates are maximized at or above  $\text{pH} = 7$ . The kinetics and growth mechanisms of the reaction depend on the pH value of the solution. With acidic pH, particle growth stops once the size of 2 to 4 nm is reached. Above  $\text{pH} = 7$  particle growth is mainly dependent on the temperature and particles of more than 100 nm in diameter can be formed (particulate sols). Above  $\text{pH} = 7$  particles are negatively charged and they repel each other and no aggregation of particles occurs (particulate sols). At low pH, near the isoelectric point (IEP), repulsive forces between particles are low and particles collide and form continuous networks leading to gels (Figure 2.2). Generally, silica particles are positively charged at low pH and negatively charged at high pH. Weakly basic to moderate acidic sols have significant amounts of deprotonated silanol groups ( $\text{SiO}^-$ ) which increase the condensation rate causing a formation of highly branched silica species. Gelation of these branched species results in the formation of mesoporous regions with a pore size between 2 nm and 50 nm.

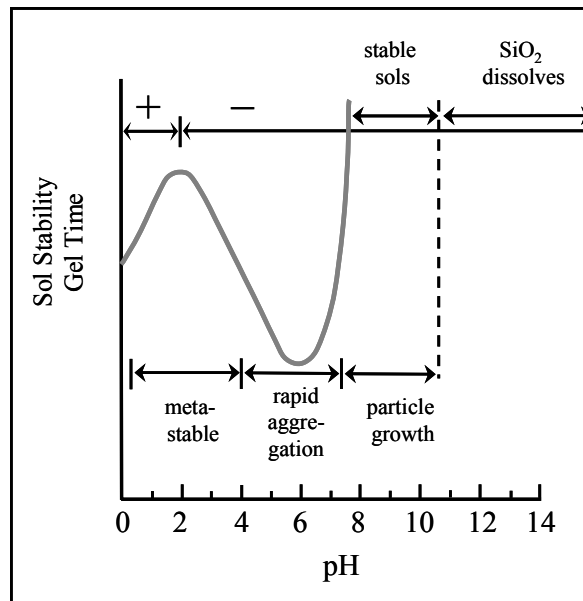


*Figure 2.2: Effect of pH on colloidal silica-water system.*<sup>91</sup>

## 2.2 Physisorption<sup>97</sup>

Adsorption is brought about by the interactions between the solid and the molecules in the fluid phase. Adsorption occurs whenever a solid surface is exposed to a gas or liquid. The physical adsorption of gases by solids increases with decreasing temperature and increases with pressure. The process is exothermic. An adsorption (or desorption)

isotherm is a measure of the standard volume of gas  $V_a$ , taken up, (or released), at a constant temperature  $T$  by an initially clean solid surface as a function of relative gas pressure  $p/p^0$ . The sorption (adsorption + desorption) measurements are conducted at boiling point of liquid  $N_2$  at one atmospheric pressure. Porosity is defined as the ratio of the volume of pores and voids to the volume occupied by the solid and pore volume is regarded as the volume of open pores.

### 2.2.1 Classification of pore sizes<sup>98</sup>

The pore systems of solids are of different kinds. The individual pores may vary greatly both in size and in shape within a given solid, and between one solid and another. A feature of special interest for many purposes is the width  $w$  of the pores, e.g. the diameter of a cylindrical pore or the distance between the sides of a slit-shaped pore. The basis of classification is that each of the size ranges corresponds to characteristic adsorption effects as manifested in the isotherm. In micropores, the interaction potential is significantly higher than in wider pores owing to the proximity of the walls and the amount adsorbed (at a given relative pressure) is correspondingly enhanced. The pore diameter of these materials is less than 2 nm. In mesopores, capillary condensation, with its characteristic hysteresis loop, takes place. The pore diameter ranges from 2 to 50 nm. In the macropore range the pores are so wide that it is virtually impossible to map out the isotherm in detail because the relative pressures are so close to unity. The pore diameter of these materials is larger than 50 nm.

### 2.2.2 Types of adsorption isotherms

The experimental adsorption isotherm is usually presented in graphical form. Adsorption isotherms are grouped into six classes in the IUPAC classification, Figure 2.3. Type *I* isotherm is concave to the relative pressure axis. It rises sharply at low relative pressures and reaches a plateau. The narrow range of relative pressures necessary to attain the plateau is an indication of a limited range of pore size and the appearance of a nearly horizontal plateau indicates a very small external surface area. The type *II* isotherm is concave to relative pressure axis, then almost linear and finally convex to the  $p/p^0$  axis. It indicates the formation of an adsorbed layer whose thickness increases progressively with increasing relative pressure until  $p/p^0 \rightarrow 1$ . Type *II* isotherms are obtained with non-porous or macroporous adsorbents, which allow unrestricted monolayer-multilayer

adsorption to occur at high  $p/p^0$ . Complete reversibility is the first condition to be satisfied for normal monolayer-multilayer adsorption on an open and stable surface. Type *III* isotherm is convey to the  $p/p^0$  axis over the complete range. This feature is indicative of weak adsorbent–adsorbate interactions.

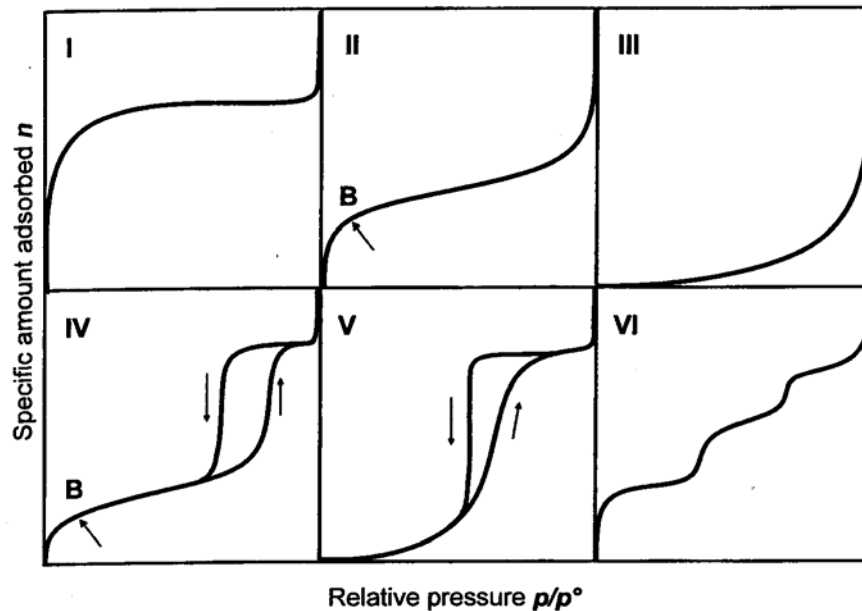


**Figure 2.3:** The six main types of gas physisorption isotherms, according to the IUPAC classification.

The type *IV* isotherm, whose initial region is closely related to the type *II* isotherm, tends to level off at high relative pressures. It exhibits a hysteresis loop, the lower branch of which represents measurements obtained by progressive additions of gas of the adsorbent, and the upper branch by progressive withdrawal. The hysteresis loop is usually associated with the filling and emptying of the mesopores by capillary condensation. Type *IV* isotherms are common for mesopores adsorbents. Type *V* and type *VI* isotherms are relatively rare.

### 2.2.3 The BET Model<sup>99</sup>

One of the most important methods in order to determine the area of a porous material is the determination of the BET (Brunauer Emmet Teller) adsorption isotherm. This method is based on a kinetic model of the adsorption process developed by Langmuir. One regards the surface of the solid as an array of adsorption sites. As soon as the state of dynamic equilibrium is reached the rate at which molecules arrive from the gas phase and

condensing on to bare sites equals the evaporation rate of these molecules. BET theory incorporated the concept of multi-molecular layer adsorption. By equating the rate of condensation of gas molecules onto an already adsorbed layer to the rate of evaporation from that layer and summing for an infinite number of layers, the expression

$$\frac{\frac{p}{p^0}}{V_a \left(1 - \frac{p}{p^0}\right)} = \frac{1}{V_m C} + \frac{\left((C-1) \frac{p}{p^0}\right)}{V_m C}$$

is obtained where  $C$  is a constant,  $p/p^0$  is the relative pressure,  $V_a$  is the volume of gas adsorbed and  $V_m$  is the volume of monolayer capacity. The value of  $C$  in simple terms is

$$C \propto \exp\left(\frac{Q_1 - Q_L}{RT}\right)$$

where  $Q_1$  is the heat of adsorption of the first layer,  $Q_L$  the heat of liquefaction of the adsorptive,  $R$  the gas constant and  $T$  the absolute temperature. The BET equation is of the form of straight line with intercept,  $1/V_m C$  and slope,  $(C-1)/V_m C$ . The value of  $V_m$  is obtained as the reciprocal of the sum of the slope and intercept.

The specific surface area  $s$  ( $\text{m}^2/\text{g}$ ) of the material can be calculated from  $V_m$  by the following equation,

$$s = \frac{V_m \sigma N_A}{m V_0}$$

Where  $\sigma$  is the molecular cross-sectional area of adsorbed gas molecule,  $N_A$  the Avogadro constant,  $m$  mass of the adsorbing material and  $V_0$  is the standard molar volume of the gas.<sup>100</sup>

## 2.3 Semi-empirical equation for describing drug release

A semi-empirical exponential relation was introduced by Ritger and Peppas<sup>101</sup> to describe the general drug release behaviour of controlled release polymeric devices.

$$\frac{M}{M_0} = kt^n$$

Where  $M/M_0$  is the fractional drug release,  $t$  is the release time,  $k$  is a constant, incorporating structural and geometric characteristics of the release device, and  $n$  is the diffusional exponent characteristic of the release mechanism. This equation applies until 60% of the total amount of drug released. It predicts that the fractional release of drug is

exponentially related to the release time and it adequately describes the release of drug from slabs, spheres, cylinders and tablets from both swellable and non-swellable matrices. In case of pure Fickian release the exponent  $n$  has the limiting value of 0.50, 0.45 and 0.43 for release from slabs, cylinders and spheres, respectively. For tablets, the Fickian diffusion mechanism is described by  $0.43 < n < 0.50$ . For drug release from spherical polymer particles of a wide distribution, the value of the exponent  $n$  for Fickian diffusion depends on the width of the distribution. An anomalous non-Fickian diffusion pattern ( $n = 0.5 - 1.0$ ) is observed when the rates of the solvent penetration and drug release are in the same range. This deviation is due to increasing drug diffusivity in the matrix by the solvent induced relaxation of the polymers. Zero order drug release ( $n = 1$ ) can be achieved when drug diffusion is rapid compared to the constant rate of solvent induced relaxation and swelling in the polymer. Use of this equation to analyze data of drug release from a porous system will lead to  $n < 0.5$ , since the combined mechanisms (diffusion through the matrix and partially through water-filled pores) will shift the release exponent toward smaller values.<sup>102</sup> A detailed mathematical modeling has been described and reviewed in the literature.<sup>103,104</sup> However, the model has been treated with caution, since the diffusional exponent can be markedly biased by polydispersity of the sample.<sup>101</sup> Sinclair<sup>103</sup> and Peppas<sup>105</sup> also demonstrated that  $n$  is strongly influenced by the precision of the release data, often suggesting erroneous conclusions about the release mechanism despite satisfactory data fitting by the model.

## 2.4 Nuclear magnetic resonance<sup>106</sup>

### 2.4.1 Introduction

The fundamental property of the atomic nucleus is the nuclear spin ( $I$ ), which has values of 0,  $\frac{1}{2}$ ,  $I$ , etc. in units of  $h/2\pi$  ( $\hbar$ ). The nuclear magnetic moment ( $\mu$ ) is directly proportional to the spin  $I$ , i.e.

$$\mu = \hbar\gamma I \quad (2.1)$$

where  $\gamma$ , the proportionally constant, is called the gyromagnetic ratio, which is constant for particular nucleus. A nucleus of spin  $I$  has  $2I+ 1$  possible orientations, which are given by the value of the magnetic quantum number  $m_I$ , which has values of  $-I, -I+1, \dots, I- 1$  and  $I$ ; i.e. for a nucleus of spin  $\frac{1}{2}$ ,  $m_I$ , has values of  $-\frac{1}{2}$  and  $\frac{1}{2}$ . Examples of the spin  $\frac{1}{2}$  nuclei are  $^1\text{H}$ ,  $^{13}\text{C}$  and  $^{29}\text{Si}$ .

The energy of interaction is proportional to the nuclear moment and the applied field. By using Eq. (2.1) one gets

$$E = \hbar I \gamma m_I B_0 \quad (2.2)$$

where  $B_0$  is the main magnetic field.<sup>106</sup>

The spin can flip spontaneously from one energy state to the other as the spin is in a large magnetic field. Such a flip is a relatively infrequent spontaneous event, but if energy that is equal to the differences in energy ( $\Delta E$ ) of the two nuclear spin orientations is applied more flipping will occur. The irradiation energy is in the RF range. The absorption of energy by the nuclear spins causes transitions from higher to lower energy levels as well as from the lower to the higher energy level. The energy absorbed by the spins induces a voltage that can be detected by a suitably tuned coil. This voltage, after being amplified, can be displayed as free induction decay (FID).

The energy required to induce spin flip and cause an NMR signal appearance is just the energy difference between the two nuclear orientations, and is dependent on the strength of the magnetic field  $B_0$  (Figure 2.4).

$$\Delta E = \hbar \gamma B_0 \quad (2.3)$$

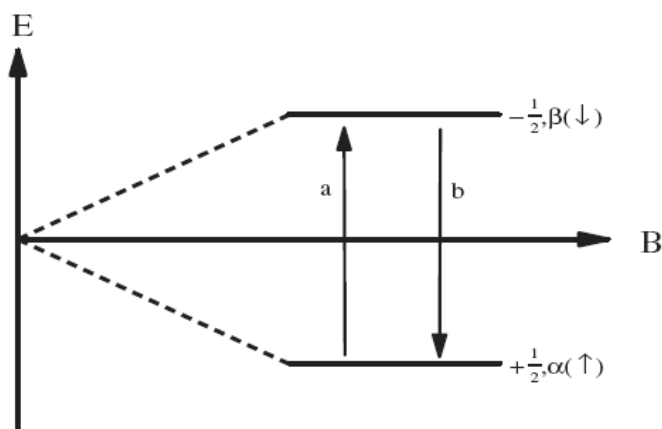


**Figure 2.4:** Energy levels and transitions for a nucleus ( $I = \frac{1}{2}$ ) in a magnetic field  $B$ .

### 2.4.2 Boltzmann distribution

The whole phenomenon of magnetic resonance depends on the difference in population between the two energy states,  $\alpha$  and  $\beta$ . The Boltzmann equation



$$\frac{N_{\beta}}{N_{\alpha}} = e^{-\Delta E/kT} = e^{-h\nu/kT}, \quad (2.4)$$

where  $k$  is the Boltzmann constant,  $T$  is the absolute temperature. From the equation one can calculate that at room temperature in an 11.4 T magnetic field, which corresponds to the 500 MHz proton frequency, the ratio has a value of 0.999919998, which corresponds to the situation where we would have, for every million spins, an excess of 40 spins in the lower energy state.

## 2.5 NMR of solids<sup>107</sup>

The main interactions involving a nucleus with a magnetic moment which may occur in the solid state are; (a) the Zeeman interactions with magnetic field, (b) the dipole-dipole interactions with other nuclei, (c) magnetic shielding by the surrounding electrons giving chemical shifts, (d) spin-spin coupling to other nuclei and (e) quadrupolar interactions which will be present for nuclei with spin  $> \frac{1}{2}$  only, and often dominate the spectra of these nuclei.

Conventional utilization of solution phase NMR data acquisition techniques on solid samples yields broad, featureless spectra. There are three main practical reasons which prevent the observation of high resolution NMR spectra in organic solids by normal Fourier Transform techniques.<sup>108</sup> The first reason is that normally the resonance lines are highly broadened by anisotropic dipole-dipole interactions leading to line widths in the kHz range or even more. The second reason is the phenomenon of the chemical shift anisotropy, which for powders leads to broad complex line shapes even when dipolar broadening is absent or eliminated. These anisotropic interactions are in principle also present in liquids, but fortunately are averaged to zero by the rapid Brownian motion of the molecules. Finally the third reason is that, solids show extremely long spin lattice relaxation times. Therefore, Fourier transform experiments require long pulse repetition times resulting in a reduced convenience of signal accumulation and thus in low sensitivity.

### 2.5.1 Line broadening by Dipole-Dipole interactions<sup>109</sup>

Dipole-dipole interaction is the direct magnetic coupling of two nuclei through space. This interaction may involve two nuclei of equivalent spin, or non equivalent spin, and is

depend upon the internuclear distance and dipolar coupling tensor. Additionally, the total interaction, labeled  $H_D$ , is the summation of all possible pair wise interactions (homo- and heteronuclear). The interaction is dependent on the magnitude of the magnetic moments which is reflected in the gyromagnetic ratio and the angle ( $\theta$ ) that the internuclear vector makes with  $B_0$ . Therefore, this interaction is significant for spin  $\frac{1}{2}$  nuclei with large magnetic moments such as  $^1\text{H}$ . Also, the interaction decreases rapidly with increasing internuclear distance ( $r$ ), which generally corresponds to contributions only from directly bound and nearest neighbor nuclei.

$$H_D^{IS} = \frac{\gamma_I \gamma_S \hbar^2}{r^3} \vec{I} \cdot \hat{D} \cdot \vec{S} \quad (2.5)$$

Equation (2.5) describes the dipole interaction for a pair of nonequivalent, isolated spins  $I$  and  $S$ . Since the dipole coupling tensor,  $D$ , contains a  $(1 - 3 \cos^2 \theta)$  term, this interaction is depend on the orientation of the molecule. In solution-phase studies where the molecules are rapidly tumbling, the  $(1 - 3 \cos^2 \theta)$  term is integrated over all angles of  $\theta$  and subsequently disappears. Within solid-state NMR, the molecules are fixed with respect to  $B_0$ , thus the  $(1 - 3 \cos^2 \theta)$  term does not approach zero. This leads to broad resonances within the spectra since dipole-dipole interactions typically range from 0 to  $10^5$  Hz in magnitude.

In the case of organic solids which are dominated by carbon and proton nuclei, the dipole-dipole interactions may be simplified. The carbon and proton nuclei may be perceived as dilute and abundant based upon their natural abundance, respectively. Homonuclear  $^{13}\text{C} - ^{13}\text{C}$  dipolar interactions essentially do not exist because of the low concentration of  $^{13}\text{C}$  nuclei. On the other hand,  $^1\text{H} - ^{13}\text{C}$  dipolar interactions contribute significantly to the broad resonances.

### 2.5.2 Chemical shift interactions

The chemical shift interaction ( $H_{CS}$ ) is the most sensitive interaction to changes in the immediate environment of the nucleus and provides the most diagnostic information in the measured spectrum. The external magnetic field induces magnetic moments due to circulation of electrons which are associated with an atom or a chemical bond and give rise to chemical shift contributions for nuclei in the molecule. These small perturbations upon the nucleus are reflected in a change in the magnetic field experienced by the

nucleus. Therefore, the field at the nucleus is not equal to the externally applied field and hence the difference is the nuclear shielding, or chemical shift interaction [Eq. 2.6].

$$H_{CS} = \gamma_I \hbar \vec{I} \cdot \hat{\sigma} \cdot \vec{B}_0 \quad (2.6)$$

In a powdered or amorphous sample each molecule or molecular group may be oriented in all possible directions and due to this we have a spread of chemical shifts resulting in a broad resonance line. The chemical shift contribution  $\sigma$  is again proportional to  $(1 - 3 \cos^2 \theta)$  term, a fact which is common to all the anisotropic interactions and is also proportional to the applied field, hence need for chemical shift reference material such as TMS.

Solution state NMR spectra yield average chemical shift values which are characteristic of the magnetic environment for a particular nucleus. The average signal is due to the isotropic motion of the molecule in solution. For solid-state NMR, the chemical shift value is also characteristic of the magnetic environment of a nucleus, but normally, the molecules are not free to move, although, shielding will be characteristic of the nucleus in a particular orientation of the molecule with respect to  $B_0$ . Therefore, a specific functional group oriented perpendicular to the magnetic field will give a sharp signal characteristic of this particular orientation, Figure 2.5. Analogously, if the functionality is oriented parallel to  $B_0$ , then a sharp signal characteristic of that particular orientation will be observed, Figure 2.5. For most polycrystalline pharmaceutical samples, a random distribution of all orientations of the molecule will exist. This distribution produces all possible orientations and is thus observed as a very broad NMR signal, Figure 2.5. The magnitude of the chemical shift anisotropy is typically between 0 to  $10^5$  Hz.

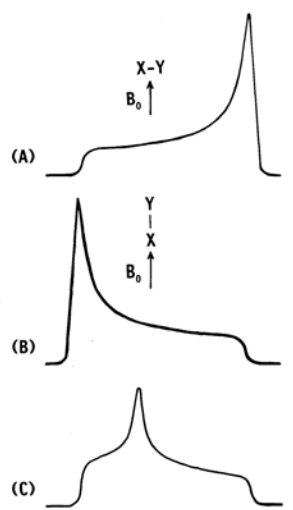


**Figure 2.5:** Schematic representation of the  $^{13}\text{C}$  NMR signal of a single crystal containing the functional group A-B, oriented (A) perpendicular and (B) parallel to the applied field and also depends on tensor values. The line shape (C) represents the NMR signal of a polycrystalline sample with a random distribution of orientations yielding the chemical shift anisotropy pattern displayed.

Two additional interactions experienced by the nucleus in the solid state are spin-spin couplings to other nuclei and quadrupolar interactions, which involve nuclei of spin greater than  $\frac{1}{2}$ . Spin-spin ( $H_{SC}$ ), or  $J$  coupling, originates from indirect coupling between two spins by means of their electronic surroundings and are several orders of magnitude smaller ( $0 - 10^4$  Hz) than dipole interactions. Since organic/pharmaceutical compounds are primarily hydrocarbons, quadrupolar interactions ( $0 - 10^9$  Hz) do not interfere with the spectra.

### 2.5.3 Long spin lattice relaxation times

After a perturbation the nuclear magnetization of a sample returns to equilibrium exponentially within a certain time characterized by a time constant  $T_1$ , the spin lattice relaxation time. Therefore, in order to measure the full nuclear magnetization, that means maximum signal strength, in repetitive experiments it is necessary to wait approximately  $5 \cdot T_1$  between single measurements. The success of Fourier transform technique lies in the measurement of less sensitive nuclei, where within a given time the NMR signal is very often produced, measured and accumulated to result in a great signal-to-noise ratio improvement. Unfortunately, long  $T_1$  times are more typical in solids due to the reduced

molecular motions, requiring in ordinary FT experiments repetition times of minutes or even longer and therefore only small number of accumulation.

#### 2.5.4 Highly resolved solid state NMR spectra

The three principal reasons for broad, featureless spectra, of solids are very different in origin and therefore one simple manipulation cannot help in the solution of the problem. High-resolution NMR in solids came of age with the development of high power decoupling,<sup>110</sup> cross polarization (CP)<sup>111</sup> and Magic angle spinning (MAS)<sup>112</sup>.

##### High power decoupling

For the study of dilute nuclei such as  $^{13}\text{C}$  the elimination of dipolar broadening is relatively simple, since the local field must arise from the abundant nuclei, for example from the protons in organic solids. The hetero nuclear interaction can be removed by decoupling the unobserved protons from the observed  $^{13}\text{C}$  spins. The concept of decoupling is similar to the solution phase NMR, but needs to expand for solid-state studies. In solution-phase studies, the decoupling eliminates the scalar spin-spin coupling, not the dipole-dipole interactions (this averages out to zero due to isotropic motions of the molecules). Irradiation of the sample at the resonant frequency of the nucleus to be decoupled causes the  $z$  component of the spins to flip rapidly compared to the interaction one wishes to eliminate (Figure 2.6)

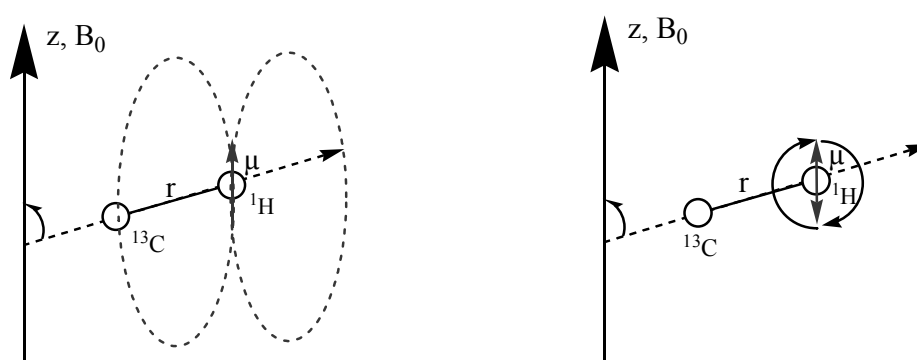


**Figure 2.6:** Local magnetic field at  $^{13}\text{C}$  spin produced by a nuclear magnetic dipole moment of proton spin at a distance  $r$  (left). The effect of high power decoupling (right). Due to rapid rotation of proton spin the time averaged local field at the  $^{13}\text{C}$  spin vanishes.

Scalar interactions usually require 10 W of decoupling power or less. In organic and pharmaceutical solids work, decoupling is used primarily to remove the heteronuclear dipolar interactions between protons and carbons. The magnitude of the dipolar interactions (~50 KHz) usually requires decoupling fields of 100 W and subsequently removes both scalar and dipole interactions. Applying dipolar decoupling, leads to considerable sharpening of the solid state resonances and therewith also an improvement of signal-to-noise ratios. The residual line widths are then affected by CSA interactions and homonuclear interactions between the rare spins themselves. Homonuclear dipolar interaction cannot be eliminated by high power decoupling.

## Magic Angle Spinning (MAS)

Molecules in solid state are in fixed orientations with respect to the magnetic field. This produces chemical shift anisotropic powder patterns for each carbon atom since all orientations are possible. It was shown as early as 1958, that rapid sample rotation of solids narrowed dipolar broadened signals.<sup>112</sup> A number of years later, it was recognized that spinning could remove broadening caused by CSA yet retain the isotropic chemical shift.<sup>113</sup> The concept of magic-angle spinning arises from the understanding of the shielding constant,  $\sigma$ . This constant is a tensor quantity and, thus, can be related to three principal axes where  $\sigma_i$  is the shielding at the nucleus when  $B_0$  aligns along the  $i^{\text{th}}$  principal axis, and  $\theta_i$  is the angle this axis makes with  $B_0$ . Earlier it has been shown that the dipolar coupling tensor  $D$  and chemical shift contribution  $\sigma$  is proportional to  $(1 - 3 \cos^2 \theta)$  term.

$$\sigma_{zz} = \sum_{i=1}^3 \sigma_i \cos^2 \theta_i \quad (2.7)$$

Under conditions of mechanical spinning, this relationship becomes time dependent and a  $(3 \cos^2 \theta - 1)$  term arises. By spinning the sample at the magic angle of  $54.7^\circ$ , this term becomes zero and thus removes the spectral broadening due to CSA, providing that the sample rotation (kHz) is greater than the magnitude of the CSA (kHz).

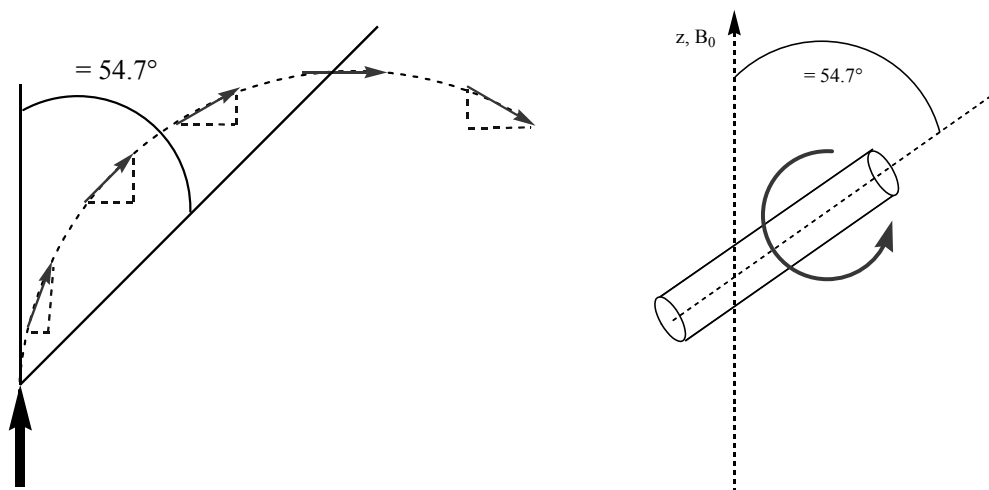


**Figure 2.7:** (left) Magnetic field line of a magnetic dipole showing positive and negative  $z$ -components. At  $\theta = 54.7^\circ$  the  $z$ -component is zero. (Right) Magic angle spinning of a specimen in a field of a solenoid under the magic angle of  $54.7^\circ$ .

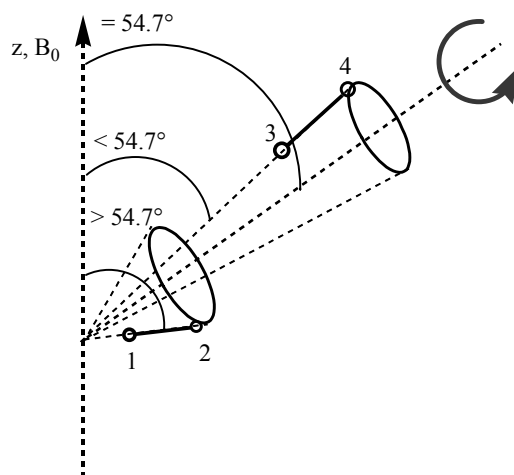


**Figure 2.8:** Effect of magic angle spinning: By rotation about the magic angle the time averaged value of all binding vectors becomes  $54.7^\circ$ , e.g.  $\langle \theta_{1,2} \rangle = \langle \theta_{3,4} \rangle = 54.7^\circ$ , in spite of  $\langle \theta_{1,2} \rangle \neq \langle \theta_{3,4} \rangle$ .

CSA may range from 0 to 20 kHz, so our spin rates must exceed this value or spinning side bands are observed. To eliminate chemical shift anisotropy interactions for  $^{13}\text{C}$  in organic/pharmaceutical molecules, spinning rates of some kHz are necessary. Since the chemical shift is field dependent the required spinning rates are proportional to  $B_0$ . From the above it is clear that dipolar interaction between the rare spins themselves are also averaged to zero and one obtains finally line widths which are comparable to those in liquid samples. The final resolution obtainable with MAS depends highly on the precision which is possible for the magic angle adjustment. Especially for very large CSA, very accurate angle setting is necessary, otherwise powder pattern line shapes will result. This is most critical with aromatic or carbonyl type resonances. In case of homonuclear coupling of protons, where high power decoupling fails, in principle MAS also narrows the resonance lines. However, since these line widths are some tens of kHz, extraordinary high spinning rates are required, which are possible to do today. Unfortunately, there is an inherent lack of sensitivity in the general NMR experiment because of the nearly equivalent population of the two spin states for spin  $\frac{1}{2}$  nuclei. In addition, the sensitivity of the experiment is decreased with organic/pharmaceutical compounds since they are composed primarily of carbon atoms where the  $^{13}\text{C}$  observable nuclei have a natural abundance of only 1%. The long relaxation times of specific carbon nuclei also pose a problem since quick, repetitive pulsing cannot occur. The technique of



cross-polarization provides a means of both signal enhancement and reduction of long relaxation times.

### **Cross-polarization**

In liquid-state experiments that measure  $^{13}\text{C}$  or  $^{15}\text{N}$  chemical shifts, the magnetization is often initially transferred from neighboring protons and then transferred back to the protons for detection to exploit the higher sensitivity.<sup>114</sup> In addition, the relaxation is usually more rapid for protons, and the acquisition time is shorter. It is difficult to obtain high-resolution solid-state  $^1\text{H}$  NMR spectra due to the dominant homonuclear proton-proton dipolar interactions which leads to broad proton resonances, the majority of solid-state NMR experiments detect the magnetization of other nuclei such as  $^{13}\text{C}$  and  $^{15}\text{N}$ . The drawbacks of directly detecting low  $\gamma$  nuclei such as  $^{13}\text{C}$  and  $^{15}\text{N}$  are low isotopic abundances, low spin polarization, and low signal intensity. These drawbacks can be circumvented by a solid-state NMR technique that combines both the high polarization and short relaxation time and the enhancement of the signals from rare nuclei involve the transfer of polarization from abundant nuclei by using cross polarization. The rare spin system is classified as  $^{13}\text{C}$  nuclei and the abundant system as  $^1\text{H}$  spins for pharmaceutical solids. The process of CP occurs through the tendency of the magnetization to flow from highly polarized  $^1\text{H}$  to less polarized  $^{13}\text{C}$  when they are brought into contact, similar to heat flow from a hot object to a cold object when the two are in thermal contact. For homonuclear spins, the magnetization can be exchanged through mutual energy conserving spin flips and for heteronuclear spins, these spin flips are not energy conserving at high magnetic fields. The exchange of magnetization must be driven externally by the application of RF fields.

Figure 2.9 describes the cross-polarization pulse sequence and the behavior of the  $^1\text{H}$  and  $^{13}\text{C}$  spin magnetization during the pulse sequence in terms of the rotating frame of reference.

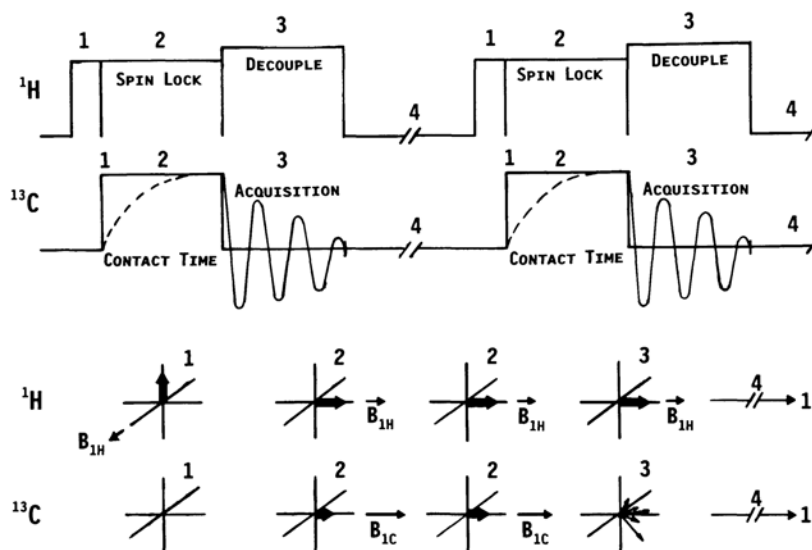


**Figure 2.9:** The top diagram represents the pulse sequence for the cross-polarization experiment, whereas the bottom describes the behavior of the  $^1\text{H}$  and  $^{13}\text{C}$  spin magnetization during the sequence. The steps in the two diagrams correspond to each other and are fully explained in the text.<sup>107</sup>

Step 1 of the sequence involves rotation of the proton magnetization onto the  $y'$  axis by application of a  $90^\circ$  pulse (rotating frame magnetic field  $B_{1H}$ ). Subsequent spin-locking occurs along  $y'$  by an on resonance pulse along  $y'$  for a specific period of time,  $t$ . At this point, a high degree of proton polarization occurs along  $B_{1H}$  which will decay with a specific time referred to as  $T_{1\rho H}$ . As the proton spins are locked along  $y'$ , an on resonance pulse,  $B_{1C}$ , is applied to the  $^{13}\text{C}$  spins. The  $^{13}\text{C}$  spins are also locked along the  $y'$  (step 2). By correctly choosing the magnitude of the spin-locking fields  $B_{1H}$  and  $B_{1C}$ , the Hartmann-Hahn<sup>115</sup> condition (Eq. 2.8) will be satisfied and transfer of magnetization will occur from the  $^1\text{H}$  spin reservoir to the  $^{13}\text{C}$  spin reservoir.

$$\gamma_{^1\text{H}} B_{1H} = \gamma_{^{13}\text{C}} B_{1C} \quad (2.8)$$

Once this quantity is obtained by the correct spin-locking fields, the dilute  $^{13}\text{C}$  spins will be more intense. In the end, a maximum magnetization enhancement equal to the ratio of the gyromagnetic ratios may be achieved ( $\gamma_H/\gamma_C$ ). Once the carbon magnetization has built up during this contact time ( $t$ ),  $B_{1C}$  is switched off and the carbon free induction decay is recorded (step 3). During this data acquisition period, the proton field is maintained for heteronuclear decoupling of the  $^1\text{H}$ - $^{13}\text{C}$  dipolar interactions. Step 4

involves a standard delay period in which no pulses occur and the two spin systems are allowed to relax back to their equilibrium states.

The entire CP pulse sequence provides two advantages for the solid state NMR spectroscopist. Significant enhancement of the rare spin magnetization and reduction of the delay time between successive pulse sequence since the rare spin system takes on the relaxation character of the abundant spin system. Signal enhancement for less sensitive nuclei is immediately apparent from the CP process. The rare spin system signal does not depend on the recycle time in step 4 (re-growth of carbon magnetization), but on the transfer process in step 2 and the relaxation behavior of the proton spin system in step 4. Since the spin lattice relaxation time of the proton system is typically much shorter than the carbon system, the delay time is much shorter. This corresponds to a greater number of scans per unit time yielding better S/N.

Throughout the CP pulse sequence, a number of competing relaxation processes are occurring simultaneously. The recognition and understanding of these relaxation processes are critical in order to apply CP pulse sequence for quantitative solid-state NMR data acquisition or ascertaining molecular motions occurring in the solid state.

## Relaxation

The spin-lattice relaxation time,  $T_1$ , is defined as the amount of time for the net magnetization ( $M_z$ ) to return to its equilibrium state ( $M_0$ ) after a spin transition is induced by a radiofrequency pulse. The process of transferring spin energy to other modes of energy may be classified as relaxation mechanism. For  $T_1$  in solids, all of the following mechanisms may contribute: dipole-dipole ( $T_{1DD}$ ), spin rotation ( $T_{1SR}$ ), quadrupolar ( $T_{1Q}$ ), scalar ( $T_{1SC}$ ) and chemical shift anisotropy ( $T_{1CSA}$ ). To understand cross-polarization process, two other rate processes must be defined: (a) spin-lattice relaxation in rotating frame ( $T_{1\rho}$ ) and (b) the cross-polarization time ( $T_{CH}$ ). The spin-lattice relaxation in the rotating frame characterizes the decay of magnetization in a field  $B_I$  which is normally much smaller than the externally applied field  $B_0$ . In step 1 and 2 of the CP sequence, the carbon and proton spin systems are locked by the application of the fields  $B_{IH}$  and  $B_{IC}$  and each system decays with its characteristic time. Figure 2.10 represents a thermodynamic model for the kinetic process during CP. During contact between the two spin systems, magnetization is transferred at the rate  $T_{CH}$ . Since

competing processes are occurring, the following conditions must be met to obtain a spectrum by CP:  $T_{1C} > T_{1H} \geq T_{1\rho H} > \text{CP time} > T_{CH}$ .

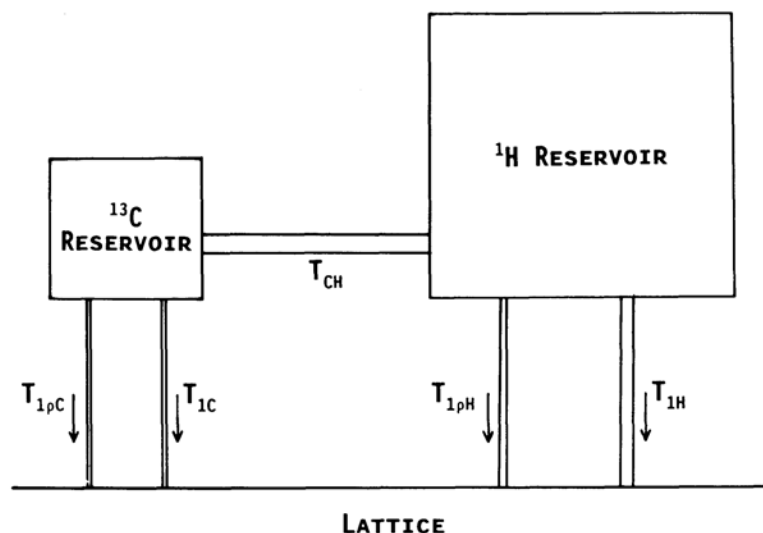


**Figure 2.10:** Thermodynamic model of the cross-polarization sequence and representation of the competing relaxation processes.

A combination of high-power CW decoupling, cross-polarization and high-speed MAS, can rapidly yield one dimensional solid state spectra of compounds containing spin  $\frac{1}{2}$  nuclei of low natural abundance such as  $^{13}\text{C}$ ,  $^{15}\text{N}$  and  $^{29}\text{Si}$ , with sufficient spectral sensitivity and resolution. However as in liquid-state NMR, more advanced multipulse and multidimensional techniques can be utilized to perform more detailed analysis of the structure and dynamics of the sample.

### 2.5.5 2D NMR spectroscopy

Although 2D NMR spectroscopy has many different applications, the basic form of all these experiments is essentially the same.<sup>116</sup> The pulse sequence of a 2D NMR experiment may be divided into the following blocks:<sup>117</sup>

Preparation-evolution ( $t_1$ )-mixing-detection ( $t_2$ )

The detection period corresponds exactly to the one for 1D NMR spectroscopy. The time  $t_2$  provides (after Fourier transformation) the  $\omega_2$  frequency axis of a 2D NMR spectrum. The trick of 2D NMR spectroscopy is that a second time variable, the evolution time  $t_1$ , is

introduced. The evolution time  $t_1$  is made stepwise longer, i.e., incremented, in analogy to the detection time  $t_2$ . For each  $t_1$  increment a separate FID is detected in  $t_2$ . Thus a signal is obtained which is a function of two time variables,  $t_1$  and  $t_2$ . A series of  $\omega_2$  spectra is then obtained upon Fourier transformation of each of the FIDs. They differ from one another in the intensities and/or phases of the individual signals, according to the different  $t_1$  increments. A second Fourier transformation over  $t_1$ , perpendicular to the  $\omega_2$  dimension, results in a spectrum as a function of two frequencies ( $\omega_2$  horizontal,  $\omega_1$  vertical).

### 2.5.6 2D FSLG HETCOR NMR

Heteronuclear correlation (HETCOR) spectroscopy is an important tool for resolution enhancement in multidimensional NMR spectroscopy. For solids, line narrowing in the proton dimension is achieved by suppressing the strong homonuclear dipolar interactions between the abundant protons. Line narrowing can be achieved by manipulating spin interactions either on the space part or on the spin part. Both manipulation techniques correspond to rotations, MAS in real space and pulses in spin space.<sup>118</sup> Pulsed averaging is much more flexible than a simple mechanical rotation because amplitudes, phases and frequencies can be changed and with them the effective rotation angle and direction. While MAS only reduces spin interactions, pulsed modulations can be applied to generate a variety of effective spin interaction Hamiltonian from them. In the Lee-Goldburg-type sequences the averaging is performed continuously using an appropriate offset frequency to adjust the effective rotation axis at the magic angle in spin space. It was shown by Lee and Goldburg<sup>119</sup> that the application of RF field off-resonance according to  $\Delta LG/\omega_1 = \frac{1}{2}\sqrt{2}$  produces an effective field in the rotating frame inclined at the magic angle  $\theta_m = \tan^{-1}(\sqrt{2})$  to the static field  $B_0$ . A  $360^\circ$  pulse at this offset then causes the spin magnetization to precess completely by one turn around this effective field. The average homonuclear dipolar coupling between the spins over this period is then zero if the effective field is at the magic angle. The effects of homonuclear dipolar coupling are removed from the spectrum under this scheme, providing the averaging of the dipolar coupling take place at a rate which is significantly faster than the strength of the dipolar coupling in frequency units. The rate of averaging process is simply the nutation frequency of the spin magnetization about the effective field, which is the effective field strength in frequency units, i.e.  $\sqrt{(\omega_1^2 + \Delta\omega^2)}$  where  $\omega_1$  is the RF

amplitude of the  $360^\circ$  pulses and  $\Delta\omega$  is the offset of the pulse frequency from resonance, so providing reasonable high-power pulses are used, this condition is easily met. The  $360^\circ$  pulses are alternated in phase to reduce errors which occur from the fact that it is not possible to set the off-resonance condition required exactly for all parts of the sample. When the LG irradiation is both frequency and phase switched (FSLG)<sup>120</sup> after successive periods  $\tau = (2\pi/\omega_1)\sqrt{2/3}$ , corresponding with the time to complete  $2\pi$  rotation around the tilted axis, the efficiency of decoupling is significantly improved. The details of pulse sequence and coherence transfer pathways with phase cycles are given in the next chapter.

## 2.6 Spray Drying: A theoretical investigation<sup>121</sup>

### Introduction<sup>122,123</sup>

Spray drying is the transformation of feed from a fluid state into a dried particulate form by spraying the feed into a hot drying medium. The central element of a spray dryer is the spray dry chamber. In the chamber, atomized liquid is brought into contact with hot gas resulting in the evaporation of the solvent contained in the droplets in a matter of a few seconds. The structural stability of the droplet and the hydrodynamic effects during the drying process play important roles in controlling the morphology of the resulting particles. The size of the sol in the droplet, droplet size, viscosity of droplet, drying temperature, gas flow rate and addition of surfactant are all crucial parameters that affect the morphology of particles. Pauchard and Couder<sup>124</sup> proposed that tiny concentration of suspended particles can dramatically alter the behavior of a drying droplet. Rather than simply shrinking isotropically, drying colloidal droplet can undergo striking mechanical instabilities, such as fracture and buckling. Tsapis et al.<sup>125</sup> suggests that forces between particles in a drying droplet play an important role in determining the onset of buckling. They hypothesize that buckling occurs when the capillary forces drive the deformation and flow of a shell overcome the electrostatic forces stabilizing the particle aggregation. Therefore, at a critical value of the capillary forces, the particles undergo a sol-gel transition, transforming the shell from a viscous fluid to an elastic solid, and triggering the onset of buckling.

The main concern with spray drying is the lack of ability to predict or control particle morphology. Under some conditions solid particles are formed and under other conditions, however, hollow or porous particles are formed.<sup>122</sup> The nature of the precursor is the most important factor that determines powder morphology. Solvent evaporation up to the onset of solute nucleation is another critical step in determining powder morphology. Different models have been proposed to predict the onset of solute nucleation during spray drying process. Every model has been built on some assumptions such as; (a) only laminar flow is considered, (b) free convection is not considered, (c) Kelvin effect is ignored due to dry solute particle size is much larger than  $0.1\ \mu\text{m}$ , the size below which Kelvin effect is significant,<sup>126</sup> (d) droplet coagulation, diffusion, thermophoresis and diffusiophoresis are ignored.

Figure 2.12 shows the scheme used in the preparation of micrometer-sized particles using spray drying method. The precursor is atomized to form spherical droplets with a diameter  $d_d$ , which contain nanometer-sized solid particles (sol) with a diameter  $d_p$ . Droplets with diameters in the range between 1 and  $100\ \mu\text{m}$  are usually produced by an atomizer. The droplets are carried into a drying chamber by a carrier gas for drying. The dispersion water is evaporated inside the chamber, resulting in micrometer-sized nanostructured particles.

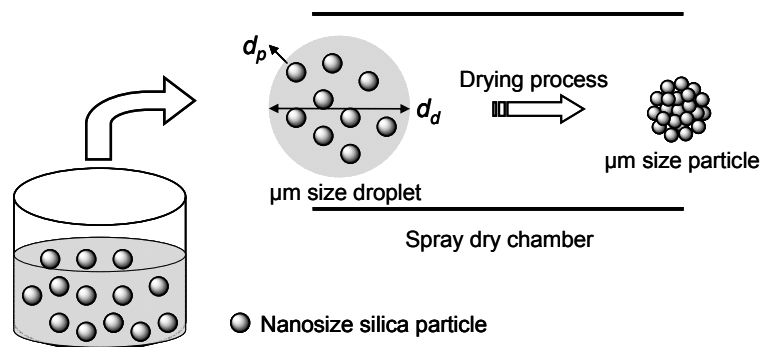


**Figure 2.12:** Schematic of the preparation of micrometer-sized nanostructured particle by spray drying.

Parameters that control the formation of microsized particle shape and morphology in a spray drying method can be considered as follows:

(1) The properties of the precursors, i.e., the viscosity of sol, the diameter of the colloidal nanoparticles ( $d_p$ ) and surface tension at the droplet–carrier gas interface.

(2) The conditions for particle formation, i.e., the droplet diameter ( $d_d$ ), the flow rate, which determines the velocity  $V_d$  (cm/s) of the droplets inside the chamber and the temperature of the chamber ( $T$ ), which can determine the evaporation rate of the droplets.

(3) Mass fraction of small particles in the initial droplet ( $\varphi$ ).

Toroid morphology of the produced particles can be considered to be the result of an initial deformation of the droplet, which, changes its initial spherical shape to a “mushroom-like” shape or a “double convex disc” form.

This is possible due to the loss of structural stability of a droplet in a two-phase flow field because of additional macro- and micro-hydrodynamic effects during the drying process.

### Structural stability of droplets

The structural stability of droplets can be explained by Bond's number  $\beta$ , the ratio of the inertial force and surface tension effects. The Bond number is given by

$$\beta = \frac{\Delta\rho a d_d^2}{\sigma}$$

where  $\Delta\rho$  is the difference in the densities of the droplet and the surrounding fluid,  $d_d$  the droplet size,  $\sigma$  the interfacial/surface tension force and  $a$  the acceleration.<sup>127</sup> The acceleration,  $a$  is related to the mass of the particle, particle velocity, particle diameter, gas velocity, gas viscosity and external force field. A particle can lose its stability due to aerodynamical drag by its acceleration. The droplet is nearly spherical at values of  $\beta \rightarrow 0$  and becomes flat when the values of  $\beta$  increase. The values of  $\beta$  can be set experimentally by varying the densities of the two-phase droplets or the size of the droplets or by adding appropriate surfactants. It is likely that inertial effects are able to drive the deformation of a droplet and that interfacial/surface tensions forces will maintain them in a spherical shape. The destabilization of the initial shape of a droplet could be achieved by (i) increasing the droplet size, (ii) increasing the droplet density and (iii) decreasing the surface tension  $\sigma$  of the droplet. Reduction of the  $\sigma$  value by introducing a surfactant into the water will result in a less stable droplet. For droplets in the presence of surfactants, values of  $\beta > 1$  are accessible and a “mushroom-like” form or “double convex disc” form can be obtained (Figure 2.13). Detailed formulas for the calculation of shape in all cases are available.<sup>128</sup>



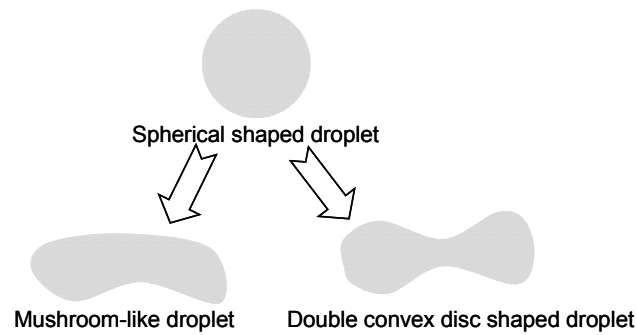


**Figure 2.13:** Deformation of an unstable droplet.

### Hydrodynamic Effects

Hydrodynamic (internal and external with respect to the droplet) effects also play an important role in controlling particle morphology. The carrier gas velocity and the drying temperature are the principal quantities affecting this, which influence the final shape and structure of the particle. An increase in airflow velocity in the reactor causes the destabilization of the droplet shape as shown in Figure 2.14. Reduction of the residence time of the droplet in the reactor due to an increase in droplet velocity should be compensated by increasing the air temperature needed to give a completely dry particle.

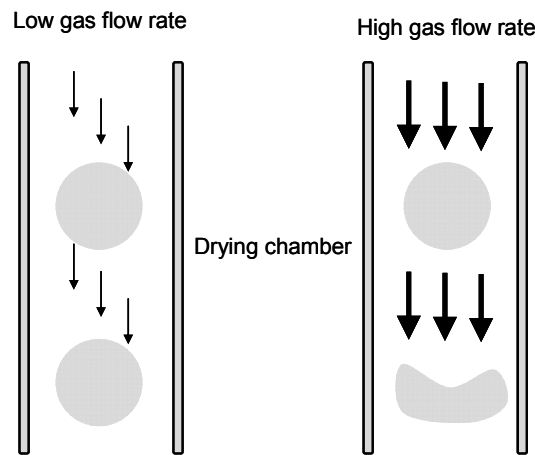


**Figure 2.14:** The effect of flow rate on the stability of droplets.

When a small amount of water evaporates, a strong flux of heat is transmitted from the surface of the droplet into the gas stream. Local temperature gradients are created on the droplet surface (Figure 2.15). This causes two types of effects - the thermophoretic displacement of the sol toward the surface of the droplet and specific microcirculations inside a droplet, near the edge, due to surface tension gradient. The sol particles move

toward the peripheral regions of the droplet, and, as a result, the inertial effect is enhanced, leading to a stronger deformation of the droplet toward the toroid shape of the final particle.<sup>129</sup>

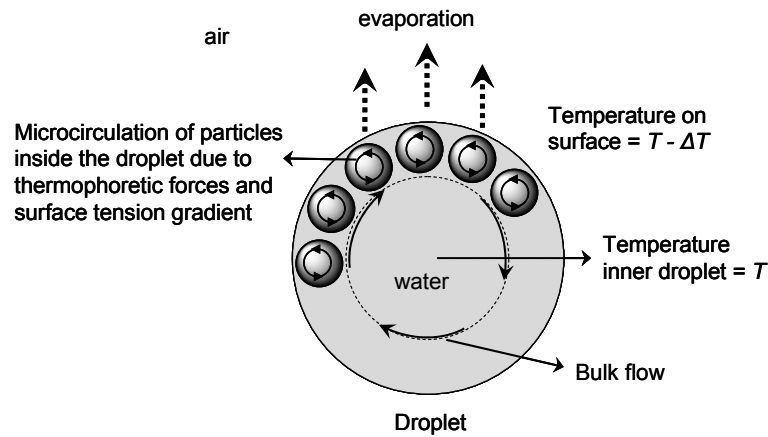


**Figure 2.15:** Hydrodynamic effects inside the droplet; temperature gradient at the surface creates thermophoretic forces that move particles towards the interfaces.

Surface tension gradients cause a hydrodynamic effect in the region near a droplet surface. This effect is enhanced in the presence of an active surfactant adsorbed as a monolayer on the liquid–gas interface. The surface tension gradient leads to induced motion tangential to the surface and away from the point of local cooling due to evaporation. Thermophoresis and microcirculation inside a droplet lead to the reorganization of sol particles.

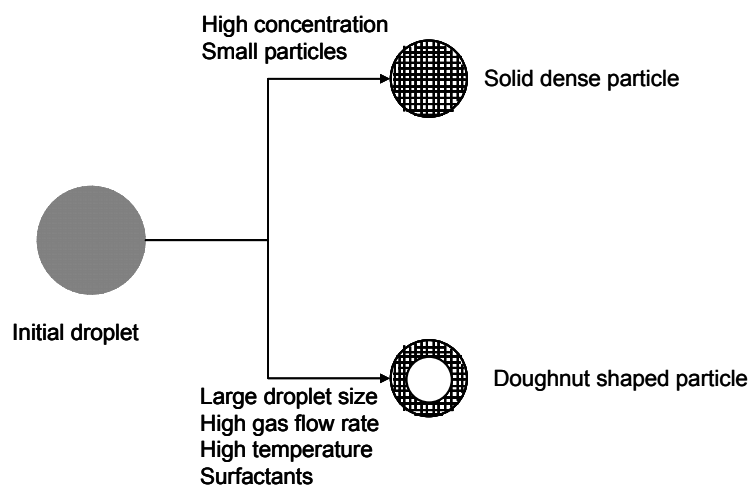


**Figure 2.16:** Morphology changes of particles prepared by spray drying.

Evaporation of the atomized droplets during spray drying leads to high solute supersaturation at the receding vapor/liquid interface. A fast drying rate, where the time for the liquid to evaporate is much less than the time required homogenizing the droplet, is one of the prerequisites to form hollow particles with a thin shell thickness.<sup>130</sup>

### 3. Methods and Materials

#### 3.1 Silica precursors

A basic requirement for successful molecular imprinting is the selection of suitable functional silane monomers that can create the molecular site by interacting in noncovalent fashion with the drug molecules. By careful tailoring of specific functional T monomers and Q monomers to a particular drug, desired end properties can be achieved for hybrid materials. The design stage considers the structure and features of drug molecules including the size, polarity, hydrophobicity and acidity for the selection of organically functionalized T monomers.

**Table 3.1:** Silica precursors employed for the hybrid gel preparations.

<p><i>Tetraethoxysilane (TEOS)</i></p>	<p><i>Methyltriethoxysilane (MTS)</i></p>
<p><i>Ethyltriethoxysilane (ETS)</i></p>	<p><i>n-Propyltriethoxysilane (PTS)</i></p>
<p><i>Acetoxypropyltrimethoxysilane (ATS)</i></p>	<p><i>Benzyltriethoxysilane (BTS)</i></p>
<p><i>Phenyltriethoxysilane (PhTS)</i></p>	<p><i>Diphenyldiethoxysilane (DPhDS)</i></p>

Different silica precursors were employed for the synthesis of hybrid gels. This includes Q monomer and a variety of T monomers. In this study, different alkyl substituted

(hydrophobic as well as hydrophilic) and aromatic substituted monomers were used. The detailed lists with structures are given in Table 3.1. All the chemicals were purchased from ABCR GmbH & Co. KG (Karlsruhe, Germany) and were used as received.

### 3.2 Model Drugs and their physicochemical characteristics

Propranolol Hydrochloride (PP, racemic mixture) was purchased from Sigma-Aldrich Chemie GmbH (Steinheim, Germany) and was used as received. Persantin (PS) was used as obtained from Boehringer Ingelheim Pharma GmbH & Co. KG Company.

#### 3.2.1 Persantin

Persantin, 2-[[3-[bis(2-hydroxyethyl)amino]-5,10-bis(1-piperidyl)-2,4,7,9-tetraza-bicyclo[4.4.0]deca-2,4,7,9,11-pentaen-8-yl]-(2-hydroxyethyl)amino]ethanol, is a yellow crystalline powder, with molecular weight of 504.6 g/mol. It is a coronary vasodilator and is also used to prevent platelet aggregation after heart valve disease. It is monobasic with a  $pK_a$  value of 6.4.<sup>104</sup> Persantin is sparingly soluble in pure water, but readily soluble in organic solvents like chloroform, ethanol and acetone. The physicochemical properties of the drug have been summarized in Table 3.2 and the structure is given in Figure 3.1.

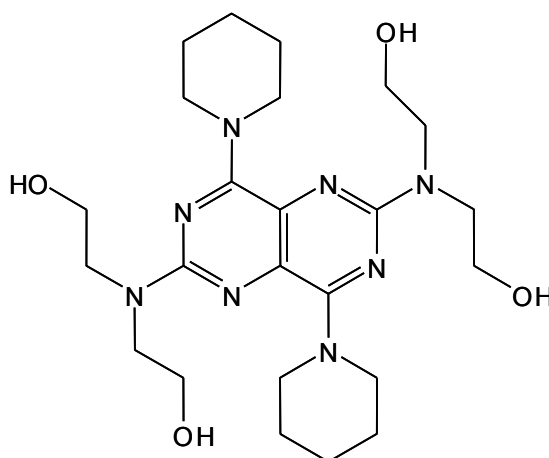


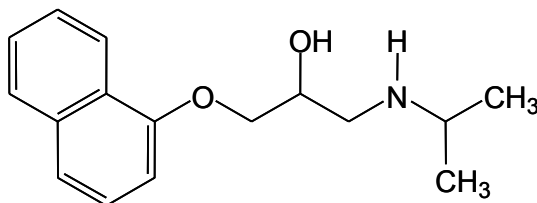
*Figure 3.1: Structure of Persantin.*

**Table 3.2:** Physicochemical properties of model drug Persantin

<i>Molecular Weight</i>	504.6 g/mol
<i>Chemical formula</i>	$C_{24}H_{40}N_8O_4$
<i>Melting point</i>	435-441 K
<i>pK<sub>a</sub></i>	6.4
<i>UV/VIS absorption in HCl (0.1 M), Max.</i>	400 nm, 283 nm, 237 nm
<i>UV/VIS absorption in HCl (0.1 %), Max.</i>	402 nm
<i>Solubility</i>	0.05 mg/mL in water (310 K)
	53.0 mg/mL in HCl (0.1 M, at 310 K)
	> 100 mg/mL in chloroform

### 3.2.2 Propranolol

Propranolol, DL-1-(Isopropylamino)-3-(1-naphthoxy)-2-propanol hydrochloride, is a colourless crystalline powder with molecular weight of 295.8 g/mol. Propranolol Hydrochloride is a beta-adrenergic antagonist (beta-blocker) used extensively in the treatment of cardiovascular disorders such as hypertension, cardiac arrhythmias and angina pectoris. It is weakly basic with a pK<sub>a</sub> value of 9.2<sup>131</sup> and has a nearly pH-independent solubility over a physiological pH-range (1-7). Propranolol Hydrochloride is soluble in water and ethanol. The physical properties of the PP have been summarized in Table 3.3 and the structure is given in Figure 3.2.

**Figure 3.2:** Structure of Propranolol

**Table 3.3:** Physicochemical properties of model drug Propranolol Hydrochloride

<i>Molecular Weight</i>	<i>295.8 g/mol</i>
<i>Chemical formula</i>	<i>C<sub>16</sub>H<sub>21</sub>NO<sub>2</sub>.HCl</i>
<i>Melting point</i>	<i>436-439 K</i>
<i>pK<sub>a</sub></i>	<i>9.2</i>
<i>UV/VIS absorption in water, Max.</i>	<i>289 nm</i>
<i>Solubility</i>	<i>50 g/l in water (at 298 K)</i>

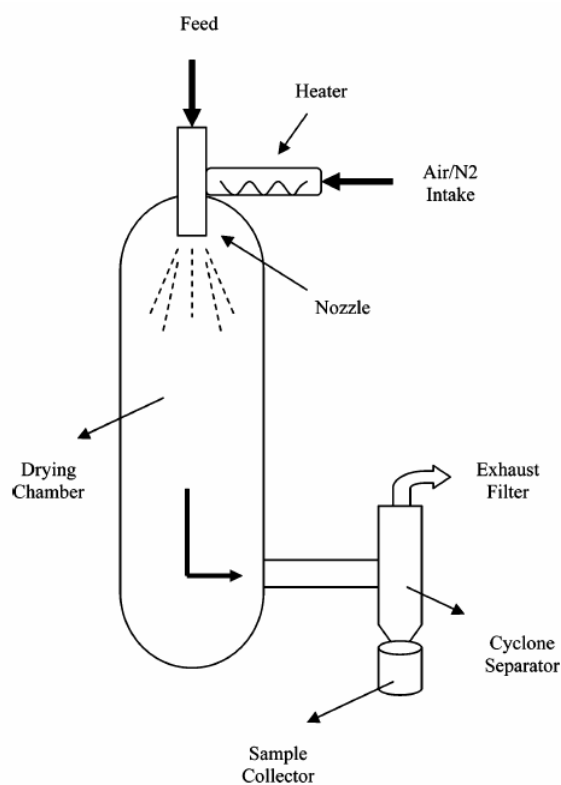
### 3.3 Preparation of Hybrid silica gels

#### 3.3.1 Evaporation Induced Self Assembled (EISA) gels

Silica sols were prepared at room temperature by acid hydrolysis of the monomer precursors. For the preparation of hybrid gels, both Q and T monomers were hydrolyzed in a water/ethanol/drug mixture by acid catalysis. The synthesis parameters like Q/T ratio, composition, drug loading and pH were adjusted before placing for stirring in a closed vessel. After that the silica sol was cast into an open vessel and kept at 323 K for self assembly and gelation. The polymerized silica gels were dried at 323 K for constant weight. The drug concentration in the EISA gels were calculated by assuming that the entire drug dissolved in the silica sol was incorporated into the final gel.

### 3.3.2 Spray dried (SD) gels

The hydrolyzed silica sol was spray dried with a mini spray dryer (B-290, Büchi Labortechnik AG, Switzerland). During the spray drying process, the silica sol was introduced through a nozzle to a hot drying medium ( $N_2$ ) in a chamber (Scheme 3.1). When the droplets of the silica sol come into contact with the hot gas, evaporation takes place from the vapour film. The spray dried particles exiting the drying chamber are passed into a cyclone separator, where the gas is exhausted after filtering and the dried particles are collected. Spray drying process parameters are given in Table 3.4. The drug concentration in the spray dried gels was calculated by assuming that the entire drug dissolved in the silica sol was incorporated into the final spray dried gel.



**Scheme 3.1:** Schematic diagram of the Büchi B-290 Mini spray dryer.



**Table 3.4:** *Spray drying process parameters.*

<i>Parameters</i>	<i>Values</i>
<i>Inlet air temperature</i>	<i>393 K</i>
<i>Outlet air temperature</i>	<i>338 K</i>
<i>Pump</i>	<i>20 – 30 %</i>
<i>Aspirator capacity</i>	<i>90 – 95 %</i>
<i>Spray flow rate</i>	<i>5.0 ml/min</i>
<i>Nozzle size</i>	<i>0.77 mm</i>

### 3.3.3 Gel notations

The hybrid gels are labeled according to their synthetic conditions. Gel label include the number, second precursor name, ratio between TEOS and second precursor and pH. Additional parameters are given at the end of the name. For example, MTS<sub>400</sub>(3:1,2.5) represents MTS gel with TEOS:MTS ratio 3:1 and a synthesis pH of 2.5 with gel number 400. In figures and tables, the complete name is emphasized whereas in text only gel number is used. Washed gels are marked with “w”. All the drug extraction has been carried out on dissolution medium for 24 h. Samples treated at higher temperatures are marked with respective temperatures. For example, “Gel 189 @ 1173 K”, represents Gel 189 treated at 1173 K. All SS NMR measurements are carried out at room temperature.

## 3.4 Characterization techniques

Different characterization techniques such as Dissolution Rate Test (DRT), N<sub>2</sub> sorption, Scanning Electron Microscopy (SEM) and solid state Nuclear Magnetic Resonance (NMR) spectroscopy has been employed to study the properties of the organic-inorganic hybrid gels.

### 3.4.1 Drug release studies *in vitro*

The drug release from the silica gels was evaluated by *in vitro* dissolution testing. All dissolution tests were performed in a VK 7010 dissolution bath with an auto sampler (VanKel industries, NJ, USA). 900 ml of double distilled water was used as dissolution medium for Propranolol Hydrochloride and 900 ml solution of 0.1% HCl was used as a dissolution medium for Persantin. The system operated at 310 K and 100 rpm, using the paddle method. Sink conditions were maintained. The Japanese sinker baskets were used to retain the dosage form at the bottom of the vessel. Full flow filters were used before the absorbance measurement. Dissolution continues until the sample is filtered. The full flow filters when attached to an automated sampling cannula, provides immediate filtration which preserves the integrity of the dissolution sample. Samples for UV-VIS absorbance of 5 ml were taken at 5 min intervals for the first 180 min and at 15 min intervals for the rest of 22 hour dissolution studies. The drug concentration in the dissolved samples were measured at 289 nm for Propranolol Hydrochloride and 402 nm for Persantin with an UV-Visible spectrophotometer (Cary 100 Tablet, Varian). The gel samples were packed in a gelatin capsule and approximately 50 mg drug amount per capsule. The UV-VIS spectra of the two drug molecules are given below in Figure 3.3 and 3.4.

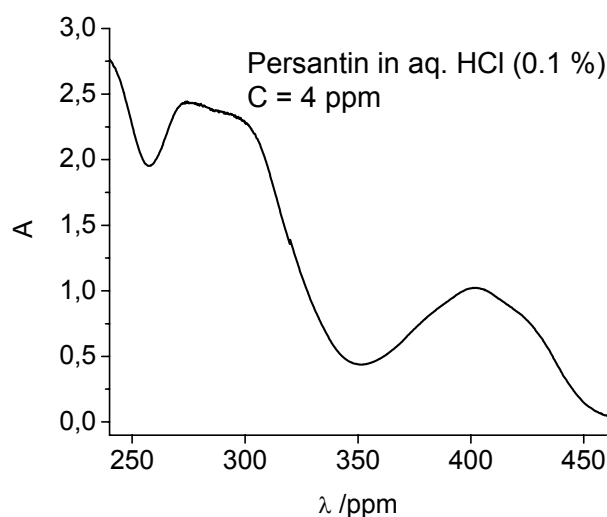


**Figure 3.3:** UV-VIS spectrum of Persantin in aq. HCl (0.1 %).

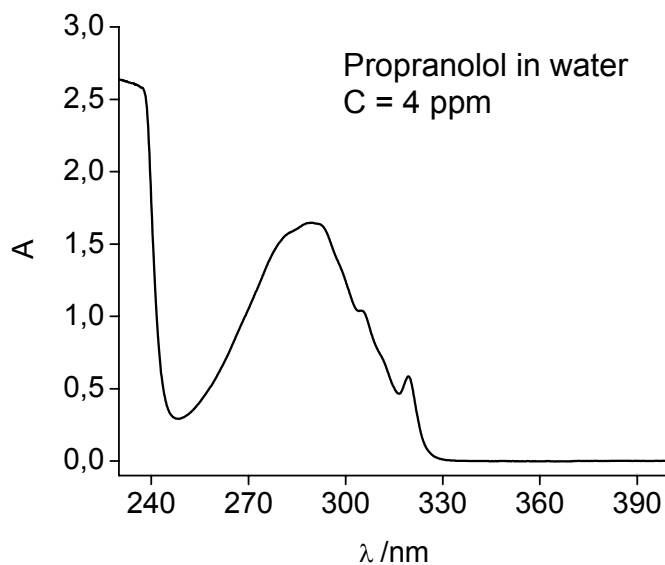


**Figure 3.4:** UV-VIS spectrum of Propranolol Hydrochloride in water.

Drug release mechanisms from the silica gels were studied by *in vitro* dissolution testing. The studies were conducted at 310 K for 22 hours and the drug concentrations in the dissolved samples were measured by UV-VIS spectroscopy. The details of standard dissolution parameters are given in Table 3.5. The concentration of the released drug was monitored as a function of time. The release kinetics as well as the total amount of drug dissolved depends on the synthesis and processing parameters of the final hybrid gel. Plots of amount dissolved (%) against time (min) were used to evaluate the kinetics and mechanisms of drug release. The release kinetics of Propranolol from the gels was evaluated using the equation<sup>101</sup>  $M/M_0 = kt^n$ , which describes the release of drugs from various geometrical forms and diffusion mechanisms.

**Table 3.5:** Standard dissolution rate testing parameters.

<i>Dissolution Medium</i>	(1) Double distilled water (PP) (2) 0.1% HCl (PS)
<i>Wavelength</i>	(1) 289 nm (PP) (2) 402 nm(PS)
<i>Sample volume</i>	900 ml
<i>Standard volume</i>	900 ml
<i>Tablet potency</i>	40 – 60 mg per capsule

### 3.4.2 Nitrogen sorption technique

Both pore size distribution and surface area of hybrid gels were measured using nitrogen adsorption/desorption technique. Nitrogen adsorption-desorption experiments were carried out at liquid N<sub>2</sub> temperature (77 K) on a Micromeritics ASAP 2010 sorption analyzer. All the samples were outgassed at 373 K under vacuum until the test of outgas pressure rise was passed by 10  $\mu$ mHg per min prior to their analysis. The data collected and processed automatically using the software ASAP 2010. Different inbuilt methods have been used to calculate the surface area and pore size distribution from the collected data. Plots of  $V_a$  (volume adsorbed cm<sup>3</sup>/g) against the reduced gas pressure  $p/p^0$  reveal the pore structure of the adsorbing material by its shape. BET (Brunauer, Emmett, Teller) surface areas were measured from the linear part of the plot ( $0.06 < p/p^0 < 0.2$ ). For the mesoporous gels, average mesopore radii were calculated from adsorption branch of the isotherms by the BJH (Barrett-Joyner-Halenda) method.<sup>132</sup> Total mesopore volume were derived from the liquid volume of adsorbed nitrogen at  $p/p^0 = 0.9$ . For the microporous gels, HK (Horvath and Kawazoe) method<sup>133</sup> was used for the micropore size distribution and micropore volume calculations.<sup>134</sup> Drug loaded and drug extracted hybrid gels has been studied by N<sub>2</sub> sorption technique.

### 3.4.3 Scanning Electron Microscopy (SEM)

The microscopic analysis by scanning electron microscopy was carried out in a LEICA 420 I instrument that allows a direct examination of the hybrid gel structures and approximately estimates the morphology, size and shape. Both, drug loaded and drug extracted gels has been examined using SEM. The sample was placed on a conducting polymer foil on an aluminum holder. The high magnification of the microscope allowed visualizing details of the morphology of gels and taking photographs. Since the silica samples are nonconducting, they were sputtered with gold before the examination. High resolution SEM was carried out in a JEOL 840 instrument.

### 3.4.4 Solid state NMR spectroscopy

The solid state nuclear magnetic resonance experiments were performed on different Bruker FT-NMR spectrometers operating at  $^1\text{H}$  Larmor frequencies of 300.13, 400.29, 500.12 and 800.05 MHz. A suite of one-dimensional (1D) and two-dimensional (2D) NMR was used, including 1D MAS NMR ( $^1\text{H}$  and  $^{29}\text{Si}$ ), 1D cross polarization (CP) MAS NMR ( $^{13}\text{C}\{^1\text{H}\}$  and  $^{29}\text{Si}\{^1\text{H}\}$ ) and 2D frequency switched Lee-Goldburg (FSLG) heteronuclear correlation (HETCOR) NMR ( $^1\text{H}$ - $^{13}\text{C}$  and  $^1\text{H}$ - $^{29}\text{Si}$ ). The data were acquired and Fourier transformed (FT) by using the programs XWINNMR and TOPSPIN. The spectrum was analyzed, deconvoluted and plotted with the help of the program DMFIT. The nuclei studied and their properties are presented in Table 3.6.

**Table 3.6:** NMR properties of the nuclei studied.

<i>Nuclei</i>	<i>Spin</i>	<i>Natural abundance (%)</i>	<i>Magnetogyric ratio <math>\gamma/10^7</math> (rad T<sup>-1</sup>s<sup>-1</sup>)</i>	<i>Standard</i>
$^1\text{H}$	$1/2$	99.985	26.752	TMS
$^{13}\text{C}$	$1/2$	01.108	06.728	TMS/Adamantane
$^{29}\text{Si}$	$1/2$	04.700	-5.319	TMS/ $\text{Q}^8\text{M}^8$

## **<sup>1</sup>H MAS NMR**

<sup>1</sup>H MAS NMR spectra were recorded at 9.4 T on a Bruker DSX 400 spectrometer operating at a <sup>1</sup>H Larmor frequency of 400.29 MHz using a 4 mm MAS probe. The sample was packed on a ZrO<sub>2</sub> rotor and spun at different MAS rate between 0 to 15 kHz. Additional <sup>1</sup>H data was recorded at 18.8 T on a Bruker ultrashield 800 plus Avance *II*<sup>+</sup> spectrometer operating at a <sup>1</sup>H Larmor frequency of 800.05 MHz and at 11.7 T on a Bruker ultrashield 500 Avance *II*<sup>+</sup> spectrometer operating at a <sup>1</sup>H Larmor frequency of 500.12 MHz. For high speed sample rotation, a 2.5 mm probe capable of MAS 35 kHz was used. Essential experimental parameter such as  $\nu_{\text{rf}}$ , the magnitudes of radio frequency (RF) fields was 100 kHz. The relaxation delay between accumulations was 6 s, as the typical  $T_1$  values measured by using saturation recovery were around 1.0 s. <sup>1</sup>H chemical shifts are reported using the  $\delta$  scale and are externally referenced to tetramethylsilane (TMS) at 0 ppm.

## **<sup>29</sup>Si MAS NMR**

<sup>29</sup>Si MAS NMR spectra were recorded at 7.1 T on a Bruker CXP 300 spectrometer operating at a <sup>29</sup>Si Larmor frequency of 59.63 MHz using a 7 mm MAS probe and a spinning rate of 4 kHz. The values of  $T_1$  relaxation times for selected hybrid silica gels varied between 30 and 50 s. Therefore, a 45° pulse with a relaxation delay of 120 s at  $\nu_{\text{rf}}$  of 30 kHz was chosen to ensure sufficient restoration of the initial <sup>29</sup>Si magnetization. <sup>29</sup>Si chemical shifts are reported using the  $\delta$  scale and are externally referenced to tetramethylsilane (TMS) at 0 ppm. The isotropic chemical shifts<sup>135</sup> of Q, T and D groups are shown below.

Q<sup>4</sup>:  $\delta = -109$  to  $-112$  ppm

Q<sup>3</sup>:  $\delta = -100$  to  $-102$  ppm

Q<sup>2</sup>:  $\delta = -90$  to  $-92$  ppm

T<sup>3</sup>:  $\delta = -64$  to  $-67$  ppm

T<sup>2</sup>:  $\delta = -53$  to  $-60$  ppm

D<sup>2</sup>:  $\delta = -15$  to  $-17$  ppm

D<sup>1</sup>:  $\delta = -6$  to  $-8$  ppm

$^{13}\text{C}\{^1\text{H}\}$  CPMAS NMR

$^{13}\text{C}\{^1\text{H}\}$  CPMAS experiments were performed at 9.4 T on a Bruker DSX 400 spectrometer operating at a  $^{13}\text{C}$  Larmor frequency of 100.65 MHz using a 4 mm double resonance MAS probe. Spinning rates of 10 kHz, 12.5 kHz and 15 kHz were employed and the spectra were recorded with a standard pulse sequence described in Figure 3.5.

The sequence starts with a  $^1\text{H}$   $90^\circ$  pulse (with RF field  $\nu_{\text{rf}(90)}^{\text{H}}$ ) that rotates magnetization from  $z$  to  $-y$ . Once it is along this axis a pulse on  $y$  is applied to keep it there and often called the spin lock pulse (with field  $\nu_{\text{rf}(\text{spin-lock})}^{\text{H}}$ ), simultaneously a pulse on  $^{13}\text{C}$  (with field  $\nu_{\text{rf}(\text{contact})}^{\text{C}}$ ). The duration of these two pulses can be varied from 50  $\mu\text{s}$  to several milliseconds and often called contact time. After that a decouple pulse is irradiated on the proton channel (with field  $\nu_{\text{rf}(\text{decouple})}^{\text{H}}$ ) while observing the  $^{13}\text{C}$  channel.

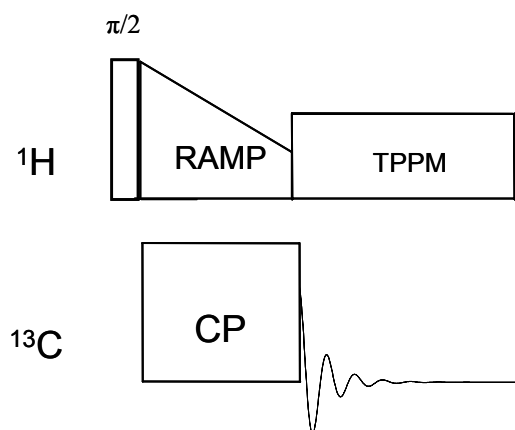


**Figure 3.5:** Pulse sequence used to perform 1D  $^{13}\text{C}\{^1\text{H}\}$  CPMAS experiments.

The magnetic fields  $\nu_{\text{rf}}^{\text{H}}$  of 100 kHz and 50 kHz were used for initial excitation and decoupling, respectively. During the CP period the  $^1\text{H}$  RF field  $\nu_{\text{rf}}^{\text{H}}$  was ramped using 64 increments, whereas the  $^{13}\text{C}$  RF field  $\nu_{\text{rf}}^{\text{C}}$  was maintained at a constant level. RAMP-CP<sup>136</sup> improves the Hartmann-Hahn matching condition and the efficiency (broader matching profile) of the CP step which are known to be very sensitive to RF power instabilities at high MAS rates. With this technique the CP matching profile is less dependent on the MAS rate and thus more easily adjustable and maintainable at optimum Hartmann-Hahn matching for magnetization transfer. During the acquisition, the protons are decoupled from the carbons by using a two-pulse phase-modulated (TPPM)<sup>137</sup>

decoupling scheme, which improves the high-field  $^{13}\text{C}$  resolution considerably. A moderate ramped RF field  $\nu_{\text{rf}}^{\text{H}}$  of 50 kHz was used for spin locking, while the carbon RF field  $\nu_{\text{rf}}^{\text{C}}$  was matched to obtain optimal signal and the CP contact time was varied between 1.0 and 7.0 ms.  $^{13}\text{C}$  chemical shifts are reported using the  $\delta$  scale and are externally referenced to adamantane at 38.56 ppm. Taylor has published papers on the setting up and application of CPMAS experiments.<sup>138</sup> Kolodziejski and Klinowski has reviewed the kinetics of cross-polarization in solid state NMR.<sup>139</sup>

### **$^{29}\text{Si}\{^1\text{H}\}$ CPMAS NMR**

$^{29}\text{Si}\{^1\text{H}\}$  CPMAS experiments were performed at 11.7 T on a Bruker ultrashield 500 Avance *II*<sup>+</sup> spectrometer operating at a  $^{29}\text{Si}$  Larmor frequency of 99.36 MHz using a 4 mm double resonance MAS probe. A spinning rate of 12.5 kHz was employed and the spectra were recorded with a standard pulse sequence.  $^{29}\text{Si}$  chemical shifts are reported using the  $\delta$  scale and are externally referenced to shifts of  $\text{Q}^8\text{M}^8$ .

The magnetic fields  $\nu_{\text{rf}}^{\text{H}}$  of 104 kHz and 48 kHz were used for initial excitation and decoupling, respectively. During the CP period the  $^1\text{H}$  RF field  $\nu_{\text{rf}}^{\text{H}}$  was ramped using 100 increments, whereas the  $^{29}\text{Si}$  RF field  $\nu_{\text{rf}}^{\text{Si}}$  was maintained at a constant level. During the acquisition, the protons are decoupled from the silicons by using a continuous wave (CW) decoupling mode, which slightly improves the high-field  $^{29}\text{Si}$  resolution. A moderate RF field  $\nu_{\text{rf}}^{\text{H}}$  of 50 kHz was used for spin locking and the CP contact time was varied between 1.0 and 7.0 ms.

### **2D $^1\text{H}$ - $^{13}\text{C}$ and $^1\text{H}$ - $^{29}\text{Si}$ FSLG HETCOR NMR**

All the 2D spectra were acquired on a Bruker ultrashield 500 Avance *II*<sup>+</sup> spectrometer and a wide bore 11.7 T magnet with operational frequencies for  $^1\text{H}$ ,  $^{29}\text{Si}$  and  $^{13}\text{C}$  of 500.12, 99.36 and 125.77 MHz, respectively. Additional 2D  $^1\text{H}$ - $^{13}\text{C}$  FSLG HETCOR NMR experiments were performed at 9.4 T on a Bruker DSX 400 spectrometer operating at a  $^{13}\text{C}$  Larmor frequency of 100.65 MHz. A 4 mm double resonance probe with magic angle spinning rate of 12.5 kHz was employed in all the experiments. The sample was packed in a  $\text{ZrO}_2$  HRMAS rotor and the volume was restricted to the middle of the rotor. Such a procedure is necessary because the FSLG decoupling step is sensitive to RF



inhomogeneities, restricting the sample volume to the central part of the rotor leads to an improvement of the RF field homogeneity and avoids deterioration of the  $^1\text{H}$  resolution. The pulse sequence<sup>140</sup> and coherence transfer pathway used to collect 2D heteronuclear correlation spectra is depicted in Figure 3.6.

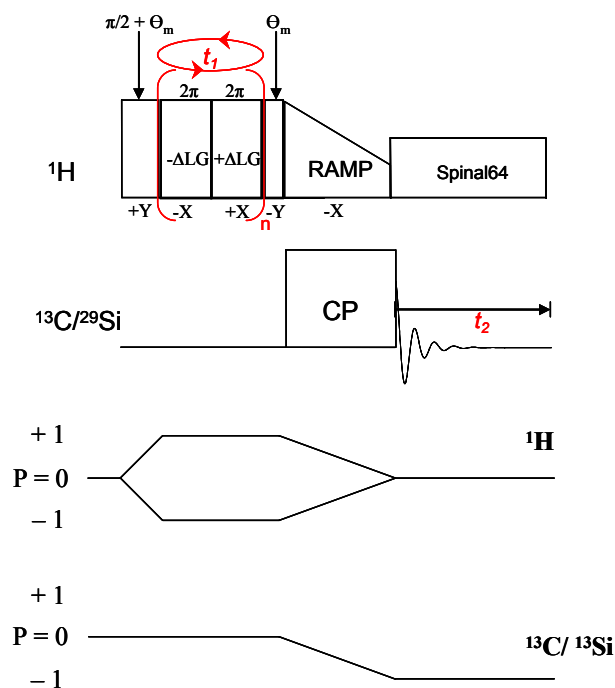


**Figure 3.6:** Pulse sequence and coherence transfer pathway diagram<sup>141</sup> for the 2D heteronuclear correlation NMR, with frequency-switched Lee-Goldburg irradiation during the evolution. The pulse angle  $\theta_m$  represents the angle between the static magnetic field and the effective field.

The sequence starts with a  $(\pi/2 + \theta_m)_y$  ( $90^\circ + 54.7^\circ = 144.7^\circ$ ) pulse on the proton channel, directly followed by a train of frequency and phase switched symmetric LG pulses in the  $xz$  plane. After the evolution period, proton magnetization is turned back by a single magic angle  $y$  pulse ( $54.7^\circ$ ) into the  $xy$  plane, and which will bring the spin-locked component along the LG-pulse back to the  $z$  axis. During the LG period the homonuclear proton dipolar coupling is averaged to zero by applying a RF pulse which initially places the effective field at the magic angle with respect to the static field. Here  $\Delta LG$  with  $-x$  refers to a RF pulse with an amplitude  $\omega_{1H}$  applied to the  $-x$  direction with a positive offset of  $\Delta\omega$  from the  $^1\text{H}$  on-resonance frequency fulfilling the condition of  $\omega_{1H}$

$= \sqrt{2}\Delta\omega$ . For FSLG, each cycle time consists of two LG blocks. The effective fields created by the two LG units have opposite phases and offset frequencies along the magic angle. The remaining part of the pulse sequence is similar to the CPMAS sequence. During the acquisition, the protons are decoupled by using a decoupling scheme, spinal 64 in the  $^1\text{H}$ - $^{13}\text{C}$  HETCOR, whereas CW is used in  $^1\text{H}$ - $^{29}\text{Si}$  HETCOR experiments. The details of essential experimental parameters for the 2D  $^1\text{H}$ - $^{29}\text{Si}$  FSLG HETCOR and  $^1\text{H}$ - $^{13}\text{C}$  FSLG HETCOR NMR are given in Table 3.7.

In theory, under FSLG decoupling, the proton chemical shift is scaled by  $1/\sqrt{3}$  (0.577) and the proton chemical shift scale has been corrected for this scaling in all of the 2D spectra. The  $^1\text{H}$  chemical shift scale and the scaling factors were determined by comparing the 1D  $^1\text{H}$  spectra recorded under fast MAS. The chemical shifts of the methyl/methylene protons of the silica matrix were used to reference (F1) the 2D spectra. The scaling factors obtained for all the 2D spectra were well within the range of the theoretical value.  $^{13}\text{C}$  and  $^1\text{H}$  chemical shifts are reported using the  $\delta$  scale and are externally referenced to adamantane.

**Table 3.7:** 2D  $^1\text{H}$ - $^{29}\text{Si}$  FSLG HETCOR and  $^1\text{H}$ - $^{13}\text{C}$  FSLG HETCOR NMR experimental parameters.

	$^1\text{H}$ - $^{29}\text{Si}$ HETCOR	$^1\text{H}$ - $^{13}\text{C}$ HETCOR
Number of $t_1$ increments	56-80	64-96
Relaxation delay [s]	2	2
Number of scans	64-336	80-400
MAS rate [kHz]	12.5	12.5
$^1\text{H}$ RF field [kHz]	104	104
$^1\text{H}$ LG offset frequency [kHz]	+1.0	+1.0
FSLG decoupling power [kHz]	127	127
Positive offset frequency (+ $\Delta\text{LG}$ ) [kHz]	+74.680	+74.680
Negative offset frequency (- $\Delta\text{LG}$ ) [kHz]	-72.680	-72.680
Contact time [ms]	0.5 – 5.0	0.1 – 2.0

The spectra are the constructive contours reflect a 2 fold change in the intensity. In all the spectra, the lowest level corresponds to 0% of maximum intensity observed, whereas skyline projections are normalized and in some cases the floor is elevated due to the low signal-to-noise ratio.

Diversity of the solid state nuclear magnetic resonance spectroscopy has been exploited to characterize the organic-inorganic hybrid silica gels. Conventional solid state NMR techniques such as MAS and CPMAS and advanced high resolution technique FSLG

HETCOR has been employed in this study. The NMR experiments were performed to probe the local environment of the drug molecules and to determine whether possible interactions between the confined drug and the silica matrix can control the release properties.  $^1\text{H}$  MAS NMR experiments were devoted to study the organic and inorganic components in the hybrid gels, whereas  $^{29}\text{Si}$  MAS NMR used to study the spatial distribution of the inorganic network.  $^1\text{H}$  MAS NMR of the as synthesized gels and various temperature treated gels were carried out in order to probe the proton sources in the hybrid silica gels and to differentiate between encapsulated drug molecules and solvents. Proton MAS NMR with different spinning rate was carried out to study the mobility and dipolar interactions in the gels and it is known that the spectra acquired at moderate spinning rate will chiefly dominate by mobile species while at high speed MAS rigid species will also be visible.

1D  $^{29}\text{Si}$  and  $^{13}\text{C}$  CPMAS NMR provides information about the distributions of local sites and the existence of the encapsulated drug molecules in the hybrid gels, respectively.  $^{13}\text{C}$  CPMAS NMR was also used to study the packing behaviour and polymorphic structures of pure drug. As CPMAS is based on heteronuclear dipolar interactions, it is sensitive to internuclear distances and the mobility of the molecules involved. The assignments of the  $^{13}\text{C}$  and  $^1\text{H}$  solid state spectral resonances of drugs and hybrid silica gels were performed on the basis of the  $^{13}\text{C}$  and  $^1\text{H}$  solution spectrum and with the help of commercial software.<sup>142</sup> The assignments were further corroborated with the high resolution 2D FSLG HETCOR NMR spectroscopy.

### 3.5 Pre-characterization techniques

Pre-characterization techniques such as Differential Scanning Calorimetry (DSC) and X-Ray powder Diffraction (XRD) were carried out on selected hybrid silica gels.

#### 3.5.1 Differential Scanning Calorimetry (DSC)

Differential scanning calorimetry measurements were carried out on a NETZSCH DSC 204 Phoenix instrument registering a temperature range between 298 and 773 K at a rate of 10 K/min.  $\text{N}_2$  was used as sweeping gas and the reference was  $\text{Al}_2\text{O}_3$ .

In Figure 3.7 the DSC traces of selected TEOS silica gels prepared in the presence of drug are shown and are compared with the physical mixture prepared with model drug molecules Persantin and Propranolol. Physical mixtures are prepared by grinding the

drug with a TEOS Gel 189 which was prepared in the absence of drug. The physical mixtures exhibit a sharp peak at around 434 K for PP and 435 K for PS, corresponding to the melting point of the drug, thus indicating that the drug is in crystalline form. However, in the thermogram of the hybrid gel there was no sharp peak at around 435 K, confirming that the drug was indeed amorphous in the hybrid gel. The silica gels 201 and 262 were spray dried gels, whereas 176 was EISA gel. The DSC graphs pinpoint that there was no crystallization of the drug molecules within the self assembled and spray dried gels and are molecularly dispersed in the hybrid silica gel.

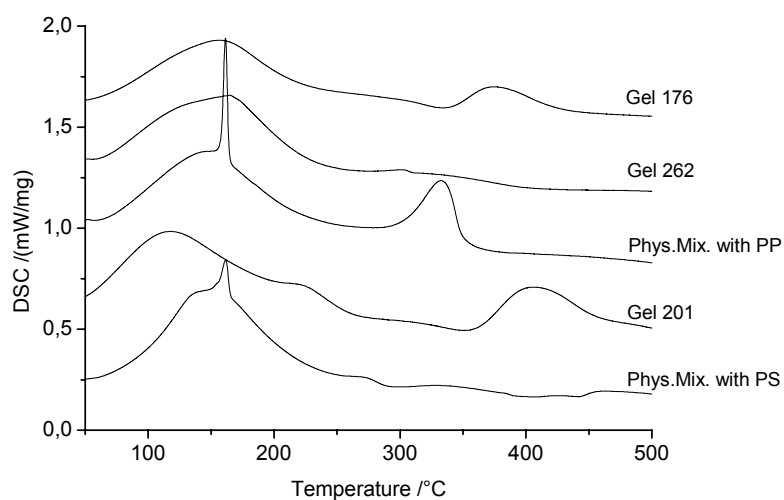


**Figure 3.7:** DSC traces of TEOS based silica gels prepared in the presence of model drug molecules, PS and PP, and physical mixtures of drug and silica gel.

### 3.5.2 X-Ray powder diffraction (XRD)

The amorphous nature of the hybrid gels were determined using X-ray powder diffraction, employing Guinier cameras. EISA gels were initially crushed in a mortar and then the resulting powder was evenly spread over the grid of a Guinier sample holder with an adhesive tape. Spray dried samples were directly used without crushing. A Guinier camera (ENRAF-NONIUS, type FR 552) with Cu  $K_{\alpha_1}$  radiation (154.051 pm) with an image plate system (Fujifilm BAS 1800) was used for characterization and registered Bragg angles between 5-60°.

The X-ray powder diffraction pattern of the two model drugs, PS and PP, are given in Figure 3.8 and are crystalline in nature. The diffraction pattern of the spray dried (Gel 262) and EISA (Gels 176, 191, 177, 182) gels are featureless and indicated the presence of amorphous material (Figure 3.9). The formation of separate drug phase and apparent crystallinity in the silica gel can be excluded by the analysis of X-ray powder diffraction patterns.

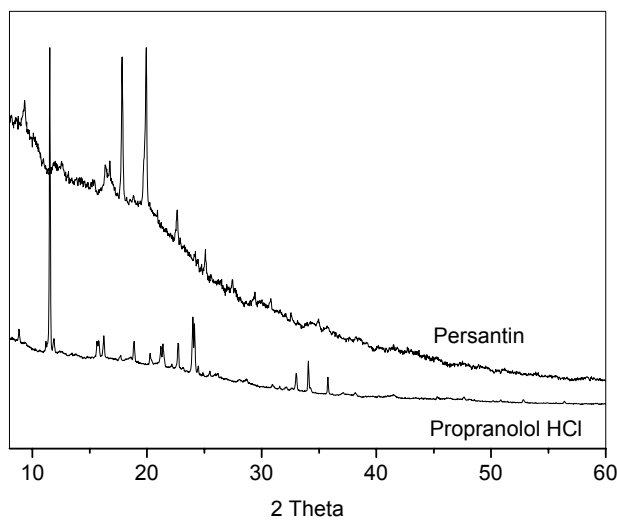


**Figure 3.8:** X-ray powder pattern of pure drugs, PS and PP showing crystallinity.

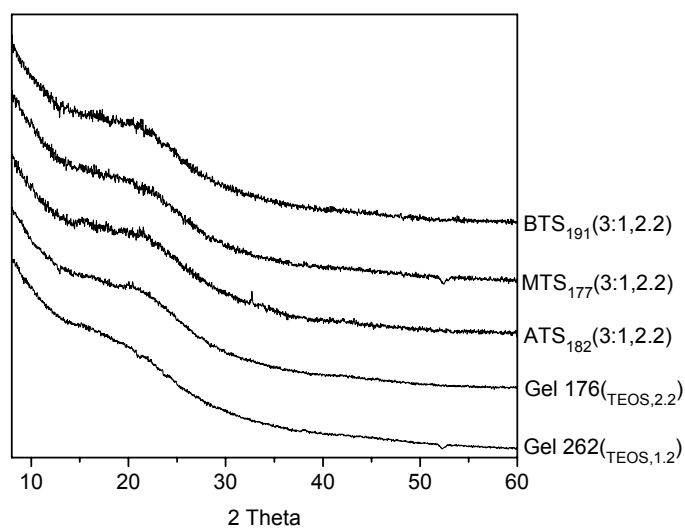


**Figure 3.9:** X-ray powder pattern of silica gels prepared with model drug molecules, PS and PP showing non-crystalline character.

---

## 4. Evaporation Induced Self Assembled Gels

---

### Introduction

Self assembly can be defined as the spontaneous organization of materials (e.g., drug molecules and silica oligomer/polymer) through noncovalent interactions such as hydrogen bonding, van der Waals forces, electrostatic forces,  $\pi$ - $\pi$  interactions etc. In EISA gels, self assembly is driven by the evaporation of solvents such as water or ethanol resulting in a semi-solid. Subsequent aging by temperature treatment solidify the silicon skeleton, thereby locking the drug molecules inside the pores. In this chapter, the preparation, characterization and properties of EISA gels synthesized in presence of pharmaceutically active drug molecule, Propranolol is presented. Attempts have been made to understand the influence of synthesis parameters such as, pH, precursor amounts and solvent content in the EISA gel formulations. The chapter is divided into two sections, the first part dealing with the silica gel formulations from single precursors followed by two precursor formulations in the second part.

### 4.1 EISA silica gel formulations from a single precursor

#### 4.1.1 Preparation

Gel 2 was prepared at pH 1.5 by mixing TEOS, H<sub>2</sub>O, Ethanol, PP and HCl in the molar ratio 1.0 : 4.9 : 1.95 : 0.029 : 0.0098. In a typical synthesis, PP was dissolved in a mixture of water and ethanol; to this solution TEOS was added. The solution was stirred while adding 0.5 M HCl till the hydrolysis was complete. The sol was stirred for 24 h at room temperature and after that subjected to evaporation induced self assembly (EISA) at 323 K. The silica sols with high synthesis pH values were prepared by two-step catalysis with aqueous HCl and aqueous NH<sub>3</sub>. The final pH of the sol after hydrolysis was controlled by the addition of aqueous NH<sub>3</sub>. The synthesis compositions are given in Table 4.1. The polymerized silica gels were dried at 323 K for constant weight. All gels were treated in a ballmill for 3 min at 200 rpm to obtain a similar particle size distribution. The drug loads in these gels are between 10-12 wt%.

**Table 4.1:** Relative molar ratios, pH and stirring time ( $t_s$ ) for single precursor gel formulations

<i>Gel</i>	<i>TEOS</i>	<i>H<sub>2</sub>O</i>	<i>Ethanol</i>	<i>HCl</i>	<i>PP</i>	<i>t<sub>s</sub> (h)/pH</i>
<i>Gel 2</i>	1	4.9	1.95	0.0098	0.029	24 / 1.5
<i>Gel 4</i>	1	4.9	1.95	0.0098	0.029	24 / 2.0
<i>Gel 5</i>	1	4.9	1.95	0.0098	0.029	24 / 2.5
<i>Gel A22</i>	1	4.9	1.95	0.002	0.029	24 / 5.5
<i>Gel A25</i>	1	4.9	1.95	0.002	0.029	24 / 6.5
<i>Gel A37</i>	1	9.8	3.9	0.0039	0.029	96 / 3.0
<i>Gel 161</i>	1	4.9	1.95	0.0708	0.029	24 / 0.5
<i>Gel 176</i>	1	4.9	1.95	0.0098	0.029	24 / 2.2
<i>Gel 174</i>	1	4.9	1.95	0.0708	0.000	24 / 0.5
<i>Gel 189</i>	1	4.9	1.95	0.0098	0.000	24 / 2.2

#### 4.1.2 Dissolution rate test

The release profiles of Propranolol from silica gels prepared at different pH are compared in Figure 4.1.1. Silica gels made at different pH values from 0.5 to 6.5 in the presence of PP, show strong pH dependence in release kinetics. Around 60 wt% of the drug was released within 22 hours, for gels synthesized between pH 1.5 and 2.5. A fast initial release occurs for gels synthesized at higher pH (above pH 3.0) and lower pH (0.6) whereas a retarding effect is observed in gels synthesized at pH around 2.0. At pH = 0.6 and above 3.0, the initial burst (referred to a fast release rate of drug) was accounted for approximately 70%. The release kinetics of Propranolol from the gels was evaluated using the equation  $M/M_0 = kt^n$ , which describes the release of drugs from various geometrical forms and diffusion mechanisms. The release of Propranolol confirmed to diffusion controlled release ( $n = 0.30-0.43$ ) for silica gels prepared at around pH = 2, as shown in the inset of Figure 4.1.1.



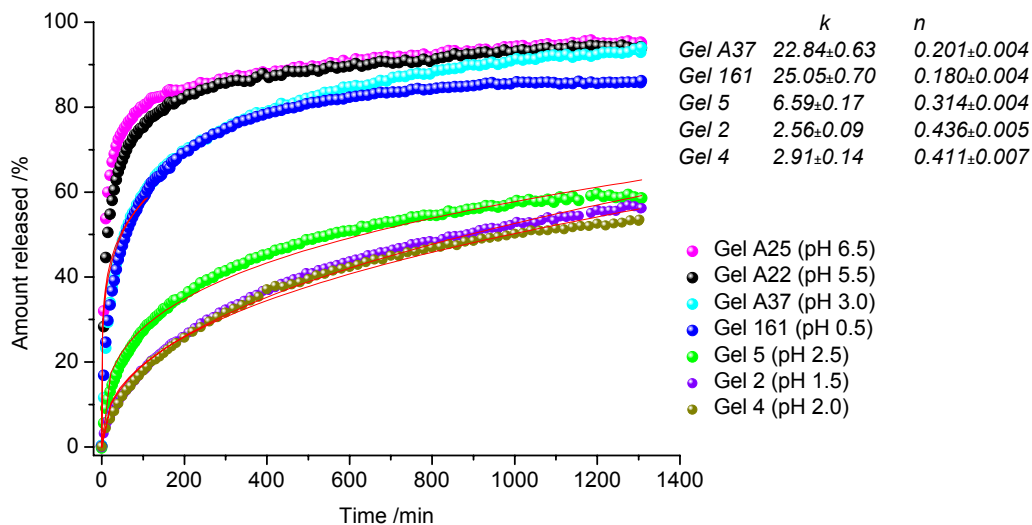


**Figure 4.1.1:** Drug release profiles of Propranolol from silica gels with different synthesis pH.

#### 4.1.3 Surface studies by SEM

The microscopic analysis by scanning electron microscopy was carried out to obtain information about the morphology and to evaluate shape, size and surface of the particles. The SEM micrographs of Gel 2 and 5 are given in Figure 4.1.2. The micrographs reveal the formation of monoliths with irregular shape and size.

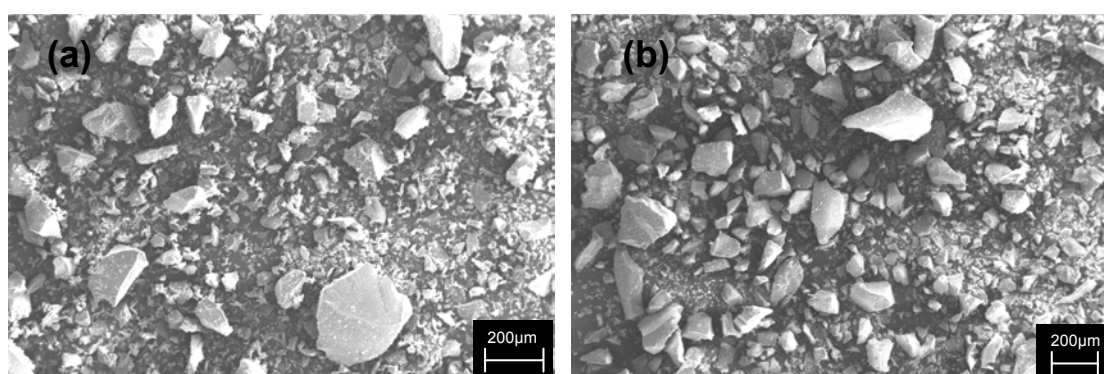


**Figure 4.1.2:** SEM micrographs of Gel 2 (a) and 5 (b).

### 4.1.4 N<sub>2</sub> Sorption studies

N<sub>2</sub> sorption studies have been carried out for the characterization of the porosity of gels, Figure 4.1.3. The N<sub>2</sub> sorption isotherm of the Gel 174, which is prepared in the absence of drug, is of type I, indicating a microporous material. The BET surface area and the micropore volume are 304 m<sup>2</sup>/g and 0.149 cm<sup>3</sup>/g, respectively. The micropore size distribution are derived from physisorption isotherm data using Horvath-Kawazoe method and found to be in the range of 0.2-0.4 nm. Although the Gel 4 and Gel 2 released considerable amount of drug within 22 h as indicated by the DRT graph, no significant porosity and hence surface area are observed in these materials. The nitrogen sorption capacity of Gel A22 is clearly higher before and after the release. The untreated sample shows a small specific surface of 114 m<sup>2</sup>/g, while the washed sample exhibits a very high specific surface area of 500 m<sup>2</sup>/g. Gel A22 was synthesized at pH 5.5 and porous silica architectures were formed. The DRT graph clearly confirms that above 90% of the loaded drug was released during the 22 h study. The pores emptied after the drug release was accessible to the nitrogen adsorption and are exhibited as high surface area material. A mixture of micropore-mesopore contribution to the total porosity of washed Gel A22w was also observed.

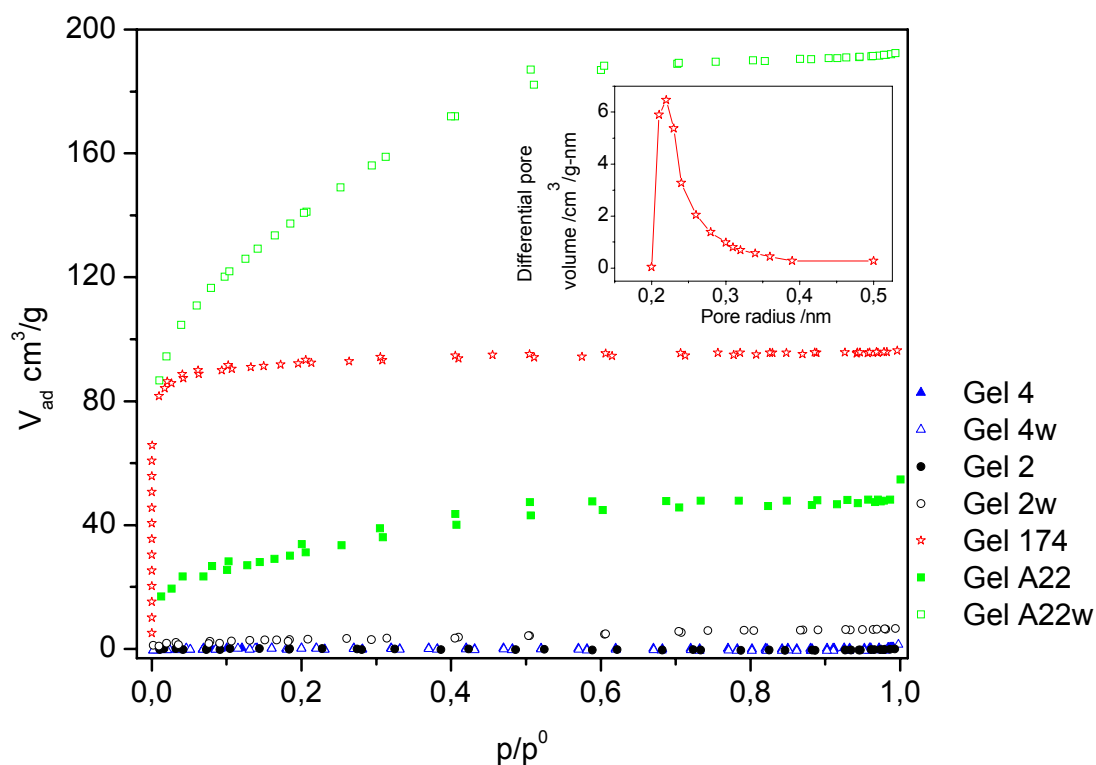


**Figure 4.1.3:**  $N_2$  sorption isotherm of various gels. Inset shows the pore-size distribution of Gel 174 according to the Horvath-Kawazoe method.

#### 4.1.5 $^{29}\text{Si}$ MAS NMR studies

Various gel samples were examined using 1D  $^{29}\text{Si}$  MAS NMR spectroscopy. The studies on gels have been carried out in order to understand the structural pattern and silicon atom connectivity in the gel network. The  $^{29}\text{Si}$  MAS NMR spectra of various gels are shown in Figure 4.1.4, together with the corresponding simulated spectra and their individual components from each silicon site.

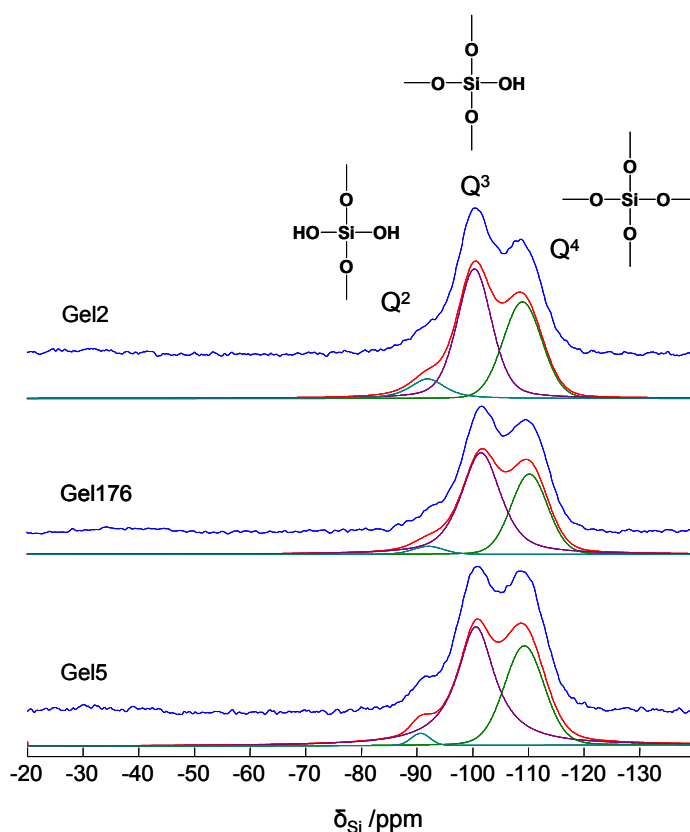


**Figure 4.1.4:**  $^{29}\text{Si}$  MAS NMR spectra of various gels. Each set of spectra includes experimental spectrum (in blue) and the simulated spectrum (in red) with individual contributions from each silicon site.

The peak around -91 ppm is attributed to silicon atom that have two hydroxyl groups attached,  $(\text{Si-O})_2\text{Si}(\text{OH})_2$ , often referred as  $\text{Q}^2$  silicons or as geminal silanols. The resonance at -99 ppm is due to silicons with only one hydroxyl group (single silanol),  $(\text{Si-O})_3\text{Si-OH}$  often referred as  $\text{Q}^3$  sites. The  $\text{Q}^4$  silicon sites,  $\text{Si}(\text{O-Si})_4$ , resonances at -110 ppm does not have hydroxyl groups.

**Table 4.2:** Peak area derived for deconvoluted peaks of the  $^{29}\text{Si}$  MAS spectra of gels.

Probe	$\text{Q}^2$ /%	$\text{Q}^3$ /%	$\text{Q}^4$ /%	$\Sigma \text{Q}$ /%	pH	$\eta$
Gel 2	9	52	39	100.00	1.5	0.82
Gel 176	3	60	37	100.00	2.2	0.83
Gel 5	2	59	39	100.00	2.5	0.84

Table 4.2 summarizes the deconvoluted peak areas of the spectra in Figure 4.1.4. Since the MAS NMR spectra provide quantitative information, the peak area represents the actual number of Si sites present in the gels. The ratio of populations of the silicon sites indicates a less condensed silica network formed at acidic pH values. The  $\eta$  value, a measure of degree of condensation is calculated by the effective and potential functionalities of Si,  $f_{eff}$  and  $f_{pot}$ , respectively.<sup>143</sup>

$$\eta = \frac{f_{eff}}{f_{pot}}$$

The effective functionality is obtained by,

$$f_{eff} = \sum_n (\chi_n \times n)$$

Where  $\chi_n$  is the percentual area of silicate structure  $Q_n$  and  $n$  varies from 2 to 4.

The  $\eta$  value, increases with pH as can be seen from the Table 4.2. The synthesis pH values of these gels are in the acidic range where silanol sites dominate over siloxane site.

#### 4.1.6 <sup>1</sup>H MAS NMR studies

Several <sup>1</sup>H MAS NMR studies has been performed to probe the proton sources in the silica gels and to differentiate between encapsulated drug molecules and solvents. The surface functionalization of silica gel was investigated by several thermal treatment and NMR spectroscopy.<sup>144</sup>

The proton NMR spectra of Gel 189 prepared in the absence of the drug are shown in Figure 4.1.5. Considerable improvement in resolution has been achieved upon increasing the sample rotation rate up to 15 kHz as shown in Figure 4.1.5. The broad line from 3 to 9 ppm is absent in the low MAS rate, (e.g. 2 kHz), a resonance originating from protons involved in strong dipolar interactions that are too intense to be averaged by low MAS rate. The appearance of a narrow peak at 1.3 ppm upon increasing the MAS rate confirms the fact that the <sup>1</sup>H-<sup>1</sup>H dipolar interactions of these protons are weak enough to be averaged by MAS.

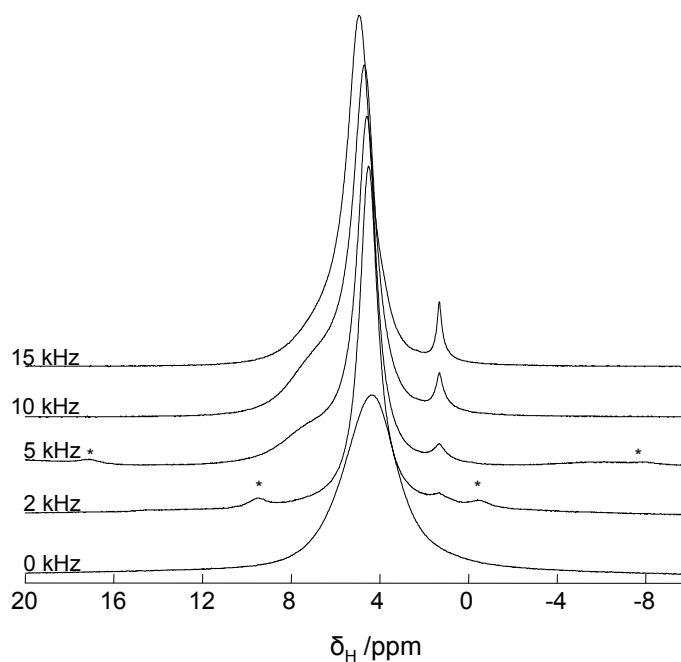


**Figure 4.1.5:** The  $^1\text{H}$  MAS NMR spectra of Gel 189 at different MAS conditions. Intensities are not in absolute scale.

The deconvolution of the spectrum of Gel 189 is shown the presence of different proton sites in the gel and is assigned to hydrogen bonded silanol groups, mobile water and also to the chemically bound ethoxy groups and physisorbed ethanol (Figure 4.1.6). The peak at 4.9 ppm is due mainly to water molecules (1) that are physisorbed on the silica surface, an assignment derived directly from the dehydration-rehydration studies (see below), and by analogy to analogous results reported previously on silica gel.<sup>145</sup> No MAS sidebands are detected for this peak which implies that the water molecules physisorbed on the silica surface have liquid like behavior, i.e., are rather mobile at the measurement temperature (298 K). The broad peak from about 3 to 9 ppm is assigned to silanol protons (2) in a variety of hydrogen bonding environments, another assignment derived directly from the dehydration-rehydration studies, and also on the basis of earlier silica gel studies.<sup>145</sup> Hydrogen bonding is commonly identified with proton shifts to lower shielding, and a distribution of types and strengths of hydrogen bonding should yield a distribution of isotropic chemical shifts, i.e., an inhomogeneously broadened peak. This broad peak overlaps with the resonance intensity arising from the protons of water molecules that are hydrogen bonded, indicating that the silanol protons are in a similar chemical and physical environment. A sharp signal at 1.3 ppm is due to the methyl protons of the physisorbed ethanol (3) and the narrow line indicates presence of sufficient

mobility in the gel. The broad signal at 3.8 ppm is due to the methylene protons of the ethanol and ethoxy group (4) and the weak broad peak at 1.2 ppm is due mainly to the methyl protons of the chemically bound ethoxide (5). The contributions from the isolated silanols cannot be identified as separate peak, but contribute to the intensity observed in the 1.0 – 2.0 ppm range.

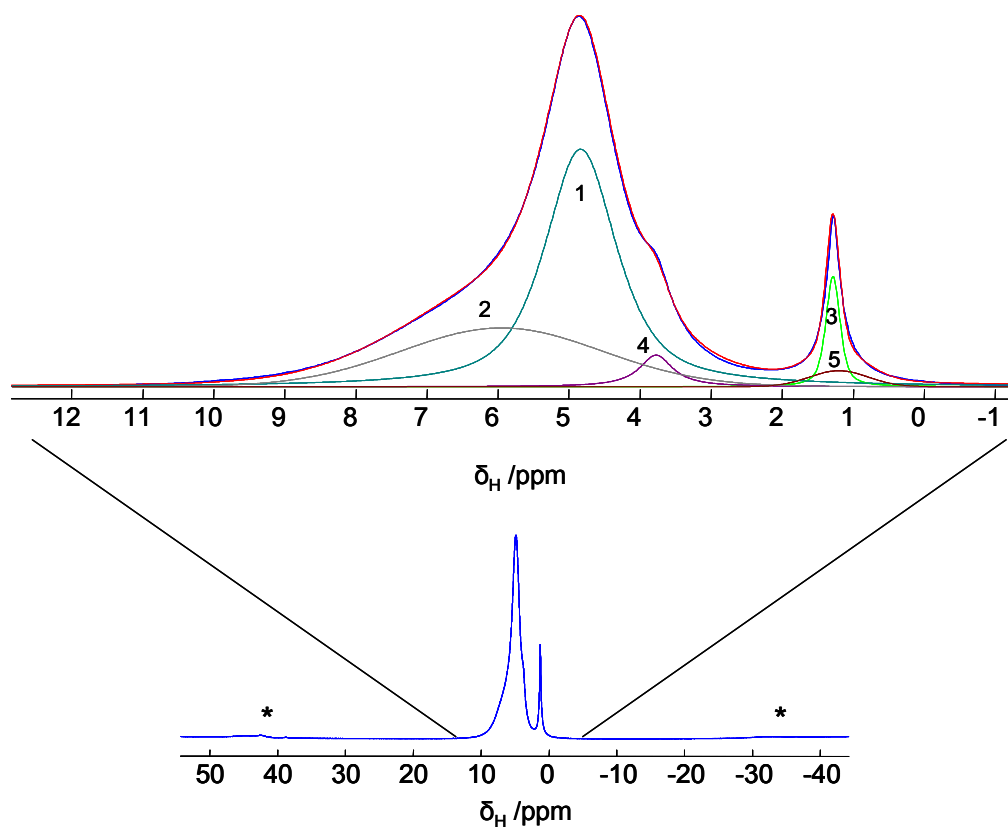


**Figure 4.1.6:** The  $^1\text{H}$  MAS NMR spectra at 15 kHz and its computer simulation/deconvolution of Gel 189.

**Table 4.3:** Chemical shift derived for deconvoluted peaks of the  $^1\text{H}$  MAS spectra of Gel 189

	Group	$\delta_{\text{H}}/\text{ppm}$
1	Mobile water	4.9
2	Hydrogen bonded silanol	3 - 9
3	$-\text{CH}_3$ of Ethanol	1.3
4	$-\text{CH}_2$ of ethoxy/ethanol	3.8
5	$-\text{CH}_3$ of ethoxy group	1.2

The above assignments are supported by the spectra obtained for the gel treated at higher temperatures, Figure 4.1.7. Elimination of physisorbed water and ethanol starts well below 393 K and are absent in the spectrum of Gel 189 treated at 393 K. After the heat treatment and followed by the exposure to the atmosphere, water reabsorbs on the silica gel and appears as a peak at 3.4 ppm. It can be argued that the environments of the water confined in the silica gel are different before and after the heat treatment. This is supplemented by the spectra of gel treated at 773 K. Readsorbed water shows a peak which is further narrowed and no overlapping with the peak from hydrogen bonded silanols. It should be emphasized that the chemically bound ethoxide is eliminated well before this temperature and contributes to the narrowing of the water peak. Hydrogen bonded silanol are not completely eliminated even at 1173 K (broad peak from 5 to 9 ppm), in addition to the existence isolated silanols (peaks at 1.35 and 1.85 ppm). High temperature treatment of the gel leads to the conversion of the hydrogen bonded silanols to isolated silanol by forming siloxane bonds at the expense of  $\text{H}_2\text{O}$ .<sup>144</sup>

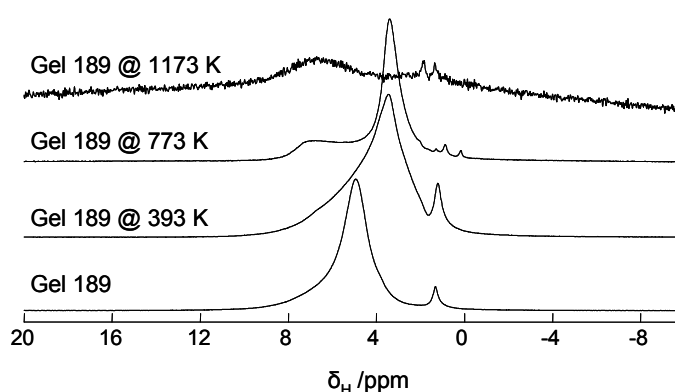


**Figure 4.1.7:** The  $^1\text{H}$  MAS NMR spectra of Gel 189 after different temperature treatment (MAS 15kHz). Intensities are not in absolute scale.



The proton NMR spectrum of Gel 176 which is prepared in presence of PP is shown in Figure 4.1.8. The deconvolution of the spectra shows the presence of different proton sites in the gel and they are assigned to hydrogen bonded silanols, mobile water, physisorbed ethanol and different groups of the drug molecule.

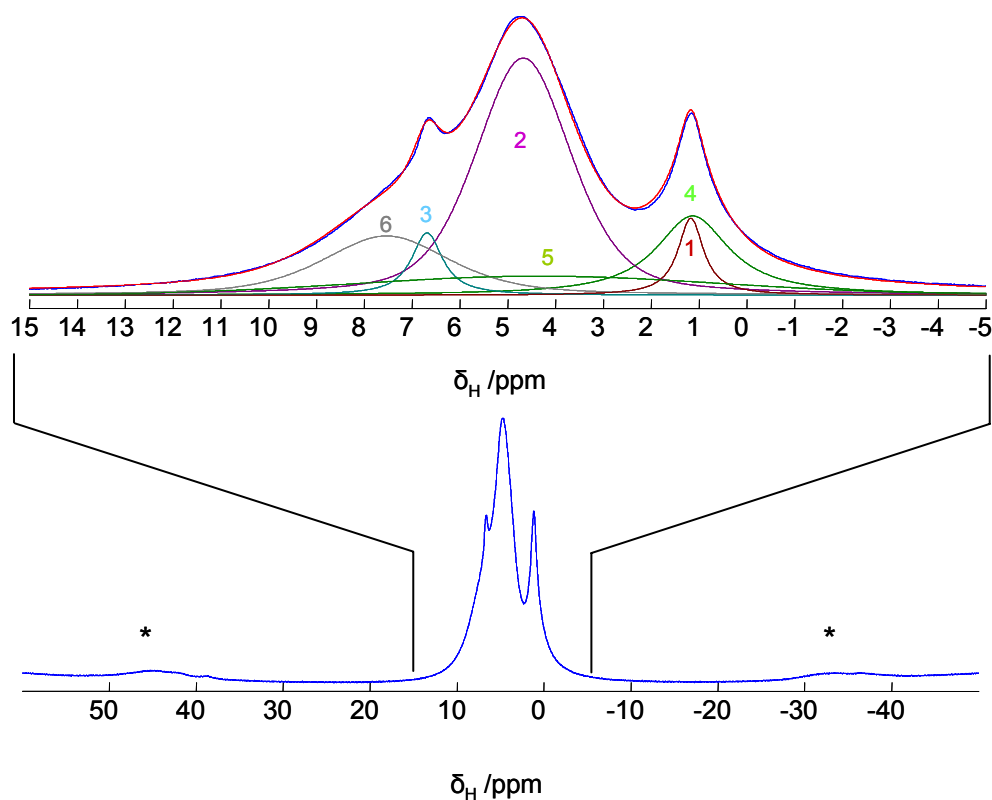


**Figure 4.1.8:** The  $^1\text{H}$  MAS NMR spectra at 15 kHz MAS and its computer simulation/deconvolution of Gel 176.

Similar to the assignment of Gel 189, there is an ethanol peak, water peak and hydrogen bonded silanol peak at 1.2, 4.7 and 6.7 ppm, respectively. Besides that, drug peaks at different chemical shift were also observed, and assigned as shown in Table 4.4. Compared to pure drug (Figure 4.1.9), only weak dipolar interactions are observed in the drug incorporated gels indicating dilution and hence a higher degree of molecular motion in the gels. As shown in Figure 4.1.10, besides the absence of the water and ethanol peaks, the broad spectrum of Gel 176 treated at 393 K is an indication of the presence of Propranolol. The broad feature of the PP signals also confirms the strong dipolar interactions between the protons of Propranolol and the absence of mobility. Hydrogen bonded silanol groups (in the range 3-12 ppm) are not completely eliminated even at 1173 K, in addition to the existence of isolated silanols. Isolated silanols resonances at

1.35 ppm as seen from the spectrum of gel treated at 1173 K, are formed from the hydrogen bonded silanols upon heat treatment.

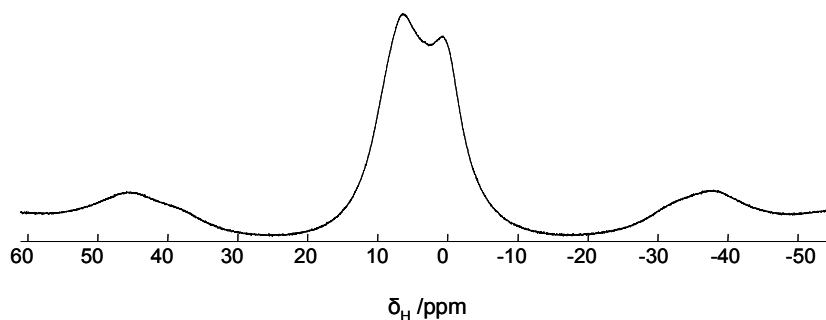


**Figure 4.1.9:**  $^1\text{H}$  MAS spectra of PP at 15 kHz.

**Table 4.4:** Chemical shift derived for deconvoluted peaks of the  $^1\text{H}$  MAS spectra of gels 176

	Group	Shift /ppm
1	-CH <sub>3</sub> of ethanol	1.2
2	Mobile water	4.7
3	Hydrogen bonded silanol	6.7
4	-CH <sub>3</sub> of Propranolol HCl	1.1
5	Aliphatic protons of drug	4.3
6	Aromatic protons of drug	7.5

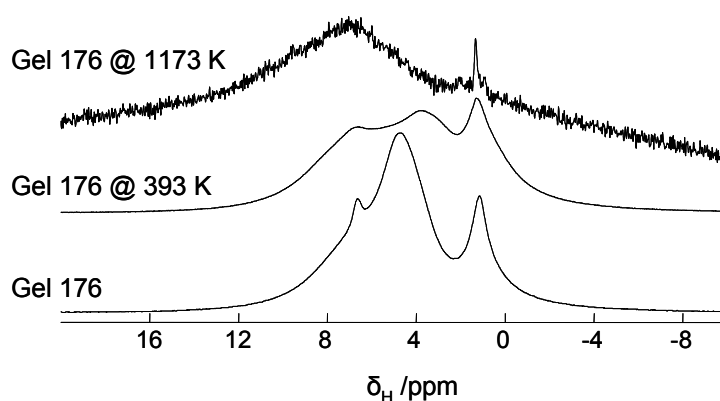


**Figure 4.1.10:** The  $^1\text{H}$  MAS NMR spectra of Gel 176 after different temperature treatment. Intensities are not in absolute scale.

#### 4.1.7 $^{13}\text{C}\{^1\text{H}\}$ CPMAS NMR studies

The CPMAS NMR spectra of various gels and PP are shown in Figure 4.1.11. The broad signals (Gel 189) at around 61.7 and 17.5 ppm are assigned to a small number of

chemically bound ethoxy groups (broken arrows).<sup>146</sup> The peaks which partly overlap with these at 59.4 and 17.6 ppm are attributed to physically adsorbed ethanol (solid arrows).<sup>147</sup> The other resonances are attributed to PP by comparison with the spectrum of the pure drug. The spectrum of the drug extracted gel is also presented, Gel 4w. The peaks from the drug molecules remains in much lower intensity after the drug extraction for 24h. From the DRT experiments it is clear that more than 40% of the drug remains in the gel, but the resonance peaks from the chemically bound ethoxy group and physisorbed ethanol are missing in the drug extracted gel. The reason for the absence of physisorbed ethanol can be attributed to extraction upon drug dissolution. During the extraction process the surface bound ethoxy groups are irreversibly converted to silanol group. However, it should be noted that the resonance from the methyl and methylene protons of drug lie in the same range and the contribution to these peaks cannot be neglected. Moreover, this evidence confirms the presence of mobile drug molecules within the silica gel.

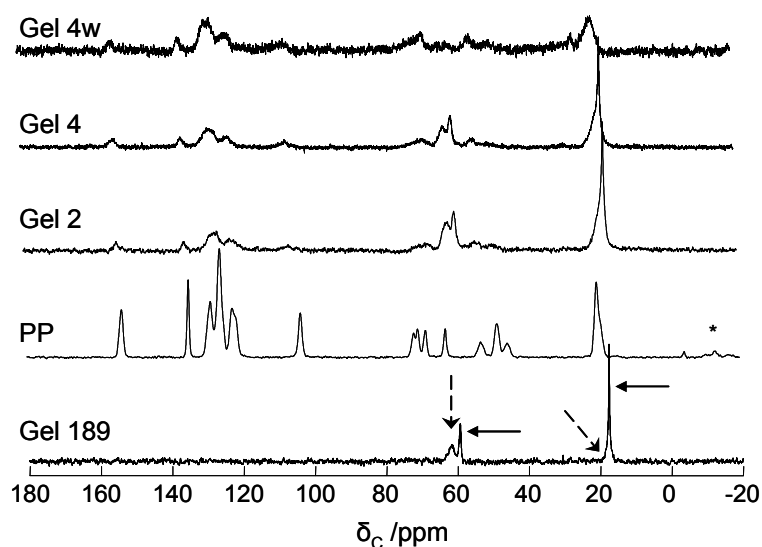


**Figure 4.1.11:**  $^{13}\text{C}\{^1\text{H}\}$  CPMAS NMR spectra of various gels and PP. Peaks from the ethanol and ethoxy group are marked with solid and broken arrows, respectively.

#### 4.1.8 Discussion

The first parameter having an influence on drug release is the synthesis pH value and a strong dependence of the release profile on the pH value was observed for TEOS gels. A fast initial release occurs for gels which were made at the higher (3.0 and above) and lower (0.5) pH values. The release parameters  $k$  and  $n$  are illustrated in Figure 4.1.12. For

the pH values in the range 1.5 to 2.0, the kinetic release parameters  $k$  and  $n$  presume a minimum and a maximum value, respectively. This corresponds to release curves with the smallest curvatures. The release curvature increases below and above this intermediate acidic pH values. The faster release from the most acidic gels (pH 0.5) is interpreted as follows. The silica gel matrix is protonated at very acidic pH values in addition to the presence of protonated PP molecules. Therefore, at pH values below 1.5, protonated Propranolol molecules would be incorporated in a protonated silica matrix, which leads to a stronger tendency for dissolution than in the pH ranges of neutral or negatively charged silica. Charge neutrality at low pH can then be rationalized by the inclusion of the desired number of counterions (e.g.,  $\text{Cl}^-$ ), resulting in a salt-in-salt inclusion model. The retarded release from the gels that are observed near the charge matching point of silica which is interpreted as follows. Gels made at pH values close to 2.0 show no sorption capacity, although they have released an appreciable amount of drug during the 24 h of extraction process. This is a clear indication that the pores formed at these pH values are much smaller after release than before. This observation is also supported by the diffusion controlled release mechanism indicated by the parameter  $n$  (value close to 0.43). At higher pH values, larger pores are formed, which also facilitates faster release. Similar observations are reported in the literature.<sup>148</sup> Figure 4.1.13 illustrates the pH regimes in which porous silica gels can be formed. To summarize, larger pores and faster release times are observed for TEOS gels prepared at weakly acidic pH values whereas, slower drug release kinetics are found at charge matching pH values.

At this point, it is impossible to predict the role of drug molecules in the evolution of silica networks. One important unanswered question is exactly what silica species are present during the formation of silica gels and what is the role of drug molecules in the nucleation of the porous structure. It is important to know the structure of the silica species present before and after drug extraction for tailor-made property achievements. These issues will be discussed in the context of hybrid gels.

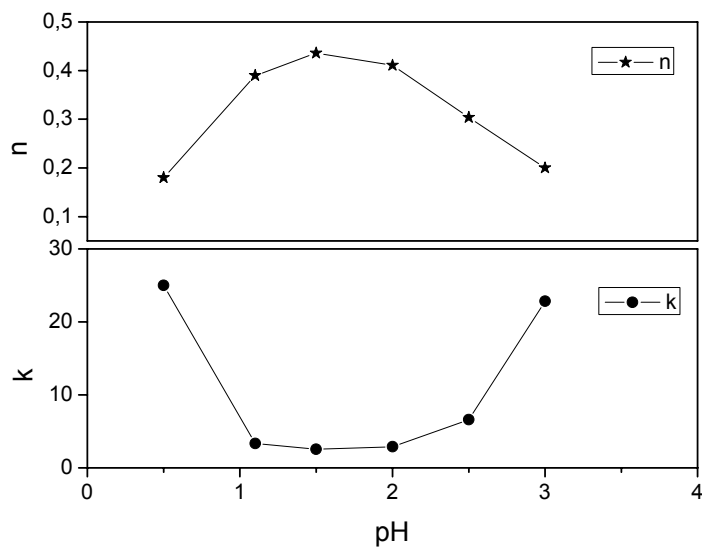


**Figure 4.1.12:** pH dependence of kinetic release parameters of TEOS based silica gels.

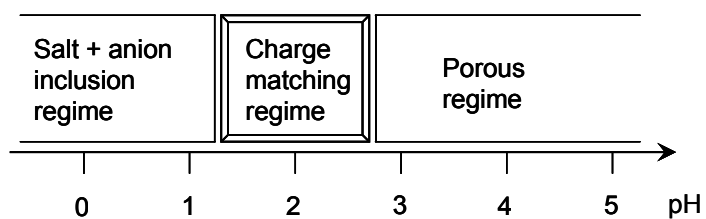


**Figure 4.1.13:** A model representing the pH ranges in which different silica gels can be formed.

## 4.2 EISA gel formulations from two precursors

### Introduction

The drug release studies from TEOS gels shown that a faster release times for gels prepared at weakly acidic as well as highly acidic conditions whereas, retarded release kinetics at charge matching pH values. The N<sub>2</sub> sorption studies shown that microporous network was formed for gels prepared at higher synthesis pH conditions. This shows that the gel network and pore structure are influenced by self-assembly with the drug molecule in the course of matrix genesis. However, tailor made controlled release kinetics and pore architectures cannot be achieved without the functionalization of silica gel. To this end, the introductions of organic functional have been proposed for a better control of the final properties and application of silica gel. The question whether better control can be achieved by the introduction of either hydrophobic/hydrophilic or aromatic substitution is studied next. The chapter is divided into different sections depending on the nature of ternary monomer precursors such as hydrophilic, hydrophobic and aromatic precursors. The drug release experiments, SEM and matrix porosities are discussed in detail and the different solid state NMR studies are given in the appendix.

### 4.2.1 Hydrophobic Precursors

#### Preparation

The hybrid MTS Gel 37 with pH 1.8 was prepared by mixing TEOS, MTS, H<sub>2</sub>O, Ethanol, PP and HCl in the molar ratio 1.0 : 0.33 : 6.53 : 2.6 : 0.039 : 0.013. In a typical synthesis, PP was dissolved in a mixture of water and ethanol; to this solution TEOS and MTS was added. The solution was stirred while adding 0.5 M HCl till the hydrolysis was complete. The sol was allowed to stir for 24 h and after that subjected to evaporation induced self assembly (EISA) at 323 K. The silica sols with high pH were prepared by two-step catalysis with aqueous HCl and aqueous NH<sub>3</sub>. The final pH of the sol after hydrolysis was controlled by the addition of aqueous NH<sub>3</sub>. The compositions for MTS, ETS and PTS gels are given in Table 4.5, 4.6 and 4.7, respectively. The polymerized silica gels were dried at 323 K for constant weight. All gels were treated in a ballmill for

3 min at 200 rpm to obtain a similar particle size distribution. The drug loads in these gels are between around 10 wt% unless otherwise specified.

**Table 4.5:** Relative molar ratios, pH and stirring time ( $t_s$ ) for hybrid MTS gel formulations

Gel	Name	TEOS	MTS	H <sub>2</sub> O	Ethanol	HCl	PP	$t_s$ (h)/pH
Gel 37	MTS <sub>37</sub> (3:1,1.8)	1	0.33	6.53	2.6	0.013	0.039	24 / 1.8
Gel 38	MTS <sub>38</sub> (3:1,1.8)	1	0.33	6.53	2.6	0.013	0.079	24 / 1.8
Gel 39	MTS <sub>39</sub> (3:1,1.8)	1	0.33	6.53	2.6	0.013	0.117	24 / 1.8
Gel 40	MTS <sub>40</sub> (3:1,1.8)	1	0.33	6.53	2.6	0.013	0.019	24 / 1.8
Gel 41	MTS <sub>41</sub> (3:1,1.8)	1	0.33	2.61	2.6	0.0026	0.039	24 / 1.8
Gel 42	MTS <sub>42</sub> (3:1,1.8)	1	0.33	13.07	2.6	0.039	0.039	24 / 1.8
Gel 43	MTS <sub>43</sub> (3:1,1.8)	1	0.33	26.13	2.6	0.052	0.039	24 / 1.8
Gel 70	MTS <sub>70</sub> (1:1,0.6)	1	1.00	9.79	3.90	0.0039	0.058	24 / 0.6
Gel 71	MTS <sub>71</sub> (3:1,0.6)	1	0.33	6.53	2.60	0.0026	0.039	24 / 0.6
Gel 72	MTS <sub>72</sub> (5:1,0.6)	1	0.20	5.88	2.34	0.0024	0.035	24 / 0.6
Gel 74	MTS <sub>74</sub> (3:1,0.6)	1	0.33	6.53	2.60	0.0026	0	24 / 0.6
Gel 177	MTS <sub>177</sub> (3:1,2.2)	1	0.33	6.53	2.60	0.0026	0.039	24 / 2.2
Gel 178	MTS <sub>178</sub> (5:1,2.2)	1	0.20	5.88	2.34	0.0023	0.035	24 / 2.2
Gel 179	MTS <sub>179</sub> (1:1,2.2)	1	1.00	9.79	3.90	0.0039	0.058	24 / 2.2
Gel A40	MTS <sub>A40</sub> (1:1,2.4)	1	1.00	9.79	3.90	0.0039	0.058	24 / 2.4
Gel A41	MTS <sub>A41</sub> (3:1,2.4)	1	0.33	6.53	2.60	0.0026	0.039	24 / 2.4
Gel A42	MTS <sub>A42</sub> (5:1,2.4)	1	0.20	5.88	2.34	0.0047	0.029	24 / 2.4
Gel A28	MTS <sub>A28</sub> (3:1,3.0)	1	0.33	6.53	2.60	0.0026	0.039	24 / 3.0
Gel A29	MTS <sub>A29</sub> (3:1,5.0)	1	0.33	6.53	2.60	0.0026	0.039	24 / 5.0
Gel A30	MTS <sub>A30</sub> (3:1,7.0)	1	0.33	6.53	2.60	0.0026	0.039	24 / 7.0
Gel A17	MTS <sub>A17</sub> (7:1,1.8)	1	0.14	5.60	2.23	0.0045	0.028	24 / 1.8

**Table 4.6:** Relative molar ratios, pH and stirring time ( $t_s$ ) for hybrid ETS gel formulations

Gel	Name	TEOS	ETS	H <sub>2</sub> O	Ethanol	HCl	PP	$t_s$ (h)/pH
Gel 80	ETS <sub>80</sub> (1:1,1.2)	1	1.00	9.79	3.90	0.0039	0.058	24 / 1.2
Gel 81	ETS <sub>81</sub> (3:1,1.2)	1	0.33	6.53	2.60	0.0026	0.039	24 / 1.2
Gel 82	ETS <sub>82</sub> (5:1,1.2)	1	0.20	5.88	2.34	0.0024	0.035	24 / 1.2
Gel 83	ETS <sub>83</sub> (10:1,1.2)	1	0.10	5.39	2.14	0.0022	0.032	24 / 1.2
Gel 165	ETS <sub>165</sub> (3:1,0.5)	1	0.33	6.53	2.60	0.0956	0.039	24 / 0.5
Gel 166	ETS <sub>166</sub> (5:1,0.5)	1	0.20	5.88	2.34	0.0861	0.035	24 / 0.5
Gel 180	ETS <sub>180</sub> (3:1,2.2)	1	0.33	6.53	2.60	0.0026	0.039	24 / 2.2
Gel 181	ETS <sub>181</sub> (5:1,2.2)	1	0.20	5.88	2.34	0.0023	0.035	24 / 2.2

**Table 4.7:** Relative molar ratios, pH and stirring time ( $t_s$ ) for hybrid PTS gel formulations

Gel	Name	TEOS	PTS	H <sub>2</sub> O	Ethanol	HCl	PP	$t_s$ (h)/pH
Gel 7	PTS <sub>7</sub> (5:1,1.9)	1	0.20	5.88	2.34	0.0023	0.035	24 / 1.9
Gel 8	PTS <sub>8</sub> (10:1,1.9)	1	0.10	5.39	2.14	0.0022	0	24 / 1.9
Gel 15	PTS <sub>15</sub> (7:1,1.9)	1	0.14	5.60	2.23	0.0022	0.033	24 / 1.9
Gel 75	PTS <sub>75</sub> (1:1,0.5)	1	1.00	9.79	3.90	0.0955	0.058	24 / 0.5
Gel 76	PTS <sub>76</sub> (3:1,0.5)	1	0.33	6.53	2.60	0.0637	0.039	24 / 0.5
Gel 77	PTS <sub>77</sub> (5:1,0.5)	1	0.20	5.88	2.34	0.0574	0.035	24 / 0.5
Gel 78	PTS <sub>78</sub> (10:1,0.5)	1	0.10	5.39	2.14	0.0523	0.032	24 / 0.5
Gel 79	PTS <sub>79</sub> (3:1,0.5)	1	0.33	6.53	2.60	0.0637	0	24 / 0.5
Gel 301	PTS <sub>301</sub> (3:1,1.3)	1	0.33	6.51	2.60	0.0078	0.039	24 / 1.3
Gel 302	PTS <sub>302</sub> (10:1,1.3)	1	0.10	5.39	2.14	0.0065	0.032	24 / 1.3
Gel 303	PTS <sub>303</sub> (3:1,2.3)	1	0.33	6.51	2.60	0.0026	0.039	24 / 2.3
Gel 304	PTS <sub>304</sub> (10:1,2.3)	1	0.10	5.39	2.14	0.0021	0.032	24 / 2.3
Gel 305	PTS <sub>305</sub> (3:1,4.0)	1	0.33	6.51	2.60	0.0026	0.039	24 / 4.0
Gel 306	PTS <sub>306</sub> (10:1,4.0)	1	0.10	5.39	2.14	0.0021	0.032	24 / 4.0

### Influence of drug loading and H<sub>2</sub>O/Si ratio ( $r$ )

The release profiles of Propranolol from hybrid silica gels prepared under different drug loading is shown in Figure 4.2.1. Propranolol release was increased during the first hours with higher drug loading in the hybrid gel. The burst effect was stronger for drug loading with 20 wt% and higher. The number of protonated Propranolol species per unit area is higher with higher loading. Larger loading of PP will create repulsive forces within the surface, where the drug molecules are weakly bound, thus resulting in a faster release.

The effect of water/Si molar ratio ( $r$ ) on the release rate of PP was studied on gels synthesized at pH 1.8 (Figure 4.2.2). Decreasing the molar ratios of water to Si from  $r = 20$  to  $r = 6$  also decreased the release rate of PP. The release kinetics parameter,  $k$  and  $n$



(inset of Figure 4.2.2), deviated from the diffusion controlled process, when the water/Si ratio of silica sol was increased to  $r = 20$ .

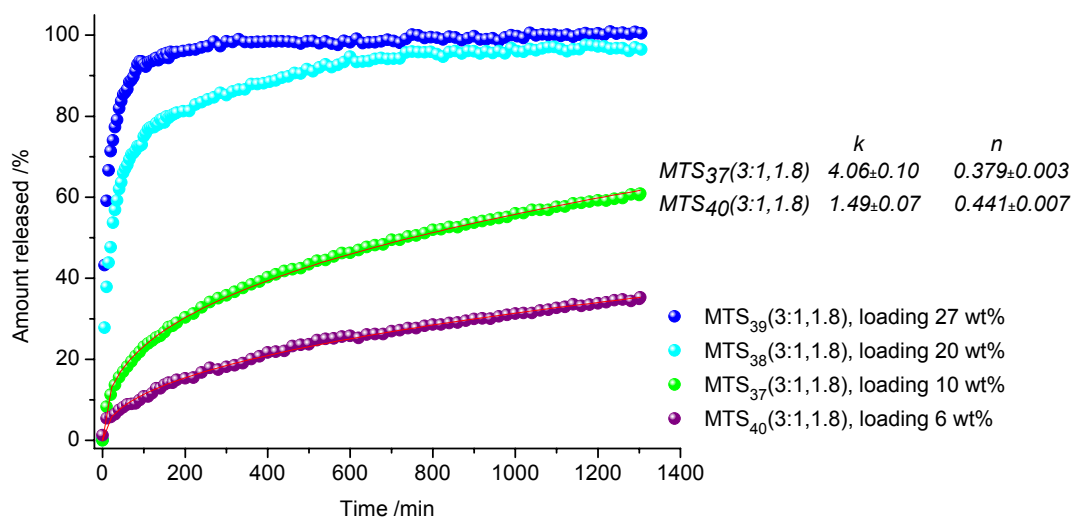


**Figure 4.2.1:** Release profiles of Propranolol from hybrid silica gels with different drug loading.

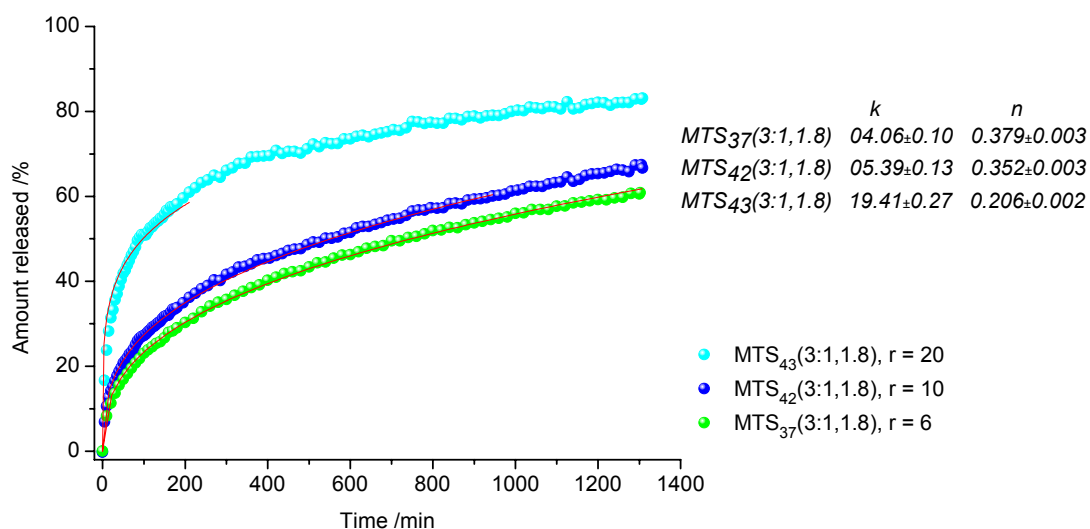


**Figure 4.2.2:** Release profiles of Propranolol from hybrid silica gels with different  $r$  values.

### Influence of pH

The effect of synthesis pH on the release rate of PP has been studied by varying the pH of the hybrid silica sol, Figure 4.2.3. Hybrid silica gels made at different pH values from

0.6 to 5.0 in the presence of PP, show strong pH dependence on release kinetics. Around 96% of the drug was released within 22 hours for gels synthesized at pH 0.6 and 5.0, whereas only 40 % released for the same period for gel synthesized at pH 2.4. As discussed in section 4.1.8, similar behavior was observed for methyl substituted hybrid gels.

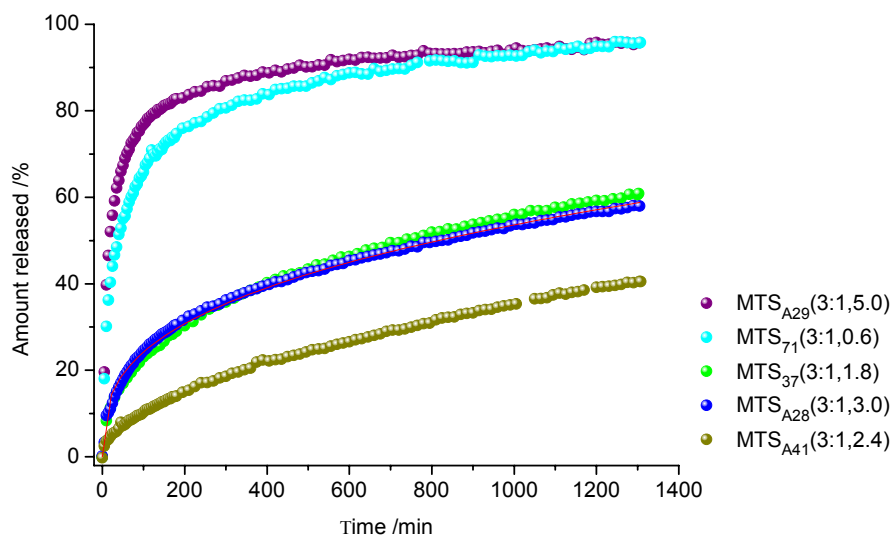


**Figure 4.2.3:** Release profiles of Propranolol from hybrid MTS silica gels with different synthesis pH.

**Table 4.8:** Kinetic release parameters of various MTS gels.

	$k$	$n$
$MTS_{37}(3:1,1.8)$	$4.06 \pm 0.10$	$0.379 \pm 0.003$
$MTS_{A28}(3:1,3.0)$	$4.95 \pm 0.09$	$0.345 \pm 0.003$
$MTS_{A41}(3:1,2.4)$	$0.90 \pm 0.07$	$0.531 \pm 0.012$

The influence of pH on the hydrophobic gels synthesized with longer alkyl chains has also been studied, Figure 4.2.4 and 4.2.5. ETS hybrid silica gels made at different pH values of 0.5 and 2.2 in the presence of PP, show strong pH dependence on release kinetics (Figure 4.2.4). Around 80% of the drug was released within 22 hours for gels synthesized at pH 0.5, whereas only below 65 % released for the same period for gel synthesized at pH 2.2. At pH = 0.5, the initial burst was accounted for approximately 60%. When the synthesis pH was very acidic, 0.5, the influence of ethyl groups on the hybrid gel was diminished and shows close to analogous release curves. A very strong composition effect was observed at a pH value close to the charge matching point for

PTS hybrid gels (Figure 4.2.5). This could be an effect from the hydrophobic nature of the propyl groups, which are on the surface of the gel particles and prevent the dissolution of the drug. Hybrid PTS silica gels made at different pH values from 1.3 to 4.0 in the presence of PP, show pH dependence on release kinetics, especially when the PTS substitution in the hybrid gel was 25 mol%. Due to the presence of propyl groups on the surface of the pores, the gel particles are hydrophobic. The poor wetting prevents water diffusion and the solvent's ability to dissolve the drug molecules from the pores. The release parameters  $k$  and  $n$  presume a minimum and a maximum value, respectively at pH close to 2.4 as shown in Table 4.9.

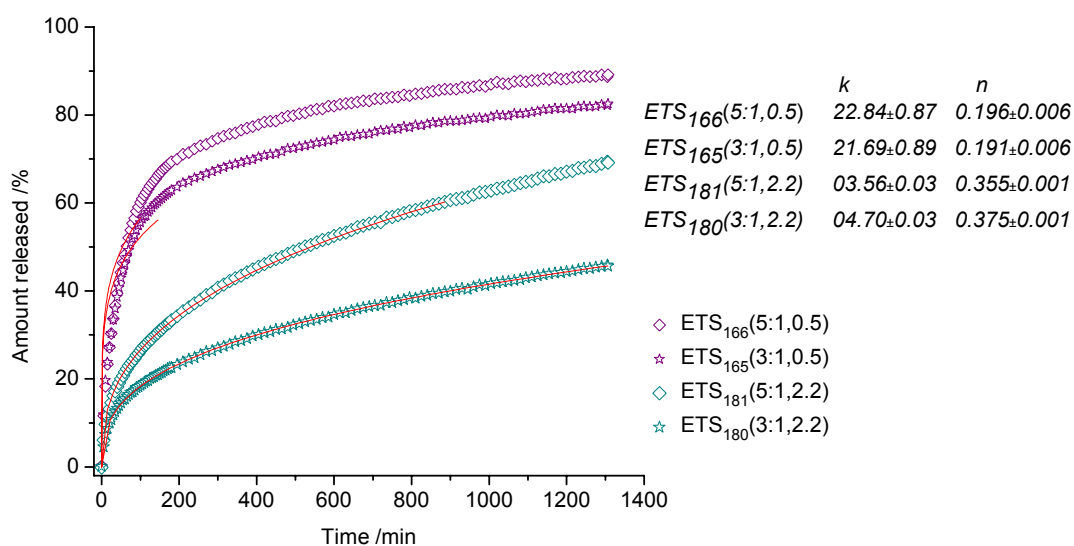


**Figure 4.2.4:** Release profiles of Propranolol from hybrid ETS silica gels with different synthesis pH.

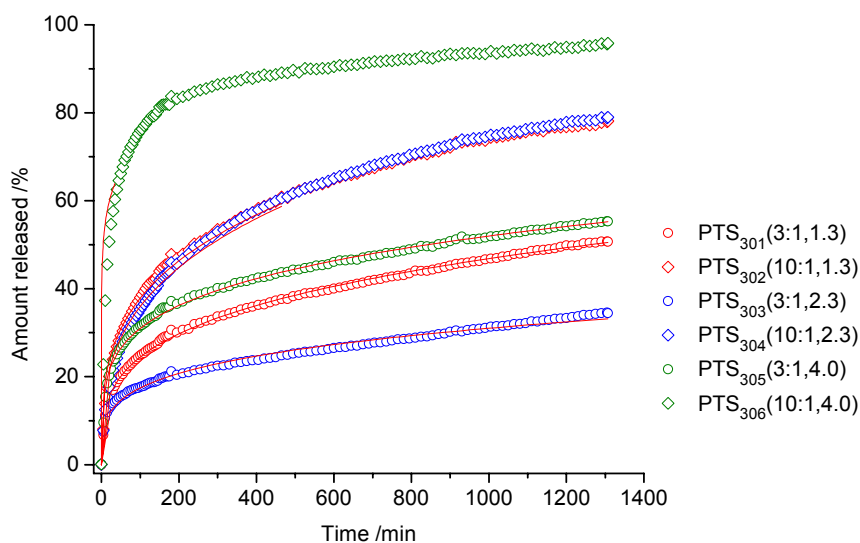


**Figure 4.2.5:** Release profiles of Propranolol from hybrid PTS silica gels with different synthesis pH.

**Table 4.9:** Kinetic release parameters of various PTS gels.

	$k$	$n$
$PTS_{301}(3:1,1.3)$	$06.66\pm0.27$	$0.282\pm0.006$
$PTS_{302}(10:1,1.3)$	$09.80\pm0.25$	$0.293\pm0.004$
$PTS_{303}(3:1,2.3)$	$05.54\pm0.31$	$0.249\pm0.008$
$PTS_{304}(10:1,2.3)$	$08.22\pm0.22$	$0.320\pm0.004$
$PTS_{305}(3:1,4.0)$	$10.98\pm0.35$	$0.224\pm0.005$
$PTS_{306}(10:1,4.0)$	$41.67\pm0.57$	$0.120\pm0.002$

### Influence of composition

The release profiles of gels made with different TEOS:MTS ratios and are compared in Figure 4.2.6. A high level of MTS in the hybrid gel leads to a decrease in the drug release. When the synthesis pH is very acidic, 0.6, the influence of MTS in the hybrid gel is diminished and shows analogous release curves. Due to the presence of methyl groups in the surface, the gel particle are hydrophobic in character and the solvent's ability to dissolve the drug molecule from the pores decreases with increase in the MTS level. At the very acidic pH, the hydrophobic effect is masked by the salt-like character of the system.

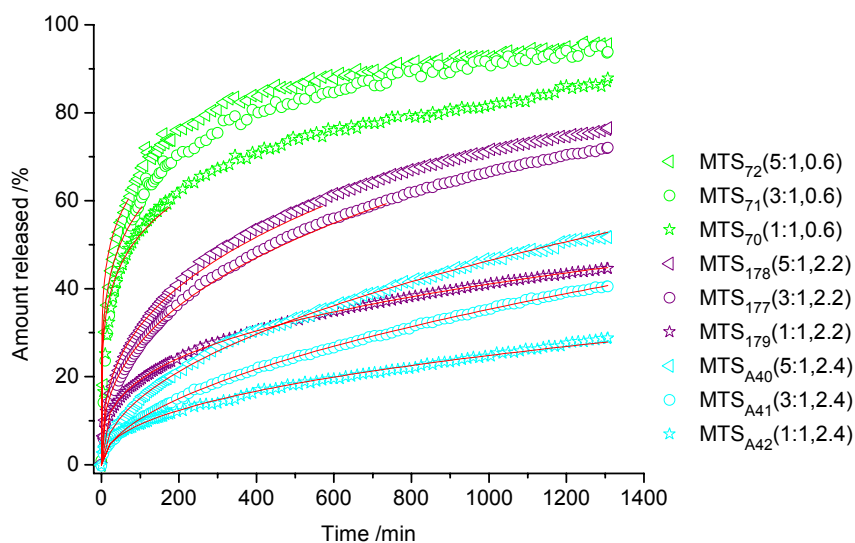


**Figure 4.2.6:** Release profiles of Propranolol from hybrid silica gels with different composition.

**Table 4.10:** Kinetic release parameters of various gels.

	$k$	$n$
MTS <sub>72</sub> (5:1,0.6)	29.45±0.43	0.169±0.002
MTS <sub>71</sub> (3:1,0.6)	22.74±0.37	0.203±0.002
MTS <sub>70</sub> (1:1,0.6)	20.60±0.37	0.202±0.002
MTS <sub>178</sub> (5:1,2.2)	06.10±0.17	0.356±0.004
MTS <sub>177</sub> (3:1,2.2)	04.79±0.15	0.380±0.005
MTS <sub>179</sub> (1:1,2.2)	04.26±0.20	0.328±0.007
MTS <sub>A40</sub> (5:1,2.4)	01.24±0.12	0.433±0.014
MTS <sub>A41</sub> (3:1,2.4)	00.90±0.07	0.531±0.012
MTS <sub>A42</sub> (1:1,2.4)	01.60±0.09	0.487±0.008

The influence of composition on the hydrophobic gels synthesized with longer alkyl chains has also been studied, Figure 4.2.7 and 4.2.8. The release profiles of gels made with different TEOS:ETS ratios are compared in Figure 4.2.7. The hybrid ETS gels were synthesized at a pH value 1.2 and a strong compositional influence is visible. A high level of ETS in the hybrid gel tends to slow down the drug release. This observation is analogous to the MTS gel and attributed to the hydrophobic effect of the alkyl chains. Close to diffusion controlled drug release was observed in all ETS gels. The effect of PTS composition on the release rate of PP has also been studied by varying the composition ratios in silica sol, Figure 4.2.8. A high level of PTS in the hybrid gel also leads to a decrease in the drug release. While the PTS substitution in the hybrid gel was less than 25 mol% (Gel 77 and 78), its influence in the release profile was lower at pH

0.5 (Figure 4.2.8). When the composition is 1:1, close to zero order type release ( $n = 0.91$ ) was achieved up to 20 % within 22 hours (Gel 75).

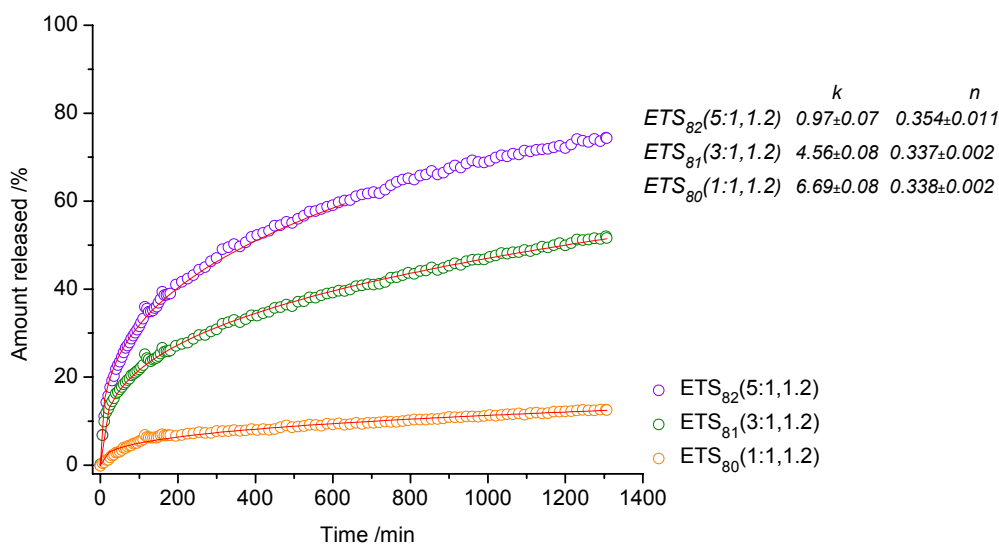


**Figure 4.2.7:** Release profiles of Propranolol from hybrid silica gels with different TEOS:ETS ratio.

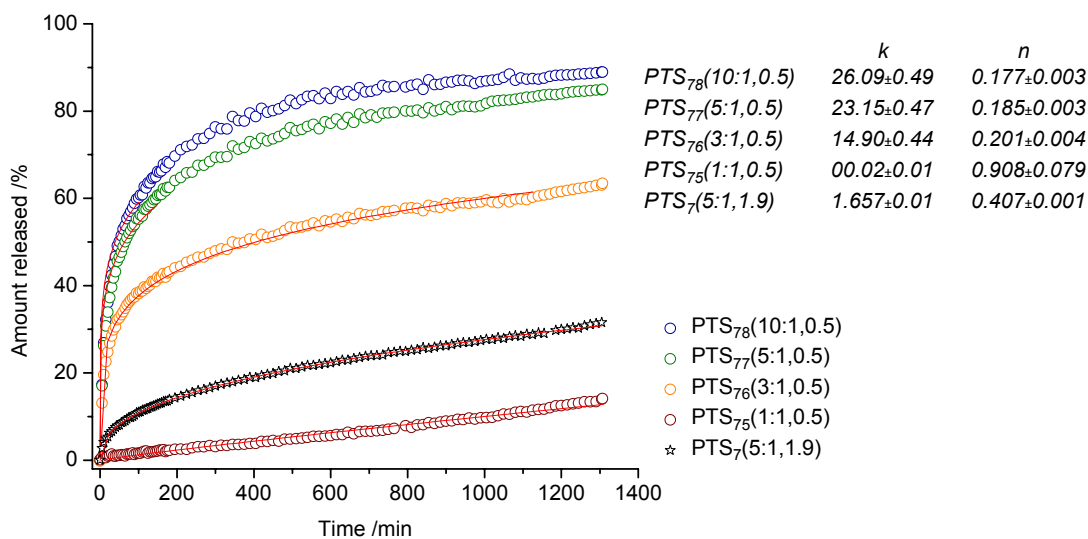


**Figure 4.2.8:** Release profiles of Propranolol from hybrid silica gels with different TEOS:PTS ratio (pH 0.5).

## N<sub>2</sub> Sorption studies

The N<sub>2</sub> sorption isotherms of hybrid gels, which are prepared in the presence of different amounts of drug, are shown in Figure 4.2.9. Drug loaded gels show no porosity before

release. Although the gels released considerable amounts of drug within 24 h, only gels with 20 and 27 wt% drug loading show higher surface area after release. Even near to charge matching point, porous silica structures can be formed and use of higher drug loading causes significant increase in the porosity of gels. The  $N_2$  sorption isotherm of the extracted gels is of type I, characteristic for microporous materials. Pore volumes for drug extracted gels are analyzed by using the Horvath-Kawazoe method and specific surface areas are given from BET analysis (Table 4.11). The DRT studies confirm that almost all loaded drug molecules are released within 22 hours for higher loaded gels (e.g. Gel 38 and 39) whereas only less than 60% release for other gels (e.g. Gel 37 and 40). Therefore, 100% of the microporous sites of the extracted gels are accessible to  $N_2$  for higher loaded gels, but only less than 60% for the lower loaded gels.

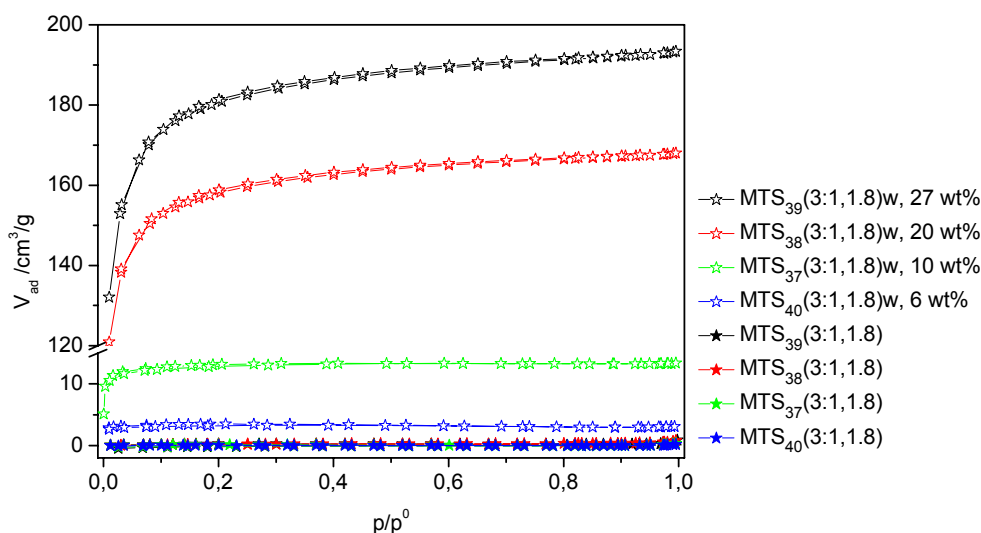


**Figure 4.2.9:**  $N_2$  sorption isotherm of various drug loaded hybrid gels prepared at pH 1.8, before and after drug extraction for 24 h (marked with w).

**Table 4.11:** Surface area and pore volumes for drug loaded and extracted gels.

sample	drug loading /wt%	BET surface area /m <sup>2</sup> /g		pore volume after drug release /cm <sup>3</sup> /g
		before drug release	after drug release	
<i>MTS</i> <sub>39</sub> (3:1,1.8)	27	< 2	612	0.299
<i>MTS</i> <sub>38</sub> (3:1,1.8)	20	< 2	535	0.260
<i>MTS</i> <sub>37</sub> (3:1,1.8)	10	< 2	43	0.021
<i>MTS</i> <sub>40</sub> (3:1,1.8)	6	< 2	15	0.005

The  $N_2$  sorption studies have been extended to investigate the effect of treatment with the dissolution medium on the porosity of hybrid MTS gels. Figure 4.2.10 shows the  $N_2$  sorption isotherms of various gels prepared in the presence (Gel 71) and absence (Gel 74) of drug. In Table 4.12, the surface area and pore volume for Gel 71 and 74 are compared. The gel prepared in the absence of drug is microporous with BET surface area  $494 \text{ m}^2/\text{g}$  whereas the drug loaded gel is nonporous. After treating both gels under similar dissolution conditions, isotherms were measured. Porosity increases for the drug extracted Gel 71 whereas porosity decreased for the unloaded Gel 74. This simple comparison of the porosity development of a loaded and unloaded gel shows that pore volume is generated upon drug release by emptying internal void space and not by swelling of the material.

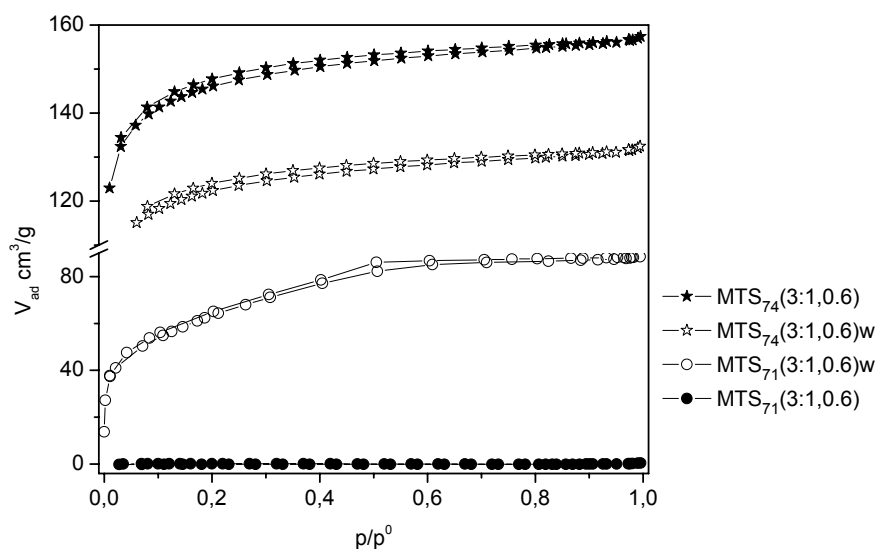


**Figure 4.2.10:**  $N_2$  sorption isotherms of various gels prepared at pH 0.6, in the presence (Gel 71) and absence (Gel 74) of drug. Washed gels are marked with w.

**Table 4.12:** Surface area and pore volumes for various drug loaded and extracted gels

Sample	drug loading /wt%	BET surface area / $\text{m}^2/\text{g}$		pore volume after drug release / $\text{cm}^3/\text{g}$
		before drug release	after drug release	
$MTS_{71}(3:1,0.6)$	10	< 2	229	0.137
$MTS_{74}(3:1,0.6)^*$	0	494	413	0.205

\* Gel 74 was treated with similar dissolution conditions.



Figure 4.2.11 shows the  $N_2$  sorption isotherms of various drug extracted gels prepared at different synthesis pH. The BET surface area and pore volume are given in Table 4.10. The observations from sorption experiments are matching with the DRT measurements which support the formation of porous structures after drug extraction at the lower and higher pH ranges. About 96 % drug was released from Gel A29 whereas only less than 40 % release for Gel A41 for the 22 h DRT study. The porosity development after the extraction is directly related to the total amount drug release. There is no gel structure shrinking upon drug release observed for MTS substituted hybrid gels whereas structure shrinking was observed for TEOS gels as reported in the literature.<sup>58</sup>

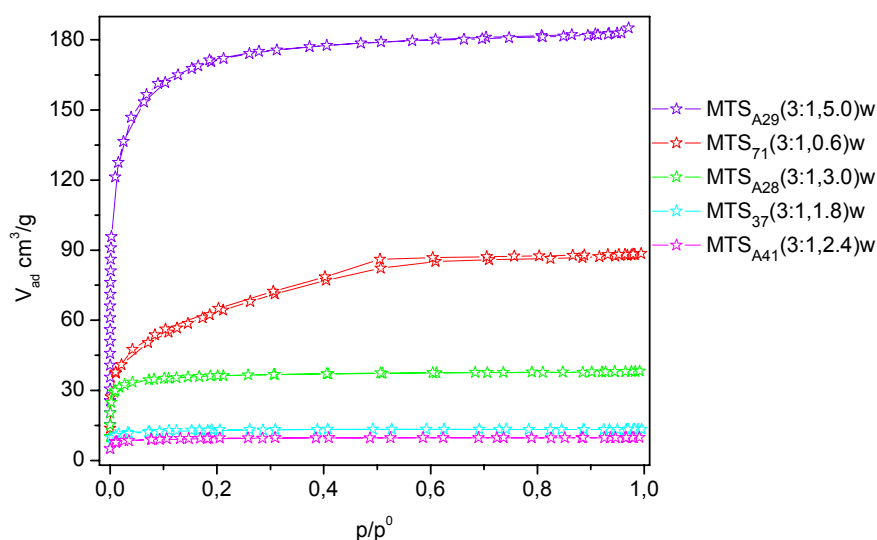


**Figure 4.2.11:**  $N_2$  sorption isotherms of various drug extracted gels prepared at different pH.

**Table 4.13:** Surface area and pore volumes for various drug extracted gels synthesized at different pH values.

sample	gel synthesis pH	BET surface area / $m^2/g$	pore volume after drug release / $cm^3/g$
		after drug release	
$MTS_{71}(3:1,0.6)w$	0.6	229	0.137
$MTS_{37}(3:1,1.8)w$	1.8	43	0.021
$MTS_{A41}(3:1,2.4)w$	2.4	32	0.015
$MTS_{A28}(3:1,3.0)w$	3.0	120	0.059
$MTS_{A29}(3:1,5.0)w$	5.0	581	0.286

The drug loaded ETS (Figure 4.2.12) and PTS (Figure 4.2.13) gels show no porosity whereas the drug extracted gels are microporous. There was no porosity observed for

drug extracted Gel 75w. According to the DRT profile only 20% of the drug was released within 22 hours of dissolution. This could be a reason for non porous nature of Gel 75w. The hybrid PTS gel synthesized at higher pH values show porosity which is also in support of the observation from pure TEOS gels. Gel 306 with a TEOS:PTS ratio 10:1 shows porosity before and after drug release. Gel 306 was synthesized at pH value of 4.0 has a surface area of 40 and 403  $\text{m}^2/\text{g}$  before and after drug release, respectively.

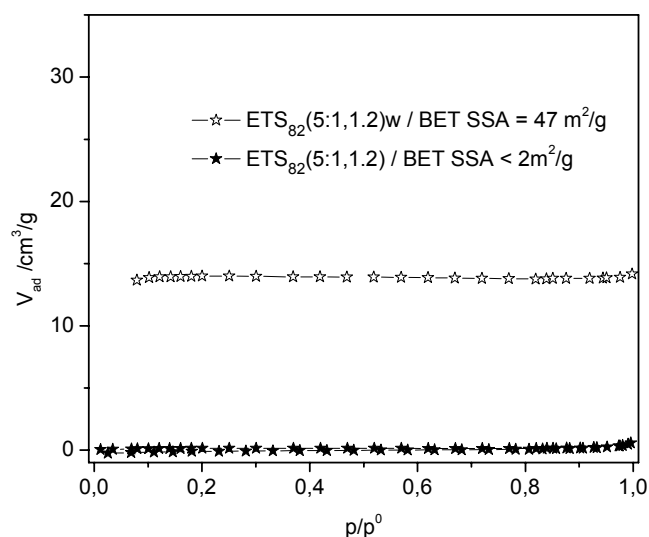


**Figure 4.2.12:**  $N_2$  sorption isotherm of drug loaded hybrid ETS Gel82, before and after drug extraction (marked with w).

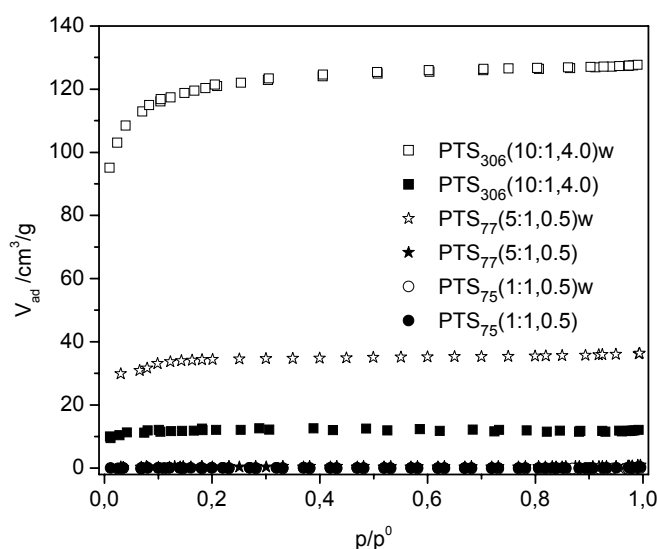


**Figure 4.2.13:**  $N_2$  sorption isotherm of various drug loaded hybrid PTS gels, before and after drug extraction (marked with w).

## <sup>29</sup>Si MAS NMR studies

Various hybrid gel samples were examined using <sup>29</sup>Si MAS NMR spectroscopy (Figure 4.2.14). The studies on gels have been carried out in order to understand the silicon atom connectivity in the gel network. The peak around -54 ppm is attributed to silicon atom that have one hydroxyl group and methyl group attached, (Si-O)<sub>2</sub>(CH<sub>3</sub>)Si(OH), often referred as T<sup>2</sup> silicons. The resonance at -63 ppm is due to silicons with methyl carbon directly bound to silicon (Si-O)<sub>3</sub>Si-CH<sub>3</sub> often referred as T<sup>3</sup> sites and does not have hydroxyl group. The Q<sup>4</sup>, Q<sup>3</sup> and Q<sup>2</sup> sites are appearing at chemical shift close to -109, -100 and -91 ppm, respectively.

The influence of synthesis pH on the final gel status has been studied (Figure 4.2.14). From Table 4.14, the deconvoluted peak areas, the ratios of siloxane to silanol sites  $[(T^3+Q^4)/(T^2+Q^3+Q^2)]$  are lowest at pH 2.4. This observation gives an insight into the drug-matrix interactions which will be discussed later. A comparison of drug extracted gels is shown in Figure 4.2.15 and Table 4.15. The ratios of siloxane to silanol sites  $[(T^3+Q^4)/(T^2+Q^3+Q^2)]$  for drug loaded and extracted gels are 0.68 and 2.4 (pH 2.4) and 1.45 and 1.07 (pH 1.8), respectively. The ratio has increased by a factor of 3.5 in the case of pH 2.4, but decreased by a factor of 0.73 at pH 1.8, for extracted gels. To summarize, more condensed gel networks are formed during the drug extraction period for gels prepared at pH close to charge matching point. This observation is also supported by the retarded drug release shown in the DRT profile of gel prepared at pH 2.4. When the synthesis pH is around 5 (Gel A29), more porous networks are formed (as seen from the N<sub>2</sub> isotherms) with less population of silanol sites compared to siloxane sites (as seen from Table 4.11) and faster drug release.

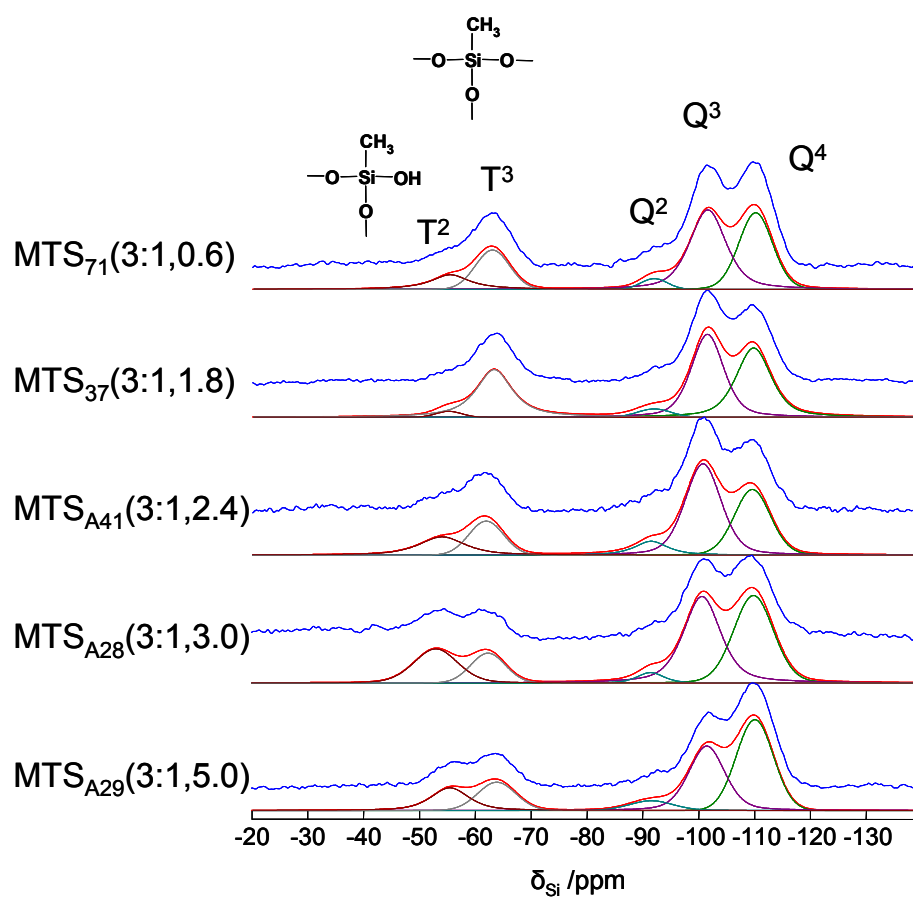


**Figure 4.2.14:**  $^{29}\text{Si}$  MAS NMR spectra of hybrid MTS gels synthesized at different pH values. Each set of spectra includes experimental spectrum (in blue) and the simulated spectrum (in red) with individual contributions from each silicon site.

**Table 4.14:** Peak area derived for deconvoluted peaks of the  $^{29}\text{Si}$  MAS spectra of hybrid MTS gels.

Probe	pH	T <sup>2</sup> /%	T <sup>3</sup> /%	Q <sup>2</sup> /%	Q <sup>3</sup> /%	Q <sup>4</sup> /%	Σ T /%	Σ Q /%
MTS <sub>71</sub> (3:1,0.6)	0.6	9	16	3	41	31	25	75
MTS <sub>37</sub> (3:1,1.8)	1.8	2	25	4	36	33	27	73
MTS <sub>A41</sub> (3:1,2.4)	2.4	12	13	7	41	27	25	75
MTS <sub>A28</sub> (3:1,3.0)	3.0	15	10	3	37	35	25	75
MTS <sub>A29</sub> (3:1,5.0)	5.0	12	13	5	30	40	25	75

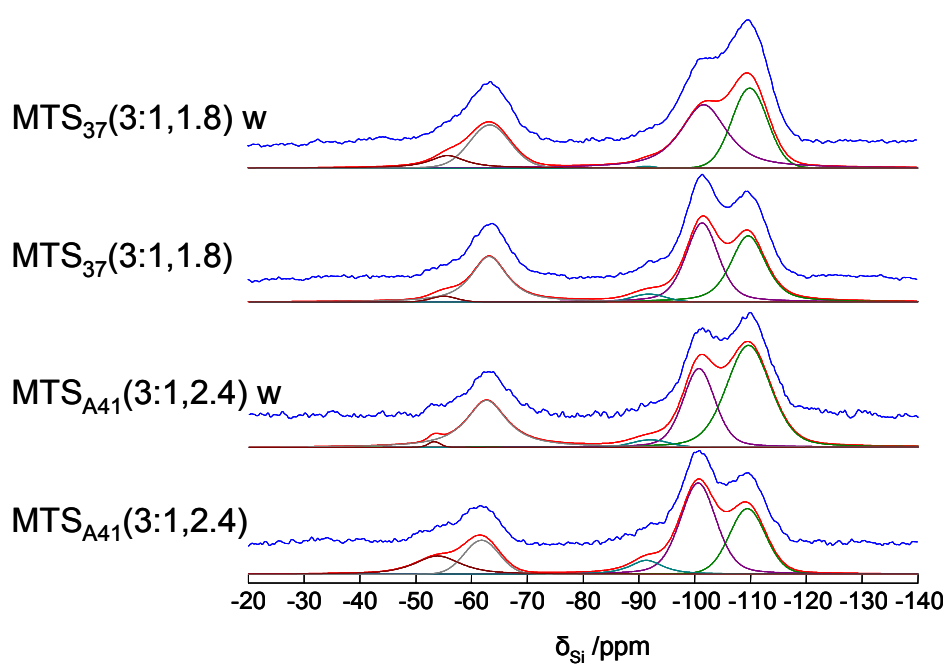


**Figure 4.2.15:**  $^{29}\text{Si}$  MAS NMR spectra of hybrid MTS gels before and after extraction of drug. Each set of spectra includes experimental spectrum (in blue) and the simulated spectrum (in red) with individual contributions from each silicon site.

**Table 4.15:** Peak area derived for deconvoluted peaks of the  $^{29}\text{Si}$  MAS spectra of hybrid MTS gels

Probe	pH	T <sup>2</sup> /%	T <sup>3</sup> /%	Q <sup>2</sup> /%	Q <sup>3</sup> /%	Q <sup>4</sup> /%	Σ T /%	Σ Q /%
MTS <sub>37</sub> (3:1,1.8)w	1.8	7	20	1	41	31	27	73
MTS <sub>37</sub> (3:1,1.8)	1.8	2	26	3	36	33	28	72
MTS <sub>A41</sub> (3:1,2.4)w	2.4	1	24	3	26	46	25	75
MTS <sub>A41</sub> (3:1,2.4)	2.4	12	13	7	41	27	25	75

### $^1\text{H}$ MAS NMR studies

Several  $^1\text{H}$  MAS NMR studies has been performed to probe the proton sources in the hybrid MTS silica gels and to differentiate between encapsulated drug molecules and solvents. The proton NMR spectra of a hybrid gel prepared in the presence (Gel 71) and absence (Gel 74) of the drug is shown in Figure 4.2.16. The peak at around 0.3 ppm is due to the methyl protons of the matrix. Rests of the resonances found are similar to the TEOS gels as discussed in section 4.1.6. The assignment of water peak and ethanol peak are also supported by the absence of the resonances in the spectrum of high temperature treated gels. The assignments are further corroborated by high resolution NMR studies discussed in the later chapter. Besides that, the observed broadening on the peaks in Gel 71 is due to the chemical shift distribution from the drug molecules. The broadening in the spectrum of Gel 71 treated at 393 K compared to Gel 74 treated at 393 K indicates that the PP molecules confined in the pores interact with the matrix, thus reducing their mobility.

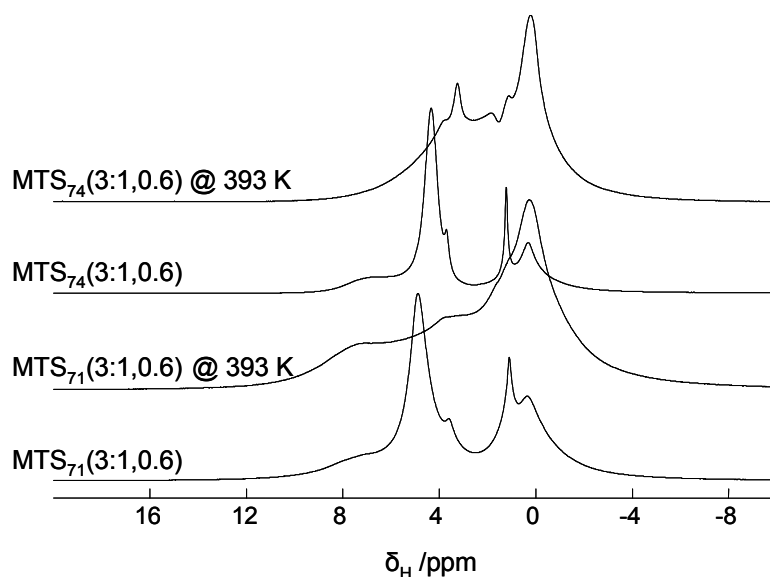


**Figure 4.2.16:** The  $^1\text{H}$  MAS NMR spectra of hybrid MTS gel synthesized in the presence (Gel 71) and absence (Gel 74) of PP (MAS 15 kHz). Gels treated at 393 K are marked. Intensities are not in absolute scale.

The effect of the synthesis pH on the final hybrid gel structure has been studied using  $^1\text{H}$  MAS NMR. The  $^1\text{H}$  MAS NMR spectra of hybrid gel synthesized at different pH are presented in Figure 4.2.17. The resonances from the methyl protons of ethoxide/ethanol and the matrix (1) are identical throughout the studied pH range (Table 4.13). The contributions from the chemically bound ethoxy group and physisorbed ethanol are very small for gels prepared at pH 1.8 and 2.4, but they are found by sharp peaks (2,3) at the higher pH values of 5.0 and 7.0. Instead, hydrogen bonded silanols appear at 7.0 ppm (5) for acidic pH values (1.8 and 2.4). Another remarkable feature is the shift in the resonance of mobile water (4), to the lower shielding region for gels prepared at very low pH (0.6) and very high pH (5.0 and 7.0). This shift in the water peak can be attributed to the fact that the water molecules confined in the MTS gels are experiencing different environment at different pH values.

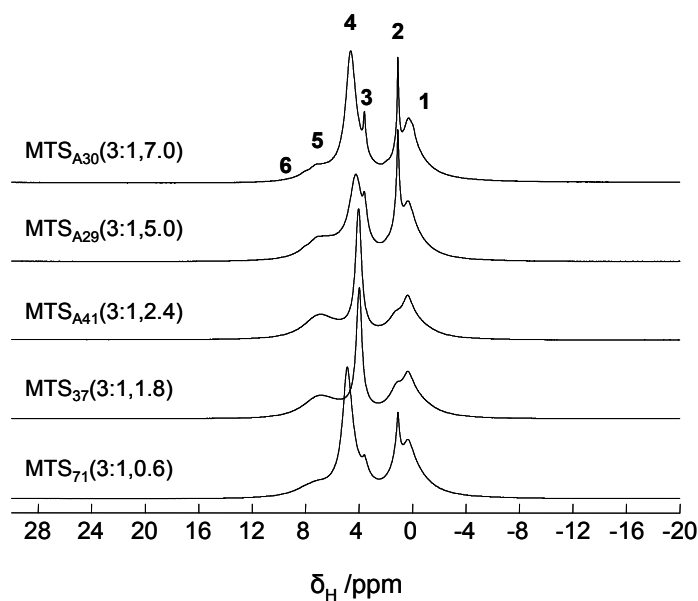


**Figure 4.2.17:** The  $^1\text{H}$  MAS NMR spectra of hybrid MTS gel synthesized at different pH. (MAS 15 kHz).

**Table 4.16:**  $^1\text{H}$  chemical shift differences as a function of pH for various hybrid gels.

Gel	pH	$^1\text{H}$ chemical shift /ppm		
		mobile $\text{H}_2\text{O}$	non-hydrogen bonded silanol	methyl protons of matrix
$\text{MTS}_{A30}(3:1,7.0)$	7.0	4.63	1.12	0.30
$\text{MTS}_{A29}(3:1,5.0)$	5.0	4.26	1.12	0.30
$\text{MTS}_{A41}(3:1,2.4)$	2.4	4.03	-	0.30
$\text{MTS}_{37}(3:1,1.8)$	1.8	3.99	-	0.30
$\text{MTS}_{71}(3:1,0.6)$	0.6	4.89	1.12	0.30

$^1\text{H}$  MAS NMR studies has been performed on longer alkyl chain hydrophobic gels and are shown in appendix. As the alkyl chain length increases, there is a restriction on the mobility in the hybrid gels observed in the proton spectra.

### $^{13}\text{C}\{^1\text{H}\}$ CPMAS NMR studies

The CPMAS NMR spectra of various hydrophobic hybrid gels prepared in the presence of PP is shown in appendix. The spectra unambiguously establish the presence of PP intact in the gels.



## 4.2.2 Hydrophilic Precursor - ATS

### Preparation

The preparations of hybrid ATS gels are similar to that of hydrophobic gels as discussed in the last section. The synthesis compositions are given in Table 4.17.

**Table 4.17:** Relative molar ratios, pH and stirring time ( $t_s$ ) for hybrid gel formulations

Gel	Name	TEOS	ATS	H <sub>2</sub> O	Ethanol	HCl	PP	$t_s$ (h)/pH
Gel A1	ATS <sub>A1</sub> (3:1,1.3)	1	0.33	13.05	5.28	0.0637	0.131	24 / 1.3
Gel A2	ATS <sub>A2</sub> (3:1,1.3)	1	0.33	13.05	5.28	0.0637	0.065	24 / 1.3
Gel A3	ATS <sub>A3</sub> (3:1,1.3)	1	0.33	13.05	5.28	0.0637	0.032	24 / 1.3
Gel A4	ATS <sub>A4</sub> (3:1,1.3)	1	0.33	13.05	5.28	0.0637	0.013	24 / 1.3
Gel A9	ATS <sub>A9</sub> (5:1,2.1)	1	0.20	11.74	4.75	0.0043	0.029	24 / 2.1
Gel A10	ATS <sub>A10</sub> (5:1,1.9)	1	0.20	11.74	4.75	0.0047	0.029	24 / 1.9
Gel A12	ATS <sub>A12</sub> (5:1,2.5)	1	0.20	11.74	4.75	0.0023	0.029	24 / 2.5
Gel A19	ATS <sub>A19</sub> (5:1,7.0)	1	0.20	5.89	2.34	0.0575	0.035	24 / 7.0
Gel A20	ATS <sub>A20</sub> (5:1,3.0)	1	0.20	5.89	2.34	0.0575	0.035	24 / 3.0
Gel A21	ATS <sub>A21</sub> (5:1,5.0)	1	0.20	5.89	2.34	0.0575	0.035	24 / 5.0
Gel167	ATS <sub>A167</sub> (5:1,0.5)	1	0.20	5.89	2.34	0.0861	0.035	24 / 0.5
Gel168	ATS <sub>168</sub> (3:1,0.5)	1	0.33	6.53	2.60	0.0956	0.039	24 / 0.5
Gel182	ATS <sub>182</sub> (3:1,2.2)	1	0.33	6.53	2.60	0.0018	0.039	24 / 2.2
Gel183	ATS <sub>183</sub> (5:1,2.2)	1	0.20	5.89	2.34	0.0016	0.035	24 / 2.2
Gel307	ATS <sub>307</sub> (3:1,1.3)	1	0.33	6.53	2.60	0.0078	0.039	24 / 1.3
Gel308	ATS <sub>308</sub> (10:1,1.3)	1	0.10	5.38	2.14	0.0064	0.032	24 / 1.3
Gel309	ATS <sub>309</sub> (3:1,2.3)	1	0.33	6.53	2.60	0.0026	0.039	24 / 2.3
Gel310	ATS <sub>310</sub> (10:1,2.3)	1	0.10	5.38	2.14	0.0021	0.032	24 / 2.3
Gel311	ATS <sub>311</sub> (3:1,4.0)	1	0.33	6.53	2.60	0.0026	0.039	24 / 4.0
Gel312	ATS <sub>312</sub> (10:1,4.0)	1	0.10	5.38	2.14	0.0021	0.032	24 / 4.0

### Influence of drug loading

The release profiles of Propranolol from hybrid silica gels prepared under different drug loading is shown in Figure 4.2.18. Propranolol release was increased during the first hours with higher amount of drug loading in the hybrid gel. The burst effect was stronger for drug loading with 15 wt% and higher. With lower drug loading (Gel A3 and A4), a retarded drug release was observed. This observation is in support of the discussion done in the context of TEOS gels. At very acidic pH, the acetoxypopyl group could also get protonated which will further enhance the drug release. Another explanation could be the

preferential electron pair donor interaction of the carbonyl oxygen with the silanol protons than the drug interaction with the silica surface.<sup>149</sup> Further studies by high resolution solid state HETCOR NMR have been carried out for an explanation of these effects.

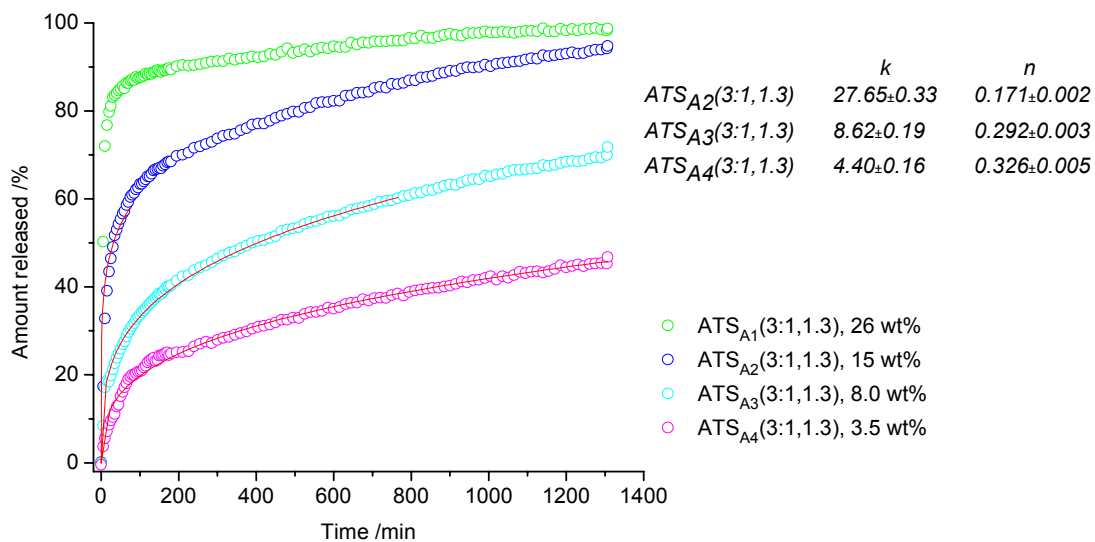


**Figure 4.2.18:** Release profiles of Propranolol from hybrid ATS silica gels with different drug loading.

## Influence of pH

The effect of synthesis pH on the release rate of PP has been studied by varying the pH of the hybrid ATS silica sol, Figure 4.2.19. Hybrid silica gels made at different pH values from 1.9 to 2.5 in the presence of PP, show strong pH dependence on release kinetics. However, above pH = 3, there is no pH influence on the drug release kinetics. 98% of the drug was released within 22 hours, for gels synthesized at pH 3.0 and higher, whereas only around 70% released for the same period for gel synthesized at pH around 2. For Gels prepared at pH = 3 and higher, the initial burst was accounted for approximately 80%.

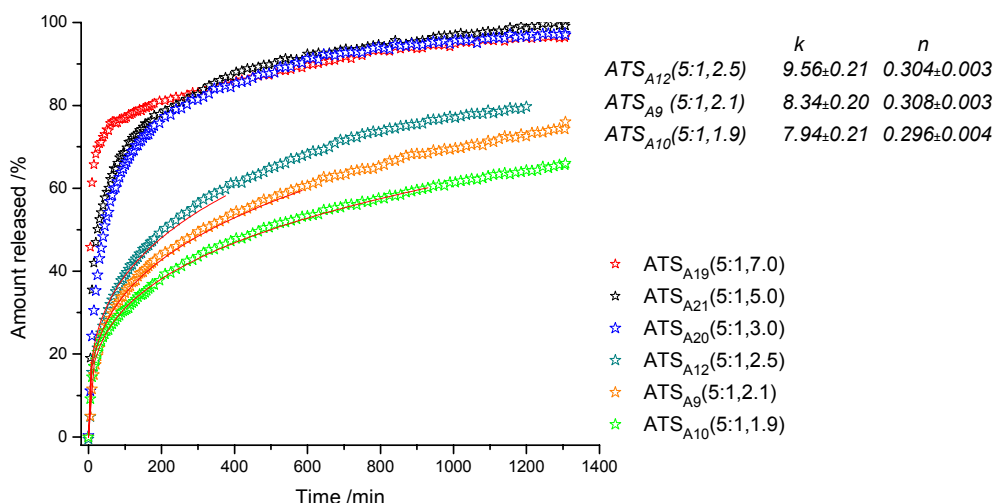


**Figure 4.2.19:** Release profiles of Propranolol from hybrid ATS silica gels with different synthesis pH.

## Influence of Composition

The release profiles of gels made with different TEOS:ATS ratios and pH values are compared in Figure 4.2.20 and 4.2.21. A high level of ATS in the hybrid gel leads to a decrease in the drug release for gels prepared at pH around 2.0 and higher (Gels 182, 309 and 311), whilst the reverse effect is observed for gels synthesized at very acidic pH (Gel 168 and 307). This effect is more pronounced at pH values close to the charge-matching

point, where a clear shift in the release mechanism occurs. The composition effect above  $\text{pH} = 2.0$  is in conjunction with other hybrid gels (MTS or PTS). At very acidic  $\text{pH}$ , the drug release is accelerated by ATS which can be explained as follows. When the synthesis  $\text{pH}$  is very acidic, 0.5, the silica matrix is positively charged, and the acetoxypopyl group can interact with the matrix. The interaction between the highly positive silica surface and the protonated drug molecules are repulsive whereas the interactions with ATS units are not repulsive. A higher amount of ATS unit in the hybrid gel will amplify a mutual preferential interaction between acetoxypopyl group and matrix and an inferior interaction with drug molecules. Close to the charge-matching point, the matrix is neutral or negatively charged and the influences of ATS units are masked. Hence a shift in the interaction mechanism occurs at around  $\text{pH} 2$ . Bögershausen have reported a similar shift for ATS gels, in the controlled release of Persantin, at  $\text{pH}$  value above 5.5. The unexpected change in the shift values could be due to the difference in the physicochemical properties of drugs.

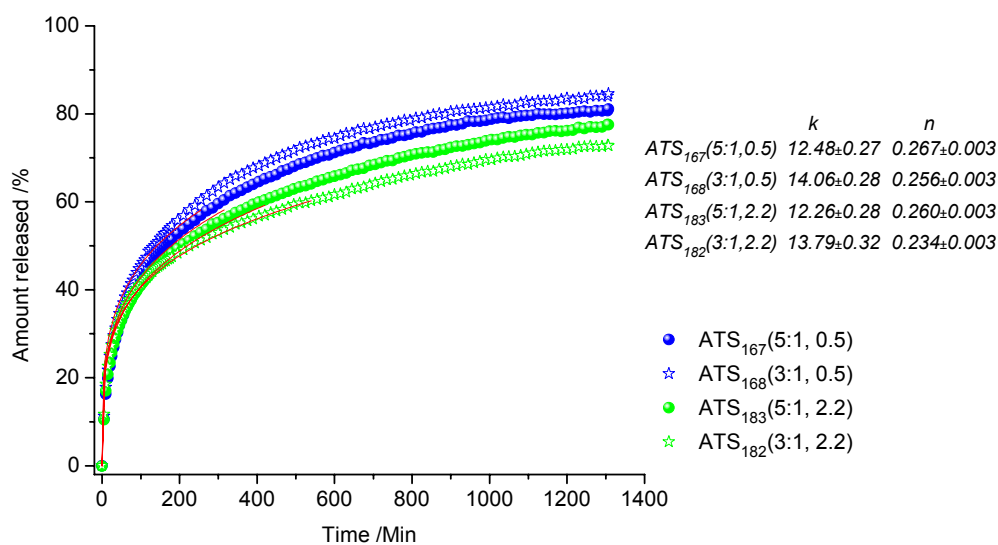


**Figure 4.2.20:** Release profiles of Propranolol from hybrid ATS silica gels with different  $\text{pH}$  and composition.

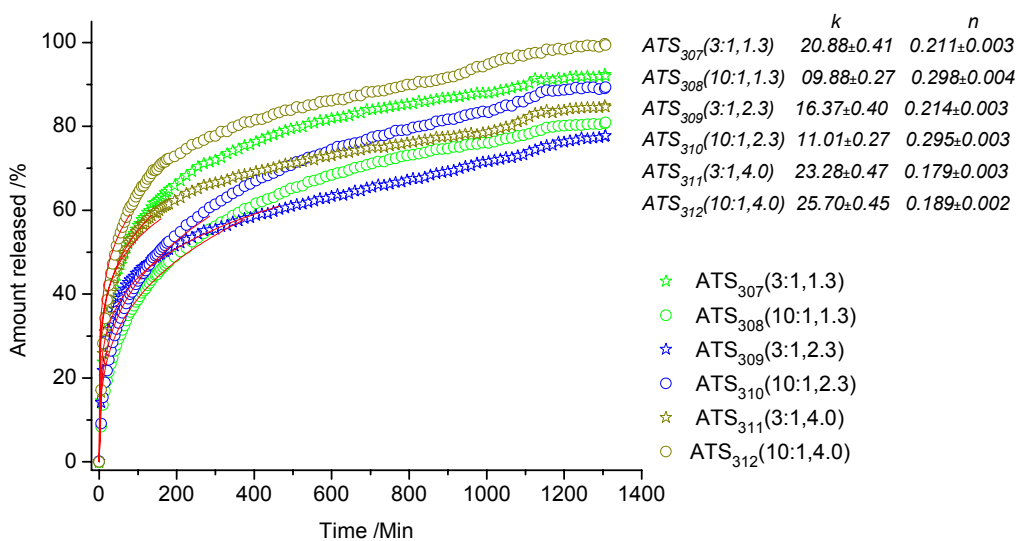


**Figure 4.2.21:** Release profiles of Propranolol from hybrid ATS silica gels with different pH and composition.

### N<sub>2</sub> sorption studies

The N<sub>2</sub> sorption isotherms of hybrid gel microparticles, for drug loaded and extracted ATS gels are shown in Figure 4.2.22. These gels were synthesized between the pH values 2 and 4. Drug loaded and drug extracted gels show no porosity which is characteristic of ATS gels as earlier reported in the literature.<sup>58</sup> Ansgar et al. have proposed that the internal pore walls are covered with acetoxypopyl groups that are rigid at N<sub>2</sub> sorption temperature of 77 K thus hindering diffusion of the N<sub>2</sub> molecules. Further studies by high resolution solid state HETCOR NMR have been carried out for an explanation of above effects.

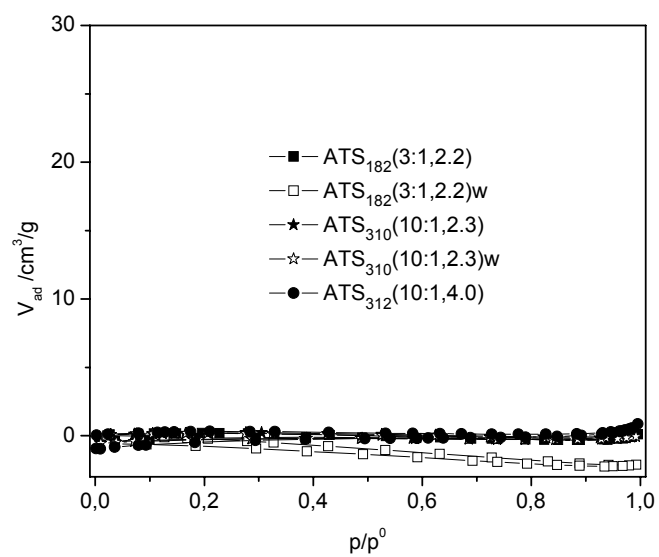


**Figure 4.2.22:**  $N_2$  sorption isotherms of various drug loaded and extracted ATS gels prepared at different pH.

### 4.2.3 Aromatic precursors

#### Preparation

Different aromatic precursors such as Benzyltriethoxysilane, Phenyltriethoxysilane and Diphenyldiethoxysilane have been employed to prepare EISA hybrid gels. The preparations of hybrid BTS, PhTS and DPhDS gels are similar to that of hydrophobic gels as discussed in the last sections. The synthesis compositions are given in Tables 4.18 – 4.20.

**Table 4.18:** Relative molar ratios, pH and stirring time ( $t_s$ ) for hybrid BTS gel formulations

Gel	Name	TEOS	BTS	H <sub>2</sub> O	Ethanol	HCl	PP	$t_s$ (h)/pH
Gel 109	BTS <sub>109</sub> (10:1,1.1)	1	0.10	5.38	2.14	0.0323	0.032	24 / 1.1
Gel 110	BTS <sub>110</sub> (5:1,1.1)	1	0.20	5.89	2.35	0.0354	0.035	24 / 1.1
Gel 111	BTS <sub>111</sub> (3:1,1.1)	1	0.33	6.53	2.60	0.0392	0.039	24 / 1.1
Gel 190	BTS <sub>190</sub> (5:1,2.2)	1	0.20	5.89	2.35	0.0047	0.035	24 / 2.2
Gel 191	BTS <sub>191</sub> (3:1,2.2)	1	0.33	6.53	2.60	0.0052	0.039	24 / 2.2

**Table 4.19:** Relative molar ratios, pH and stirring time ( $t_s$ ) for hybrid PhTS gel formulations

Gel	Name	TEOS	PhTS	H <sub>2</sub> O	Ethanol	HCl	PP	$t_s$ (h)/pH
Gel 112	PhTS <sub>112</sub> (10:1,1.1)	1	0.10	5.38	2.14	0.0323	0.032	24 / 1.1
Gel 113	PhTS <sub>113</sub> (5:1,1.1)	1	0.20	5.89	2.35	0.0354	0.035	24 / 1.1
Gel 114	PhTS <sub>114</sub> (3:1,1.1)	1	0.33	6.53	2.60	0.0392	0.039	24 / 1.1
Gel 185	PhTS <sub>185</sub> (3:1,2.2)	1	0.33	6.53	2.60	0.0026	0.039	24 / 2.2
Gel 186	PhTS <sub>186</sub> (5:1,2.2)	1	0.20	5.89	2.35	0.0024	0.035	24 / 2.2

**Table 4.20:** Relative molar ratios, pH and stirring time ( $t_s$ ) for hybrid DPhDS gel formulations

Gel	Name	TEOS	DPhDS	H <sub>2</sub> O	Ethanol	HCl	PP	$t_s$ (h)/pH
Gel 172	DPhDS <sub>172</sub> (5:1,0.5)	1	0.20	5.89	2.34	0.0863	0.035	24 / 0.5
Gel 173	DPhDS <sub>173</sub> (3:1,0.5)	1	0.33	6.51	2.60	0.0953	0.039	24 / 0.5
Gel 187	DPhDS <sub>183</sub> (5:1,2.2)	1	0.20	5.89	2.34	0.0047	0.035	24 / 2.2
Gel 188	DPhDS <sub>188</sub> (3:1,2.2)	1	0.33	6.51	2.60	0.0052	0.039	24 / 2.2

### Influence of pH and Composition

The effect of synthesis pH on the release kinetics of PP has been studied by varying the pH of the hybrid BTS silica sol, Figure 4.2.23. Hybrid BTS silica gels made at different pH values from 1.1 to 2.2 in the presence of PP, show strong pH dependence on release kinetics. A retarded drug release was observed at pH 2.2 whereas an initial fast release at pH 1.1. The release profiles of gels made with different TEOS:BTS ratios and different pH values are compared in Figure 4.2.23. A high level of BTS in the hybrid gel leads to a decrease in the drug release for gels prepared at pH around 2.2 and 1.1. This effect was more pronounced at pH values close to the charge-matching point of silica where close to zero order kinetics (kinetic parameter  $n = 0.78$ ) (Gel 191) was observed (Table 4.21). The pH and composition effects are in conjunction with other hybrid gels (MTS or PTS).

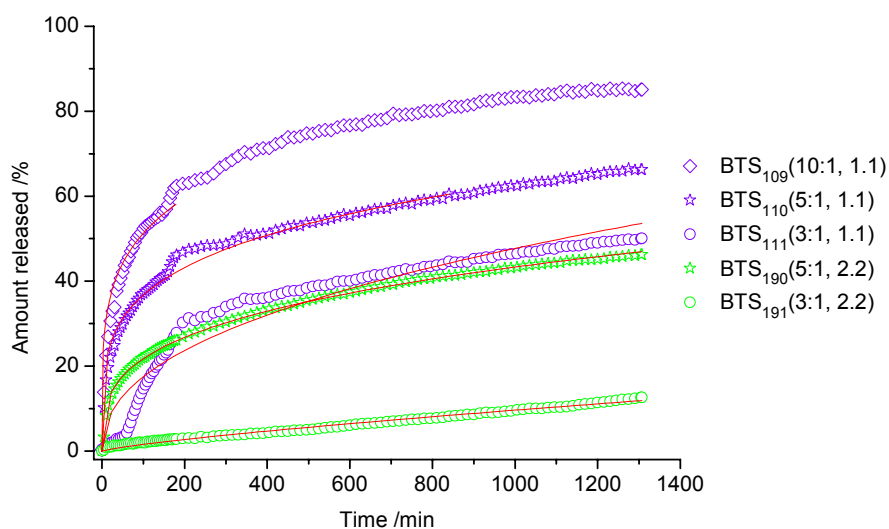


**Figure 4.2.23:** Release profiles of Propranolol from hybrid BTS silica gels with different pH and composition.

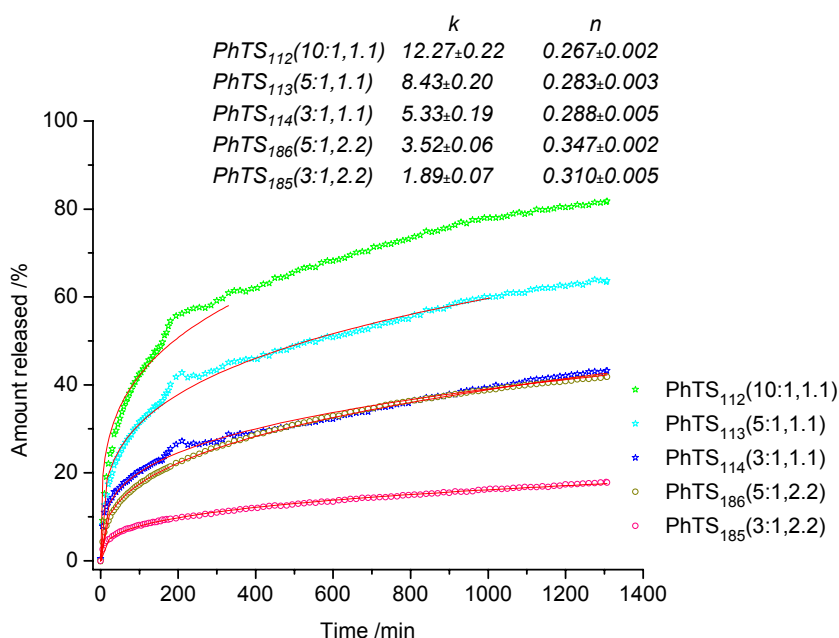


**Table 4.21:** Kinetic release parameters of various BTS gels.

	$k$	$n$
$BTS_{190}(5:1,2.2)$	$05.48 \pm 0.27$	$0.299 \pm 0.007$
$BTS_{191}(3:1,2.2)$	$00.04 \pm 0.02$	$0.782 \pm 0.072$
$BTS_{109}(10:1,1.1)$	$19.07 \pm 0.41$	$0.214 \pm 0.003$
$BTS_{110}(5:1,1.1)$	$12.51 \pm 0.38$	$0.233 \pm 0.004$
$BTS_{111}(3:1,1.1)$	$02.35 \pm 0.14$	$0.435 \pm 0.009$

Aromatic hybrid silica gels prepared with phenyl precursor also show similar release kinetics as that of benzyl substituted gels. The influences of pH and composition on phenyl substituted hybrid silica gels are given in Figure 4.2.24. A strong retarded drug release was observed at pH values 1.1 and 2.2. A high level of phenyl substitution in the hybrid gels also impedes the drug release.

The release profiles of gels made with different TEOS:DPhDS ratios and pH values are given in Figure 4.2.25. From the release profile it is clear that DPhDS substitution boost up a very strong retarding effect on the release of PP. Only 24% and 13% of the drug was released within 22h of DRT study for gels prepared at pH 0.5 and 2.2, respectively. The synthesis pH and composition has not much influence on the release of the drug from the hybrid DPhDS gel.

**Figure 4.2.24:** Release profiles of Propranolol from hybrid PhTS silica gels with different synthesis pH and composition.

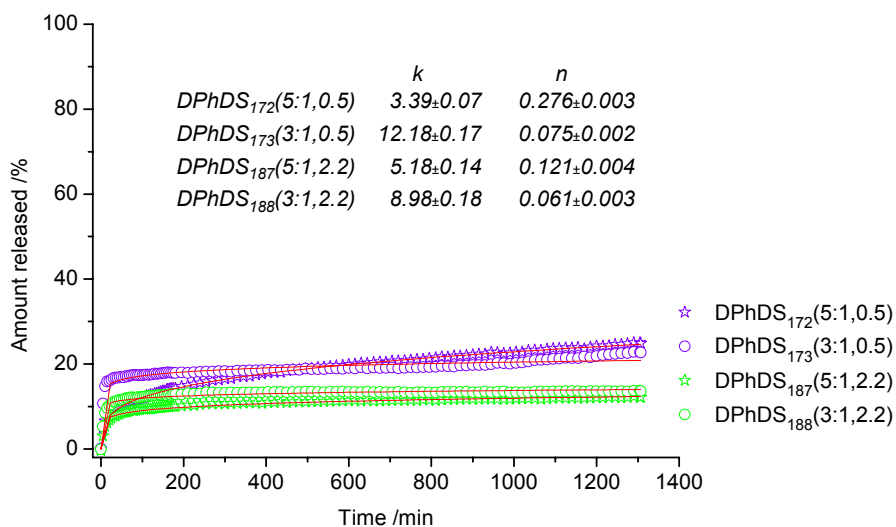


**Figure 4.2.25:** Release profiles of Propranolol from hybrid DPhDS silica gels with different pH and composition.

What more striking is the partial substitution by aromatic groups induces a strong retarding effect in the hybrid silica gels and is attributed to the hydrophobic effect. This hydrophobic effect along with pH effect dominates in the release kinetics of the benzyl and phenyl substituted hybrid gels. Since there are two phenyl groups attached to the silicon atom, a strong hydrophobic effect is expected for DPhDS gels. This strong hydrophobic effect dominates in the release kinetics of the diphenyl substituted hybrid gels than the composition and pH influences. Similar influences by aromatic group substitutions in silica gels have been reported in the literature and are attributed to the  $\pi - \pi$  interactions with drug molecules which are strongly encapsulated in these gels.<sup>58</sup>

## N<sub>2</sub> Sorption studies

N<sub>2</sub> sorption studies have been carried out for the characterization of the porosity of hybrid gels. The N<sub>2</sub> sorption isotherms of hybrid gels, which are prepared in the presence of drug, are shown in the Appendix 9.7. Drug loaded aromatic substituted hybrid gels show no porosity which means the pores are occupied by the drug molecules. Drug extracted BTS hybrid Gel 109w show porosity with BET surface area of 34 m<sup>2</sup>/g.

## **<sup>29</sup>Si MAS NMR studies**

Hybrid gels were examined using <sup>29</sup>Si MAS NMR spectroscopy and are shown in Appendix 9.3. A shift in the T group resonance to the high shielding region by roughly 8 and 15 ppm for the benzyl and phenyl substituted gels, respectively, is due to the aromatic ring current effect. A shift by roughly 30 ppm in the D group resonance to the high shielding region was observed for diphenyl substituted gels and is attributed to a very strong aromatic ring current effect.

### **4.2.4 Discussion**

The dissolution of drug molecules and the matrix porosities of hybrid gels are related to the synthesis parameters, composition and pH values. The major differences between hydrophobic, hydrophilic and aromatic hybrid gels are highlighted in the discussion below.

#### **Drug concentration**

Propranolol release was increased during the first hours with higher drug loading in hybrid gels. Both hydrophilic and hydrophobic gels show a burst effect and this was stronger for a drug loading with 15 wt% and higher. The loaded drug molecules can occupy any of the two locations of the sol-gel matrix: The interiors of the pore or the interface of the primary particles. The encapsulation in both locations occurs simultaneously during the self assembly process. The gels were synthesized at acidic pH values and the primary particles are positively charged and thus the hybrid matrix formed as well. The number of protonated PP per unit area was higher with higher loading. With higher loading, high percentage of the drug molecules interacts with surfaces of particles creating a high surface area material. The majority of the drug molecules are bound to the surfaces of the particles and are accessible to the dissolution medium. Larger loading of PP will create repulsive forces between drug adsorbed particles and retard the particle aggregation and later the densification upon processing. Thus, the drug molecules are easily accessible to the dissolution medium, resulting in a faster release. Figure 4.2.26 shows the pore volumes developed against drug loading of hybrid MTS gels measured by N<sub>2</sub> sorption measurements.

N<sub>2</sub> sorption measurements suggest that the final porosity of the hybrid silica gels is due to both primary pores (those present prior to drug extraction) and secondary pores (created by extraction of drug molecules).<sup>150</sup> Primary porosity is determined by the molecular structure of the hybrid gels, while secondary porosity is controlled by the amount, size and distribution of drug molecules in the hybrid matrix. Primary pores were inaccessible to N<sub>2</sub> as shown by the absence of porosity for drug loaded gels. The combined DRT and N<sub>2</sub> sorption results suggest that drug introduction promote a templating effect in the hybrid gel network during the drug encapsulation. The pores developed after the drug extraction are of the size and shape of drug molecules and are accessible to N<sub>2</sub>. The above observations have been further supported by the comparison of the porosity development of a drug loaded and unloaded hybrid MTS gels. Pore volumes are generated upon drug release by emptying internal void space and not by swelling of the material. In a drug unloaded gel, secondary pores are empty due to the absence of drug molecules and are easily accessible to N<sub>2</sub>. Pore structure developments upon template pyrolysis have been reported earlier in the literature.<sup>150</sup> This study of drug loading mechanism showed that drug deposition in the pores occurs during the self-assembly process, and the drug-matrix interaction is an important factor to determine the drug loading capacity.

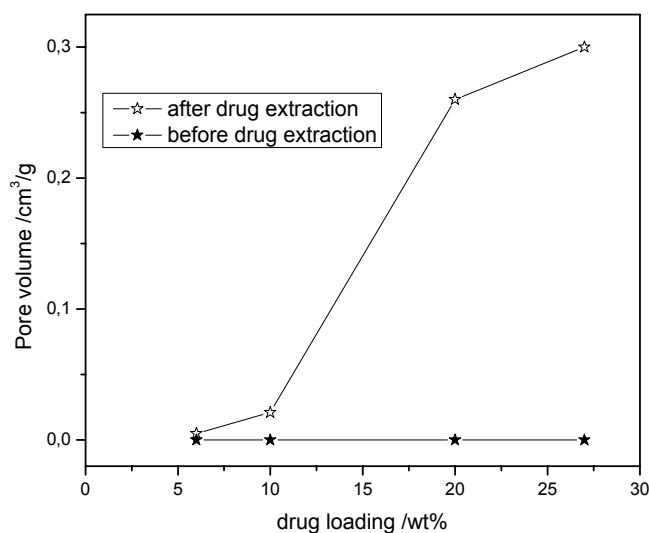


**Figure 4.2.26:** A graph representing the increase in pore volume upon drug extraction.

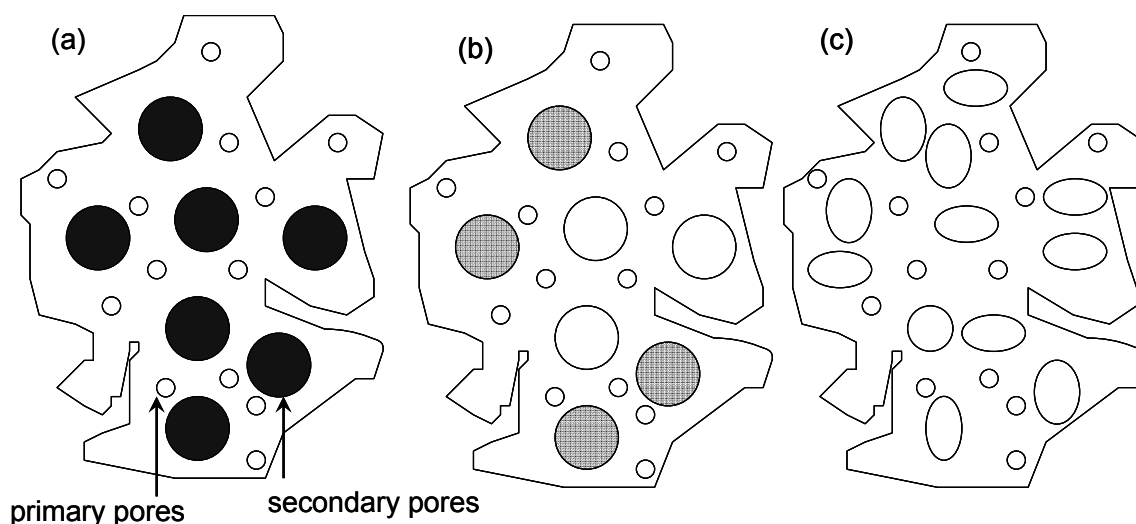


**Figure 4.2.27:** Schematic representation of template approach. (a) Drug loaded gel with secondary pores occupied by drug, (b) partially emptying of secondary pores during extraction, and (c) drug unloaded gel.

### Sol-gel synthesis pH

Similar to the TEOS based gels, strong synthesis pH dependence on drug release was observed for both hydrophilic as well as hydrophobic hybrid gels. A fast initial release occurs for gels which are made at the higher (5.0) and lower (0.6) pH values. The release curvature increases below and above intermediate acidic pH values (1.5-2.5). The retarded release from the gels with a synthesis pH value near the charge matching point of silica is due to the favorable interaction between drug and matrix. The  $N_2$  sorption experiments support the formation of porous structures after drug extraction at the lower and higher pH ranges. The porosity development after the extraction is directly related to the total amount of drug release.

The pH effect can be summarized in the model shown below. In a self assembled hybrid sol-gel synthesis in presence of drug molecules, the nature of guest-host interactions and pore structures are dictated by the synthetic pH values. Three different pH regimes can be rationalized for the easier understanding of pH effect. The first one is pH value below 1.5, the second is between 1.5 and 2.5 and the last is above 2.5. Three different drug-matrix interaction pathways can be identified in the above regimes:  $D^+X^-M^+$ ,  $D^+M^-/M^0$  and  $D^0M^-$ , where D is the drug, M is the matrix and X is the mediating ion (e.g.  $Cl^-$ ). In

the  $D^+X^-M^+$  approach, both the drug and matrix are protonated and occur at pH values below 1.5. In this regime, protonated drug molecules are incorporated in a protonated silica matrix, which leads to a stronger tendency for dissolution. Charge neutrality at low pH can then be rationalized by the inclusion of the desired number of counterions (e.g.,  $Cl^-$ ). At the charge-matching regime, overall charge between drug and matrix are matched and  $D^+M^-/M^0$  approach is valid. In this regime, a favorable interaction between drug and matrix exists. A  $D^0M^-$  approach is valid at higher pH values where the drug molecules are neutral while the matrix is negatively charged. Larger pores are formed in this pH region and no drug-matrix interaction exist which also facilitates faster drug release.

The charge matching regime is controlled by the isoelectric point of silica gels. Condensation of silanol groups at  $Q^1$  and  $Q^2$  sites are acid-catalyzed electrophilic substitutions at values below their respective isoelectric points (IEP). Their IEPs are around pH value of 3.0.<sup>151</sup> However, the IEP of  $Q^3$  sites is different from above and are at around 2. The absolute value of IEP of a silica gel differ due to the type of silica precursor (e.g. quaternary and/or ternary monomer), Q/T site concentrations, existence of other components (e.g. drug), temperature etc. Nevertheless, the charge matching regime can be assumed to lie within the pH value range 1.5 to 3.5 and a homogeneous gel network formation can be expected. On the other hand, the amount of water can also modify the kinetics of drug release. At very acidic conditions, a substantial fraction of water can be tied up in hydration of the acid and protonated drug as a hydration shell of  $H_3O^+$ ,  $Cl^-$  and  $D^+$ . In such cases a partly hydrolyzed/condensed silica gel network can be envisaged. At an optimal interaction pH value a combination of electrostatic attraction between positively charged PP and the negatively charged matrix followed by the occupation of PP in the nanopores and the formation of other noncovalent interactions occurs. The specific binding of Propranolol by the sol-gel material is reported in the literature<sup>152</sup> and is attributed to the different noncovalent interaction between PP and silica matrix. The two major contributions come from hydrophobic and  $\pi$ - $\pi$  interactions between matrix and PP. It is also proposed that the silanol groups on the surface of gel are responsible for nonspecific binding of drug molecules.

## Hydrophobicity vs hydrophilicity

Covalent bonding of the organic moieties to the inorganic framework imparts hydrophobicity/hydrophilicity to the silica gel depending on the choice of organic substitution in the monomer precursors. In addition to their role as pore-size directing templates, organic side chains serve as network modifiers by making the network more hydrophobic/hydrophilic. Different hydrophobic (MTS, ETS, PTS, BTS, PhTS and DPhDS) and hydrophilic (ATS) precursors have been used in this study. Phase separations have been inhibited by employing kinetically controlled faster sol-gel reactions. The reactions have been carried out at acidic pH values where a comparable hydrolysis and condensation rates of the TEOS and organoalkoxysilanes achieved. In such hybrid gels, the Q and T sites are homogeneously distributed throughout the network, avoiding aggregation and phase separation. When the sol-gel reactions were carried out with the aromatic substituted T and D monomers, the reaction kinetics have been slowed down and the tendency toward phase separation and aggregation increases. Aromatic systems are well known for their strong interactions (e.g., via  $\pi$ - $\pi$  interactions, hydrogen bonding and hydrophobic interaction) between organic moieties. Since the solvents employed for the reactions are polar in nature (water and ethanol) a less favorable polymer-solvent interactions occur during the growth of hybrid material. In short, aromatic substituted T groups are not uniformly incorporated in the matrix and undergo aggregation or phase separation and result in dense hybrid matrix. The phase separation can be in any length scale depending on the synthesis and processing conditions. The driving force for such phenomenon in the aromatic substituted hybrid gels are dissimilar reaction rates between Q and T moieties, heterocondensation rates, inductive effects etc. With increasing alkyl/aromatic T monomer amounts, progressively impart hydrophobic character. Organic groups from the T units reduce the connectivity of the network compared to a pure TEOS gel. It is quite likely that increasing hydrophobicity of the aliphatic chains shielded the attached silyl groups from further condensation promoting phase separation of the siloxane and organic groups. As pointed out by Corriu et al., in addition to the structure of the precursor, other factors such as the matrix/solvent interactions and concentration might influence the gel microstructure. The reduced connectivity of the network brought about by the incorporation of the T groups generally results in dense gels.

Based on the above findings the kinetics of drug release can be reviewed. A high level of T group in the hybrid gel leads to a decrease in the drug release. Due to the presence of alkyl/aromatic groups in the surface, the gel particles are hydrophobic in character and the solvent's ability to dissolve the drug molecule from the pores decreases with increase in the T group level. The trend on hydrophobic groups can be shown as  $MTS < ETS < PTS < BTS < PhTS < DPhDS$ . Very high level of hydrophobic units in the hybrid gel strongly retard the drug release. Super hydrophobic nature of the silica with anchored alkyl groups on the surface has been reported in the literature.<sup>153</sup>

The drug release is accelerated by ATS gels which are an anomaly with respect to the trend discussed above. This is attributed to the partly hydrophilic character of the acetoxypropyl units. Solvent ability to dissolve the drug increases with higher amount of hydrophilic group in the matrix. In addition, the synthesis pH values have also a strong influence on the release kinetics of drug from ATS based gels. As discussed earlier, drug release is also controlled by electrostatic interactions between the acetoxypropyl group and silanols of the matrix at very acidic pH conditions.

In summary, the drug release kinetics of the evaporation induced self assembled gels can be tailor made by appropriate choice of organic side groups. One of the key factors having control over the release rate is molecular level interaction which include noncovalent interactions such as hydrogen bonding, van der Waals forces, electrostatic forces,  $\pi$ - $\pi$  interactions etc. The cooperative interactions between the guest drug molecules and the host matrix influence the diffusion of drug from the hybrid gels. The drug molecules play the role of a structure directing agent (not structure determining) in the self assembled silica gel system.



## 5. Spray Dried Gels with Persantin

---

### Introduction

Self assembled silica and hybrid gel materials have been prepared in presence of guest molecule Persantin (PS) under EISA method by Bögershausen et al.<sup>58</sup> The dissolution of PS and the matrix porosities related to synthesis parameters, compositions and pH values by EISA method were studied in detail and presented in the literature. Bögershausen et al. put forward interesting alternatives for the controlled release of PS. However, the enhancement of the bioavailability of sparingly water soluble drug, PS, remains as a challenge. Spray drying process recently received great attention due to its ability to produce spherical particles with narrow particle size range. In this study, spray drying was evaluated as a potential method to enhance the bioavailability of PS. Similar to last chapter, two sections with single precursors and two precursor formulations are presented. Synthesis as well as characterization techniques are given in each section followed by discussion.

### 5.1 Spray dried gel formulations from a single precursor

#### 5.1.1 Preparation

Gel 99 with pH 1.5 was prepared by mixing TEOS, H<sub>2</sub>O, Ethanol, PS and HCl in the molar ratio 1.0 : 4.9 : 1.95 : 0.02 : 0.0295. In a typical synthesis, PS was dissolved in a mixture of water, ethanol and HCl. The solution was stirred while adding TEOS till the hydrolysis was complete. The sol was stirred for 24 h at room temperature and after that subjected to spray drying. The silica sols with high synthesis pH values were prepared by two-step catalysis with aqueous HCl and aqueous NH<sub>3</sub>. The final pH of the sol after hydrolysis was controlled by the addition of aqueous NH<sub>3</sub>. The synthesis compositions are given in Table 5.1. It was assumed that the amount of drug added to the solution was entirely incorporated into the microspheres. The yield of the spray dried microparticles

was in the range of 80-90 % compared to the oven dried gel. The reduced yield is accounted for the loss in the spray drying process.

**Table 5.1:** Relative molar ratios, pH and stirring time ( $t_s$ ) for single precursor gel formulations

Gel	TEOS	H <sub>2</sub> O	Ethanol	HCl	PS	$t_s$ (h)/pH
Gel 201	1	4.9	1.95	0.0343	0.04	24 / 1.2
Gel 99	1	4.9	1.95	0.0295	0.02	24 / 1.5
Gel 58	1	4.9	1.95	0.0236	0.02	24 / 2.0

The *in vitro* release profiles of Persantin from silica gel microparticles prepared under different pH and drug loading are compared in Figure 5.1.1. An initial burst release of PS was observed from Gel 201 and Gel 99, and accounted for around 90%. The effect of drug loading in the release rate has been studied. The release profile of Gel 58 shows, with lower drug loading a slower release was achieved compared to gels with higher drug loading. The Silica gel microparticles made at pH 2.0 show a retarded drug release. The initial burst release from Gel 58 is accounted for 15% followed by a retarded release. The release kinetic parameters are given in the inset of Figure 5.1.1.

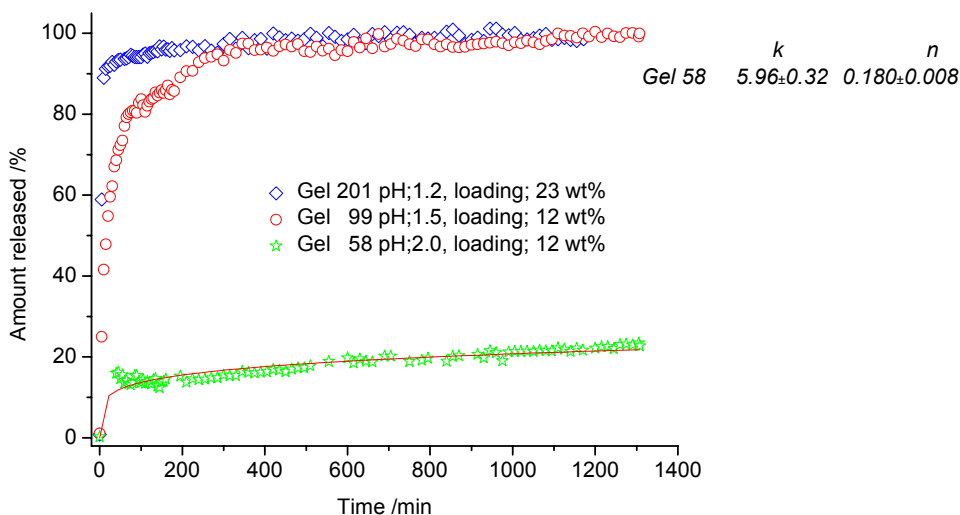


**Figure 5.1.1:** Drug release profiles of Persantin from spray dried silica gels with different pH and drug loading.

### 5.1.2 Surface studies by SEM

The microscopic analysis by scanning electron microscopy was carried out on microparticles to obtain information about the morphology and to evaluate their shape, size and surface. The SEM micrographs of Gel 201 and 201w are given in Figure 5.1.2.

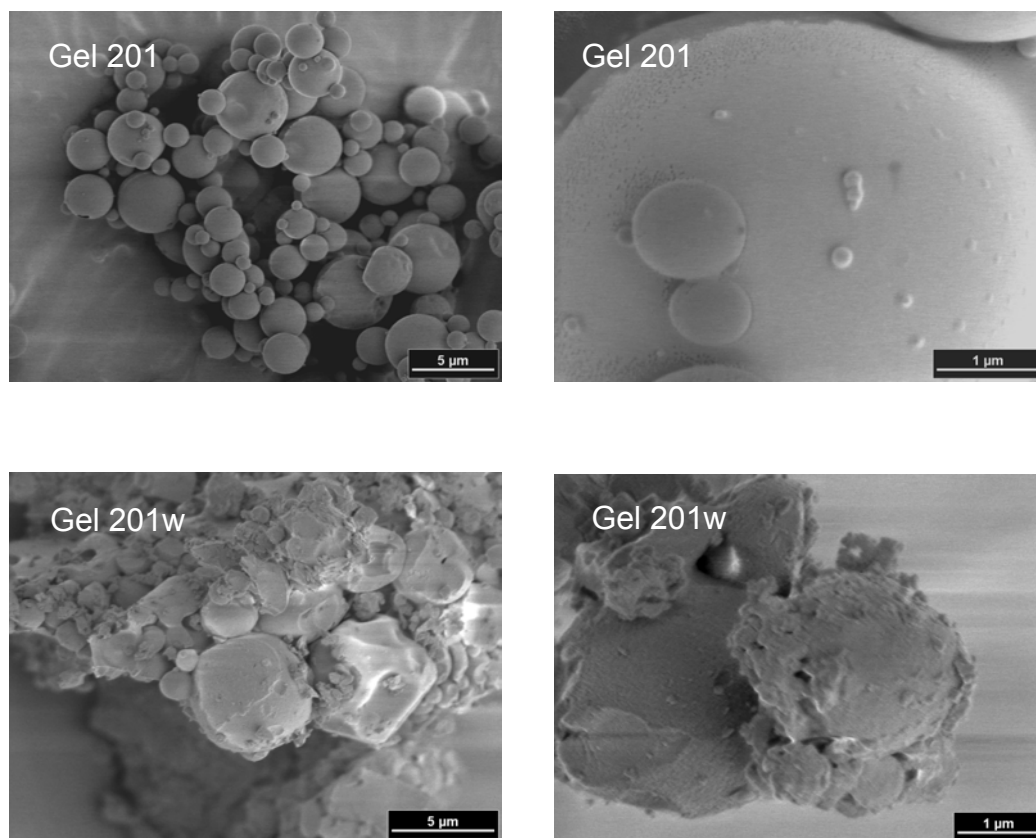


**Figure 5.1.2:** SEM micrographs of Gel 201 before and after drug dissolution (marked by w). The amplified micrographs are given on the right side.

The SEM micrographs reveal the agglomeration of spherical with nearly uniform sized particles before the drug dissolution. Despite of this agglomeration all the spherical particles are in dispersed state and have an average diameter around 2  $\mu\text{m}$ . The amplified micrographs reveal the formation of microstructures on the surface of particles with silica nanoparticles adsorbed on the surface of larger spheres. The microparticles are examined by SEM after the drug dissolution and show a significant difference in the surface morphology. The dissolution of the drug leads to the collapse of the structure and the degraded particles are more aggregated. The amplified micrograph shows the surface

erosion and presence of open pores on the surface. The structural transformations in the degraded particles are further studied by solid state NMR and will be discussed in the following sessions.

### 5.1.3 N<sub>2</sub> Sorption studies

N<sub>2</sub> sorption studies have been carried out for the characterization of the porosity of microparticles. The N<sub>2</sub> sorption isotherm of a spray dried gel, which is prepared in the presence of PS, is shown in Figure 5.1.3. Drug loaded gels show no porosity whereas the drug extracted gels are microporous with type I isotherm. Significant pore volumes for drug extracted gels are originated as observed using the Horvath-Kawazoe method. The BET surface area and micropore volume for Gel 201w are 443 m<sup>2</sup>/g and 0.221 cm<sup>3</sup>/g and for Gel 99w are 164 m<sup>2</sup>/g and 0.082 cm<sup>3</sup>/g, respectively.

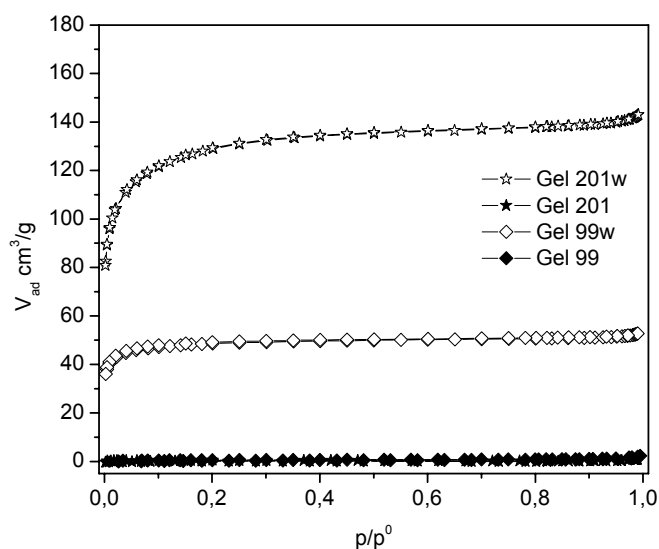


**Figure 5.1.3:** N<sub>2</sub> sorption isotherm of spray dried gels before and after drug extraction.

#### 5.1.4 $^1\text{H}$ MAS NMR studies

The proton NMR spectra of spray dried hybrid Gel 201 prepared in the presence of the drug Persantin is shown in Figure 5.1.4. Resonances from the drug molecules cannot be identified as a separate peak in the 1D proton spectrum, but contribute to the intensities observed in the range 1-8 ppm. The broad spectrum of Gel 201 treated at 393 K is a clear indication of the presence strong dipolar interactions between the protons of Persantin in the spray dried gel.

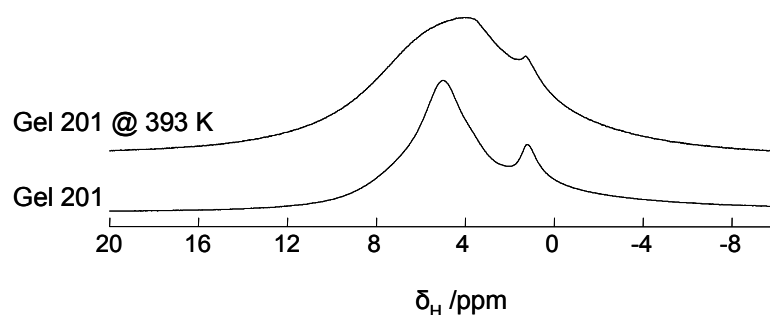


**Figure 5.1.4:** The  $^1\text{H}$  MAS NMR spectra of spray dried hybrid Gel 201 prepared in the presence of Persantin (MAS 15 kHz). Intensities are not in absolute scale.

#### 5.1.5 $^{29}\text{Si}$ MAS NMR studies

Various spray dried gel samples were examined using  $^{29}\text{Si}$  MAS NMR spectroscopy. The studies on gels have been carried out in order to understand the silicon atom connectivity in the gel network. The  $^{29}\text{Si}$  MAS spectra of various gels are shown in Figure 5.1.6, together with the corresponding computer simulated spectra and their individual deconvoluted contributions from each silicon site. Table 5.1.2 summarizes the deconvoluted peak areas of the spectra in Figure 5.1.5. The spectra are similar to the EISA gels. The  $\eta$  value, a measure of degree of condensation, was 0.76 and 0.86 for Gel 201 and 201w, respectively. Increases in the  $\eta$  value after the drug release confirm the formation of a more condensed network upon drug release.

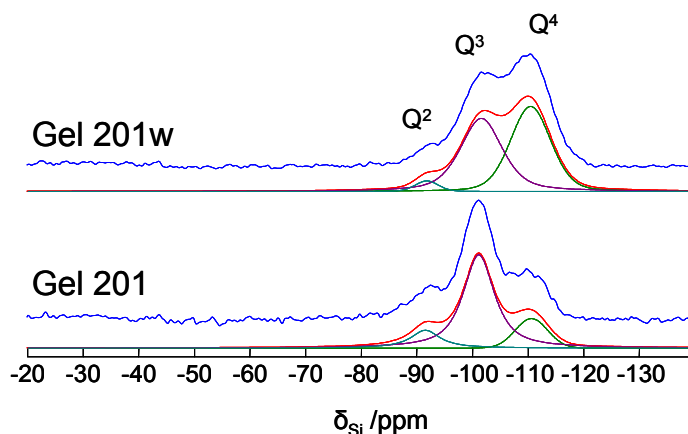


**Figure 5.1.5:**  $^{29}\text{Si}$  MAS NMR spectra of spray dried gels before and after drug extraction (w). Each set of spectra includes experimental spectrum (in blue) and the simulated spectrum (in red) with individual contributions from each silicon site.

**Table 5.1.2:** Peak area derived for deconvoluted peaks of the  $^{29}\text{Si}$  MAS spectra of spray dried Gel 201 before and after washing.

Probe	Q <sup>2</sup> /%	Q <sup>3</sup> /%	Q <sup>4</sup> /%	Σ Q /%
Gel 201	13	70	17	100.0
Gel 201w	3	48	49	100.0

The  $^{13}\text{C}\{^1\text{H}\}$  CPMAS NMR spectra of Gel 58 prepared in the presence of the drug, Persantin, is shown in appendix and confirm the presence of Persantin intact in the microparticles.

The fast release of PS from such SD gels made at very acidic pH values indicates that there is almost no retarding effect by host-guest interactions. The low pH value of 1.5 leads to a salt-like system which degrades upon washing (SEM). The connectivities of silica network undergoes dramatic change to a more condensed system, when the salt (drug,  $\text{Cl}^-$  anions) is washed out. The question whether better retardation can be achieved when organic groups are introduced in the matrix is studied next.

## 5.2 Spray dried gel formulations from two precursors

### Introduction

In this section, the preparation and properties of hybrid silica gels prepared by using two precursors will be discussed. The chapter is divided into different sections depending on the nature of second precursors such as hydrophilic, hydrophobic and aromatic precursors. The drug release experiments, SEM and matrix porosities are discussed in detail while the different solid state NMR studies are given in the Appendix.

### 5.2.1 Hydrophobic Precursors

#### Preparation

Two different hydrophobic precursors, MTS and PTS were used for the preparation of hybrid silica gel microparticles. The preparation procedure was similar to the one discussed in the earlier chapters. The details of synthesis compositions are given in Tables 5.2.1 and 5.2.2.

**Table 5.2.1:** Relative molar ratios, pH and stirring time ( $t_s$ ) for hybrid MTS gel formulations

Gel	Name	TEOS	MTS	H <sub>2</sub> O	Ethanol	HCl	PS	$t_s$ (h)/pH
Gel 140	MTS <sub>140</sub> (5:1,0.5)	1	0.20	5.88	2.34	0.1417	0.012	24 / 0.5
Gel 141	MTS <sub>141</sub> (10:1,0.5)	1	0.10	5.39	2.14	0.1299	0.011	24 / 0.5
Gel 332	MTS <sub>332</sub> (10:1,2.2)	1	0.10	5.39	2.14	0.0130	0.011	24 / 2.2
Gel 333	MTS <sub>333</sub> (5:1,2.2)	1	0.20	5.88	2.34	0.0140	0.012	24 / 2.2

**Table 5.2.2:** Relative molar ratios, pH and stirring time ( $t_s$ ) for hybrid PTS gel formulations

Gel	Name	TEOS	PTS	H <sub>2</sub> O	Ethanol	HCl	PS	$t_s$ (h)/pH
Gel 152	PTS <sub>152</sub> (5:1,0.6)	1	0.20	5.88	2.34	0.1417	0.012	48 / 0.6
Gel 153	PTS <sub>153</sub> (3:1,0.6)	1	0.33	6.51	2.59	0.1569	0.013	48 / 0.6

### Influence of pH and composition

The *in vitro* release profiles of Persantin from hybrid MTS gel microparticles prepared under different pH conditions are given in Figure 5.2.1. An initial burst release of drug occurs from Gel 140 and Gel 141, and accounted for 50 and 70%, respectively. The release profile of Gel 332 and 333 shows with higher pH (2.2), slower release was achieved compared to gels prepared at very acidic pH (0.5). In Figure 5.2.2, the *in vitro* release of PS from hybrid PTS microparticles are shown as a function of composition. A two phase drug release with an initial burst release of drug occurs from Gel 152 and Gel 153, and accounted for 50 and 60%, respectively. The burst effect was stronger although the drug loading was lower (6 wt%). After the initial burst, a retarded release was observed. However, with higher amount of propyl units in the hybrid gel, a slightly stronger retarded release was observed (Gel 153). The kinetic release parameters are given in the inset of figures and are deviated from diffusion controlled release.

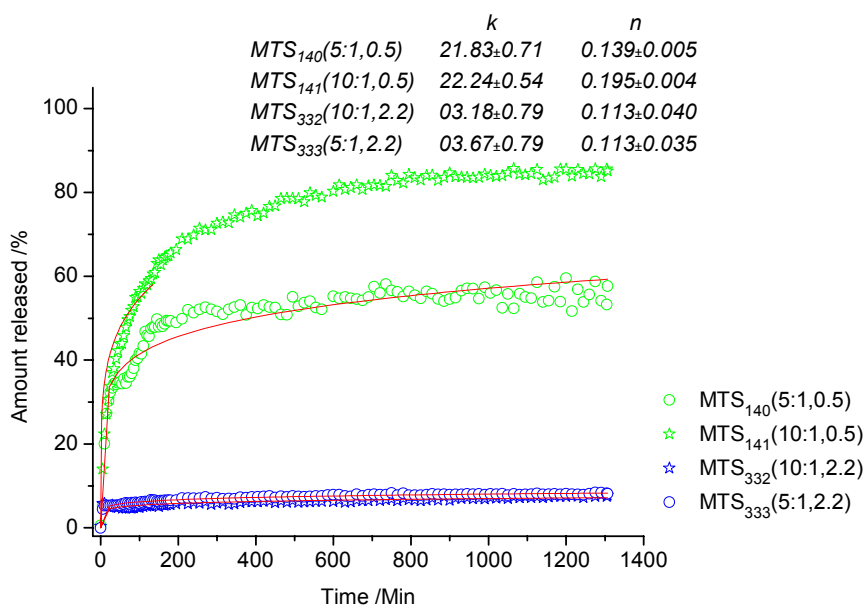


**Figure 5.2.1:** Release profiles of Persantin from hybrid MTS silica gel microparticles prepared at different pH.



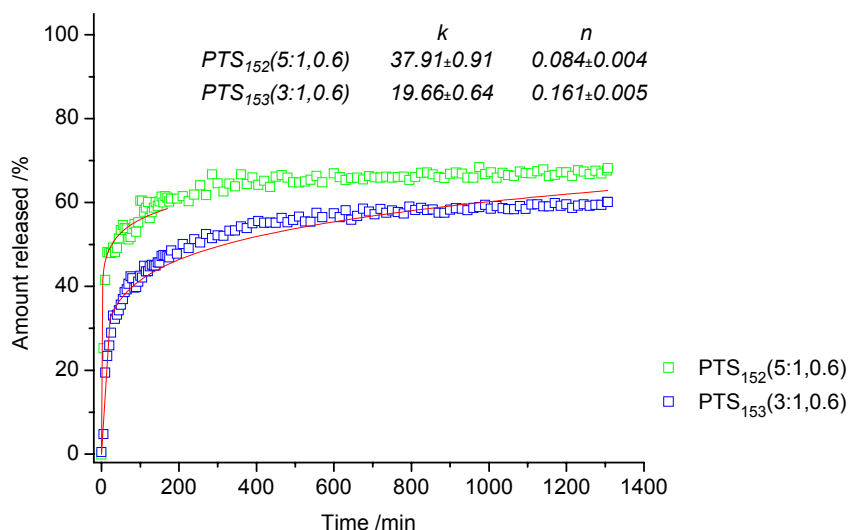


**Figure 5.2.2:** Release profiles of Persantin from hybrid PTS gel microparticles with different composition.

### **N<sub>2</sub> Sorption studies**

N<sub>2</sub> sorption studies have been carried out for the characterization of the porosity of microparticles. The N<sub>2</sub> sorption isotherm of hybrid Gel 153 and 141, which was prepared in the presence of drug, is shown in Figure 5.2.3. Drug loaded gel show no porosity and this observation is attributed to the pores being occupied by the drug molecules. After the drug extraction, there is no significant pore development for both MTS and PTS gels. This unexpected behavior is attributed to the pore collapse upon drug extraction rather than pore blocking because of the small size of alkyl groups.

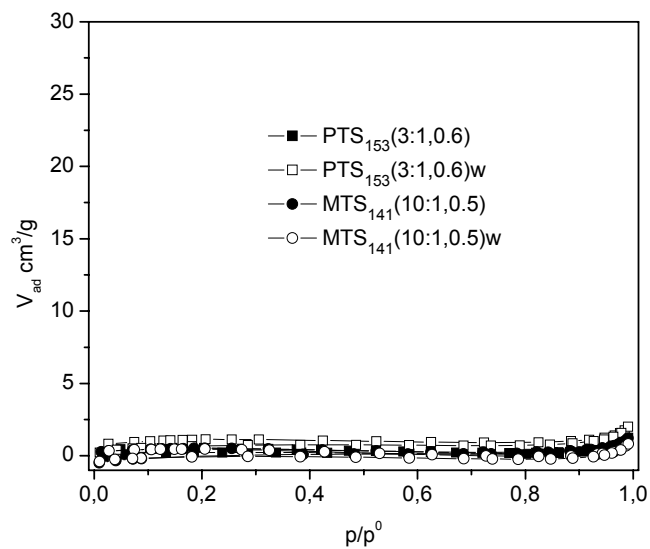


**Figure 5.2.3:**  $N_2$  sorption isotherm of drug loaded and extracted hybrid MTS and PTS gels.

## 5.2.2 Hydrophilic Precursor - ATS

### Preparation

Hydrophilic precursor, Acetoxypopyltrimethoxysilane, ATS were used for the preparation of hybrid silica gel microparticles. The preparation procedure was similar to the one discussed in the earlier chapters. The details of synthesis compositions are given in Tables 5.2.3.

**Table 5.2.3:** Relative molar ratios, pH and stirring time ( $t_s$ ) for hybrid ATS gel formulations

Gel	Name	TEOS	ATS	H <sub>2</sub> O	Ethanol	HCl	PS	$t_s$ (h)/pH
Gel 62	ATS <sub>62</sub> (5:1,1.0)	1	0.20	5.89	4.76	0.0570	0.024	24 / 1.0
Gel 103	ATS <sub>103</sub> (5:1,3.0)	1	0.20	5.89	4.76	0.0295	0.024	24 / 3.0
Gel 148	ATS <sub>148</sub> (3:1,0.5)	1	0.33	6.53	2.60	0.1570	0.013	3 / 0.5
Gel 149	ATS <sub>149</sub> (5:1,0.5)	1	0.20	5.89	2.35	0.1420	0.012	3 / 0.5
Gel 150	ATS <sub>150</sub> (10:1,0.5)	1	0.10	5.38	2.14	0.1300	0.011	3 / 0.5
Gel 203	ATS <sub>203</sub> (3:1,3.5)	1	0.33	6.53	2.60	0.0523	0.053	24 / 3.5
Gel 204	ATS <sub>204</sub> (5:1,3.5)	1	0.20	5.89	2.35	0.0472	0.048	24 / 3.5
Gel 206	ATS <sub>206</sub> (3:1,1.1)	1	0.33	6.53	2.60	0.1084	0.053	24 / 1.1
Gel 207	ATS <sub>207</sub> (5:1,1.1)	1	0.20	5.89	2.35	0.1120	0.048	24 / 1.1
Gel 208	ATS <sub>208</sub> (10:1,1.1)	1	0.10	5.38	2.14	0.2391	0.043	24 / 1.1
Gel 209	ATS <sub>209</sub> (3:1,0.6)	1	0.33	6.53	2.60	0.2770	0.053	24 / 0.6
Gel 210	ATS <sub>210</sub> (5:1,0.6)	1	0.20	5.89	2.35	0.2594	0.048	24 / 0.6
Gel 211	ATS <sub>211</sub> (10:1,0.6)	1	0.10	5.38	2.14	0.2391	0.043	24 / 0.6

### Influence of pH, composition and drug loading

In Figure 5.2.4, the *in vitro* release profiles of Persantin from hybrid ATS silica gel microparticles prepared under different pH and drug loading are shown. An initial burst release of drug occurs from Gel 103, and accounted for 80%, followed by a retarded release. The synthesis pH value for Gel 103 was 3.0 and the drug loading was around 12 wt%. A retarded release was observed for gel synthesized at pH 1.0 with similar loading, Gel 62. The release profile of Gels 148, 149 and 150 shows a retarded drug release and the drug loading was around 6 wt%. The composition effect on the release of PS has also been studied. Gel 148 (ATS mol% 25) release drug faster than Gel 150 (ATS mol% 10), which indicate that acetoxypopyl group accelerate the Persantin release. This effect was also observed for oven dried gels. The initial burst releases from Gels 203 to 211 are

accounted for 85 to 95%. The drug loading in these gels were between 18 to 20%. There was no composition influence observed in the gels with higher drug loading compared to lower drug loading. The influences of composition and pH on the release of PS were masked by the higher drug loading (Figure 5.2.5). The kinetic release parameters are given in the inset of figures and are deviated from diffusion controlled release.

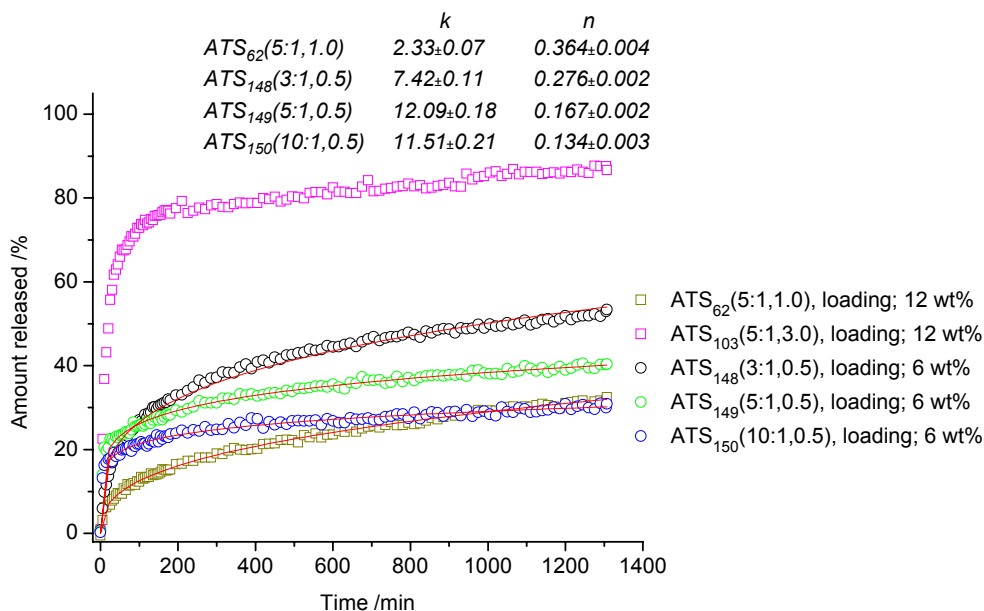


**Figure 5.2.4:** Release profiles of Persantin from hybrid ATS silica gel microparticles with different pH and composition.

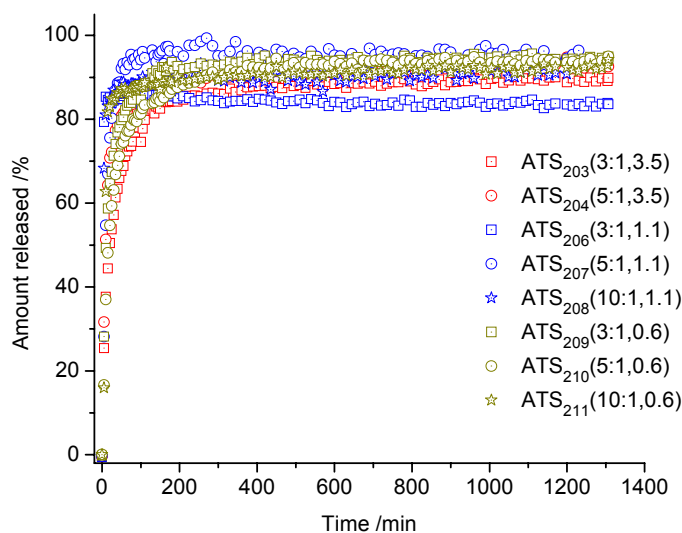


**Figure 5.2.5:** Release profiles of Persantin from hybrid ATS silica gel microparticles with different pH and composition.

### Surface studies by SEM

The SEM micrographs of Gel 203 and 209 are shown in Figure 5.2.6. The SEM micrographs reveal the agglomeration of spherical with nearly uniform sized particles before the drug dissolution. Despite of this agglomeration, all the spherical particles are in dispersed state in Gel 209, whereas in Gel 203 the particles are fused to form irregular morphologies. The fused particles are bigger than that of dispersed particle. This difference in morphology is attributed to pH effect. The synthesis pH values of the two gels were 0.6 and 3.5 for Gel 209 and 203, respectively. At very acidic pH the primary silica particles formed are positively charged and repel each other whereas at pH 3.5 the particles are neutral to weakly negatively charged and attract each other. The dispersity of the primary particles increases with increasing pH and the interfacial energy is an important factor in controlling the properties of the primary particles formed.

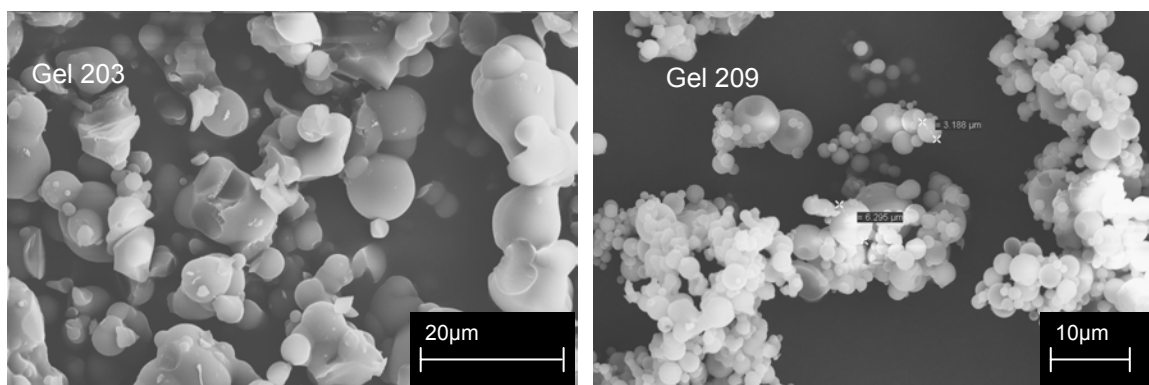


*Figure 5.2.6: SEM micrographs of Gel 203 and Gel 209*

### N<sub>2</sub> Sorption studies

The N<sub>2</sub> sorption isotherms of hybrid gel microparticles, before and after drug extraction, are shown in Figure 5.2.7 and 5.2.8. Drug loaded and drug extracted gels show no porosity. This phenomenon is characteristic of ATS gels as discussed in the last chapter.

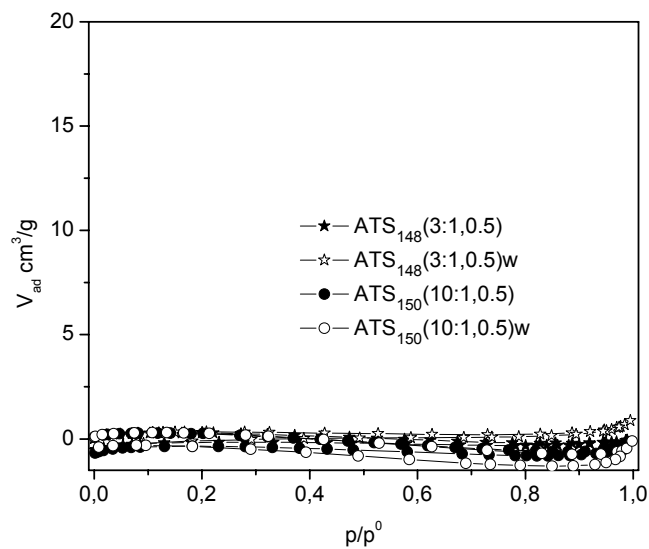


**Figure 5.2.7:**  $N_2$  sorption isotherm of drug loaded hybrid gel microparticles, before and after drug extraction (marked with w).

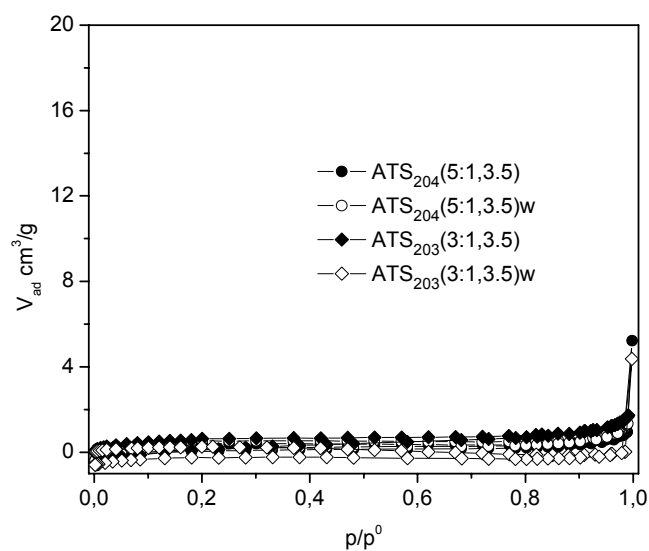


**Figure 5.2.8:**  $N_2$  sorption isotherm of hybrid Gel microparticles before and after drug extraction (marked with w).

### 5.2.3 Aromatic Precursors

#### Preparation

Different aromatic precursors, BTS, PhTS and DPhDS, were used for the preparation of aromatic substituted hybrid silica gel microparticles. The preparation procedure was similar to the one discussed in the earlier chapters. The details of synthesis compositions are given in Tables 5.2.4 to 5.2.6. There was an attempt to prepare gels at high pH values and higher concentration of second precursor but failed due to the fast gelation kinetics.

**Table 5.2.4:** Relative molar ratios, pH and stirring time ( $t_s$ ) for hybrid BTS gel formulations

Gel	Name	TEOS	BTS	H <sub>2</sub> O	Ethanol	HCl	PS	$t_s$ (h)/pH
Gel 90	BTS <sub>90</sub> (10:1,1.0)	1	0.10	5.38	4.34	0.0323	0.022	24 / 1.0
Gel 92	BTS <sub>92</sub> (5:1,1.0)	1	0.20	5.89	4.76	0.0354	0.024	24 / 1.0

**Table 5.2.5:** Relative molar ratios, pH and stirring time ( $t_s$ ) for hybrid PhTS gel formulations

Gel	Name	TEOS	PhTS	H <sub>2</sub> O	Ethanol	HCl	PS	$t_s$ (h)/pH
Gel 94	PhTS <sub>94</sub> (10:1,1.0)	1	0.10	5.38	4.34	0.0323	0.022	24 / 1.0
Gel 95	PhTS <sub>95</sub> (5:1,1.0)	1	0.20	5.89	4.75	0.0354	0.024	24 / 1.0
Gel 100	PhTS <sub>100</sub> (10:1,5.0)	1	0.10	5.38	4.34	0.0108	0.022	24 / 5.0
Gel 155	PhTS <sub>155</sub> (5:10.5)	1	0.20	5.89	2.34	0.1420	0.012	24 / 0.5
Gel 156	PhTS <sub>156</sub> (3:1,0.5)	1	0.33	6.51	2.59	0.1569	0.013	24 / 0.5
Gel 215	PhTS <sub>215</sub> (3:1,0.5)	1	0.33	6.51	2.59	0.1569	0.026	24 / 0.5
Gel 217	PhTS <sub>217</sub> (10:1,0.5)	1	0.10	5.38	2.14	0.1298	0.022	24 / 0.5

**Table 5.2.6:** Relative molar ratios, pH and stirring time ( $t_s$ ) for hybrid DPhDS gel formulations

Gel	Name	TEOS	DPhDS	H <sub>2</sub> O	EtOH	HCl	PS	$t_s$ (h)/pH
Gel 142	DPhDS <sub>142</sub> (3:1,0.6)	1	0.33	6.53	2.60	0.1575	0.053	24 / 0.5
Gel 143	DPhDS <sub>143</sub> (5:1,0.6)	1	0.20	5.88	2.34	0.1417	0.048	24 / 0.5
Gel 144	DPhDS <sub>144</sub> (10:1,0.6)	1	0.10	5.38	2.14	0.1298	0.044	24 / 0.5
Gel 218	DPhDS <sub>218</sub> (3:1,0.3)	1	0.33	6.53	2.60	0.1575	0.026	24 / 0.5
Gel 219	DPhDS <sub>219</sub> (5:1,0.3)	1	0.20	5.88	2.34	0.1417	0.024	24 / 0.5
Gel 220	DPhDS <sub>220</sub> (10:1,0.3)	1	0.10	5.38	2.14	0.1298	0.022	24 / 0.5

### Influence of composition

The release profiles of PS from gels made with different TEOS:BTS ratios are compared in Figure 5.2.9. A high level of BTS in the hybrid gel leads to a decrease in the drug release for gels prepared at a pH value around 1.0. What is more striking is the partial substitution by benzyl group induces a strong retarding effect in the hybrid gel. There is an influence of composition on the release of drug even at pH 1.0 for benzyl substituted gels. The release kinetics parameters indicate a deviation from diffusion controlled release (inset of Figure 5.2.9).

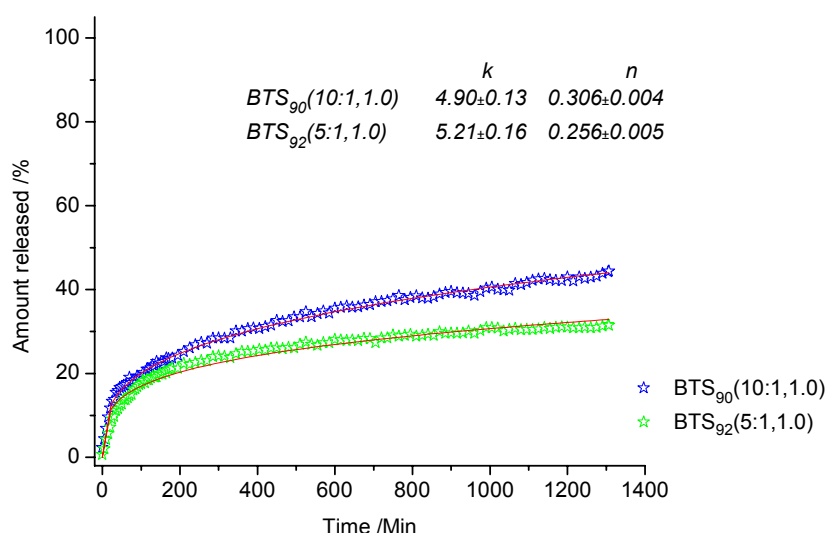


**Figure 5.2.9:** Release profiles of Propranolol from hybrid BTS silica gels with different composition.

### Influence of pH and drug loading

In Figure 5.2.10 and 5.2.11 the release profiles of Persantin from PhTS microparticles are shown under different drug loading and pH conditions. Whilst Gel 94 and 95 show a retarded release, an initial burst release of drug occurs from Gel 100, which prepared at pH 5.0 and accounted for 60%. Only less than 40% of drug was released from gels synthesized at pH 1.0 (Gel 94 and 95), within the 22 hours. The effect of drug loading in the release rate has also been studied. The release profile of Gel 156 shows, with lower drug loading, a slower release was achieved compared to gels with higher drug loading (Gel 215). A strong compositional influence was also observed in the PhTS gels. While



drug release from Gel 156 (3:1) was only 10% within 22 hours, 60% release was observed from Gel 155 (5:1) in the same period. With higher amount of PhTS in the hybrid gel microparticles, a stronger retarded drug release was observed. This is attributed to the hydrophobic effect of phenyl groups.

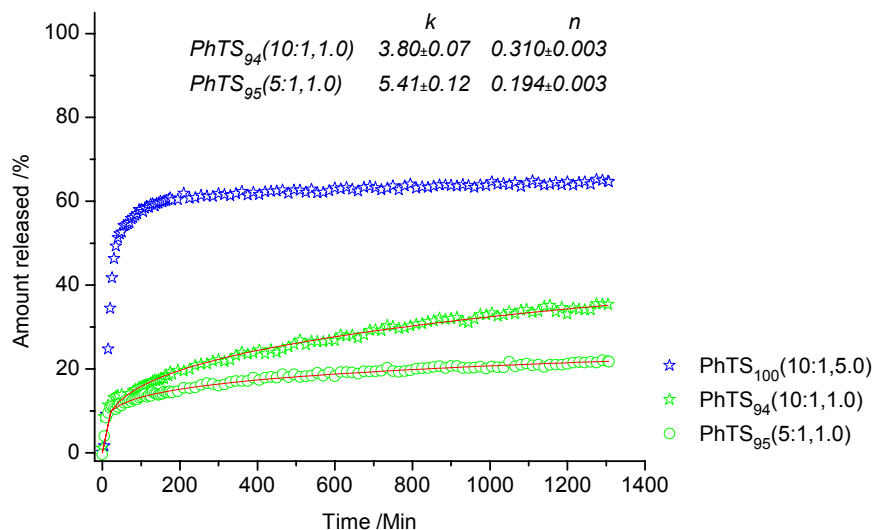


**Figure 5.2.10:** Release profiles of Persantin from hybrid PhTS silica gels with different pH.

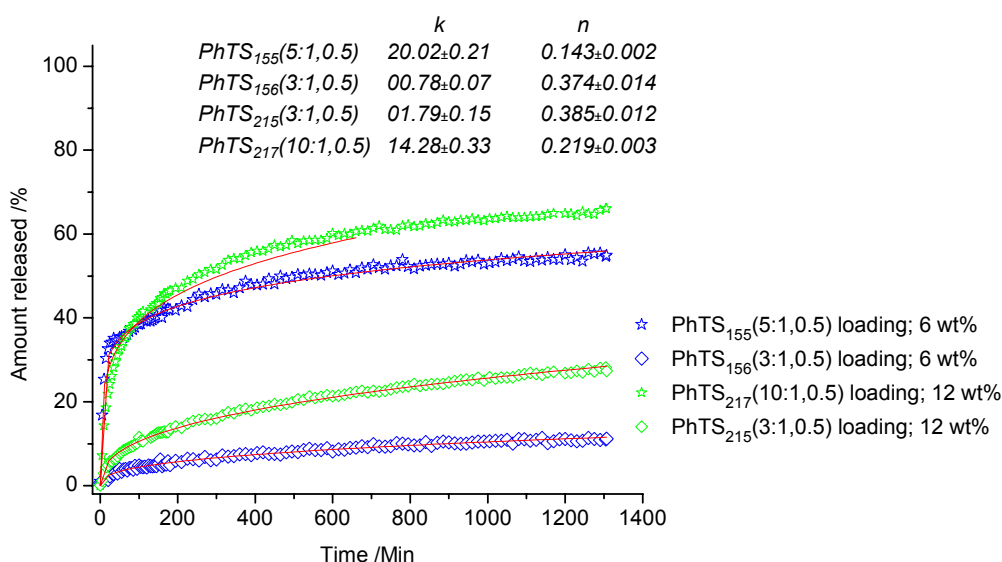


**Figure 5.2.11:** Release profiles of Persantin from hybrid silica gels with different drug loading.

### Influence of composition and drug loading

The release profiles of Persantin from hybrid silica gel microparticles prepared under different drug loading and composition conditions are shown in Figure 5.2.12. All the DPhDS hybrid gels show very strong retarded release within the drug loading range of this study. When the TEOS:DPhDS ratio in the hybrid gel was (3:1), no significant influence on the release of PS was observed for drug loading between 9 and 18 wt% (Gel 142 and 218). Faster drug release was observed for gels with higher drug loading, when the TEOS:DPhDS ratio was 10:1 in the hybrid gel (Gel 144 and 220). With a higher amount of diphenyl units in the hybrid gel, a stronger retarded drug release was observed. No burst release was observed for these DPhDS substituted microparticles. The retarded releases from the diphenyl substituted gels are attributed to the hydrophobic effect. The kinetic release parameter  $n$  shows the release from the DPhDS gels with 9 wt% drug loading were close to diffusion controlled, Gel 218 ( $n = 0.41$ ) and Gel 219 ( $n = 0.36$ ) (inset of Figure 5.2.12).

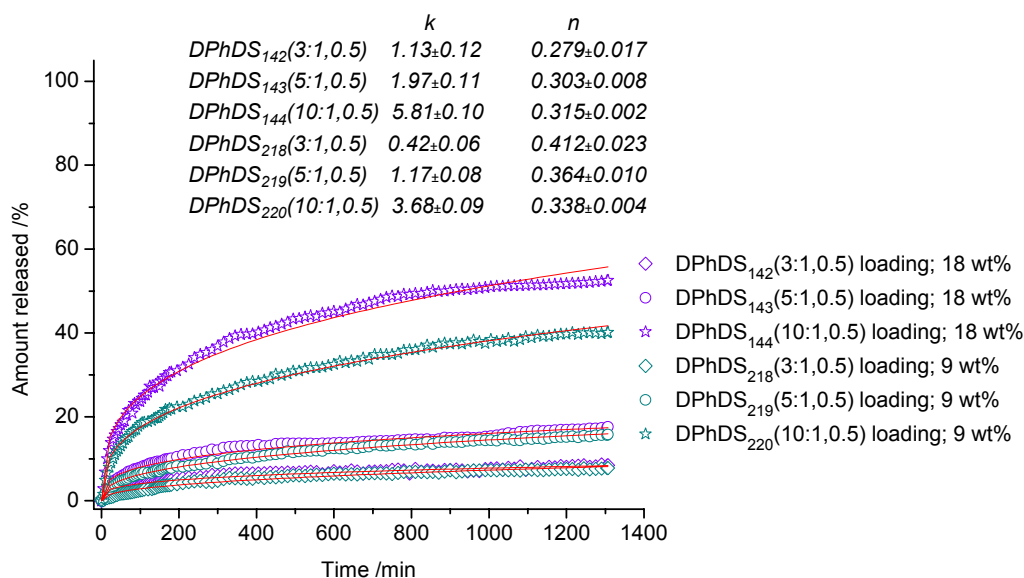


**Figure 5.2.12:** Release profiles of Persantin from spray dried hybrid DPhDS silica gels with different composition and drug loading.

## N<sub>2</sub> Sorption studies

The N<sub>2</sub> sorption isotherms of hybrid BTS and PhTS gel microparticles are shown in Figure 5.2.13 and 5.2.14, respectively. Drug loaded and drug extracted gels show no porosity. Only less than 50 % of the drug came out within 22 hours of drug extraction for BTS as well as PhTS gels and the remaining drug molecules exist in the pores, lowering the N<sub>2</sub> sorption capacity. These gels were prepared at a synthesis pH value of 1.0.

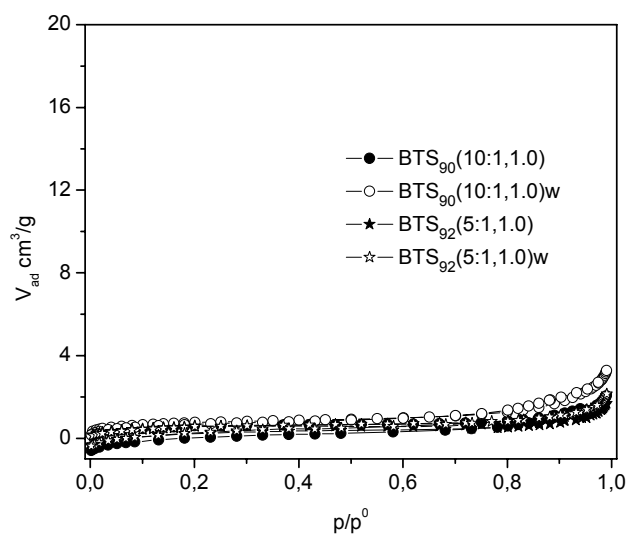


**Figure 5.2.13:** N<sub>2</sub> sorption isotherm of drug loaded hybrid BTS gel, before and after drug extraction (marked with w).

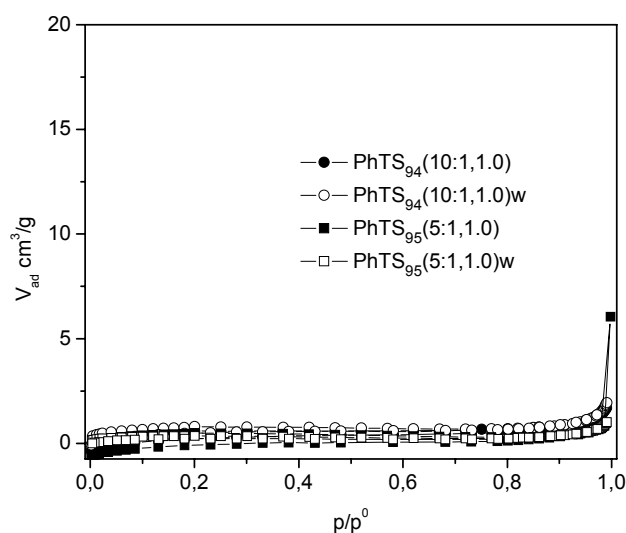


**Figure 5.2.14:** N<sub>2</sub> sorption isotherm of drug loaded hybrid PhTS gel, before and after drug extraction (marked with w).

$N_2$  sorption isotherms of hybrid PhTS gels 215 and 217, which were prepared at synthesis pH value 0.5 and with a 12 wt% drug loading, are shown in Figure 5.2.15. After the drug extraction for 22 h, hybrid Gel 217w with TEOS: PhTS ratio 10:1 shows microporosity. From the DRT data it is clear that about 70% drug are released within 22 hours. The  $N_2$  sorption isotherms of the drug extracted Gel 217w is of type I, characteristic of microporous materials. Significant pore volumes for drug extracted gels are originated as observed using the Horvath-Kawazoe method. The BET surface area and the micropore volume are  $280 \text{ m}^2/\text{g}$  and  $0.143 \text{ cm}^3/\text{g}$ , respectively. There is no porosity for drug extracted Gel 215w. Only less than 20% drug was released within 22 hours for Gel 215, as shown by the DRT data. Therefore, most of the pores in Gel 215 are occupied by the drug molecules and are not accessible for  $N_2$  molecules. The void space generated by the 20 % release is not reflected in the  $N_2$  adsorption. Pore blocking or gel collapse may be the reason. The PhTS hybrid Gel 100 prepared at pH value of 5.0, show no porosity although it lies in the porous regime. The drug extracted gel show relatively small BET surface area ( $99 \text{ m}^2/\text{g}$ ).

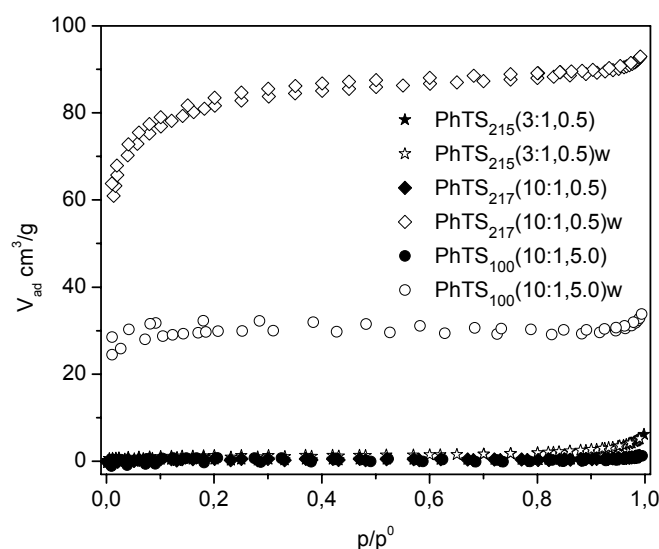


**Figure 5.2.15:**  $N_2$  sorption isotherm of drug loaded hybrid PhTS gel microparticles, before and after drug extraction (marked with w).

The  $N_2$  sorption isotherms of hybrid DPhDS gel microparticles, which are prepared in the presence of drug, are shown in Figure 5.2.16. Generally drug loaded and drug extracted gels show no porosity, however, drug extracted Gel 220w show little porosity. The BET surface area and micropore volume are  $11.3 \text{ m}^2/\text{g}$  and  $0.014 \text{ cm}^3/\text{g}$ , respectively.

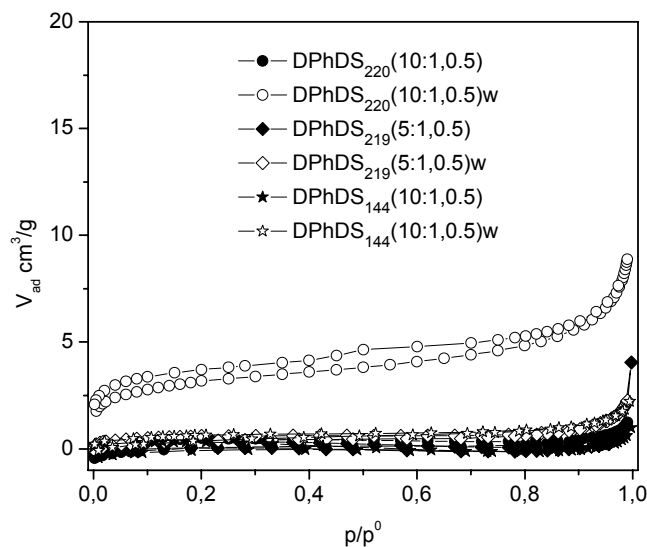


**Figure 5.2.16:**  $N_2$  sorption isotherm of drug loaded hybrid gel microparticles, before and after drug extraction (marked with w).

### Surface studies by SEM

The microscopic analysis by scanning electron microscopy was carried out on microparticles to obtain information about the morphology and to evaluate their shape, size and surface. The SEM micrographs of Gel 215 and 217 are given in Figure 5.2.17. The SEM micrographs reveal the agglomeration of spherical with nearly uniform sized particles before and after the drug dissolution. Despite of this agglomeration all the spherical particles are in dispersed state and have an average diameter around 3  $\mu\text{m}$ . The amplified micrographs reveal the formation of hollow spheres upon spray drying. The micrograph also shows that a mixture of buckled spherical particles and fine spherical particles are formed during spray drying. A mixture of spray dried particles was generated as a result of a broad size distribution of the atomized droplet that was present in a spray drying process. Dimpled spherical particles were formed as a result of buckling of the shell during in which capillary force driving the shell deformation overcome the steric or electrostatic forces stabilizing against aggregation.<sup>154</sup> The microparticles after drug dissolution show no collapse of structure. However, there is a significant change in the surface morphologies as can be clearly seen in the amplified micrograph of Gel 217W. The appearance of rough surface indicates the dissolution of salt and subsequent degradation of the particles.

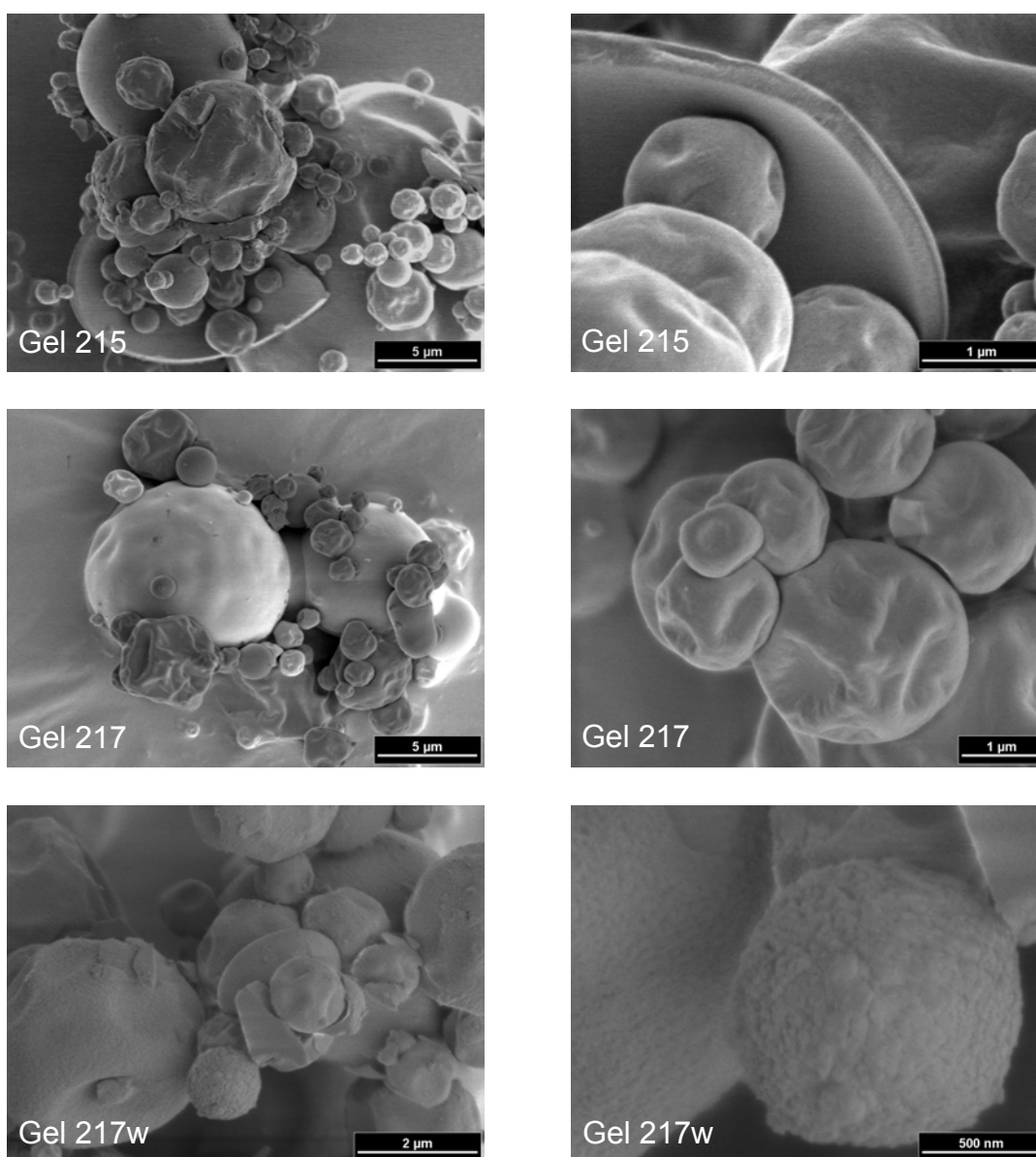


**Figure 5.2.17:** SEM micrographs of Gel 215 and 217 before and after drug dissolution. The amplified micrographs are given on the right side.

The SEM micrographs of hybrid DPhDS Gels 219 and 220 are given in Figure 5.2.18. The SEM micrographs reveal the agglomeration of spherical with nearly uniform sized particles before and after the drug dissolution. The micrograph of Gel 219 shows the shooting out of microparticles from larger spheres. The amplified micrographs reveal the formation of hollow spheres as well as a mixture of buckled spherical particles and fine spherical particles. The microparticles after drug dissolution show no collapse of structure.

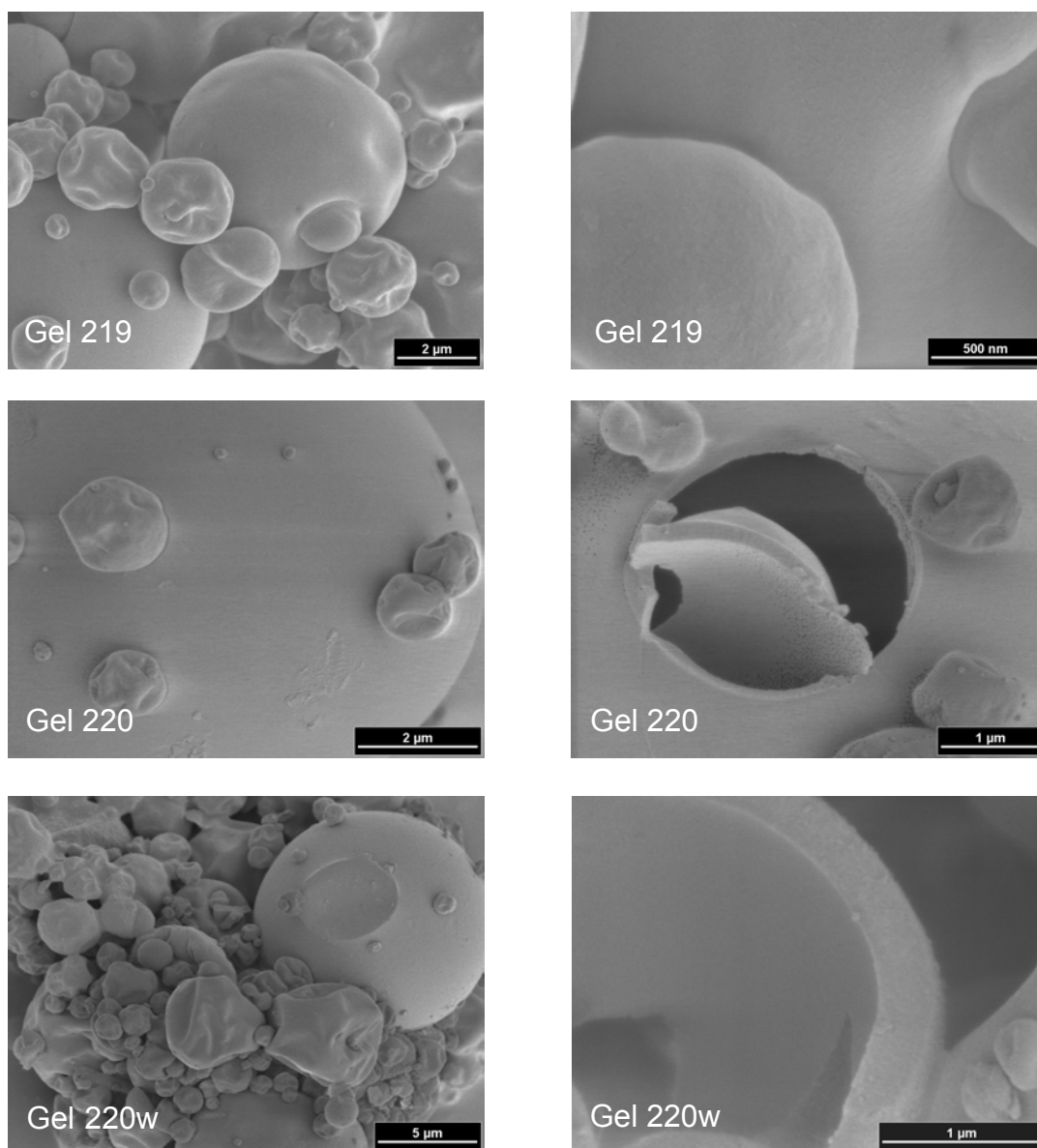


*Figure 5.2.18: SEM micrographs of Gel 219 and 220 before and after drug dissolution. The amplified micrographs are given on the right side.*

## 5.2.4 Discussion

### Hydrophilicity vs Hydrophobicity

Drug release from spray dried microparticles prepared with hydrophobic substitution tends to retard the drug release compared to single precursor gels made with TEOS. This

observation is in support of the earlier reports appeared in the literature.<sup>58</sup> The poor wettability and favorable drug-matrix interactions, compared to drug-water (dissolution medium) interaction, are the limitations of hydrophobic substituted microparticles.

### **EISA vs SD**

The release of PS has been enhanced by the spray drying route compared to EISA gels.<sup>104</sup> Generally faster drug release was observed for SD gels. However, Aromatic substituted gels show a sustained release at lower drug loadings. A higher drug loading in gels could increase the release of PS and further the bioavailability. There are two main factors affecting the drug release from EISA and SD gels: the rate of removal of solvent and the size and shape of drug carrier gel particles. In the EISA method, a slow evaporation of solvent induces an assembly between drug and silica oligomer through short range interactions. After the drying step, irregularly sized and shaped monoliths are formed from the EISA method. It can be argued that the EISA and SD gels have different drug distribution and interactions in the solid dispersions because of their different solvent evaporation rates. The drug release from the crushed monoliths is diffusion controlled whereas SD particles often show a burst release. It has been proposed by Mathiowitz et al.<sup>155</sup> that the short release rates of spray dried particles find applications in cases where fast drug releases is needed. The spray dried microparticles are very small and the release of the incorporated material occurs via two independent processes. The first is diffusion of the drug through fluid-filled pores, formed by the dissolution of the incorporated drug particles; the second is via erosion of the matrix.



**Porosity development in SD gels**

Similar to EISA gels, porosity development was observed for drug dissolved SD gels. In case on TEOS gels, drug extraction pilots to a structure collapse of microparticles. This was observed by the scanning electron microscopy and was later confirmed by solid state NMR. This observation is in correlation with the template effect of drug molecules discussed in the earlier chapters.

## **6. Spray Dried Gels with Propranolol**

---

### **Introduction**

Evaporation induced self assembled silica and hybrid gel materials prepared in presence of guest molecule Propranolol has been discussed in chapter 4. It has been shown that EISA processes represent interesting alternatives because of their intrinsic characteristics: the use of sol-gel method, the absence of macroscopic phase separation and simultaneous formation of the microporous and the functionalized channels. Different characterization techniques have been adopted to understand the underlying physico-chemical phenomena as well as to improve and expand the final properties of such systems. However, the silica gel monolith production is time consuming. Crushed silica gel particles are irregular in shape and size. These facts led to evaluate spray drying as a production method for silica gel microspheres with a narrow particle size range and to evaluate these microspheres as a carrier for controlled administration of PP. In this chapter the potentials of spray dried silica gels for controlled release of PP with and without different organic functionalization have been focused. In section 6.1, formulations from single precursors are discussed whereas in 6.2, formulations from two precursors are discussed.

### **6.1 Spray dried gel formulations from a single precursor**

#### **6.1.1 Preparation**

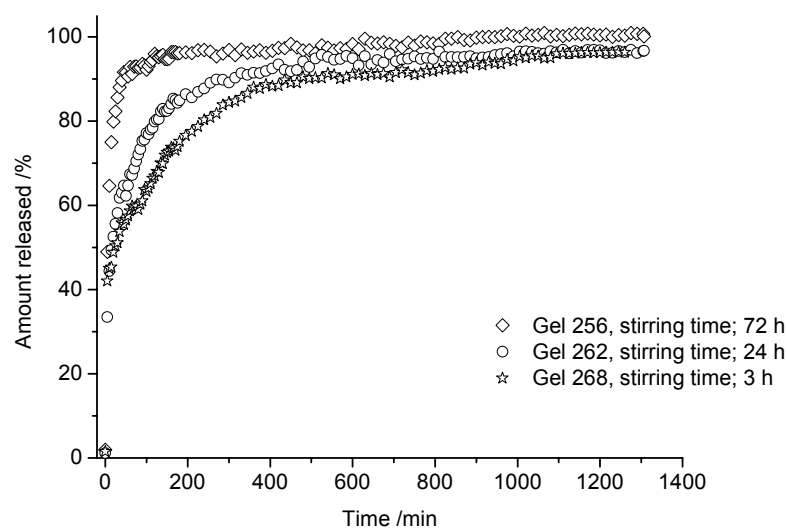
Spray dried silica gels were prepared from pure TEOS precursor. The preparation and spray drying procedure are similar to the one discussed in the earlier chapters. The details of synthesis compositions are given in Table 6.1.1. The yield of the spray dried microparticles was in the range of 80-90 % compared to the oven dried gel.

**Table 6.1.1:** Relative molar ratios, pH and stirring time ( $t_s$ ) for single precursor gel formulations

Gel	TEOS	H <sub>2</sub> O	Ethanol	HCl	PP	$t_s$ (h)/pH
Gel 256	1	4.9	1.95	0.0588	0.015	72 / 1.2
Gel 262	1	4.9	1.95	0.0588	0.015	24 / 1.2
Gel 268	1	4.9	1.95	0.0588	0.015	3 / 1.2
Gel 17	1	4.9	1.95	0.0098	0.029	24 / 2.0
Gel 323	1	4.9	1.95	0.0011	0.015	24 / 2.0

### 6.1.2 Drug release studies

The *in vitro* release profiles of Propranolol from silica gel microparticles prepared under different sol stirring time are shown in Figure 6.1.1. An initial burst release of drug occurs from all the three gels and was accounted for about 80 %. After the initial burst, a slower release phase was observed for gels prepared with shorter stirring time (Gel 268). This observation is unexpected and further studies have to be carried out for a feasible explanation. The effect of drug loading in the release rate has also been studied. In Figure 6.1.2, the release profiles shows, with lower drug loading (Gel 323) a slower release was achieved compared to gels with higher drug loading (Gel 17). A fast initial release occurs for gel synthesized at lower pH (Gel 262, pH = 1.2) whereas a retarding effect was observed for gel synthesized at pH around 2.0, Gel 323 as shown in Figure 6.1.2. Since the burst release of Propranolol was higher than 60 %, no kinetic studies conducted.

**Figure 6.1.1:** Drug release profiles of Propranolol from spray dried silica gels with different sol stirring time.

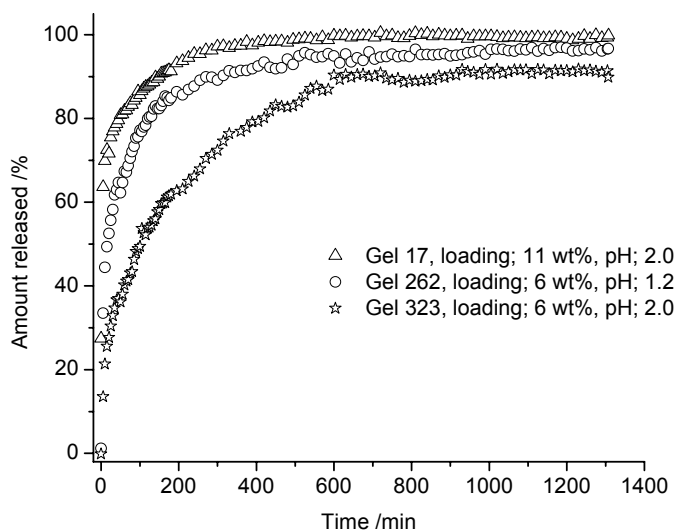


**Figure 6.1.2:** Drug release profiles of Propranolol from silica gels with different synthesis pH and drug loading.

### 6.1.3 Surface studies by SEM

The SEM micrograph of Gel 17 is shown in Figure 6.1.3. It can be seen that there are many fine spherical particles and few doughnut like particles were formed from the fraction of larger droplets produced by the spray dryer. As discussed in section 2.6, there are different factors influences the morphology of particle. The deformation of spherical shape could be due to the increase in the droplet size or increase in the droplet density. When the size of the primary particles is between 25 to 50 nm, deformed spherical particles can be formed.<sup>154</sup> The absence of surface porosity is in good agreement with that of the N<sub>2</sub> sorption measurement.

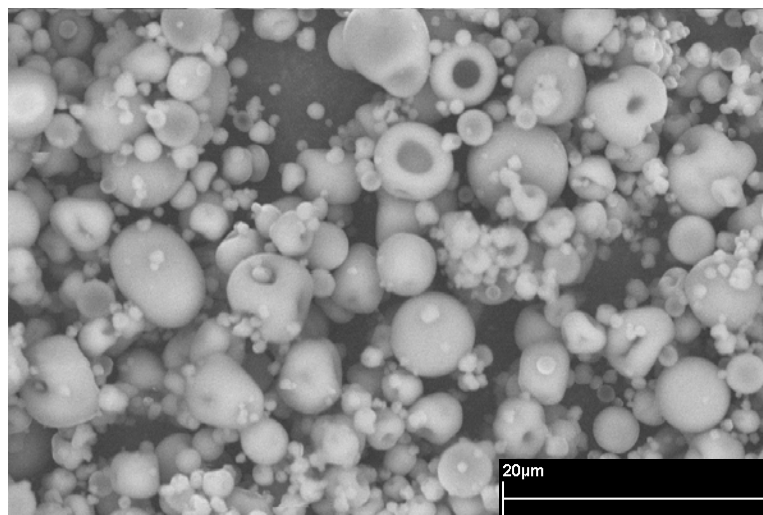


*Figure 6.1.3: SEM micrograph of Gel 17 prepared in the presence of Propranolol.*

#### 6.1.4 N<sub>2</sub> Sorption studies

N<sub>2</sub> sorption studies have been carried out for the characterization of the porosity of microparticles. The N<sub>2</sub> sorption isotherms of the drug loaded Gel 17 and 323 show nonporous materials (Figure 6.1.4). The absence of porosity can be attributed to the fact that the pores are occupied by the drug molecules. In washed gels the porosity appears with specific surface area of 194 and 211 m<sup>2</sup>/g for Gel 17w and 323w, respectively. These gels were synthesized at the pH value of 2.0, where generally dense materials are formed. The generation of porosity after the drug extraction is attributed to the emptying of drug filled pore upon extraction.

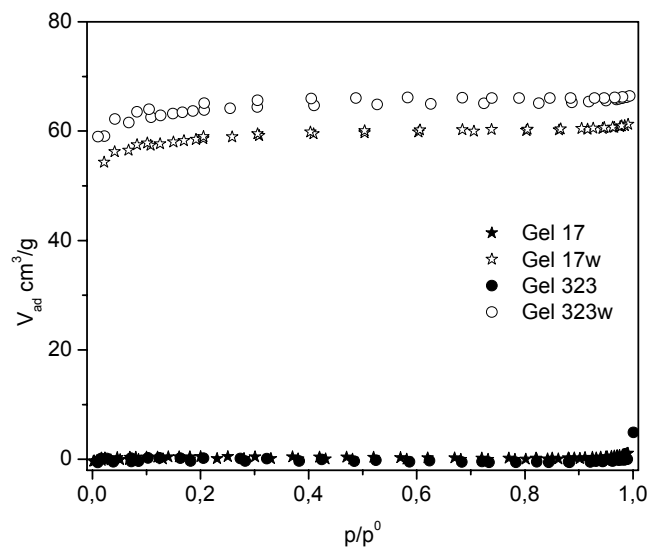


*Figure 6.1.4: N<sub>2</sub> sorption isotherm of spray dried gel, Gel 17.*

### 6.1.5 <sup>1</sup>H MAS NMR studies

The proton MAS NMR spectrum of spray dried Gel 268 prepared in the presence of the drug Propranolol is compared with spectrum of pure drug and is shown in Figure 6.1.5. The spectrum of spray dried microparticles and their assignments are similar to that of EISA gels. The sharper lines compared to EISA gels in the spectrum confirm the presence of mobility in the gel.

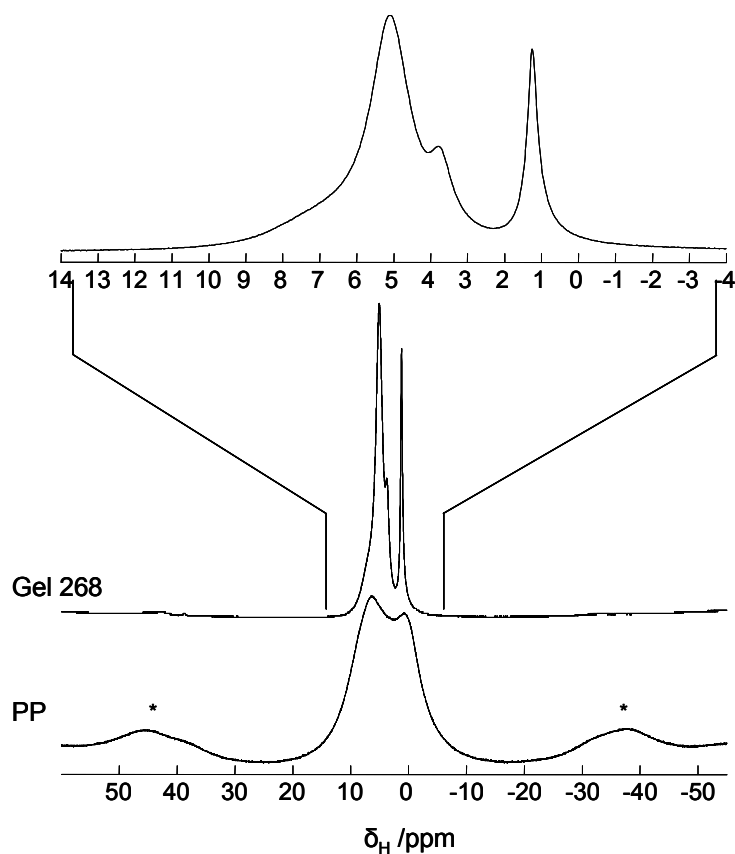


**Figure 6.1.5:** The  $^1\text{H}$  MAS NMR spectra of spray dried Gel 268 and pure drug at 15 kHz. Intensities are not in absolute scale.

### 6.1.6 $^{13}\text{C}\{^1\text{H}\}$ CPMAS NMR studies

The  $^{13}\text{C}\{^1\text{H}\}$  CPMAS NMR spectra of Gel 17 prepared in the presence of the drug, Propranolol, is shown in Figure 6.1.6. It is compared with the spectra of the pure drug. The assignments of the peaks are similar to the ones reported in the earlier chapters. The spectra unambiguously establish the presence of PP intact in the microparticles.

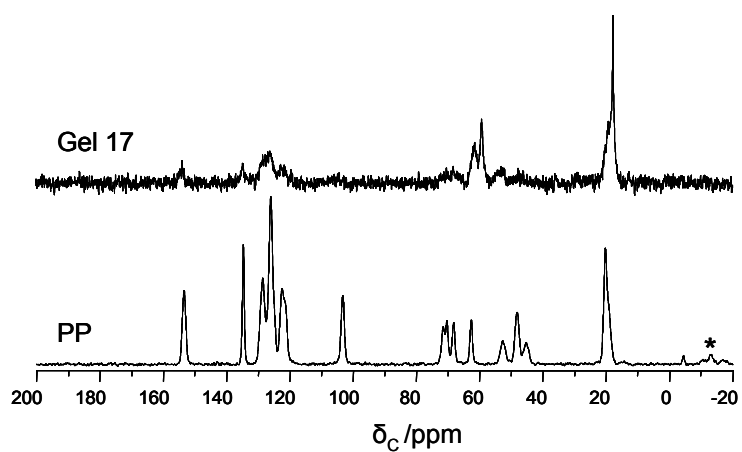


*Figure 6.1.6:  $^{13}\text{C}\{^1\text{H}\}$  CPMAS NMR spectra of Gel 17.*



## 6.2 Spray dried gel formulations from two precursors

### Introduction

In this chapter, the preparation and properties of hybrid silica gel microparticles prepared by using two precursors will be discussed. The chapter is divided into different sections depending on the nature of second precursors such as hydrophilic, hydrophobic and aromatic precursors. The drug release experiments, SEM and matrix porosities are discussed in detail and the different solid state NMR studies are given in the Appendix.

### 6.2.1 Hydrophobic Precursors

#### Preparation

Two different hydrophobic precursors, MTS and ETS were used for the preparation of hybrid silica gel microparticles. The preparation procedure was similar to the one discussed in the earlier chapters. The details of synthesis compositions are given in Tables 6.2.1 and 6.2.2.

**Table 6.2.1:** Relative molar ratios, pH and stirring time ( $t_s$ ) for hybrid MTS gel formulations

Gel	Name	TEOS	MTS	H <sub>2</sub> O	Ethanol	HCl	PP	$t_s$ (h)/pH
Gel 119	MTS <sub>119</sub> (10:1,1.0)	1	0.10	5.39	2.14	0.0323	0.032	24 / 1.0
Gel 120	MTS <sub>120</sub> (5:1,1.0)	1	0.20	5.88	2.34	0.0353	0.035	24 / 1.0
Gel 271	MTS <sub>271</sub> (5:1,1.0)	1	0.20	5.88	2.34	0.0706	0.018	24 / 1.0
Gel 315	MTS <sub>315</sub> (10:1,2.2)	1	0.10	5.39	2.14	0.0011	0.016	24 / 2.2
Gel A47	MTS <sub>A47</sub> (5:1,1.4)	1	0.20	19.60	4.90	0.0392	0.049	24 / 1.4
Gel A48	MTS <sub>A48</sub> (3:1,1.4)	1	0.33	19.60	4.90	0.0392	0.049	24 / 1.4

**Table 6.2.2:** Relative molar ratios, pH and stirring time ( $t_s$ ) for hybrid ETS gel formulations

Gel	Name	TEOS	ETS	H <sub>2</sub> O	Ethanol	HCl	PP	$t_s$ (h)/pH
Gel 123	ETS <sub>123</sub> (5:1,1.2)	1	0.20	5.88	2.34	0.0353	0.035	24 / 1.2
Gel 124	ETS <sub>124</sub> (10:1,1.2)	1	0.10	5.39	2.14	0.0323	0.035	24 / 1.2
Gel 272	ETS <sub>272</sub> (5:1,1.0)	1	0.20	5.88	2.34	0.0706	0.018	03 / 1.0
Gel 320	ETS <sub>320</sub> (5:1,2.2)	1	0.20	5.88	2.34	0.0012	0.018	24 / 2.2

### Influence of drug loading, pH and composition

The release profiles of Propranolol from hybrid silica gels prepared under different drug loading is shown in Figure 6.2.1. Propranolol release was increased during the first hours with higher amount of drug loading in the hybrid gel (Gel 119 and 120). The burst effect was stronger when the drug loading was 10 wt%. Almost 99 % of the drug was released within the first hours. There was no influence of composition observed on the release of drug when the drug loading was higher. With lower drug loading (6 wt%), a retarded drug release was observed (Gel 271 and 315). In Figure 6.2.2 is shown the release profile from microparticles synthesized with higher  $r$  value. A two phase release was observed with 90 % release in the first phase followed by a retarded release (Gel A47 and A48). The observed increase in the release rate may be attributed to the fact that the drug molecules which are molecularly dispersed on the microparticles are easily dissolved into the solution.

The release profiles of Propranolol from hybrid ETS silica gels prepared under different drug loading is shown in Figure 6.2.3. ETS gels show release kinetics similar to MTS gels.

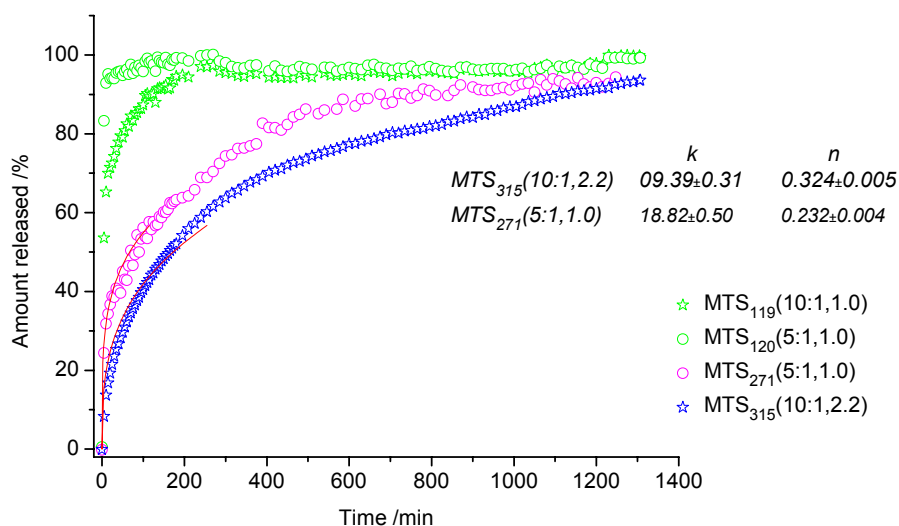


**Figure 6.2.1:** Release profiles of Propranolol from hybrid MTS silica gel microparticles with different drug loading and pH.

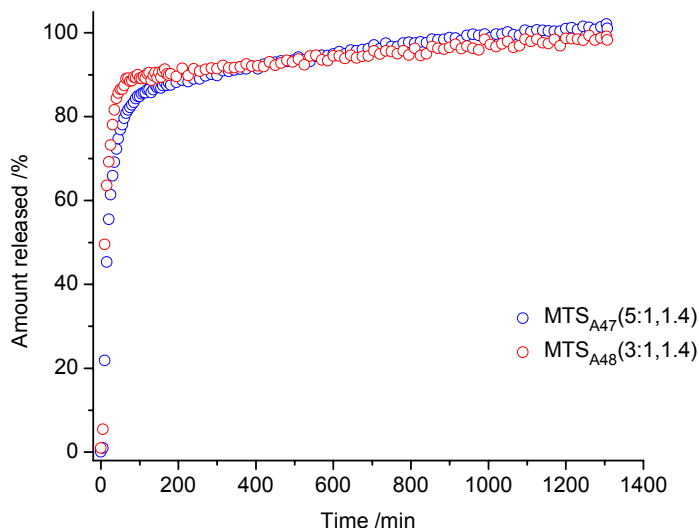


**Figure 6.2.2:** Release profiles of Propranolol from hybrid MTS silica gel microparticles with different composition.

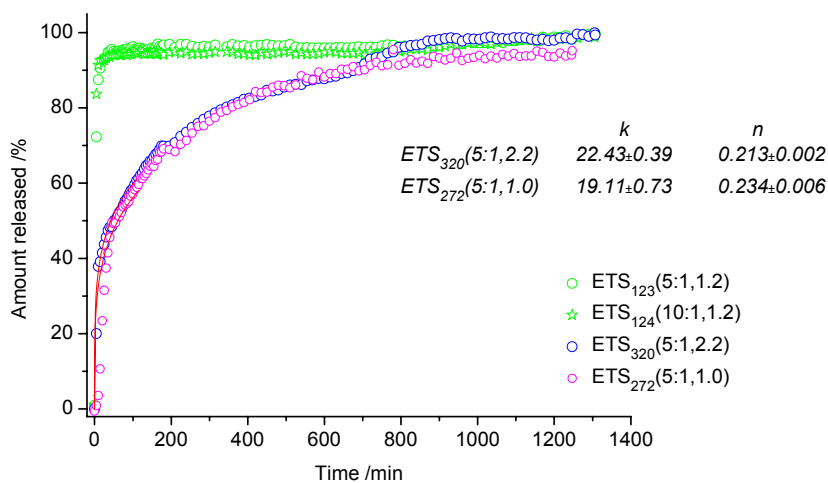


**Figure 6.2.3:** Release profiles of Propranolol from hybrid ETS silica gels with different pH and drug loading.

## N<sub>2</sub> Sorption studies

The N<sub>2</sub> sorption isotherm of a spray dried hybrid MTS gel, which was prepared in the presence of drug, is shown in Figure 6.2.4. The drug loaded gel show no porosity (Gel A47) whereas the drug extracted gel is microporous (Gel A47w) with a type I isotherm.

Significant pore volume for the drug extracted gel was originated as observed using the Horvath-Kawazoe method. Also the BET surface area is much higher for the drug extracted gel. The BET surface area and micropore volume for Gel A47w are  $310 \text{ m}^2/\text{g}$  and  $0.152 \text{ cm}^3/\text{g}$ , respectively.

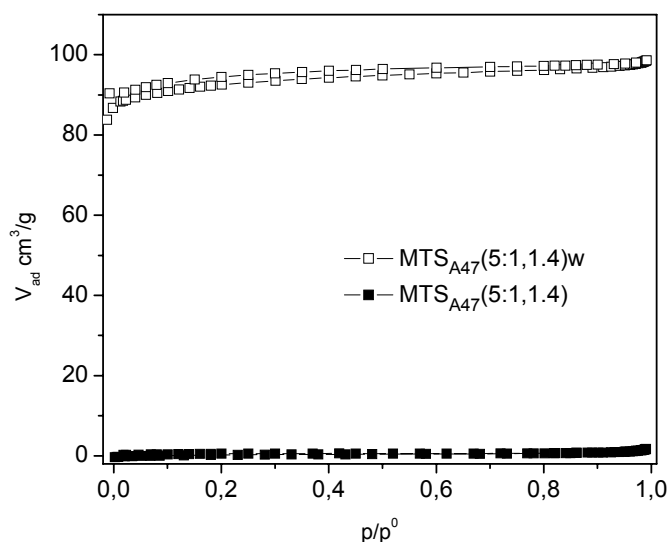


**Figure 6.2.4:**  $N_2$  sorption isotherm of drug loaded hybrid MTS gel microparticles, before and after drug extraction (marked with w).

The  $N_2$  sorption isotherms of hybrid ETS gels, which are prepared in the presence of drug, are shown in Figure 6.2.5. The drug extraction was done here by heating the sample at 623 K and the encapsulated drug was burned out. There was no porosity observed for the same gel heated at 423 K. The  $N_2$  sorption isotherm of the drug unloaded gels is of type I, characteristic of microporous materials. A significant pore volume for the calcined gel was observed using the Horvath-Kawazoe method. The BET surface area and micropore volume for Gel 123@623 K are  $114 \text{ m}^2/\text{g}$  and  $0.056 \text{ cm}^3/\text{g}$ , respectively.

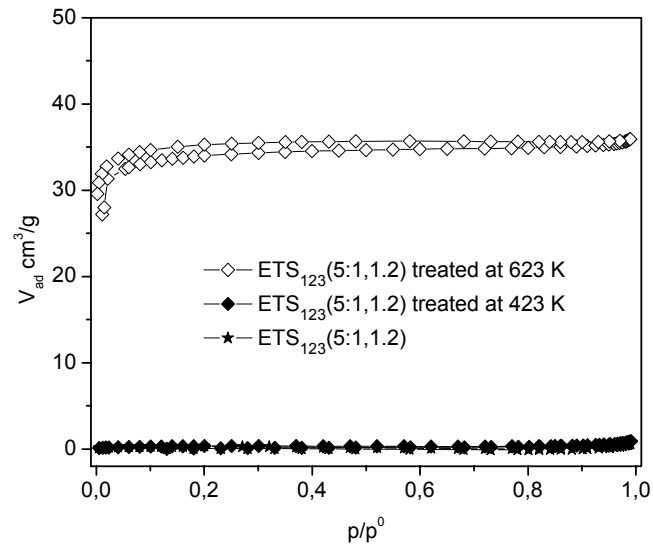


**Figure 6.2.5:**  $N_2$  sorption isotherm of various drug loaded hybrid ETS gel microparticles, before and after calcinations at different temperatures.

## 6.2.2 Hydrophilic Precursor - ATS

### Preparation

Hydrophilic precursor, acetoxypolytrimethoxysilane was used for the preparation of hybrid silica gel microparticles. The preparation procedure was similar to the one discussed in the earlier chapters. The details of synthesis compositions are given in Tables 6.2.3. The yield of the spray dried microparticles was in the range of 70-85 % compared to the oven dried gel.

**Table 6.2.3:** Relative molar ratios, pH and stirring time ( $t_s$ ) for hybrid gel formulations

Gel	Name	TEOS	ATS	H <sub>2</sub> O	Ethanol	HCl	PP	$t_s$ (h)/pH
Gel 125	ATS <sub>125</sub> (5:1,1.0)	1	0.20	5.88	2.34	0.0354	0.035	24 / 1.0
Gel 126	ATS <sub>126</sub> (10:1,1.0)	1	0.10	5.38	2.14	0.0323	0.032	24 / 1.0
Gel A39	ATS <sub>A39</sub> (3:1,3.0)	1	0.33	13.07	5.20	0.0392	0.033	24 / 3.0
Gel 313	ATS <sub>313</sub> (10:1,2.3)	1	0.10	5.38	2.14	0.0011	0.016	24 / 2.3
Gel 261	ATS <sub>261</sub> (5:1,1.0)	1	0.20	5.88	2.34	0.0707	0.018	72 / 1.0
Gel 267	ATS <sub>267</sub> (5:1,1.0)	1	0.20	5.88	2.34	0.0707	0.018	24 / 1.0
Gel 273	ATS <sub>273</sub> (5:1,1.0)	1	0.20	5.88	2.34	0.0707	0.018	03 / 1.0

### DRT - Influence of pH and composition

The release profiles of Propranolol from hybrid ATS silica gels prepared under different drug loading and pH are shown in Figure 6.2.6. About 95 % of the drug was released within the first hours from Gels 125, 126 and A39. The initial burst effect was stronger in these gels and are attributed to the higher drug loading (10 wt%) effect. However, with lower drug loading (6 wt%), a retarded drug release was observed (Gel 313) in the initial stages of drug release. There was no influence of composition on the release of drug observed when the drug loading was higher. In Figure 6.2.7, the release profiles of PP are compared in terms of sol stirring time. Gel 273 was spray dried after stirring for 3 hours and shows a retarded release. With higher sol stirring time a faster release was observed (Gel 261 and 267).

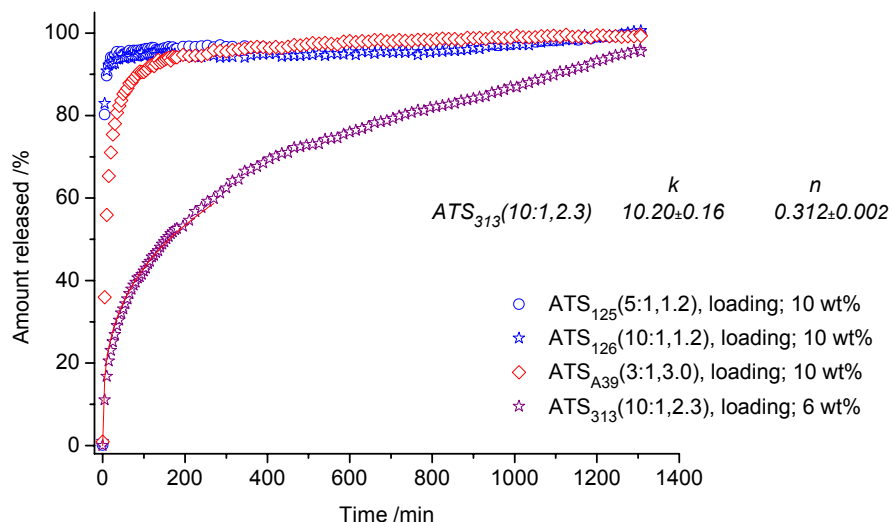


**Figure 6.2.6:** Release profiles of Propranolol from hybrid silica gels with different pH and composition.

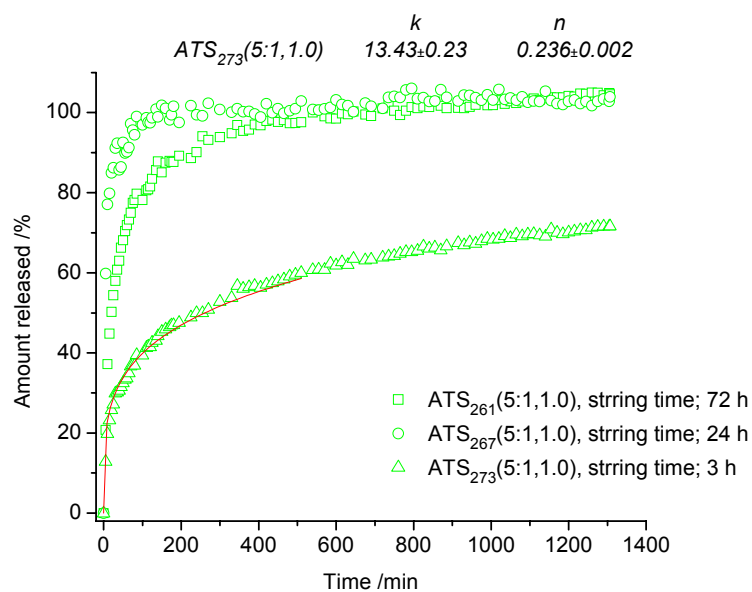


**Figure 6.2.7:** Release profiles of Propranolol from hybrid silica gels with different stirring time.

## N<sub>2</sub> Sorption studies

The N<sub>2</sub> sorption isotherms of hybrid gels, which are prepared in the presence of drug, are shown in Figure 6.2.8. Drug loaded and drug extracted gels show no porosity.

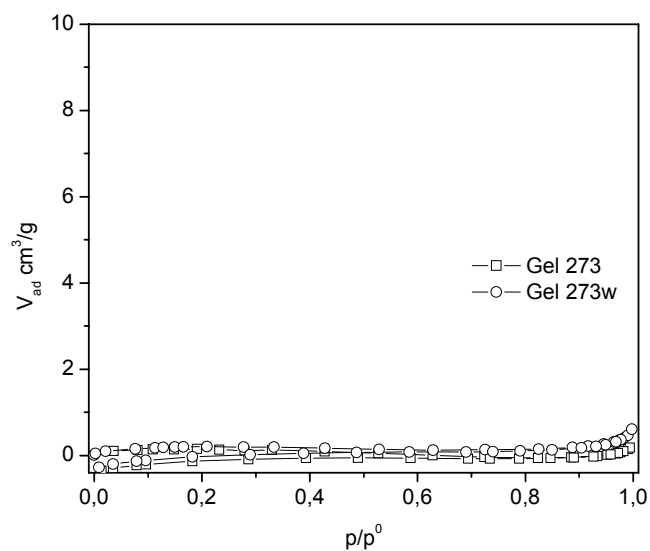


**Figure 6.2.8:** N<sub>2</sub> sorption isotherm of drug loaded hybrid ATS gel microparticles, before and after drug extraction (marked with w).



### 6.2.3 Aromatic Precursors

#### Preparation

Different aromatic precursors, BTS, PhTS and DPhDS, were used for the preparation of aromatic substituted hybrid silica gel microparticles. The preparation procedure was similar to the one discussed in the earlier chapters. The details of synthesis compositions are given in Tables 6.2.6 to 6.2.8.

**Table 6.2.4:** Relative molar ratios, pH and stirring time ( $t_s$ ) for hybrid gel formulations

Gel	Name	TEOS	BTS	H <sub>2</sub> O	Ethanol	HCl	PP	$t_s$ (h)/pH
Gel 115	BTS <sub>115</sub> (10:1,1.0)	1	0.10	5.38	2.14	0.0323	0.032	24 / 1.0
Gel 116	BTS <sub>116</sub> (5:1,1.0)	1	0.20	5.89	2.35	0.0354	0.035	24 / 1.0
Gel 317	BTS <sub>317</sub> (10:1,2.2)	1	0.10	5.38	2.14	0.0011	0.016	24 / 2.2

**Table 6.2.5:** Relative molar ratios, pH and stirring time ( $t_s$ ) for hybrid gel formulations

Gel	Name	TEOS	PhTS	H <sub>2</sub> O	Ethanol	HCl	PP	$t_s$ (h)/pH
Gel 117	PhTS <sub>117</sub> (10:1,1.0)	1	0.10	5.38	2.14	0.0323	0.032	24 / 1.0
Gel 118	PhTS <sub>118</sub> (5:1,1.0)	1	0.20	5.89	2.35	0.0354	0.035	24 / 1.0
Gel 257	PhTS <sub>257</sub> (5:1,1.0)	1	0.20	5.89	2.35	0.0707	0.018	72 / 1.0
Gel 263	PhTS <sub>263</sub> (5:1,1.0)	1	0.20	5.89	2.35	0.0707	0.018	24 / 1.0
Gel 322	PhTS <sub>322</sub> (5:1,2.2)	1	0.20	5.89	2.35	0.0012	0.000	24 / 2.2

**Table 6.2.6:** Relative molar ratios, pH and stirring time ( $t_s$ ) for hybrid gel formulations

Gel	Name	TEOS	DPhDS	H <sub>2</sub> O	Ethanol	HCl	PP	$t_s$ (h)/pH
Gel 258	DPhDS <sub>258</sub> (5:1,1.0)	1	0.20	5.89	2.34	0.0707	0.018	72 / 1.0
Gel 270	DPhDS <sub>270</sub> (5:1,1.0)	1	0.20	5.89	2.34	0.0707	0.018	3 / 1.0

#### DRT - Influence of pH, composition and drug loading

In Figure 6.2.9, the *in vitro* release profiles of PP are shown as a function of drug loading and pH. Propranolol release was increased during the first hours with higher amount of drug loading in the hybrid BTS gels (Gel 115 and 117). The burst effect was stronger for drug loading with 10 wt%. However, with lower drug loading (6 wt%), a retarded drug

release was observed (Gel 317). At around pH 2.2 the strongest retarding effect was observed. The release kinetics of drug from Gel 317 was diffusion controlled as shown by the parameter,  $n$ .

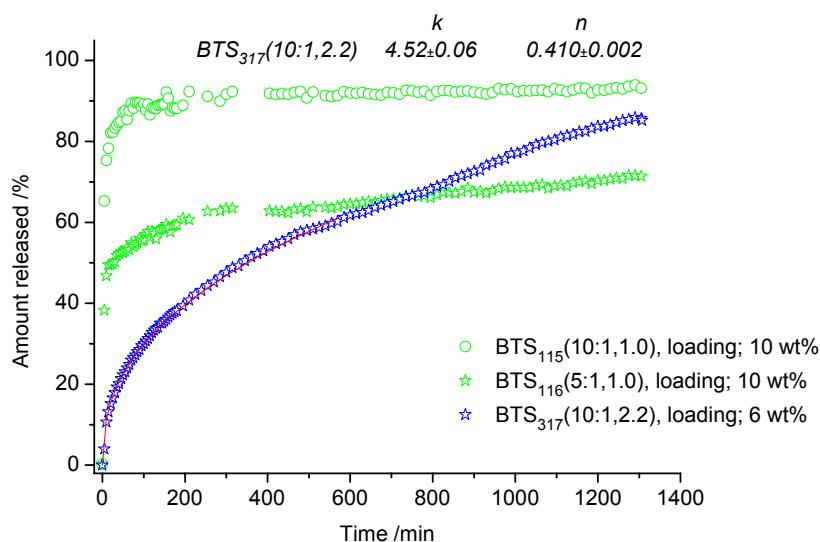


**Figure 6.2.9:** Release profiles of Propranolol from hybrid silica gels with different pH and drug loading.

The effect of synthesis pH, drug loading and composition on the release of PP from hybrid PhTS silica gels has been studied, Figure 6.2.10. Hybrid PhTS silica Gels 117 and 118 with different composition show analogous release curves. Burst release was observed for both gels in the early stages of release. The drug loading was around 10 wt% in both the gels. Propranolol release was decreased during the first hours with lower amount of drug loading (6 wt%) in the hybrid gels (Gel 257 and 263). Although a strong retarded release was observed for oven dried hybrid PhTS gels, burst release was dominated in the spray dried gels.

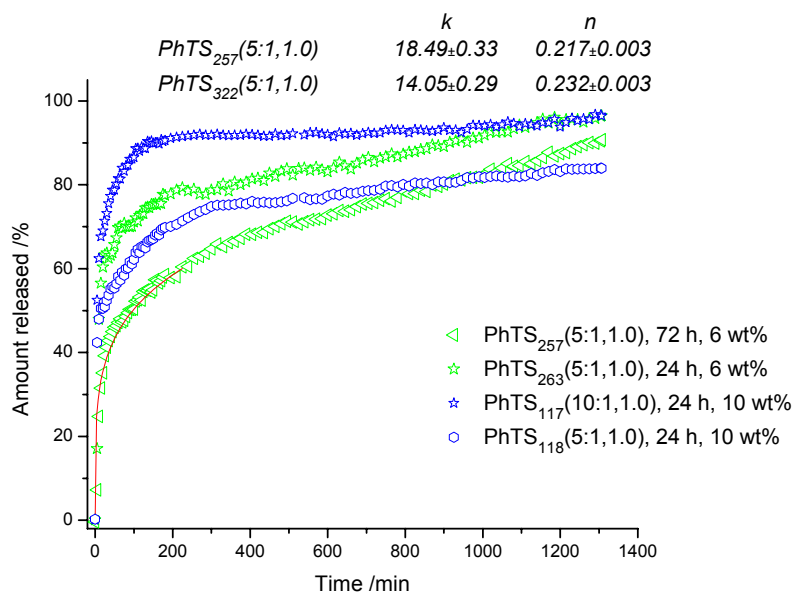


**Figure 6.2.10:** Release profiles of Propranolol from hybrid PhTS silica gels with different composition, stirring time and drug loading.

The release profiles of Propranolol from hybrid DPhDS silica gels prepared under different sol stirring time are shown in Figure 6.2.11. Propranolol release was retarded very strongly by DPhDS gels although the pH was very acidic. The burst effect was stronger for gel prepared with short sol stirring time (Gel 270) and was accounted for 40%. After the initial burst a retarded release was observed. Although the retarded release was observed at the early stages of drug release for Gel 258, higher amount of drug could diffuse out from the gel in the long run. The kinetic parameter  $n$  shows the release from the Gel 258 were diffusion controlled.

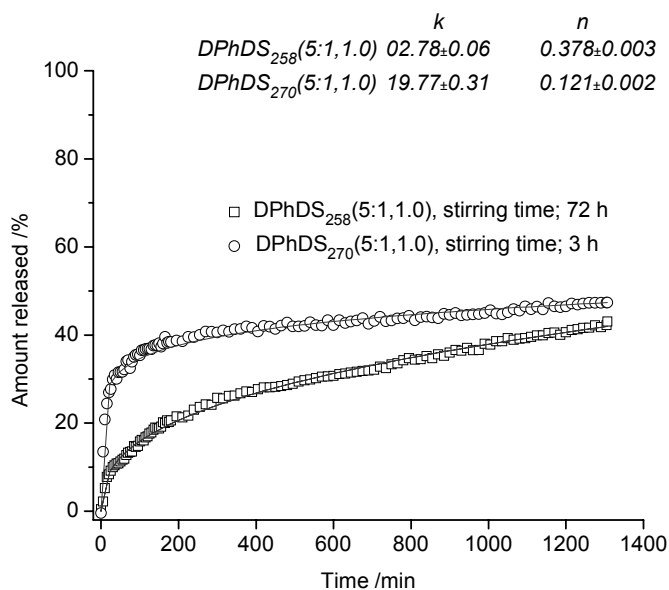


**Figure 6.2.11:** Release profiles of Propranolol from spray dried hybrid silica gels with different sol stirring time.

## **N<sub>2</sub> Sorption studies**

The N<sub>2</sub> sorption isotherm of the Gel 117 and 115, before and after washing are given in Figure 6.2.12. Both BTS and PhTS hybrid gels show no porosity before washing. However, porosity appears after drug extraction and was more pronounced for PhTS gel. The BET surface areas are 174 and 15 m<sup>2</sup>/g for Gel 117 and 115, respectively. The type I isotherm of Gel 117 confirm the microporous nature of the material. In Figure 6.2.13 showed the sorption isotherm of a DPhDS Gel 270, before and after drug extraction and are nonporous.

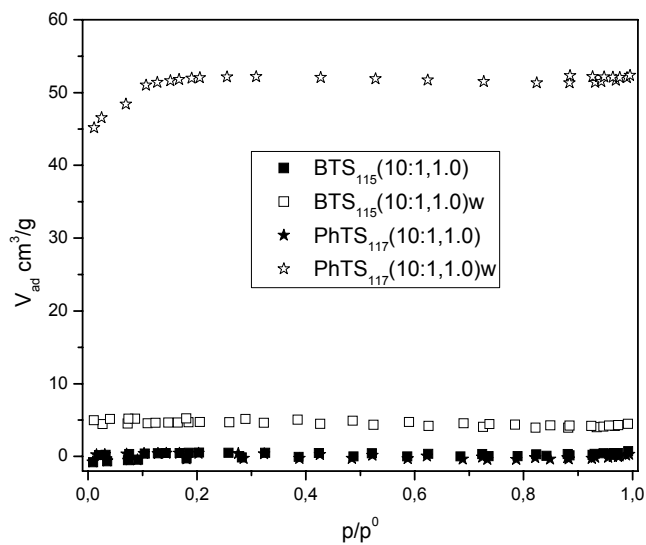


**Figure 6.2.12:**  $N_2$  sorption isotherm of drug loaded hybrid gel microparticles, before and after drug extraction (marked with w).

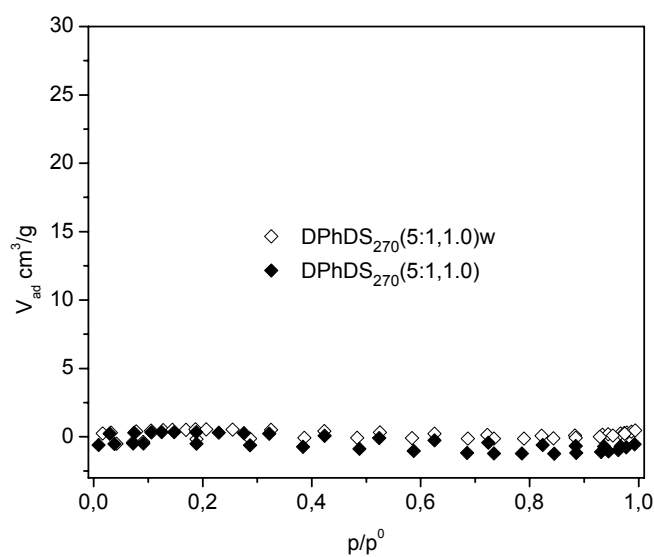


**Figure 6.2.13:**  $N_2$  sorption isotherm of drug loaded hybrid gel microparticles, before and after drug extraction (marked with w).

### 6.2.4 Discussion

PP release from SD microparticles was clearly different to that of PS. Although SD gels exhibit faster releases, PP release was faster than PS. The structure of SD microparticles and the release rate of PP were controlled by the synthesis parameters. Compared to EISA gels, Propranolol release was faster from spray dried gels. The drug loading capacity of SD particles are much less compared to EISA gels. A retarded release was observed for microparticles prepared at synthesis pH value close to 2.0. Aromatic substitution on the hybrid gel microparticles leads to a sustained release of PP compared to alkyl substitution and pure silica gels. Aromatic substitution on hybrid gel leads to a denser network formation. In addition, the hydrophobicity and non wettability of these microparticles retard the drug release.

Similar to EISA gels, porosity development was observed for drug dissolved SD gels. Porosity was measured for a spray dried sample after treating at different temperatures. Samples treated below 423 K show no porosity whereas, adsorption capacity was observed for microparticles treated at 623 K. This simple experiment proves that the porosity was developed not by the removal of physisorbed solvents, but by the emptying of templated pores.

#### **PS vs PP**

The drug release from evaporation induced self assembled gels and spray dried gels was studied both with PS and PP. The release rate of PS was slower than that of PP from both EISA and SD gels. This is attributed to the difference in the physicochemical properties of the drugs. PS is a bulky drug molecule with large number of centers with hydrogen bonding capacity. This will help the molecule to interact with matrix and strongly encapsulated in the silica gel. PP is a small molecule which can be easily extracted from the pores by dissolution medium. In general, the physicochemical properties such as size, solubility, hydrophobicity,  $pK_a$  and crystallinity of the pharmaceutically active substance affect the drug release behavior. Inhomogeneous distribution and crystallization of the drug molecules in the silica gels were excluded on the basis of PXRD and DSC studies. The stability of drug in the silica matrix was examined with the help of solid state NMR and found to be intact.

The release of drug from hybrid silica gels synthesized at charge-matching pH regime show striking differences compared to other pH regimes. Retarded drug dissolution was observed for gels synthesized at charge-matching regime despite the different processing conditions. Aromatic substituted hybrid gels show the most retarded drug release kinetics. One important question unanswered is exactly what is the role of host-guest interactions in these self-assembled systems for such release behaviors. With the help of DRT and adsorption studies, it is impossible to determine the molecular level host-guest interactions. Another important unanswered question is what are the reasons for the anomaly in the drug release trend as well as the sorption capacity shown by ATS gels. One dimensional  $^{29}\text{Si}$ ,  $^{13}\text{C}$  and  $^1\text{H}$  solid state NMR analysis of different hybrid gels provided crucial information such as the physical form of the drug and its stability in the carrier systems. However, detailed information about the structure, topology, dynamics and interactions on molecular level cannot be provided by 1D NMR experiments. To this end, high resolution solid state two dimensional heteronuclear correlation NMR techniques have been proposed to obtain detailed structural information and to probe the nature of intermolecular interactions in various hybrid gels.

## **7. High resolution solid state NMR spectroscopy**

---

### **Introduction**

The material properties of the hybrid gels depend on the molecular structure and their organization and dynamics in the solid state. High resolution solid state NMR spectroscopy plays a key role in characterization of inorganic-organic hybrid materials generated by sol-gel route. Both evaporation induced self assembled gels and spray dried gels contains NMR active nuclei such as  $^1\text{H}$ ,  $^{13}\text{C}$  and  $^{29}\text{Si}$ . The hybrid gels contain protons in the organic and inorganic components and thus, the attributions of the  $^1\text{H}$  MAS NMR resonances are not trivial and require high resolution spectra. In order to obtain detailed structural information and to probe the nature of intermolecular dynamics within the hybrid gels, high resolution multidimensional NMR spectroscopy is a prerequisite. For this purpose, different high resolution solid state NMR techniques such as high field and high speed  $^1\text{H}$  MAS NMR and  $^1\text{H}$ - $^{29}\text{Si}$  and  $^1\text{H}$ - $^{13}\text{C}$  heteronuclear dipolar correlation (HETCOR) NMR spectroscopy with frequency switched Lee-Goldburg (FSLG) homonuclear decoupling has been employed. In addition, conventional solid state NMR techniques, such as MAS and CPMAS have been applied.

### **7.1 2D $^1\text{H}$ - $^{13}\text{C}$ FSLG HETCOR NMR - Propranolol Hydrochloride**

The 2D spectra of Propranolol hydrochloride with 0.1 ms contact time are shown in Figure 7.1 and the projection along the F2 dimension of the 2D spectrum is identical to a 1D  $^{13}\text{C}\{^1\text{H}\}$  CPMAS spectrum.



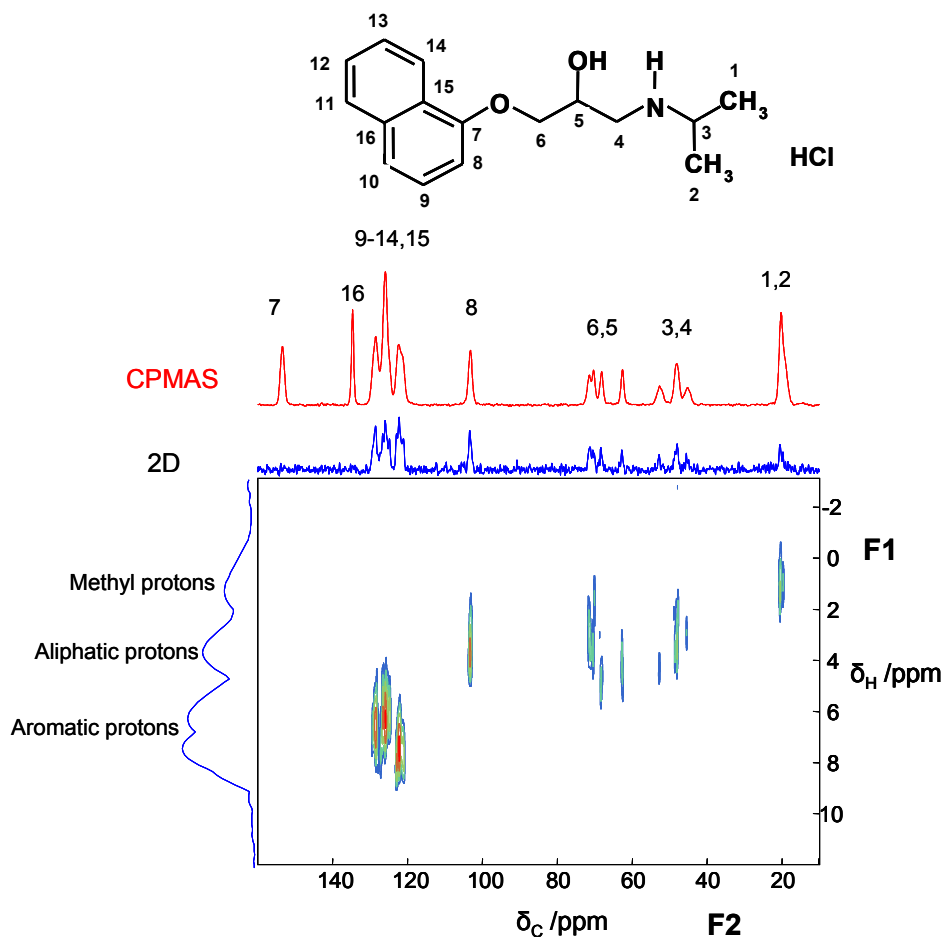


**Figure 7.1:** 2D  $^1\text{H}-^{13}\text{C}$  FSLG HETCOR spectrum of PP with skyline projections (bottom) and 1D  $^{13}\text{C}\{^1\text{H}\}$  CPMAS spectrum (top).

The assignment of the  $^{13}\text{C}$  spectral resonances of Propranolol Hydrochloride to different carbons shown in the spectrum are performed on the basis of the  $^{13}\text{C}$  solution NMR spectrum, because the solid state chemical shifts are usually quite similar, the only difference arising from conformational and/or packing effects. It must be noted that the signals in the range 40 to 74 ppm arise from the four carbon atoms, namely C3, C4, C5 and C6, for which four distinct resonances are present in the solution spectrum. The inequivalence in the solid state must be associated to the restricted motional behavior of these carbons, which are substantially “frozen” in a definite conformation and the different peaks are due to the different chemical environment of the carbon nuclei.<sup>156</sup> The broad signal centered at 20.5 ppm is assigned to the two methyl carbons and the peaks in the 120.0 – 160.0 ppm range are assigned to the aromatic carbons. The assignments are

further corroborated by the 2D FSLG HETCOR experiments. In the 2D spectrum, the peaks at 135.0 and 153.0 ppm (C16 and C7, respectively) show no correlations with the protons. This can be easily understood since no protons are directly bound to these carbons, and the magnetization transfer is too weak at longer distances for 0.1 ms contact time. Mutual correlations between aliphatic carbons and an aromatic carbon C8 with a proton source at 3.8 (F1) ppm is observed and is attributed to the packing effect because of the absence in the liquid spectrum. From the crystal structure,<sup>157</sup> it is clear that the carbon C8 lies within very close proximity of protons of C6 which can transfer the magnetization intramolecularly with short contact time. The 2D HETCOR spectra measured without suppression on <sup>1</sup>H spin diffusion during CP, and during the on resonance CP, transverse dephasing of CH coherences is much faster than the CH<sub>2</sub> protons.<sup>158</sup> Consequently these CH<sub>2</sub> hydrogen atoms become the main source of proton magnetization transferred to carbon (C6), and their signals dominate in <sup>1</sup>H projection of 2D HETCOR spectra. Although it is an unusual observation, no further studies has been carried out, as it is a minor point in the thesis.

## 7.2 Methyl Substituted Hybrid EISA Gel – Gel 37

### 7.2.1 <sup>1</sup>H High Field High Speed MAS NMR

By employing MAS rates approaching 35 kHz, high-resolution <sup>1</sup>H MAS NMR spectra of Gel 37 [MTS<sub>37</sub>(3:1,1.8)], without homonuclear decoupling were obtained. Figure 7.2 shows the improvement in the resolution observed in the <sup>1</sup>H NMR spectra of Gel 37 taken with increasing MAS frequency.

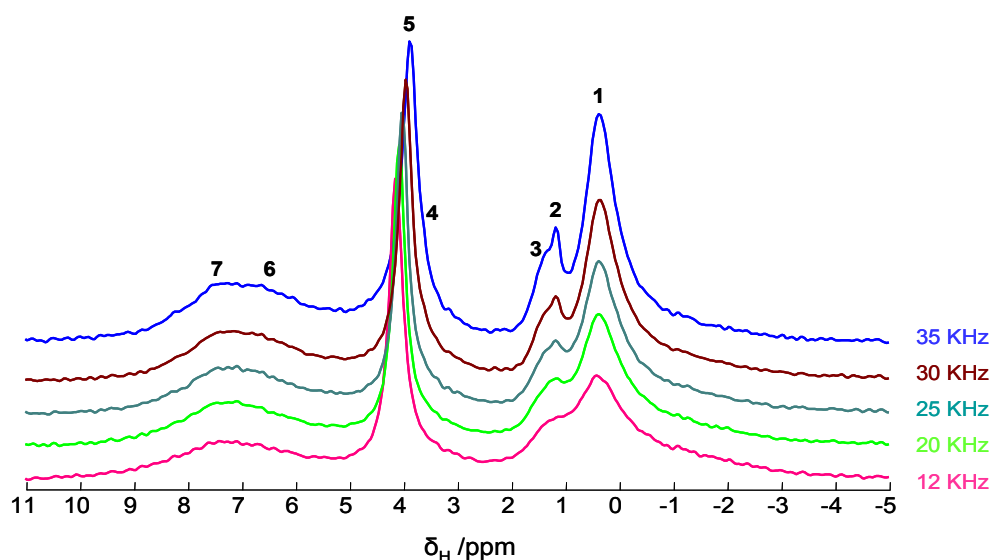


**Figure 7.2:** The  $^1\text{H}$  MAS NMR spectra of Gel 37 in a static magnetic field of 18.8 T at different MAS conditions.

The line broadening is smaller than expected in strongly coupled  $^1\text{H}$  spin systems, which implies that some degree of molecular mobility exists in the hybrid silica gel. The  $^1\text{H}$ - $^1\text{H}$  dipolar coupling was almost completely eliminated by sample spinning at 35 kHz. The residual line width under MAS is controlled by the exchange processes and inhomogeneous contribution due to the distribution of chemical shifts.<sup>80</sup> The interpretation of the spectra is straightforward. The resonance at 0.40 ppm (1) is assigned to methyl protons of the matrix. The signals at 1.2 ppm (2) and 1.4 ppm (3) are due to the protons of chemically bound ethoxy group/physisorbed ethanol and the methyl protons of the drug, respectively. The weak signal at 3.6 ppm (4) is assigned to  $-\text{CH}_2$  units of the chemically bound ethoxy group and physisorbed ethanol remaining in the silica gel as well as the drug molecules. The peak at 3.95 ppm (5) is due mainly to water molecules that are physisorbed on the silica surface. The broad peak with two maxima centered at 6.7 and 7.3 ppm in the spectrum are assigned to silanol protons in a variety of hydrogen bonding environments and aromatic protons of the drug, respectively. The rest of the resonances from the drug molecules cannot be identified as a separate resonance in the 1D MAS spectrum, but contribute to the intensity observed in the range of 1-7 ppm. These assignments will be further corroborated by  $^1\text{H}$ - $^{29}\text{Si}$  and  $^1\text{H}$ - $^{13}\text{C}$  2D FSLG HETCOR NMR experiments and will be reviewed in the following section.

7.2.2 2D  $^1\text{H}$ - $^{29}\text{Si}$  FSLG HETCOR NMR

The solid state 2D HETCOR NMR technique has been successfully used to obtain detailed structural information and to probe the nature of intermolecular interactions in the hybrid gels. It is also a powerful tool to analyze peaks that consist of strongly overlapping components. All neighboring protons participate in CP, creating multiple pathways for magnetization transfer and the proton chemical shifts of the different polarization sources can be distinguished in a 2D experiment. The FSLG HETCOR NMR experiment is based on the through-space  $^1\text{H}$ - $^{29}\text{Si}$  interactions and is more sensitive to long-range couplings.<sup>158,159</sup> The HETCOR experiments of Gel 37 obtained using different contact times are reported in Figure 7.3 to 7.5. The projection along the F2 dimension resembles the 1D  $^{29}\text{Si}\{^1\text{H}\}$  CPMAS NMR spectrum. Solid-state  $^{29}\text{Si}\{^1\text{H}\}$  CPMAS NMR and  $^1\text{H}$  MAS NMR spectra are shown in F2 and F1 dimension, respectively.

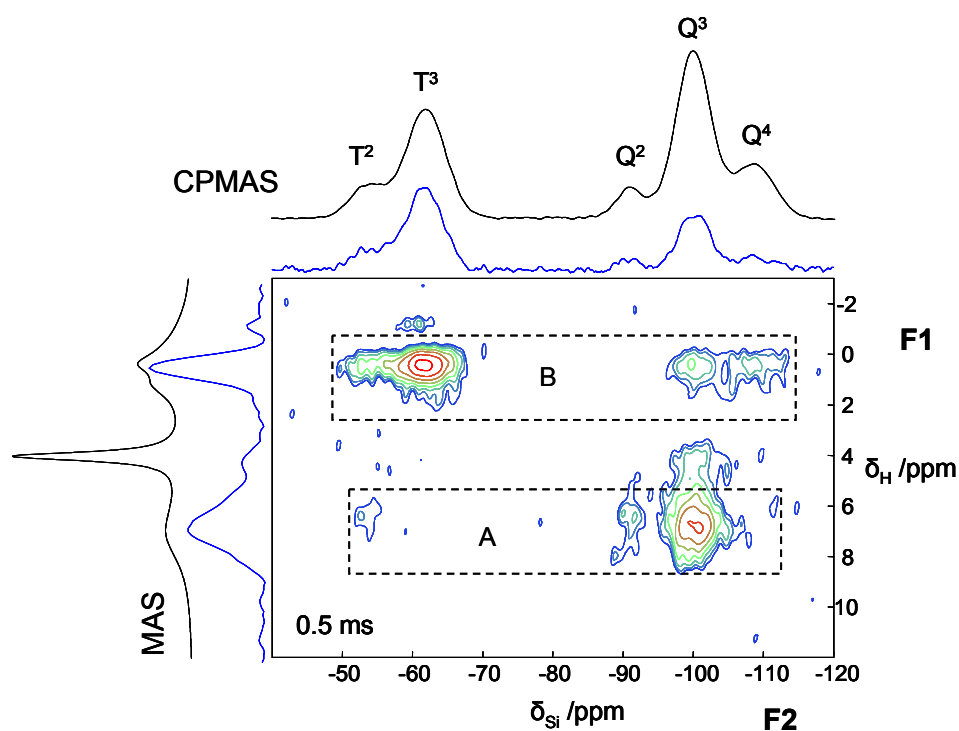


**Figure 7.3:** 2D  $^1\text{H}$ - $^{29}\text{Si}$  FSLG HETCOR spectra of Gel 37 at MAS 12.5 kHz and a mixing time of 0.5 ms. The 1D projections are shown in skyline mode.  $^{29}\text{Si}\{^1\text{H}\}$  CPMAS and  $^1\text{H}$  MAS NMR spectra are shown in F2 and F1 dimension, respectively.

The HETCOR map of Gel 37 recorded with short contact time, 0.5 ms, to minimize spin-diffusion effect, is reported in Figure 7.3. The most intense correlation peaks are ascribed to the correlation of next neighbors and lower intense peaks arise from unbonded couples. The strongest cross-peak observed in this spectrum represents a correlation between silicon site  $T^3$  and protons of the methyl group attached to this site. The resonance is centered at around -62.0 ppm (F2) and 0.40 ppm (F1). As expected, the  $T^2$  sites are also correlated with methyl protons. A resonance involving these methyl protons with adjacent  $Q^4$  and  $Q^3$  sites are also observed. These correlation peaks are strong evidence for the homogeneously distributed Q and T sites throughout the network. The resonance involving  $Q^2$  and methyl protons was not observed, most likely due to the presence of  $Q^2$  sites on the surfaces only and/or the low intensity of  $Q^2$ . A very strong cross-peak is observed at around -100.7 ppm (F2) and 6.9 ppm (F1). This resonance is attributed to the silanol protons which are hydrogen bonded. As expected, only  $Q^3$ ,  $Q^2$  and  $T^2$  sites are correlated with silanol protons. The hydrogen bonded silanol correlations with  $Q^2$  and  $T^2$  silicons are centered at around 6.4 ppm (F1). The difference in the proton resonances establish the occurrence of different types of hydrogen bonding in the hybrid gel. The silicons that resonate at -110 and -62 ppm ( $Q^4$  and  $T^3$ , respectively) show no correlations with hydrogen bonded silanol protons. This can be easily understood since no silanol protons are directly bound to these two silicon sites. In addition, cross peaks are observed between silanol site  $Q^3$  and water confined in the pores, which is a species of type  $Si-OH \cdots (H_2O)_n$ .<sup>160</sup> The rapidly exchanging hydrogen bonded water resonance at 4.1 ppm is only correlated with  $Q^3$  sites. The pores and channels of the gel are mainly composed of the  $Q^3$  sites and the water molecules reside in the vicinity of this site. Probably  $H_2O$  molecules are forming multiple layers in the pores and are exhibiting a variety of hydrogen bondings with the silanols.<sup>80</sup>

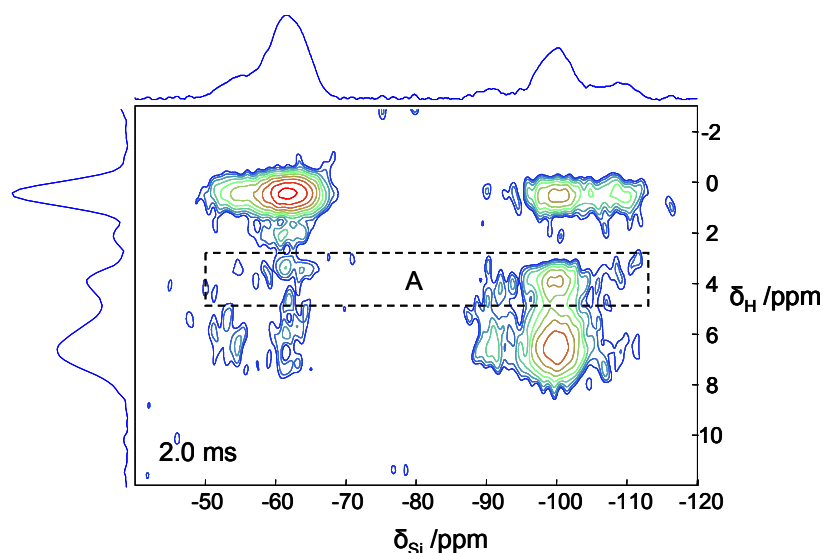


**Figure 7.4:**  $2\text{D } {}^1\text{H}$ - ${}^{29}\text{Si}$  FSLG HETCOR spectra of Gel 37 at MAS 12.5 kHz and a contact time of 2.0 ms. The 1D projections are shown in skyline mode.

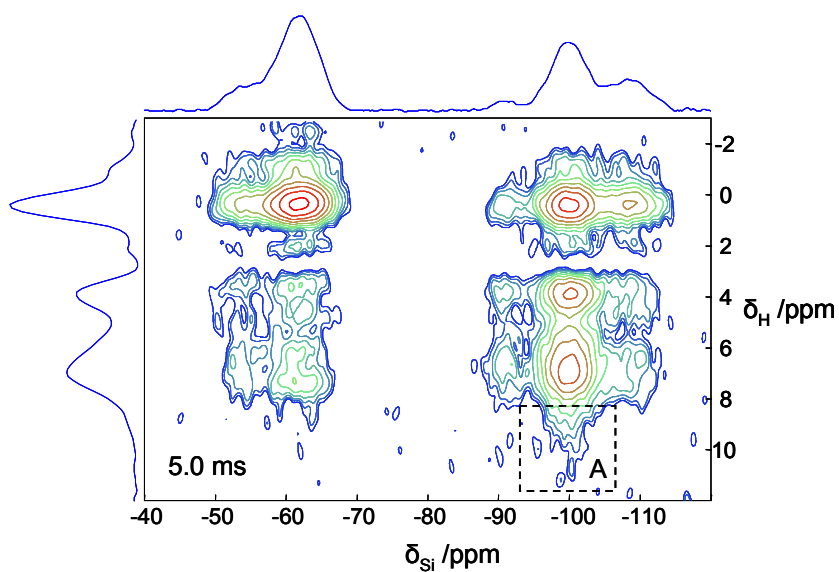


**Figure 7.5:**  $2\text{D } {}^1\text{H}$ - ${}^{29}\text{Si}$  FSLG HETCOR spectra of Gel 37 at MAS 12.5 kHz and a contact time of 5.0 ms. The 1D projections are shown in skyline mode.

All resonances found in the spectrum with 0.5 ms contact time were also detected with higher contact time (2.0 ms, Figure 7.4 and 5.0 ms, Figure 7.5) values. In addition, correlations of the  $\text{T}^3$  site with a proton pool are observed as overlapping peaks within

the range of 1 to 8 ppm (Figure 7.4). This proton pool is assumed to be the encapsulated drug, Propranolol. In addition, weak correlation peaks between  $Q^4$ ,  $Q^2$  and water as well as  $Q^4$  and hydrogen bonded silanols are also observed. With 5.0 ms contact time, very strong correlations between  $Q^3$  and silanol protons are observed at 6.9 ppm (F1). Moreover, these correlation peaks extended to 9-10 ppm in the proton dimension, indicating further coupling with the protonated amine group and hydroxyl group of the drug molecules.<sup>161</sup> Since hydrogen atoms involved in the  $^+NH_2 \cdots O-Si$  interactions are generally less shielded, the resonances are shifted to higher frequencies. This is a result of spatial proximity rather than  $^1H-^1H$  spin diffusion because in the latter case, strong correlations would be also expected between these protons and the T sites. Such nonspecific hydrogen bonds between amino group of PP and the silanol groups of the matrix have been reported in the literature.<sup>162</sup> A correlation between  $Q^2$  site and the methyl protons of the matrix is observed at 0.4 ppm (F1), which were absent in the spectra of 0.5 and 2.0 ms contact time. As expected there is no resonance observed involving  $T^3$  and hydrogen bonded silanols, but what is more striking is the presence of a cross peak centered at 7.5 ppm (F1), attributed to the aromatic protons, with the  $T^3$  site. For longer contact times, the dominant correlation originates from the aromatic region of the proton spectrum with the  $^{13}C$  signal of the  $T^3$  sites. Similarly, a cross peak between silicon sites and a protons source is observed at -1 ppm (F1) and is attributed to the methyl protons of the matrix which are in the close vicinity of the negative ring current region of the aromatic rings of the drug molecules. With longer contact time, the coherence transfer proceeds over larger distances involving several protons and silicons.<sup>163</sup> Thus, varying the contact time can provide information about the different possible pathways of magnetization transfer.

Complementary supporting evidence for the existence of correlations can be inferred from the 1D cross sections obtained from the 2D spectrum. The cross sections corresponding to  $Q^3$  and  $T^3$  sites shown in Figure 7.6 indicate that methyl protons of the matrix correlate with both,  $Q^3$  and  $T^3$  sites, whilst hydrogen bonded silanols and physisorbed water correlate mainly to  $Q^3$  site. The drug protons correlate with both Q and T sites. These results strongly suggest that the drug molecules reside in the pores of silica surface and the correlation between drug protons and silica sites provide unambiguous evidence for different types of molecular level interactions.

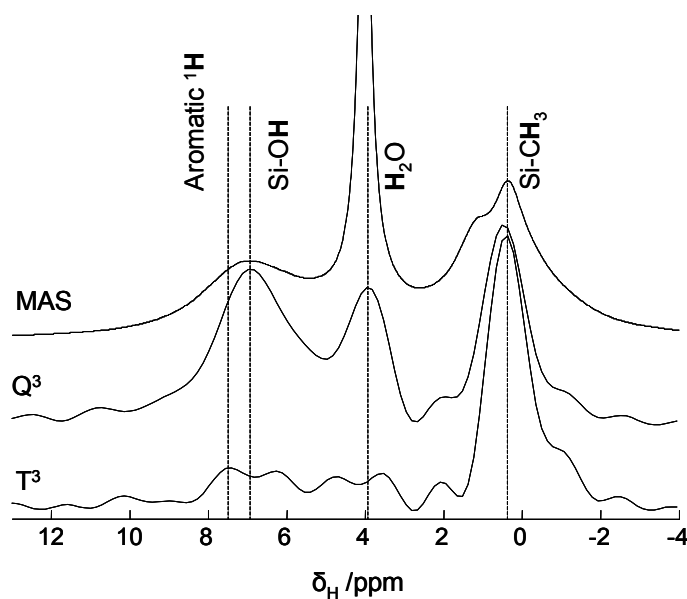


**Figure 7.6:**  $^1\text{H}$  slices for  $Q^3$  and  $T^3$  from the  $2\text{D } ^1\text{H}-^{29}\text{Si}$  FSLGHETCOR NMR experiment with 5.0 ms contact time, compared with the 1D proton MAS NMR spectrum of Gel 37.

### 7.2.3 $2\text{D } ^1\text{H}-^{13}\text{C}$ FSLG HETCOR NMR

It has been possible to use the chemical shift of heteronuclei to resolve complicated 1D proton NMR spectra by dispersing them into a second dimension. As the hybrid gel contains several proton sources, which give overlapping resonances, 2D HETCOR experiments with variable contact times were performed. The  $2\text{D } ^1\text{H}-^{13}\text{C}$  FSLG HETCOR NMR spectrum of Gel 37 obtained using 0.2 ms CP contact time is shown in Figure 7.7. The projection along the F2 dimension is identical to a 1D  $^{13}\text{C}$  CPMAS spectrum. Solid-state  $^{13}\text{C}\{^1\text{H}\}$  CPMAS NMR and  $^1\text{H}$  MAS NMR spectra are shown in F2 and F1 dimension, respectively.



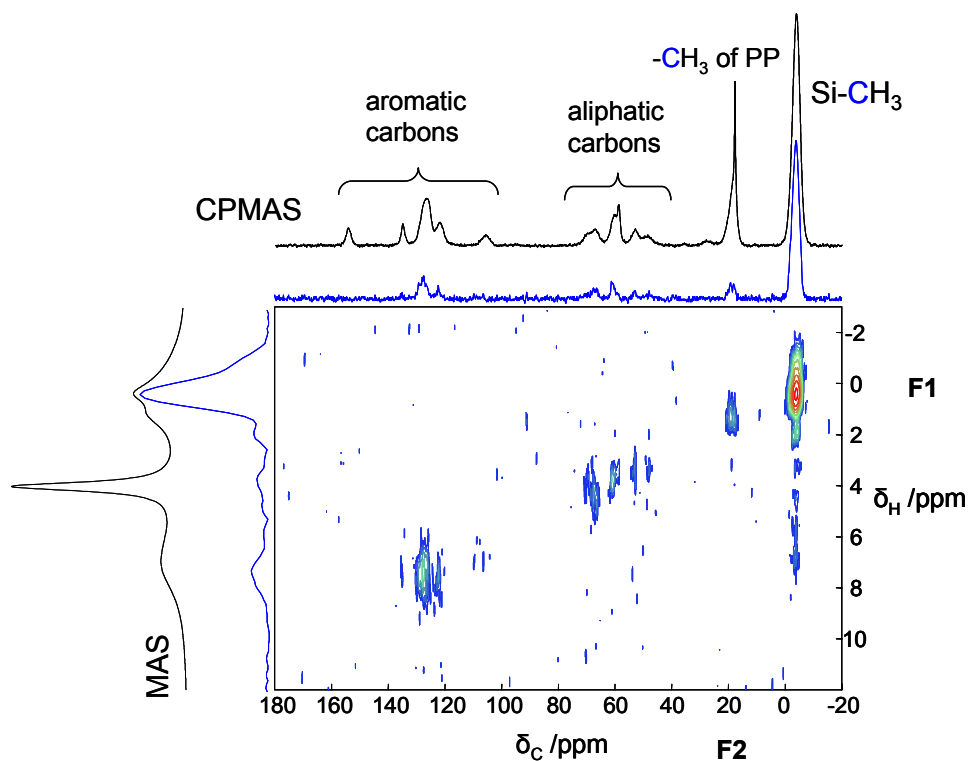


**Figure 7.7:** 2D  $^1\text{H}$ - $^{13}\text{C}$  FSLG HETCOR spectra of Gel 37 at MAS 12.5 kHz and a contact time of 0.2 ms. The 1D projections are shown in skyline mode.  $^{13}\text{C}\{^1\text{H}\}$  CPMAS and  $^1\text{H}$  MAS NMR spectra are shown in F2 and F1 dimension, respectively.

The strongest correlations observed are between carbons and directly bound protons. Both intra-molecular and through space intermolecular correlations with distinct protons occur at lower levels of cross-peak intensity. The aromatic carbon from the drug molecule at 154.0 ppm shows no correlations with the protons. This can be understood since no protons are directly bound to this carbon. The strongest cross-peak observed in this spectrum represents a correlation between methyl carbon of the matrix and directly bound protons. This resonance is centered at -3.9 ppm in the F2 dimension and 0.4 ppm in the F1 dimension. In addition, correlation between carbons of the drug molecules and directly bound protons are observed. The aromatic carbons (120-135 ppm) are correlated to directly bound protons and the chemical shifts are centered at 7.5 ppm. As far as aliphatic carbons are concerned, the correlation peaks relative to the different carbon nuclei can be clearly distinguished. A cross-peak between methyl carbons of the drug ( $\delta_{\text{C}} = 19.3$  ppm) and directly bound protons are observed at  $\delta_{\text{H}} = 1.3$  ppm. All other aliphatic protons resonances in the range from 47 to 71 ppm are correlated to their respective protons in the range from 2.7 to 5.2 ppm. In addition very weak correlation peaks from

physisorbed ethanol are observed. Weak correlation between methyl carbons of the matrix and different inorganic hydrogen species, which include pore confined water and hydrogen bonded silanols are also observed at  $-3.9$  ( $\delta_C$ ) ppm /  $2 - 8$  ( $\delta_H$ ) ppm. The correlations between methyl groups of the matrix and Propranolol cannot be resolved from other correlations. This spectrum provides further supporting evidence for the solid state  $^1\text{H}$  and  $^{13}\text{C}$  assignments discussed in earlier chapters.

When the CP contact time is longer, the coherence transfer during Hartmann-Hahn matching proceeds over larger distances, involving several protons and carbons.

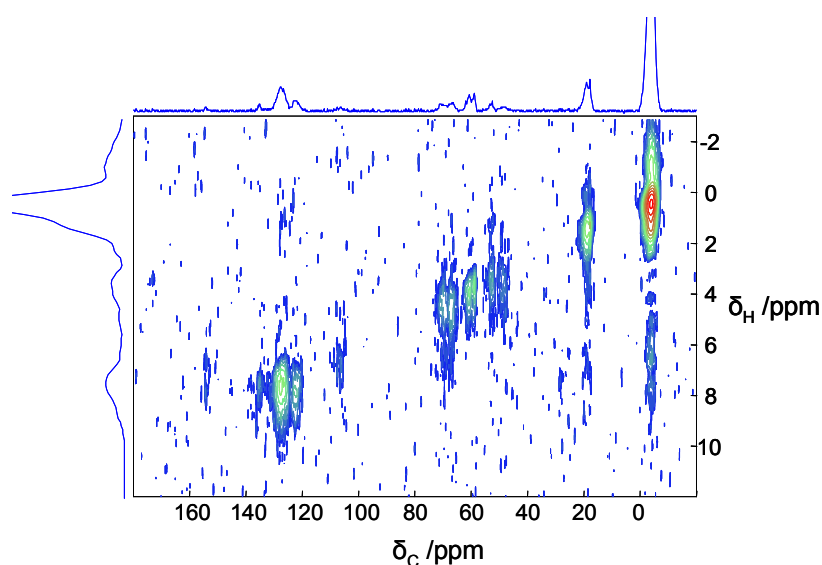


**Figure 7.8:**  $2\text{D } ^1\text{H}-^{13}\text{C}$  FSLG HETCOR spectra of Gel 37 at MAS 12.5 kHz and a contact time of 0.5 ms. The 1D projections are shown in skyline mode.

All resonances found with 0.2 ms contact time spectrum were also detected with 0.5 ms. In addition, small cross peaks between aromatic carbons of the drug and methyl protons of the matrix as well as methyl carbons of the matrix and aromatic protons of the drug are observed. The resonance from the methyl groups of the physisorbed ethanol and Propranolol are clearly distinguishable in the 2D spectrum. Similarly, a cross peak between methyl carbon of the matrix and a protons source is observed at  $-1$  ppm (F1) and is attributed to the methyl protons of the matrix which are in the close vicinity of aromatic rings of the drug molecules. The F1 projection of the 2D HETCOR experiment at 0.5 ms contact time is slightly less resolved than that of the 0.2 ms contact time experiment, probably due to spin-diffusion occurring during CP.

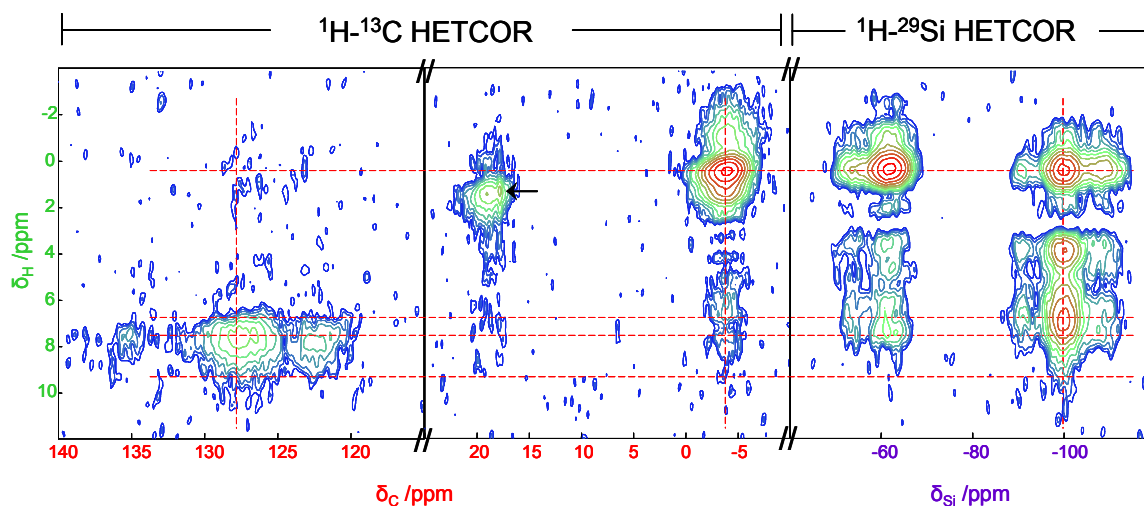


**Figure 7.9:** The amplified 2D  $^1\text{H}$ - $^{13}\text{C}/^{29}\text{Si}$  FSLG HETCOR spectra of Gel 37 at MAS 12.5 kHz. A contact time of 0.5 ms and 5.0 ms was used for the carbon and silicon HETCORs, respectively.

In Figure 7.9 the  $^1\text{H}$ - $^{13}\text{C}$  and  $^1\text{H}$ - $^{29}\text{Si}$  HETCOR maps are compared. The correlations from the methyl protons of the matrix to the directly bound carbons and to the attached silicons are clearly visible (highlighted with dashed red line). These protons are also correlated to the methyl carbons of the drug and physisorbed ethanol. It is also possible to distinguish between the resonances from the methyl protons of the rigid drug and mobile drug (marked with solid arrow). The signals from the aromatic protons (7.4 ppm) and silanol protons (6.9 ppm) are clearly distinguishable by their different correlations with aromatic carbons and  $\text{Q}^3$ , respectively. Additional correlations from the low shielding protons to the aromatic carbons and  $\text{Q}^3$  silicons are observed at around 9.0 ppm and attributed to  $^+\text{NH}_2$  and OH of the drug molecules. This is remarkable, since the same proton source correlate with the matrix and the drug and indicates that some of the drug molecules reside in the vicinity of  $\text{Q}^3$  site and form intermolecular interactions between the drug molecules and matrix. These maps help to distinguish the magnetic communication between carbon, silicon and proton with one another and provide direct proof of the intimate relationship between the organic and inorganic components of the hybrid gel.

### 7.3 Methyl Substituted Hybrid EISA Gel – Gel 177

High resolution 2D HETCOR NMR studies has been carried out on a methyl substituted EISA gel [MTS<sub>177</sub>(3:1, 2,2)] synthesized at pH value 2.2. In this study longer CP contact times have been used in the <sup>1</sup>H-<sup>13</sup>C HETCOR experiments to probe the drug-matrix interactions.

#### 7.3.1 2D <sup>1</sup>H-<sup>29</sup>Si FSLG HETCOR NMR

The HETCOR spectra of Gel 177 obtained using 2.0 ms CP contact time are shown in Figure 7.10. The projection along F2 dimension is identical to a 1D <sup>29</sup>Si CPMAS spectrum. Solid-state <sup>29</sup>Si{<sup>1</sup>H} CPMAS NMR and <sup>1</sup>H MAS NMR spectra are shown in F2 and F1 dimension, respectively.

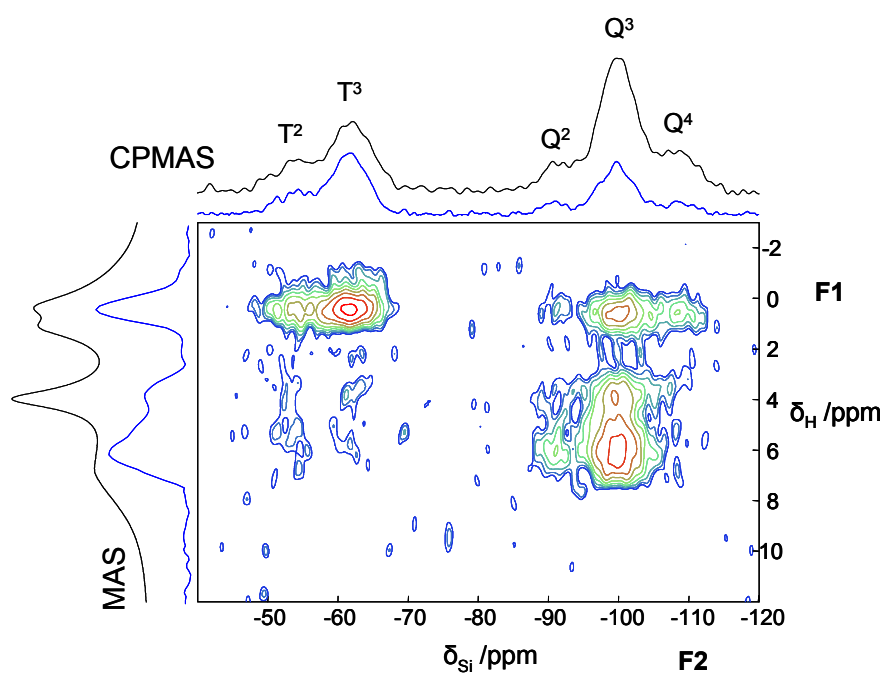


**Figure 7.10:** 2D <sup>1</sup>H-<sup>29</sup>Si FSLG HETCOR spectra of Gel 177 at MAS 12.5 kHz and a contact time of 2.0 ms. The 1D projections are shown in skyline mode. <sup>29</sup>Si{<sup>1</sup>H} CPMAS and <sup>1</sup>H MAS NMR spectra are shown in F2 and F1 dimension, respectively.

The strongest correlations in Figure 7.10 are between silicons and directly attached protons. Both intramolecular and intermolecular correlations with distant protons occur at lower levels of cross peak intensity. Mutual correlations between Q<sup>3</sup>, Q<sup>2</sup> and T<sup>2</sup> are observed at 6.0 ppm in the <sup>1</sup>H dimension and are originated from the hydrogen bonded silanol protons attached to the sites directly. The very weak/no correlations to the Q<sup>4</sup> and T<sup>3</sup> sites can be easily understood since no silanol protons are directly bound to these two silicon sites. As can be observed from the 2D spectrum, the T<sup>3</sup> and T<sup>2</sup> silicons have a strong heteronuclear correlation with the methyl protons (0.4 ppm, F1), which are directly attached to the sites. Interestingly, all the Q silicon sites receive polarization through intramolecular transfer from the methyl protons (0.4 ppm) of the T sites, and appear cross peaks at respective resonances. While the water protons (3.9 ppm) predominantly exchange polarization with the Q<sup>3</sup> site, weak polarization transfer appear to contribute little to the Q<sup>2</sup>, T<sup>3</sup> and T<sup>2</sup> sites. In addition, correlations of T<sup>2</sup> site with a proton pool observed as overlapped peaks within the range of 1 to 7 ppm. This proton pool is assumed to be the encapsulated drug, Propranolol.

### 7.3.2 2D <sup>1</sup>H-<sup>13</sup>C FSLG HETCOR NMR

Figure 7.11 shows a contour plot of a <sup>1</sup>H-<sup>13</sup>C heteronuclear dipolar correlation spectrum recorded from Gel 177 with a contact time of 0.8 ms.

Selective magnetization transfer was achieved by applying shorter contact time. All resonances found in Gel 37 were also detected in Gel 177. In addition, strong cross peaks are observed between aromatic carbons and methyl protons of the matrix as well as between aromatic protons and methyl carbons of the matrix as highlighted in Figure 7.12, with dashed blue line. These correlations are direct proof for the long-range heteronuclear coherence transfer containing structural and interaction information. Recently, it has been shown that protons in CH<sub>3</sub> groups can transfer magnetization over considerable distances, providing thus an attractive route to the detection of long-range transfer events.<sup>164</sup> Mutual correlations between methyl and methylene carbons and protons are observed as cross peaks at 1.1 (δ<sub>H</sub>) / 58.5 (δ<sub>C</sub>) ppm and 3.5 (δ<sub>H</sub>) / 17.8 (δ<sub>C</sub>) ppm, respectively (marked with dashed red line) in addition to the correlations from directly bound carbons and protons. Figure 7.12 also highlights the through-space interactions of inorganic hydrogen species, which include pore confined water and

hydrogen bonded silanols with methyl carbon of the matrix ( $-3.9$  ( $\delta_C$ ) ppm /  $2 - 8$  ( $\delta_H$ ) ppm). The correlations between methyl groups of the matrix and Propranolol overlap with the above cross peaks.

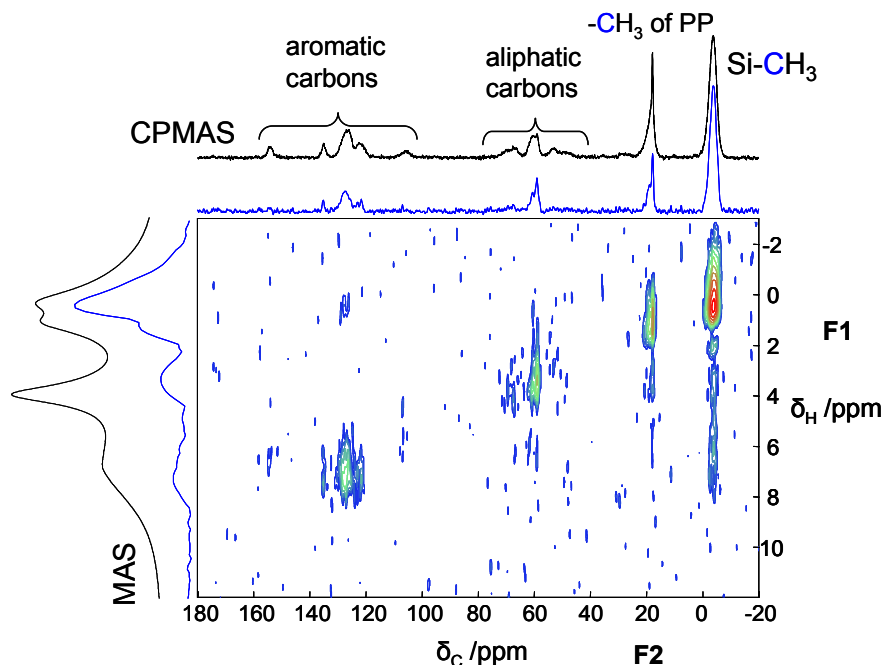


**Figure 7.11:** 2D  $^1\text{H}$ - $^{13}\text{C}$  FSLG HETCOR spectra of Gel 177 at MAS 12.5 kHz and a contact time of 0.8 ms. The 1D projections are shown in skyline mode.  $^{13}\text{C}\{^1\text{H}\}$  CPMAS and  $^1\text{H}$  MAS NMR spectra are shown in F2 and F1 dimension, respectively.

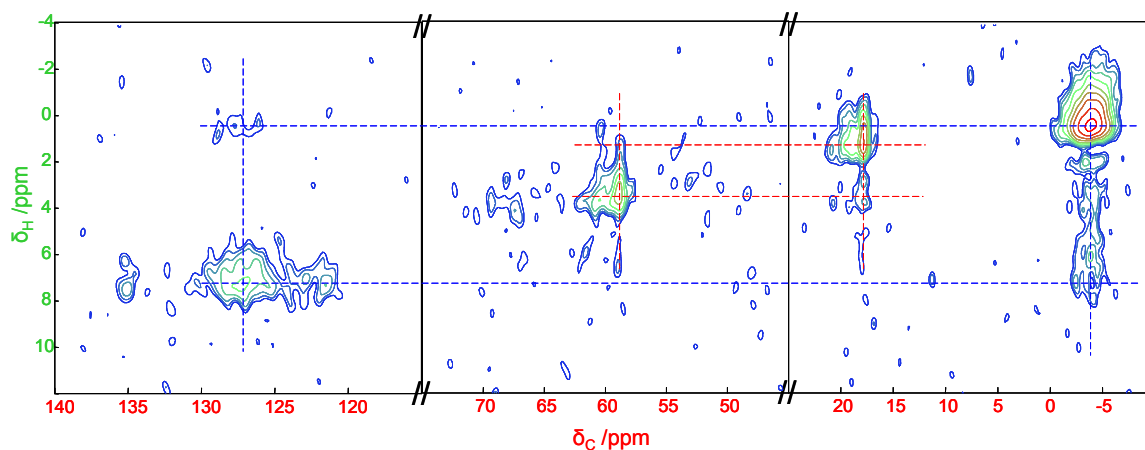


**Figure 7.12:** The amplified 2D  $^1\text{H}$ - $^{13}\text{C}$  FSLG HETCOR spectra of Gel 177 at a contact time of 0.8 ms.

In Figure 7.13, the 2D  $^1\text{H}$ - $^{13}\text{C}$  FSLG HETCOR NMR spectrum of Gel 177 at 1.0 ms contact time is presented. In additions to the correlations observed at 0.8 ms, weak cross peaks between the aliphatic and aromatic part of PP has been observed. It is also worth

noting that the cross peaks observed at 0.8 ms contact time are more intense in the 1.0 ms spectrum, and attributed to the spin diffusion influence (highlighted with dashed red lines in Figure 7.14). There are correlations between aromatic carbons and silanol protons observed at around 6.0 ppm (F1), highlighted with dashed red line. The absence of correlations between aromatic protons with silicon sites ( $Q^2$  and  $Q^3$ ) are possibly due to the larger distance between silicons and aromatic protons. What is striking is the presence of a shoulder of the main peak ( $-3.9$  ( $\delta_C$ ) /  $0.4$  ( $\delta_H$ ) ppm) at  $-1.0$  ( $\delta_H$ ) ppm which is attributed to the correlations from the methyl protons of the matrix and are in the close vicinity of aromatic rings of the drug molecules (marked with black arrow). The methyl protons interacting with aromatic rings resonate at negative values to TMS, exceptionally upfield compared to those belong to the bulk methyl group of matrix. The upfield shift is due to the intense aromatic ring currents experienced by the methyl protons of the matrix. A close contact between the aromatic ring and the methyl protons pushes the latter under the influence of strong anisotropic diamagnetic susceptibility, generating upfield shifts. Such large upfield shifts are also observed in polymer systems<sup>165,166</sup> and confirm the generality of above findings.

HETCOR maps help to distinguish the magnetic communication between carbon, silicon and proton with one another and provide direct proof of the intimate relationship between the organic and inorganic components of the hybrid gel.

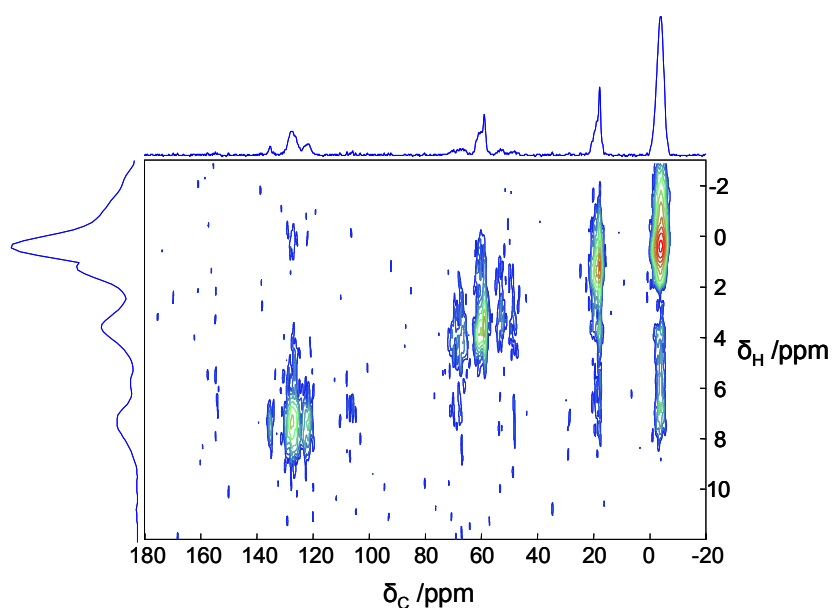


**Figure 7.13:** 2D  $^1\text{H}$ - $^{13}\text{C}$  FSLG HETCOR spectra of Gel 177 at MAS 12.5 kHz and a contact time of 1.0 ms. The 1D projections are shown in skyline mode.

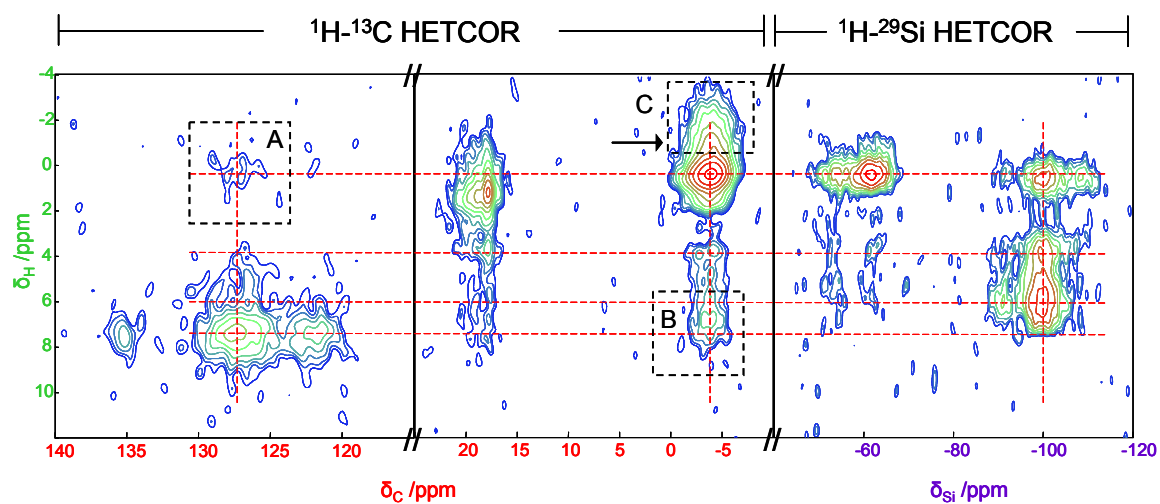


**Figure 7.14:** The amplified 2D  $^1\text{H}$ - $^{13}\text{C}/^{29}\text{Si}$  FSLG HETCOR spectra of Gel 177 at 12.5 kHz. A contact time of 1.0 ms and 2.0 ms was used for the carbon and silicon HETCORs, respectively.



## 7.4 Benzyl Substituted Hybrid EISA Gel – Gel 191

High resolution 2D HETCOR NMR studies has been carried out on a benzyl substituted EISA gel [BTS<sub>191</sub>(3:1, 2,2)] synthesized at pH value 2.2.

### 7.4.1 2D <sup>1</sup>H-<sup>29</sup>Si FSLG HETCOR NMR

The <sup>1</sup>H-<sup>29</sup>Si FSLG HETCOR spectrum of Gel 191 obtained using 2.0 ms contact time is shown in Figure 7.15.

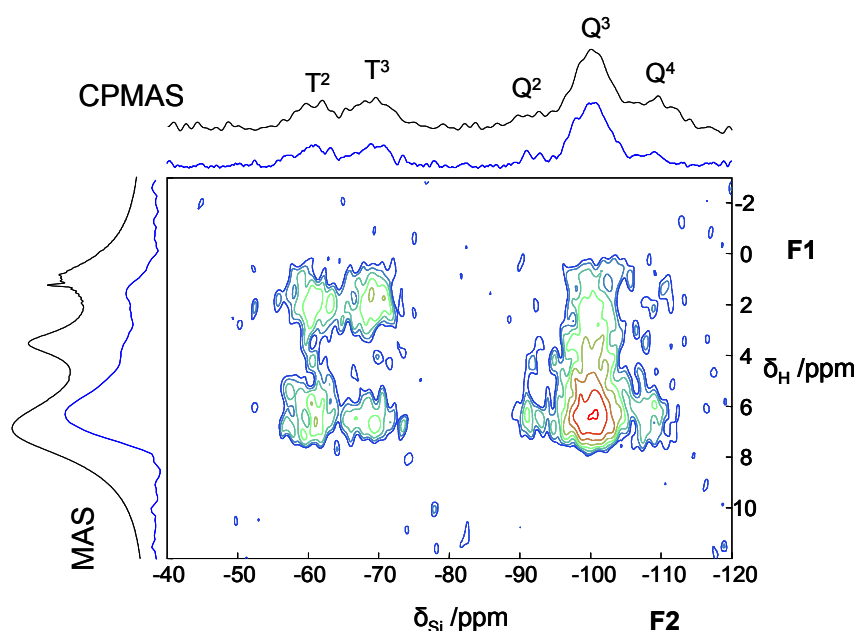


**Figure 7.15:** 2D <sup>1</sup>H-<sup>29</sup>Si FSLG HETCOR spectrum that correlates the isotropic chemical shift of <sup>1</sup>H and <sup>29</sup>Si nuclei of Gel 191 with a contact time of 2.0 ms. The 1D projections are in skyline mode. <sup>29</sup>Si{<sup>1</sup>H} CPMAS and <sup>1</sup>H MAS NMR spectra are shown in F2 and F1 dimension, respectively.

Four distinct regions of peaks in the -55.0 to -75.0 ppm (F2) range of the 2D spectrum are due to the T silicons. The top right region is due to the correlations between the T<sup>3</sup> silicon and methylene protons of the benzyl group and the top left region is due to the same protons correlating with the T<sup>2</sup> sites. The bottom left region is due to the correlation between T<sup>2</sup> sites and aromatic protons as well as with silanol protons which can be

distinguished in the spectrum. The correlations between silicon site T<sup>3</sup> and aromatic protons are seen in the bottom right region. There is no single resonance center observed in any of the four regions, instead multiple centers are observed. The observation is unique compared to the other gels and has an impact in the final properties of the gel. The resonances from the Q sites are observed in the -90.0 to -110 ppm (F2) range and are attributed to the Q<sup>4</sup>, Q<sup>3</sup> and Q<sup>2</sup> sites. A strong cross-peak observed in the spectrum represents a correlation between silicon site Q<sup>3</sup> and hydrogen bonded silanol protons at 100.7 (F2) and 6.7 ppm (F1). The shoulder of this peak extend further towards the high shielding region (F1) and is attributed to the correlations between water molecules that are in close vicinity of silanol protons and interacting with each other. The aromatic proton correlations to these sites are not identified as separate resonance, but could contribute to the intensity observed in the same range. There are no correlations between methylene protons of the T site and Q silicons (Q<sup>4</sup> and Q<sup>2</sup>) observed.

### 7.4.2 2D <sup>1</sup>H-<sup>13</sup>C FSLG HETCOR NMR

The 2D <sup>1</sup>H-<sup>13</sup>C heteronuclear correlation spectrum and its projections are shown in Figure 7.16. The spectrum was obtained with FSLG <sup>1</sup>H homonuclear dipolar decoupling during the proton evolution, at a MAS rate of 12.5 kHz and applying a contact time of 0.8 ms. The most intense correlation peaks are ascribed to directly bound couples and lower intense peaks arise from unbound couples.

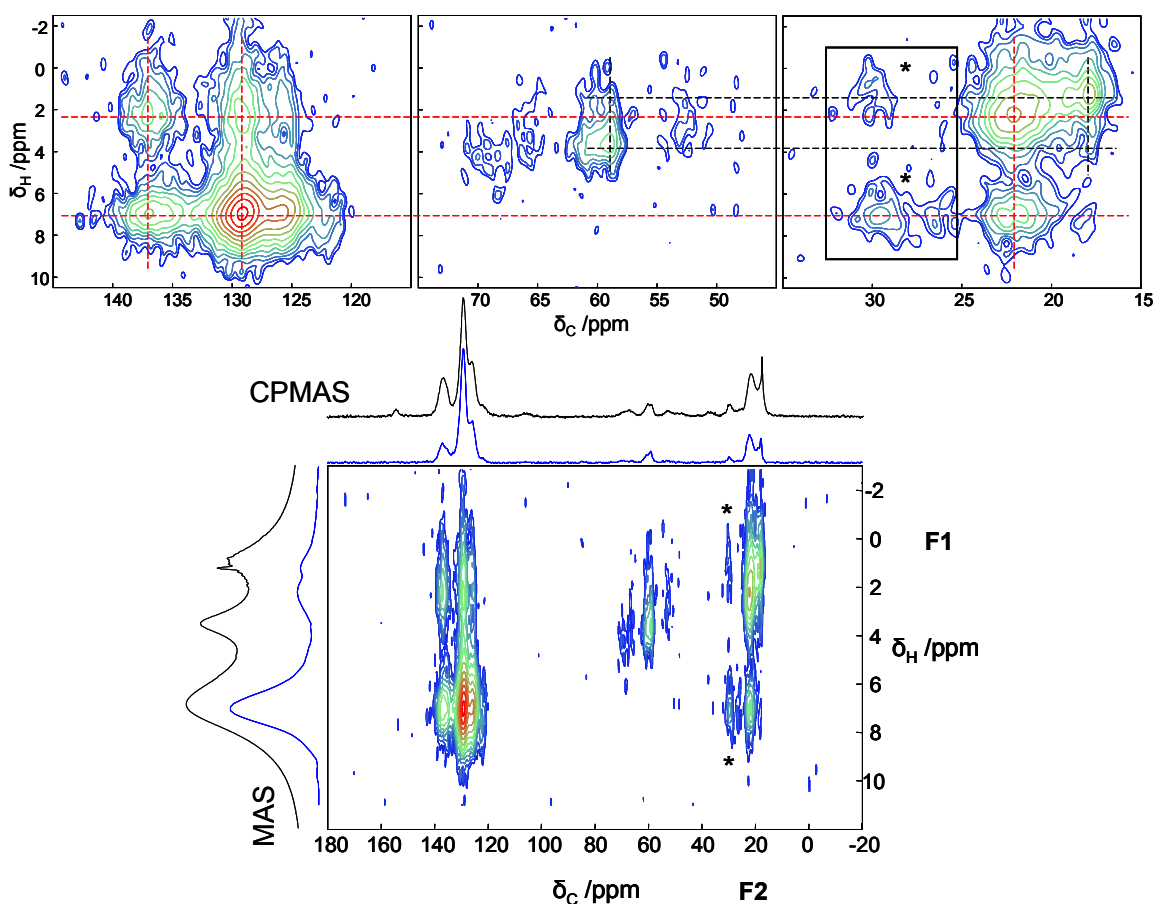


**Figure 7.16:** The 2D  $^1\text{H}$ - $^{13}\text{C}$  FSLG HETCOR spectrum of Gel 191 at MAS 12.5 kHz and a contact time of 0.8 ms. The  $^1\text{H}$  chemical shift runs vertically, while the  $^{13}\text{C}$  shift is horizontal.  $^{13}\text{C}\{^1\text{H}\}$  CPMAS and  $^1\text{H}$  MAS NMR spectra are shown in F2 and F1 dimension, respectively. The amplified regions are given on the top of the spectrum. Spinning side bands originating from the aromatic carbons are marked with asterisks.

The strongest correlations are observed in the aromatic range between 120.0-140.0 ppm (F2) and 5.0-9.0 (F1) ppm and are attributed to the aromatic part of the benzyl group. Another strong correlation observed for methylene carbons of the benzyl group and directly attached protons (centered at 22.0 (F2) and 2.2 (F1) ppm). Very strong correlations between aromatic carbons and methylene protons as well as between methylene carbons and aromatic protons are observed and are marked with dashed red line in the figure. Mutual correlations between methyl and methylene carbons and protons are observed as cross peaks at 1.2 (F1) / 59.0 (F2) ppm and 3.6 (F1) / 17.8 (F2) ppm, respectively (marked with dashed black line), besides the presence of direct correlations between carbons and bound protons. Resonances from the drug molecules are also observed in the aliphatic region of the spectrum. Resonances from the aromatic

and methyl carbons and protons of the drug cannot be identified as separate peaks, but contribute to the intensity observed in their respective regions.

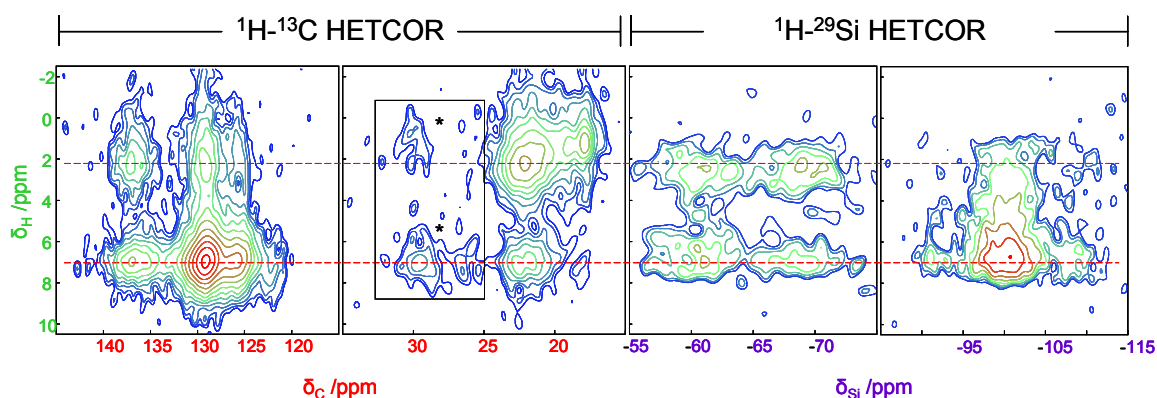


**Figure 7.17:** The amplified 2D  $^1\text{H}$ - $^{13}\text{C}/^{29}\text{Si}$  FSLG HETOR spectra of Gel 191 at 12.5 kHz. A contact time of 0.8 ms and 2.0 ms was used for the carbon and silicon HETCORs, respectively. Spinning side bands are marked with asterisks.

In Figure 7.17, the carbon and silicon heteronuclear correlation spectra are compared. The difference between the aromatic and silanol protons can be clearly distinguished. In addition, the proton correlations with different silicon and carbon sites are clearly visible. The HETCOR maps provide information about the hybrid nature of the benzyl substituted gel. The mutual correlations from the inorganic as well as the organic components of the hybrid gel confirm the formation of self assembled silica gel.

## 7.5 Acetoxypropyl substituted Hybrid EISA Gel – Gel 182

High resolution 2D HETCOR NMR studies has been carried out on a acetoxypropyl substituted EISA gel [ATS<sub>182</sub>(3:1, 2,2)] synthesized at pH value 2.2.

### 7.5.1 2D <sup>1</sup>H-<sup>29</sup>Si FSLG HETCOR NMR

The <sup>1</sup>H-<sup>29</sup>Si FSLG HETCOR spectrum of Gel 182 obtained using 2.0 ms contact time is shown in Figure 7.18.

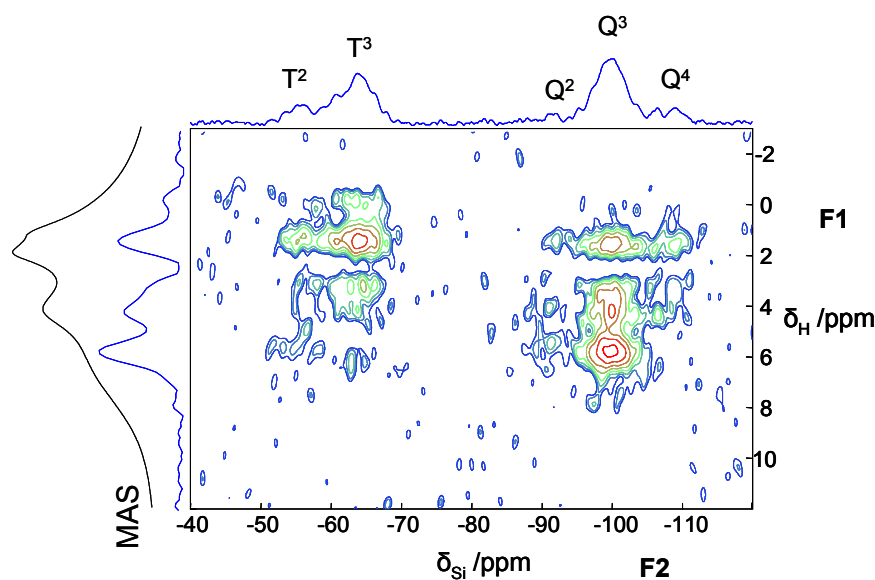


**Figure 7.18:** 2D <sup>1</sup>H-<sup>29</sup>Si FSLG HETCOR spectra of Gel 182 at MAS 12.5 kHz and a contact time of 2.0 ms. The 1D projections are shown in skyline mode. <sup>1</sup>H MAS NMR spectra is shown in F1 dimension.

A strong cross-peak at around -64 ppm (F2) and 1.40 ppm (F1) represents a correlation between silicon site T<sup>3</sup> and protons of the methylene group bound to this site. As expected, the T<sup>2</sup> sites are also correlated with these protons. A correlation involving these methylene protons with adjacent Q<sup>4</sup>, Q<sup>3</sup> and Q<sup>2</sup> sites are also observed. These correlation peaks are strong evidence for the homogeneously distributed Q and T sites throughout the gel network. Another very strong cross-peak is observed at around -99.8 ppm (F2)

and 5.8 ppm (F1). This resonance is attributed to the silanol protons, which form hydrogen bonds in Q<sup>3</sup> sites. As expected, only Q<sup>3</sup>, Q<sup>2</sup> and T<sup>2</sup> sites are correlated with silanol protons. In addition, cross peaks are observed between Q<sup>3</sup> and water, which are of the type Si-OH.....(H<sub>2</sub>O)<sub>n</sub>. While the water protons (4.2 ppm) predominantly correlate with the Q<sup>3</sup> site, weak cross peak intensities appeared to contribute from the Q<sup>4</sup>, T<sup>3</sup> and T<sup>2</sup> sites. The T sites showed a direct correlation with a proton resonance at 3.2 ppm and are attributed to the acetoxypropyl group attached to these sites.

### 7.5.2 2D <sup>1</sup>H-<sup>13</sup>C FSLG HETCOR NMR

The 2D <sup>1</sup>H-<sup>13</sup>C heteronuclear correlation spectrum with 0.5 ms contact time and its projections are shown in Figure 7.19. The most intense correlation peaks are ascribed to directly bound couples and lower intense peaks arise from unbound couples.

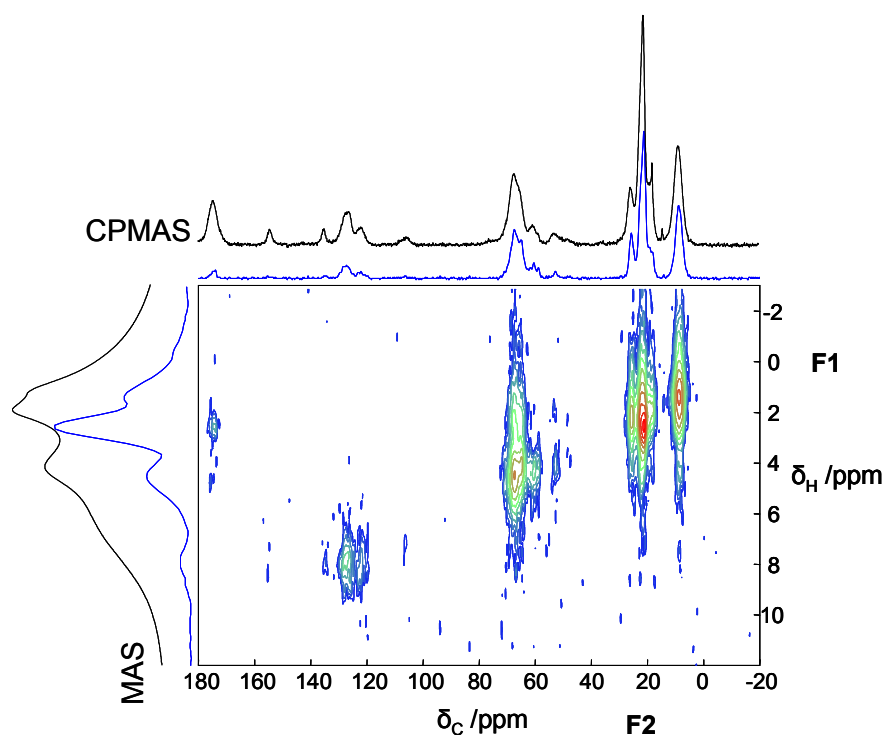


**Figure 7.19:** 2D <sup>1</sup>H-<sup>13</sup>C FSLG HETCOR spectra of Gel 182 at MAS 12.5 kHz and a mixing time of 0.5 ms. The 1D projections are shown in skyline mode.

The strongest cross-peak observed in this spectrum represents a self correlation of the methyl carbons (2.6 ppm (F1) and 21.3 ppm (F2)). The other cross peaks represent correlations between methylene carbons (-C-C-Si) at 1.4 ppm (F1) / 8.8 ppm (F2), (-C-C-C) at 2.2 ppm (F1) / 25.7 ppm (F2) and (-O-C-C) at 4.5 ppm (F1) / 67.3 ppm (F2). In

addition, a cross peak observed downfield, represents carbonyl carbon and correlated to the neighboring methyl protons (2.6 ppm (F1) and 174.0 ppm (F2)). Weak correlations between methylene carbons and adjacent protons are exhibited by the acetoxypropyl group. Mutual correlations for PP are also observed. The proton resolution for the acetoxypropyl group is rather good in the 2D projection. The 2D data also pinpoints the fact that the acetoxypropyl group stays intact in the final gel without undergoing ester hydrolysis.

With increasing contact times, from 0.5 ms to 2.0 ms, a correlation between the aromatic carbons and acetoxypropyl protons as well as aromatic protons and acetoxypropyl carbons are observed, Figure 7.20. This observation suggests that the PP molecules are in the vicinity of acetoxypropyl units.

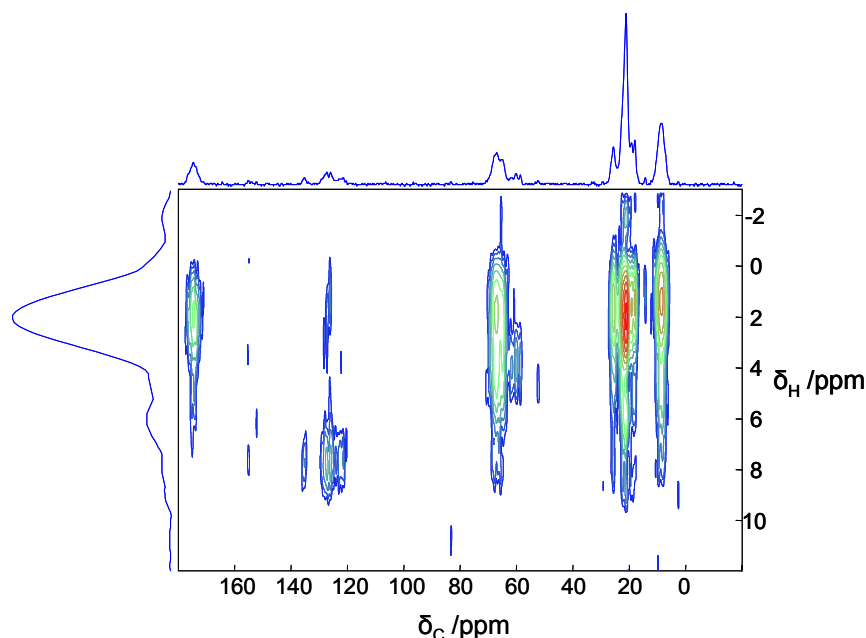


**Figure 7.20:** 2D  $^1\text{H}$ - $^{13}\text{C}$  FSLG HETCOR spectra of Gel 182 at MAS 12.5 kHz and a contact time of 2.0 ms. The 1D projections are shown in skyline mode.

Neglecting the relaxation effects, two main mechanisms take place during the contact pulse; transfer of magnetization from protons to carbon through heteronuclear dipolar interaction and spin diffusion between coupled protons (scaled down by spin-lock condition). Varying contact time from short to longer durations thus allows a description of structure relations between protons and carbons from atomic scale to larger scale. Strong correlations are observed between the carbonyl carbons and the proton spin reservoir that include methyl and methylene protons (also Figure 7.21). In addition, the

correlation peaks arising from the acetoxypropyl groups are very broad indicating that intramolecular transfer of proton magnetization via spin diffusion is very effective within the 2.0 ms contact time. The F1 projection of the 2D HETCOR experiment at 2.0 ms contact time is less resolved than that of the 0.5 ms contact time experiment, due to spin-diffusion occurring during CP.

The amplified  $^{13}\text{C}$  and  $^{29}\text{Si}$  HETCOR NMR spectra of Gel 182 are given in Figure 7.21. The comparison has been made to understand the magnetic communication between carbons, silicons and protons. The highlight of the amplified spectrum is the presence of a strong cross peak at 5.9 ( $\delta_{\text{H}}$ ) and 21.4 ( $\delta_{\text{C}}$ ) ppm (marked with dashed black circle) and is attributed to correlation between the methyl carbons of the acetoxypropyl group with highly deshielded protons. The probable sources of proton polarization in the vicinity of methyl carbons are the directly bound protons which resonate at 2.6 ppm. These are the highly polarized protons within the acetoxypropyl units due to the presence of the directly bound carbonyl group. Another source is the silanol protons capable of hydrogen bonding. The cross peak is attributed to the correlation between the silanol protons and methyl carbon of the matrix residing in the pores. In addition, polarized methyl protons of matrix can interact with the  $\text{SiO}^-$  species. In addition, correlation between the aromatic carbons and acetoxypropyl protons as well as aromatic protons and acetoxypropyl carbons are clearly visible (marked with broken red line).

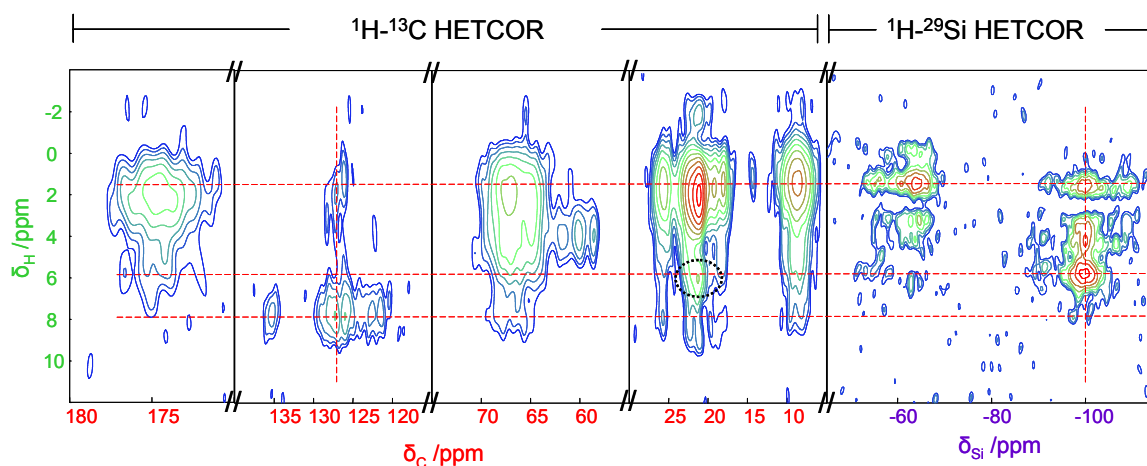


**Figure 7.21:** The amplified 2D  $^1\text{H}$ - $^{13}\text{C}/^{29}\text{Si}$  FSLG HETCOR spectra of Gel 182 at 12.5 kHz. A contact time of 2.0 ms each was used for the carbon and silicon HETCORs.



## 7.6 Acetoxypropyl Substituted Spray Dried Gel – Gel 148

High resolution 2D HETCOR NMR studies has been carried out on a acetoxypropyl substituted hybrid spray dried gel [ATS<sub>148</sub>(3:1, 0.5)] synthesized in presence of Persantin.

### 7.6.1 2D <sup>1</sup>H-<sup>29</sup>Si FSLG HETCOR NMR

The HETCOR map of Gel 148 recorded with a contact time of 2.0 ms is shown in Figure 7.22. Directly bound couples and unbound couples appear as intense and weak correlation peaks in the 2D map, respectively. The strongest cross-peak observed in this spectrum represents a correlation between silicon site Q<sup>3</sup> and silanol protons that are hydrogen bonded at around 5.8 ppm (F1) and -100.2 ppm (F2). As expected, the Q<sup>2</sup> sites are also correlated with these protons, but no correlation is observed with T<sup>2</sup> sites. Mutual correlations between all Q and T sites are observed at around 4.4 ppm in the proton dimension and originate from the water. While the Q<sup>4</sup>, T<sup>3</sup> and T<sup>2</sup> sites show this correlation as resolved cross peaks, Q<sup>3</sup> sites appear as a shoulder to the main peak. In addition, intense cross peaks are observed between T<sup>3</sup> and the methylene protons of the acetoxypropyl group at around -64 ppm (F2) and 1.5 ppm (F1). As expected, the T<sup>2</sup> sites are also correlated with these protons. A weak correlation involving these methylene protons with adjacent Q<sup>4</sup> and Q<sup>3</sup> sites are also observed. The resonance involving Q<sup>2</sup> site and methylene protons was not observed, most likely due to low probability of such neighborhoods due to the low Q<sup>2</sup> content.

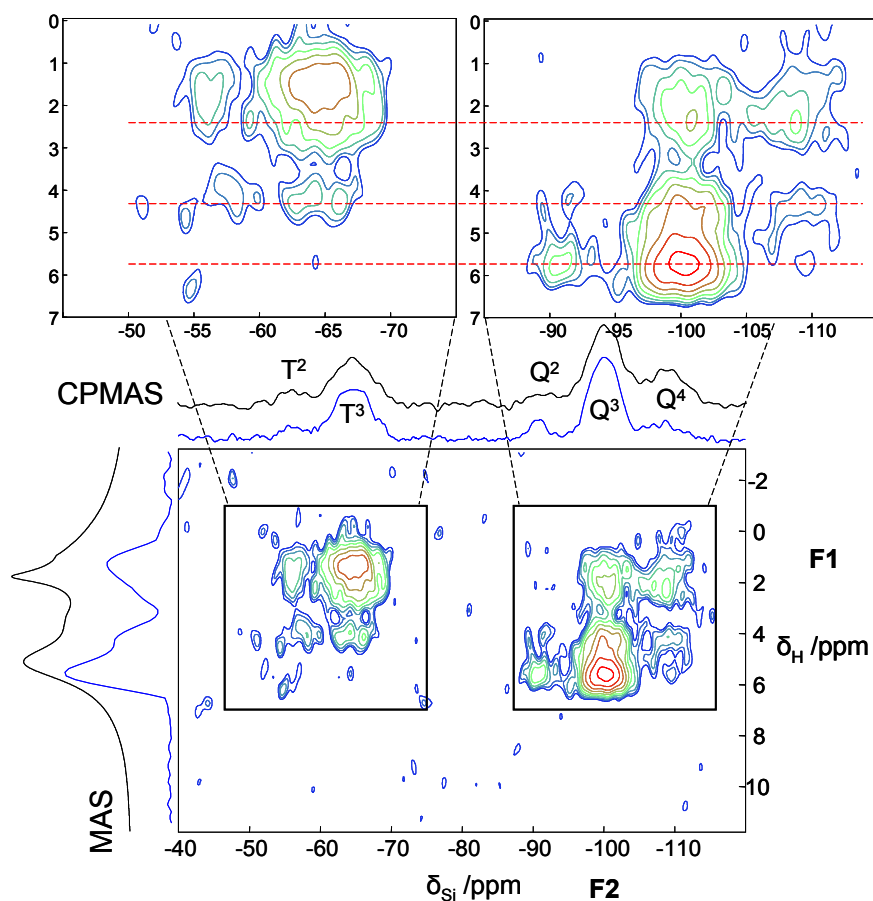


**Figure 7.22:** 2D  $^1\text{H}$ - $^{29}\text{Si}$  FSLG HETCOR spectra of Gel 148 at 2.5 kHz and a contact time of 2.0 ms. The 1D projections are shown in skyline mode. The amplified spectra are given on the top.  $^{29}\text{Si}\{^1\text{H}\}$  CPMAS and  $^1\text{H}$  MAS NMR spectra are shown in F2 and F1 dimension, respectively.

The most remarkable point about this spectrum is the mutual correlations observed between Q and T sites with a proton pool at around 2.5 ppm in the  $^1\text{H}$  dimension, (marked with dashed red line in the amplified part of Figure 7.24). It should be emphasized that, in the silica systems the water resonate in the range 3-5 ppm and hydrogen bonded silanol in the range 4-10 ppm. Due to this, the possibility of inorganic hydrogen species such as water, hydrogen bonded silanols and isolated silanols contributing to this peak can be excluded on the basis of their expected chemical shifts and the absence of direct bonding with silicon sites ( $\text{Q}^4$  and  $\text{T}^3$ ). Another potential proton polarization source is the encapsulated drug, Persantin. Owing to the lower loading of the drug in the hybrid gel, a significant contribution of detected signal from Persantin is unlikely. The remaining proton source in the hybrid gel is the acetoxypropyl units that are directly bound to the T site. From the T group concentrations in the hybrid gel and

the chemical shifts of the acetoxypropyl group, most likely the proton source contributing to the above correlation peaks are acetoxypropyl units. The methyl protons of the acetoxypropyl unit are highly polarizable due to the presence of the directly bound carbonyl group and they resonate at around 2.5 ppm. These protons can interact with the  $\text{SiO}^-$  units originating from all the silicon sites through van der Waals interactions.

The cross sections extracted from the 2D FSLG HETCOR NMR spectrum corresponding to different proton species are shown in Figure 7.23, indicating that the silanol protons at 5.8 ppm only correlate with  $\text{Q}^3$  and  $\text{Q}^2$  sites, whereas the methyl protons of the acetoxypropyl group (2.5 ppm) correlate with both, Q and T sites. The cross sections corresponding to  $\text{Q}^4$ ,  $\text{Q}^3$  and  $\text{T}^3$  sites are shown in Figure 7.24, and the correlations from different proton sources can be distinguished.

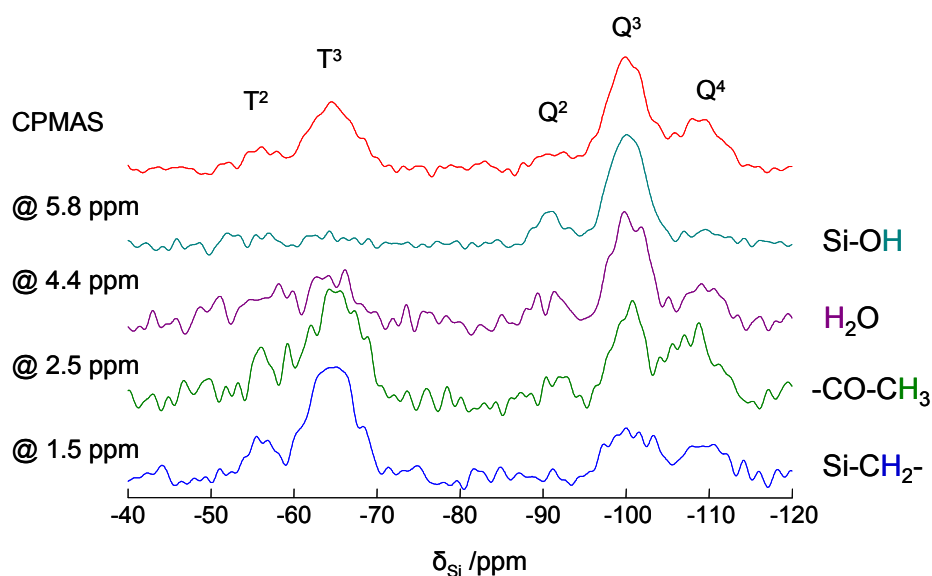


**Figure 7.23:**  $^{29}\text{Si}$  traces from the 2D  $^1\text{H}$ - $^{29}\text{Si}$  HETCOR NMR experiment with 2 ms contact time is being compared with the 1D  $^1\text{H}$ - $^{29}\text{Si}$  CPMAS spectrum of Gel 148.

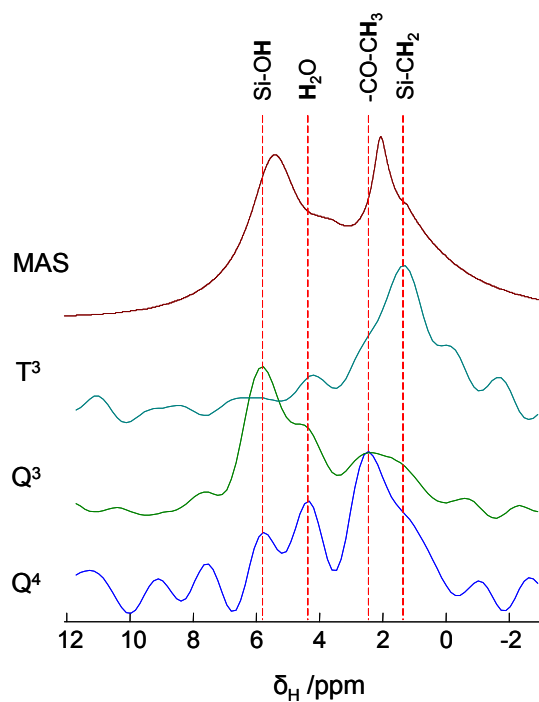


**Figure 7.24:**  $^1\text{H}$  traces from the 2D  $^1\text{H}-^{29}\text{Si}$  HETCOR NMR experiment with 2 ms contact time is being compared with the 1D proton MAS spectrum of Gel 148. Intensities are not in absolute scale.

## 7.7 Discussion

Using a series of high resolution NMR experiments, the molecular level interactions between drug and hybrid silica gel materials were revealed. In addition, different interactions within the hybrid silica gels which control their release and sorption properties are also probed. Upon encapsulation, the drug molecule experiences an increase in surface interactions, which inevitably restrict molecular motions and finally the release properties. From the 2D HETCOR NMR data of pure crystalline PP and encapsulated PP, it is clear that the drug undergoes a significant conformational and packing change. The NMR investigations have focused on the silica surface influence on drug molecules that are confined in the nanopores. The heteronuclear correlations especially favor the detection of intermolecular  $^1\text{H} - ^{13}\text{C}/^{29}\text{Si}$  interactions, since protons are located at the exterior of the molecule.<sup>164</sup> Different interactions such as Coulombic interactions, hydrogen bonding, hydrophobic interactions and other short range interactions such as van der Waals interaction surfacing between drug and matrix are discussed in the following sections.

### Water and silanol interactions

All the silica gels studied exhibit the presence of water and has a strong influence on their properties. Studies based on temperature treated samples confirm the presence of weakly bound and relatively mobile water on silica gels. From the 2D HETCOR experiment, the correlations between water protons and  $\text{Q}^3$  site at shorter contact time as well as with all Si sites at longer contact times imply the presence of different environments for water. The water molecules are hydrogen bonded to surface silanols as well as confined on the interstice pores. Figure 7.25 displays the different possible scenarios of water molecules hydrogen bonded to the silica surface. In addition, water molecules form hydrogen bonding among themselves similar to liquid water and can reside in the pores. The chemical shifts of monomer water and cluster water are around 0.8-1.5 ppm and 5.5 ppm, respectively.<sup>167</sup> Isolated silanols resonate at around 1.8 ppm. The broad proton resonances for water found in the 2D experiments were centered at around 4.0 ppm and are mainly interacting with  $\text{Q}^3$  sites (box A, Figure 7.4) at shorter contact times. From the above observations, a multimodal distribution of the water in

pores and surfaces of silica can be envisaged. There are several reports on the chemical shift of water molecules found in various environments related to this work. Most of the schemes presented in Figure 7.25 have been recognized in silica systems.<sup>168</sup> Water molecules confined in the pores and surfaces exhibit hydrogen bonding with silanols as well as drug molecules. Silanol protons can also form hydrogen bonding among themselves and these peaks are centered at around 6 -7 ppm depending on the silanol proton density (box A, Figure 7.3).

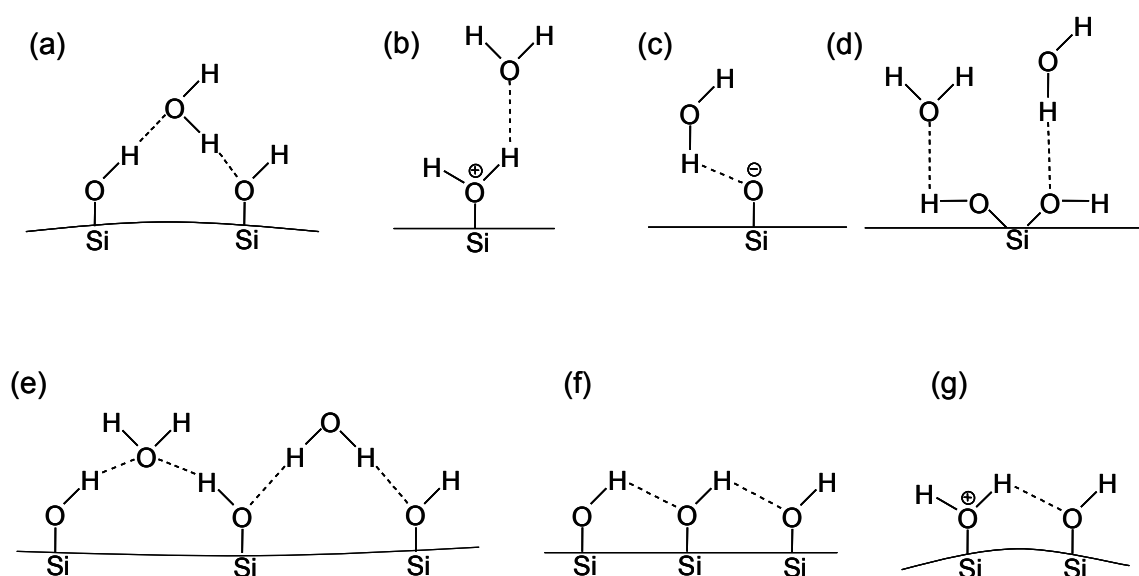


**Figure 7.25:** Schematic representation of silanol types and possible structures involving both silanol groups and water on the pore surface.

### Q and T site interactions

The dispersion of Q and T sites within the hybrid gels were investigated by HETCOR technique. The hybrid silica gel was prepared by the hydrolysis and condensation of mixtures of Q monomers (TEOS) and T monomer (e.g. MTS or ATS) under acidic conditions. The key question is if the organically modified T monomers were uniformly incorporated in the inorganic matrix without aggregation or phase separation. From the  $^1\text{H}$ - $^{29}\text{Si}$  2D HETCOR experiments, interactions between Q and T sites in hybrid gels were observed. Short contact time experiments revealed correlations among protons within its own molecules indicating confinement of polarization transfer within the same

molecule. However, the cross-peaks observed between T-protons and Q sites with short contact time indicate that they are in close proximity. From the above observation it may be concluded that the Q and T sites are mixed at molecular level and the hybrid gels are homogeneous in nature. Figure 7.26 displays possible interactions between Q and T sites in MTS and ATS gels as well as the proton polarization transfer observed in the 2D HETCOR technique. Such interaction will only appear when the Q and T sites are uniformly distributed throughout the hybrid systems (box B, Figure 7.3). All the hybrid gels investigated by 2D NMR technique exhibit Q and T interactions, which exclude phase separation and aggregation during the preparation processes.

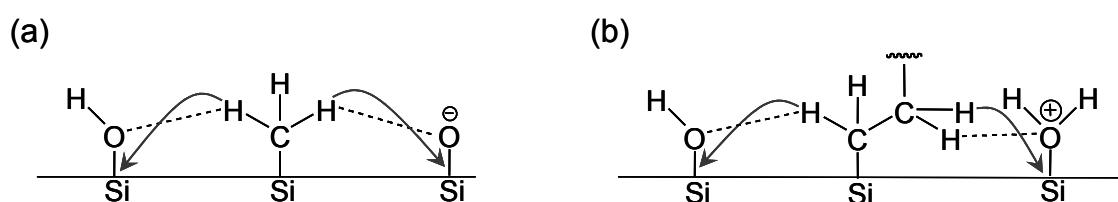


**Figure 7.26:** Schematic representation of *Q* and *T* interactions in MTS (a) and ATS (b) gels and possible polarization transfer pathways.

Two different types of gel network architecture can be imagined from the hybrid gel synthetic conditions and are given in Figure 7.27. In the first case, the T units are aggregated to form separate domain whereas in the second case Q and T sites are uniformly distributed throughout the hybrid network. From the macroscopic point of view, both types are plausible and can not be excluded in the network genesis process. Two dimensional heteronuclear correlation NMR spectroscopy gave insight into the molecular level picture of actual gel network building up process. As discussed in the previous section, the correlations observed between Q and T sites confirm the homogeneous hybrid gel formation and omit the phase separation and aggregation.

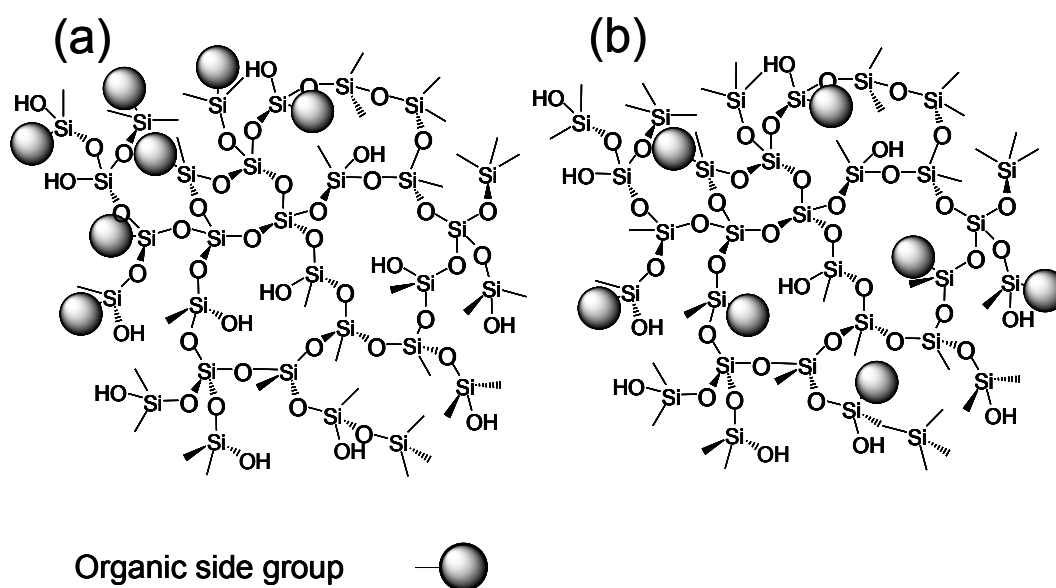


**Figure 7.27:** An illustration of the plausible hybrid silica network in gel with T group aggregation (a) and homogeneous gel (b).

### Guest-host interactions

High resolution 2D solid state NMR methods have been used to probe the through space interactions between guest and host in the complex sol-gel derived hybrid materials. Two important issues have been addressed in this discussion: (1) How the release properties of the encapsulated guest drug molecules are influenced by their interactions with the host matrix? (2) How the organic components in the inorganic matrix influence the properties of hybrid materials?

The above issues are addressed by probing the spatial proximity existing between the entities in the hybrid network (guest as well as host components) and their molecular level interactions. The efficiency of magnetization transfer between abundant and rare spins ( $^1\text{H}$  and  $^{29}\text{Si}/^{13}\text{C}$ , respectively), which occur during the contact time, is directly related to the  $^{29}\text{Si}-^1\text{H}$  and  $^{13}\text{C}-^1\text{H}$  distances and mobility.

The direct correlations (observed at short contact time) between the methyl protons of the T site with the aromatic carbons of the drug as well as between the aromatic protons of the drug and methyl carbons of T site in the methyl substituted hybrid gels supports the view that they are in very close proximity (box A and B, Figure 7.14). Furthermore, the correlations observed between the methyl protons of the drug with the Q and T sites, at short contact time suggest that the drug molecules are not far away from the matrix



surfaces. The above observation is also supported by the correlations between the silanols and aromatic protons of the drug. Figure 7.28 displays possible interactions between host matrix and guest drug molecules observed in the 2D HETCOR technique.

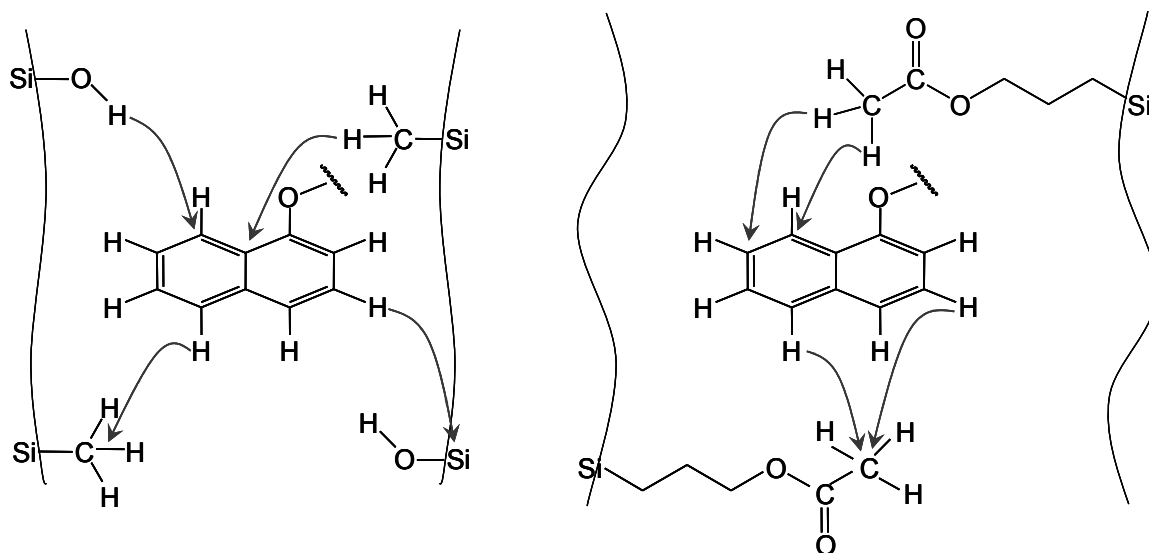


**Figure 7.28:** Schematic representation of the possible polarization transfer pathways in MTS (a) and ATS (b) gels.

### Special drug – matrix interactions

With longer contact time, correlations observed between the low shielding  $^+NH_2/OH$  protons of the drug molecules and  $Q^3$  sites (box A, Figure 7.5). Silicon sites also receive proton magnetization from methyl proton which can be envisaged as shown in Figure 7.29.

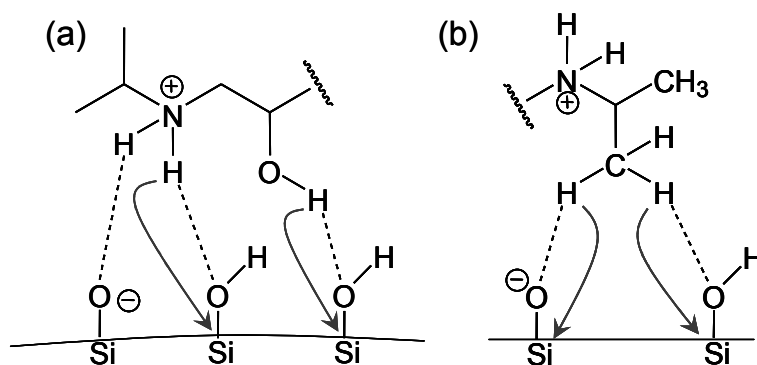


**Figure 7.29:** Schematic representation of drug-matrix interactions (a) observed at down-field and (b) observed at up-field with possible polarization transfer pathways.

Similarly, special interactions are observed for methyl protons of T sites which are in close vicinity of the negative ring current region of the aromatic rings of the drug molecules (box C, Figure 7.14). This is schematically represented in Figure 7.30. The methyl protons experience higher shielding effect than the methyl carbons due to distance considerations. Such  $\text{CH} \cdots \pi$  interactions are recognized and reported in the literature.<sup>166,169</sup> The impressive upfield shifts caused by the aromatic ring currents on the methyl group of matrix at the van der Waals contacts provide a tool for understanding the preferred topology of the drug molecules interacting with the silica matrix.

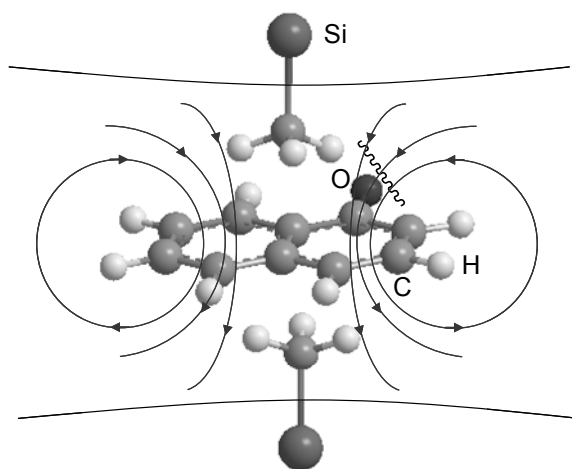


**Figure 7.30:** Topology of methyl protons located above the plane of the naphthalene rings: the ring currents generate an upfield shift.

In aromatically modified hybrid gels,  $\pi - \pi$  interactions between drug and matrix can be anticipated. Since the resonances from the aromatic carbons and protons are very broad, mutual correlations between drug and matrix cannot be separated. However, such interactions can lead to a dramatic change in the release behavior of drug molecules. Aromatic substitution in hybrid gels can impart a hydrophobic character to the silica gels which can control the release of drug in hydrophilic solvents.

### Interactions in ATS hybrid gels

Acetoxypropyl substituted hybrid gels were investigated by high resolution 2D HETCOR technique to understand the special behavior towards drug release and porosity. Bögershausen et al. found out the gated porosity in ATS gels.<sup>58</sup> Upon drug release, ATS

gels developed pore volume, but no porosity were detected by N<sub>2</sub> sorption experiment. It has been suggested that the channels were being blocked by the acetoxypropyl groups at 77 K which obstruct the N<sub>2</sub> diffusion. The blockage happens because of the organic acetoxypropyl side groups possibly form hydrogen bonds, making the chain rigid at 77 K. A detailed study by 2D HETCOR NMR technique has been carried out to understand the interactions exhibited by the ATS hybrid gels as well as to verify the hypothesis that porosity in amorphous silicates and silicate like materials arise from macromolecular phenomenon such as packing of particles and fractal topographies.<sup>146</sup>

From the HETCOR NMR experiment different correlations between acetoxypropyl group and silanols are revealed. The correlations between acetoxypropyl protons with silicon sites as well as silanol protons with acetoxypropyl carbons indicate that they are in close proximity. Different types of interactions can be envisaged from the above observations as shown in Figure 7.31.

The localization of the organic acetoxypropyl group in the hybrid gel through different short range interactions are confirmed from the through space heteronuclear dipolar interactions involving protons, carbons and silicons. Such interactions can lead to a network with three dimensional rigidity to an otherwise flexible system, thereby preventing the N<sub>2</sub> sorption at 77 K. Kurk et al. have demonstrated that the size of pore entrances can be controlled by the modification with organosilanes.<sup>170</sup> They found that by gradually increasing the alkyl chain length from methyl to octyl, the N<sub>2</sub> access partially blocked or completely shut down which is in support with the ATS scenario.

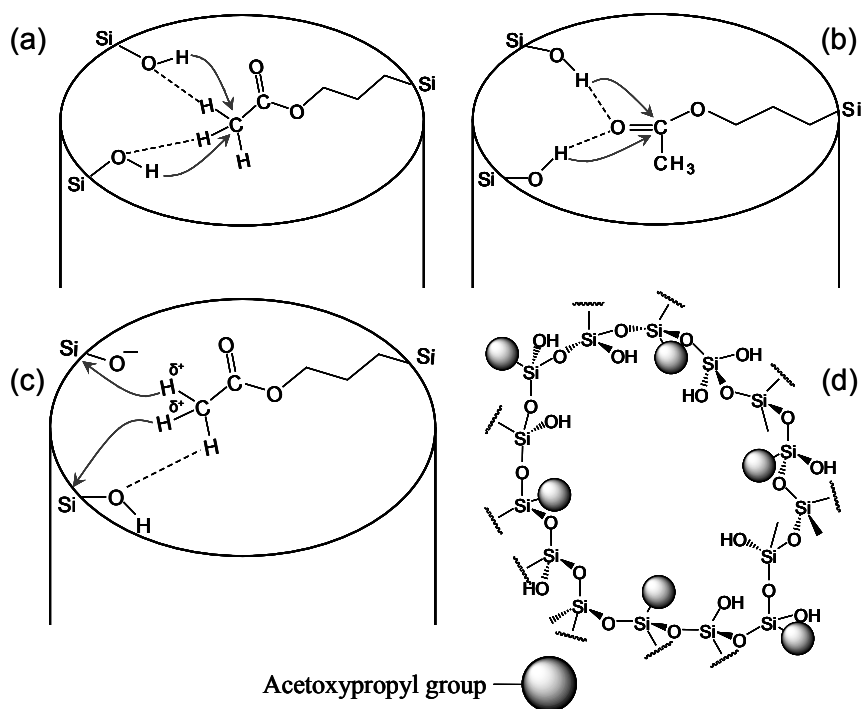


**Figure 7.31:** A plausible model representing the pore blocking ability of ATS units along with different polarization transfer pathways (a) to (c). A schematic of molecular cage opening covered by ATS units which are rigid at 77 K while flexible at 300 K (d).

Two-dimensional heteronuclear correlation data provide valuable information on the specific sites and nature of interactions of the drug with the silica surface. The observed magnetization transfer between drug and matrix is a direct proof for dipolar coupling and inversely depends on  $r^3$ , the internuclear distance. HETCOR NMR experiments with different contact times also revealed the intimacy between host and guest through the weaker interactions between dipolarly coupled nuclei. Relative distance assessment between the interacting nuclei can be made based on the intensity of the cross-peaks in the 2D plots. Together with results from PALS experiment,<sup>58,104</sup> the NMR data indicate that ATS substituted hybrid gels are inaccessible to N<sub>2</sub> molecules at 77 K. Based on the NMR data, a molecular assembly pinpointing different short range interactions between matrix and drug molecules can be envisaged. In addition to hydrogen bonding, an encapsulated drug molecule may experience Coulombic interactions, hydrophobic interactions and other nonspecific short-range interactions simultaneously. Since organically modified hybrid gels consist of alkyl chains, hydrophobic interactions

enhance interactions between drug and matrix. Thus, by using organically modified precursors, the internal hydrophobicity/hydrophilicity of silica gels can be increased. It is also quite possible that the drug molecule can act as a template for silica sol-gel matrix formation, thereby encapsulation producing a pore of similar shape and size.

High resolution 2D NMR has used to monitor the influence of different interactions on the global release behavior of hybrid silica encapsulated drug molecule at a molecular level. By directly observing the local environments of drug molecules, a rationale between release kinetics and drug – matrix interactions can be made. NMR investigations on the molecular level interactions between drug and matrix provide a deeper understanding on the kinetic release behavior as well as the effects of hydrophilicity and hydrophobicity on the hybrid silica gels.

2D NMR technique reveal drug-matrix interactions that cooperatively sustain the release of drug molecules entrapped as guests in channels formed by the hybrid silica host. These interactions are pivotal for shaping complex self-assembled architectures. In particular, hydrophobic interaction between benzene rings and hydrocarbon molecules are weak (2-8 kJ/mol).<sup>166</sup> Their strengths are 20% that of hydrogen bonds formed between water molecules; nevertheless they must be invoked for understanding molecular recognition in hybrid silica gels. Self-assembled drug encapsulated hybrid silica gel systems exploit cooperative non-covalent interactions and the decrease of overall energy drives the stabilization of complex architectures. Organized interactions of  $\pi$  – systems support the unusual arrangements of aromatic rings in the channels of hybrid gels leading to dense networks. Such dense network will sustain the drug release from aromatic substituted hybrid gels. In addition, hydrogen bonding between the aromatic part of the guest molecules and silanol groups can be expected. These interactions have recently been recognized and documented.<sup>171</sup> Attractive interactions between  $\pi$  systems are one of the principal noncovalent forces governing molecular recognition.<sup>172</sup> They influence the structures of proteins,<sup>173</sup> DNA, host-guest complexes<sup>174</sup> and self-assembled supramolecular architectures.<sup>175</sup> These  $\pi$  -  $\pi$  interactions also control the intercalation of certain drugs into DNA.<sup>176</sup> Although the importance of  $\pi$  -  $\pi$  interactions is widely recognized, a detailed understanding of their origins, strength and orientational dependence is not yet available.<sup>172</sup>

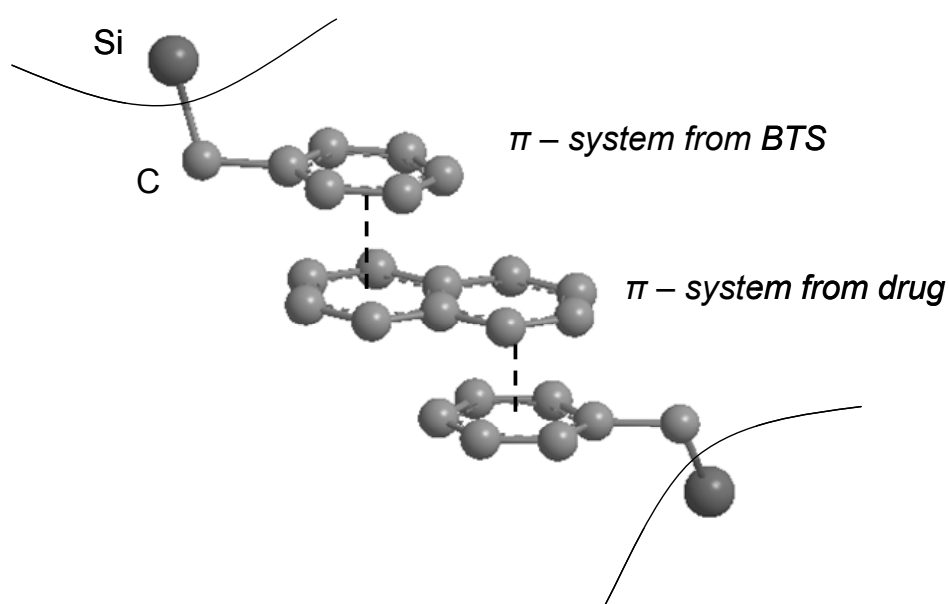


**Figure 7.32:** Schematic of the proposed  $\pi - \pi$  interactions between benzene (of matrix) and naphthalene (of drug) rings.

The results of these studies suggest that the major mechanism of naphthalene (from PP) interaction with benzene (from BTS) is of  $\pi - \pi$  nature, Figure 7.32. Despite the molecular detail of these pictures, certain aspects of the surface interactions such as the role of aliphatic part of drug in these interactions, the organization of aromatic rings and the absolute geometry of interacting molecules cannot be determined from these studies.

## 8. Conclusions and final remarks

---

The area of organic-inorganic hybrid network materials prepared by the sol-gel approach has rapidly become a fascinating new field of research interest in materials science. The outbreak of research in the past decade in this field has promoted considerable progress in both the fundamental understanding of the sol-gel process in general and its use in the development and applications of new organic-inorganic hybrid materials. As has been discussed within the thesis, a very wide range of materials properties can be generated by combining the appropriate features of a given silica precursors and synthesis conditions.

In summary, this work has shown that the diffusion rates of charged molecules trapped in a silica gel can be easily changed and tuned by modifying the charge on the matrix walls and porosity. Protonated drug molecules can be made to diffuse at rates similar to that in solution by incorporating a sufficient number of positively charged functionalities in the gel. The ability to control the rates of diffusion of different drug species in sol-gel materials will enable their performance to be enhanced in controlled drug release applications. From the NMR, adsorption and DRT studies, a picture has emerged in which sol-gel encapsulated drug molecules reside in several regions. Those within the interface region have restricted motions, while those in the surface of particles behave much as though they were in solution. An additional region is postulated here, which include pores and crevices where drug molecules are confined along with solvents.

The self assembled silica gels represent a remarkably diverse class of nanoporous materials capable of forming both Si-O-Si and Si-O-Si-C bonds with molecular scale homogeneity. For drug molecule directed self assembly, silicic acid moieties formed by alkoxide hydrolysis co-organize with protonated drug molecules to form hybrid materials. Self assembly exploits non-covalent interactions such as hydrogen bonding,  $\pi$ - $\pi$  and hydrophobic interactions to form hybrid architectures. The introduction of functionalities through organically substituted precursors serve active roles such as influencing the wetting characteristics, increasing the molecular level interactions and determining the domain sizes etc.

In this thesis it is shown that sol-gel matrix is an excellent substance for drug encapsulation along with porosity, homogeneity, ease of fabrication and stability are some of its advantages. Adding to it, the large library of existing alkoxysilanes makes the sol-gel method a versatile one for the generation of new materials. On the basis of the NMR data, it is clear that the entrapment of drug molecules into the silica gels result in significant noncovalent interactions. During the genesis process, the silica network grows around the drug molecule, and upon aging they reside in the pores. The stability of the drug molecules inside the matrix is confirmed by solid state NMR spectroscopy. The HETCOR NMR experiments are used to characterize precisely the local environments in hybrid silica gels. They also show that the scaled proton spin-diffusion occurring during the contact time of polarization transfer give valuable information about the distances in the range of nanometers.

The controlled sustained release achieved for the model drug Propranolol can be extended to the other newly discovered drugs. The enhancement of bioavailability of Persantin by the sol-gel spray drying route can be extended to the large library of sparingly water soluble drugs. I envisage that this drug encapsulated sol-gel process could be further developed into an economical and biocompatible method for day-to-day applications.



## 9. Appendix

### 9.1 $^1\text{H}$ MAS NMR spectra of various EISA hybrid gels

The proton MAS spectra were acquired at a MAS rate of 15 kHz. Washed samples and high temperature treated samples are marked. All the spectra were recorded at room temperature. The intensities of the spectra are not in absolute scale.

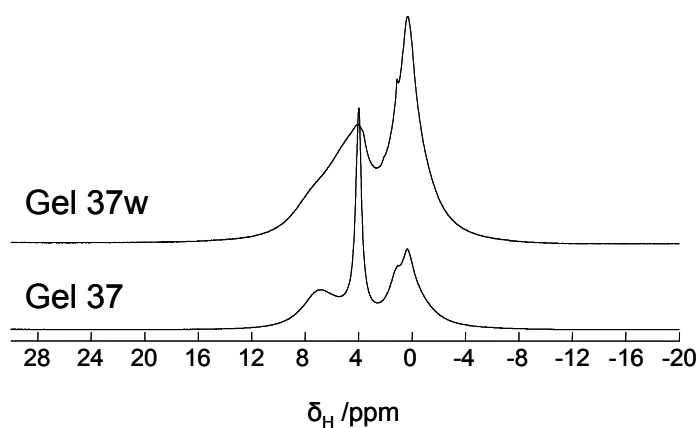


**Figure A1.1:** The  $^1\text{H}$  MAS NMR spectra of hybrid MTS gel before (Gel 37) and after extraction (Gel 37w) of drug.

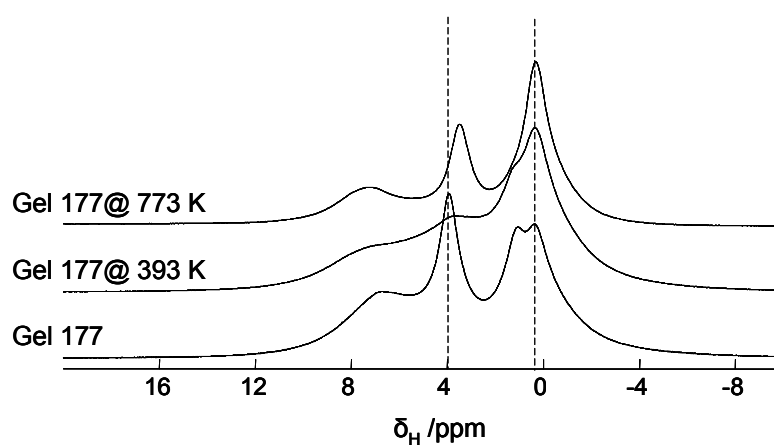


**Figure A1.2:** The  $^1\text{H}$  MAS NMR spectra of hybrid MTS Gel 177.

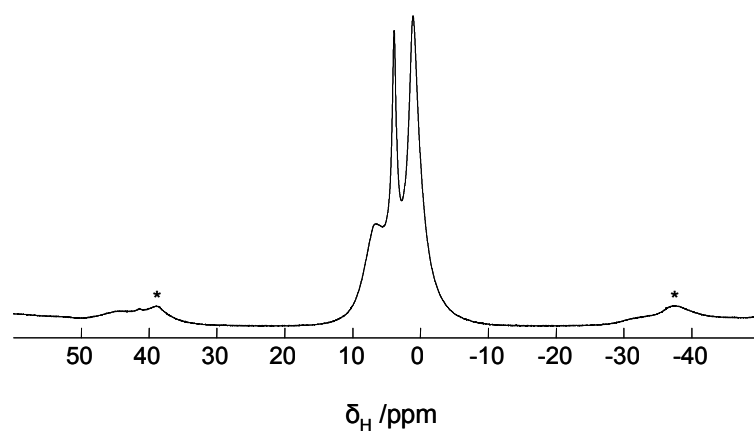


**Figure A1.3:** The  $^1\text{H}$  MAS NMR spectrum of hybrid ETS Gel 180.

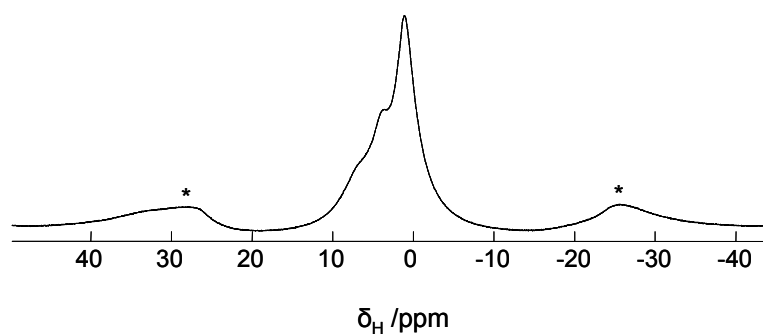


**Figure A1.4:** The  $^1\text{H}$  MAS NMR spectrum of hybrid PTS Gel 305 (MAS 10 kHz).

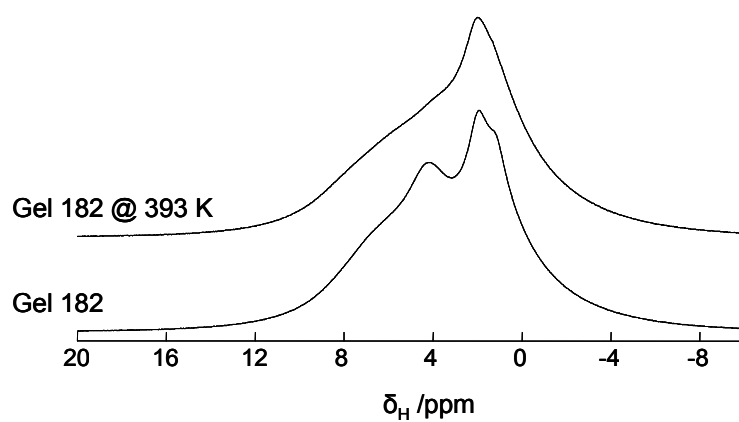


**Figure A1.5:** The  $^1\text{H}$  MAS NMR spectra of hybrid ATS Gel 182.

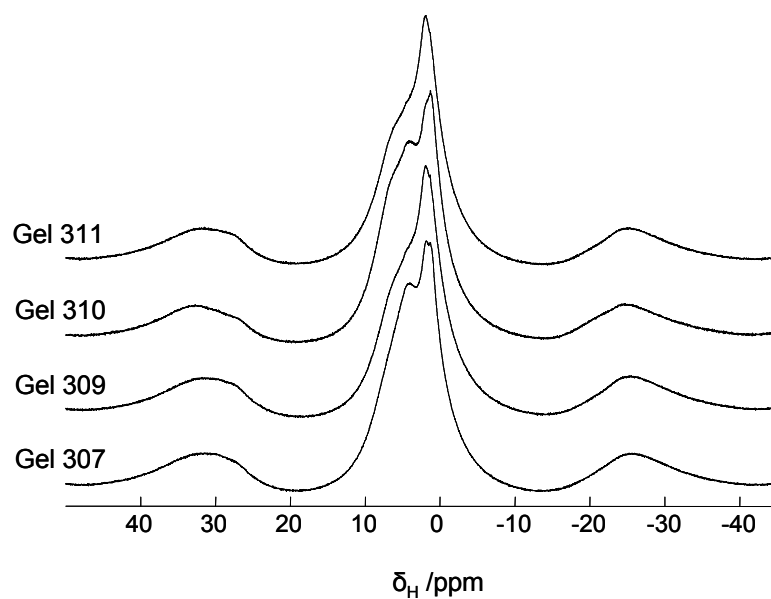


**Figure A1.6:** The  $^1\text{H}$  MAS NMR spectra of hybrid ATS gels prepared at different pH and composition, (MAS 10 kHz).

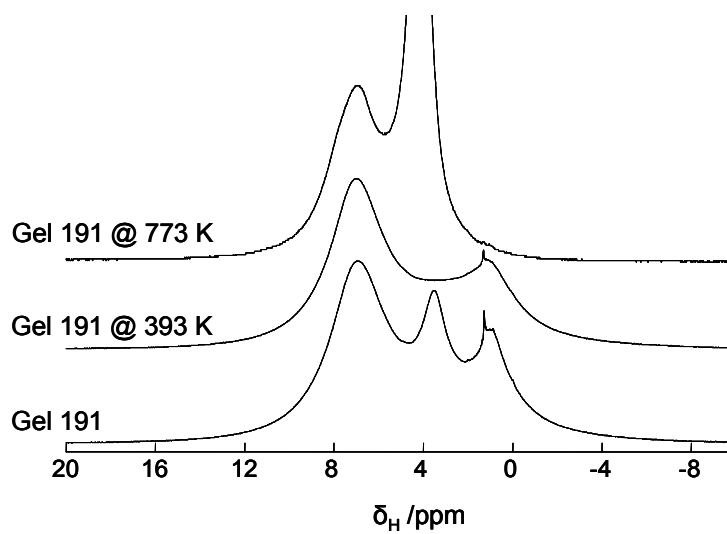


**Figure A1.7:** The  $^1\text{H}$  MAS NMR spectra of hybrid BTS Gel 191.

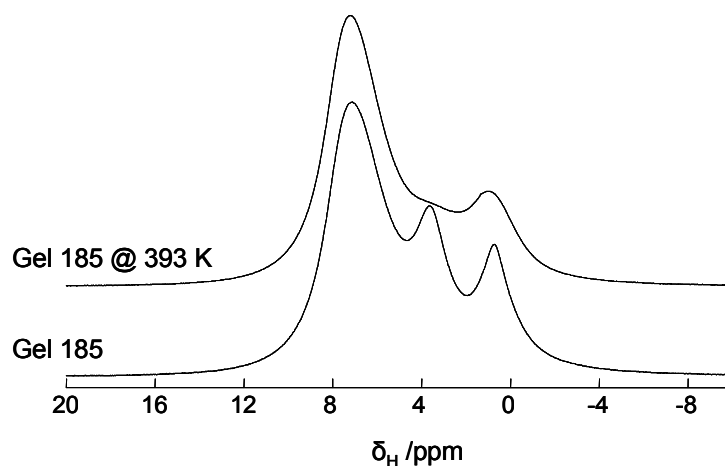


**Figure A1.8:** The  $^1\text{H}$  MAS NMR spectra of hybrid PhTS Gel 185.

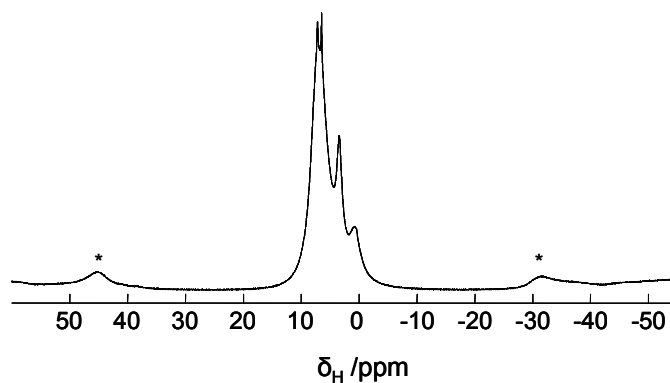


**Figure A1.9:** The  $^1\text{H}$  MAS NMR spectrum of hybrid DPhDS Gel 188.

## 9.2 $^1\text{H}$ MAS NMR spectra of various SD gels

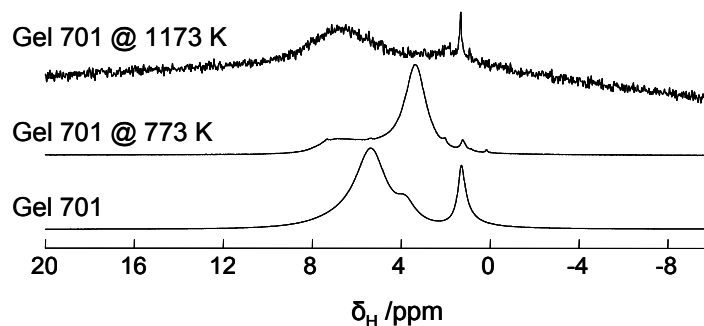


**Figure A1.10:** The  $^1\text{H}$  MAS NMR spectra of spray dried TEOS Gel 701 prepared in the absence of drug.

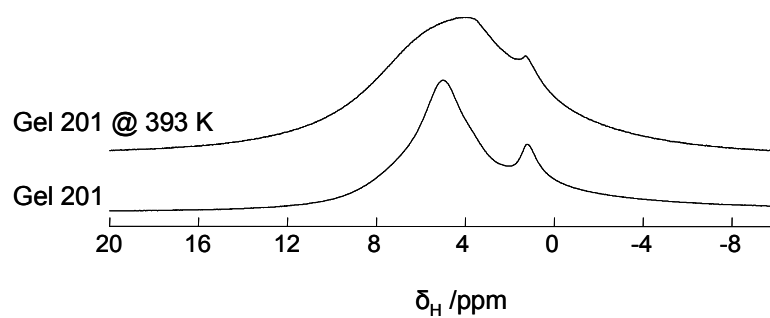


**Figure A1.11:** The  $^1\text{H}$  MAS NMR spectra of spray dried TEOS Gel 201 prepared in the presence of Persantin.

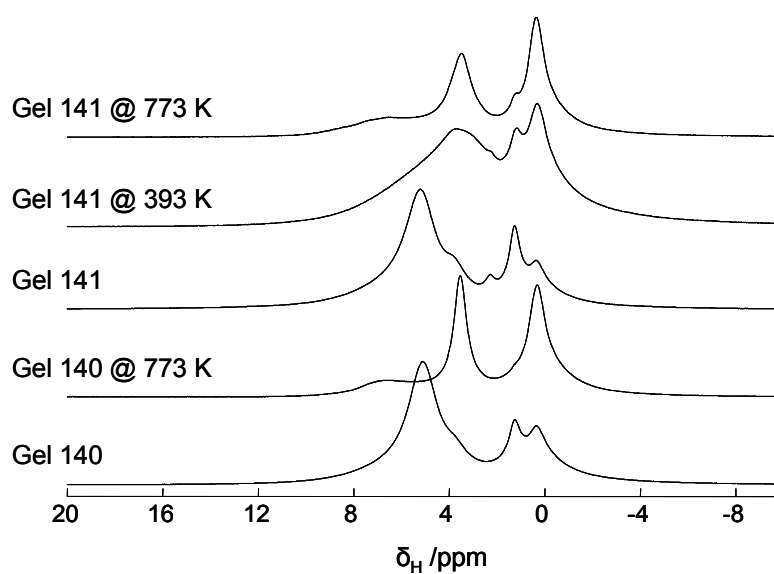


**Figure A1.12:** The  $^1\text{H}$  MAS NMR spectra of spray dried hybrid MTS gels prepared in the presence of Persantin.

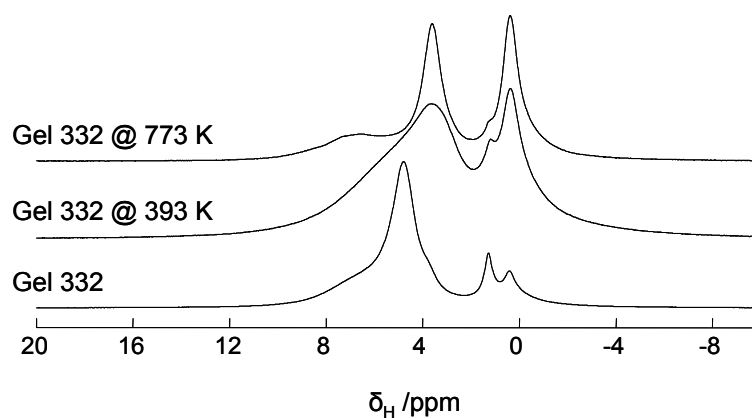


**Figure A1.13:** The  $^1\text{H}$  MAS NMR spectra of spray dried hybrid MTS Gel 332.

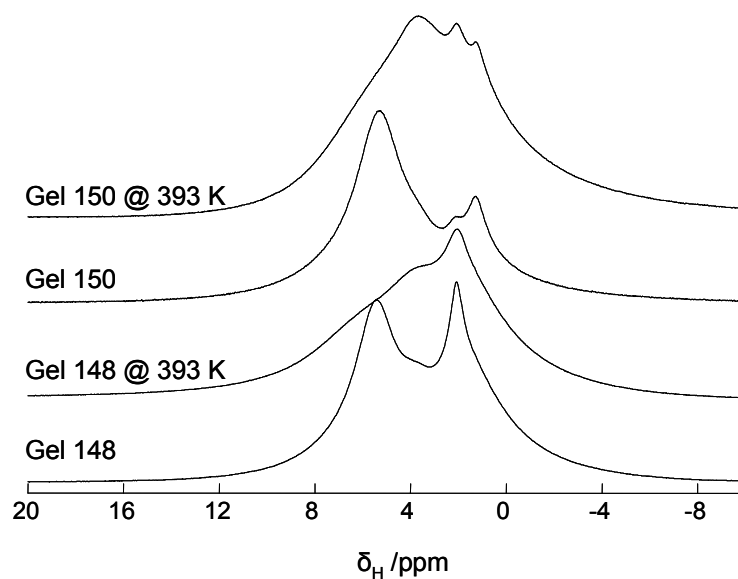


**Figure A1.14:** The  $^1\text{H}$  MAS NMR spectra of spray dried hybrid ATS Gels 148 and 150.

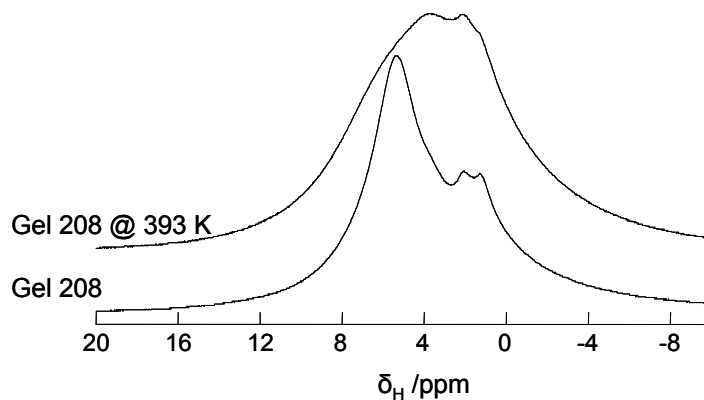


**Figure A1.15:** The  $^1\text{H}$  MAS NMR spectra of spray dried hybrid ATS Gel 208.

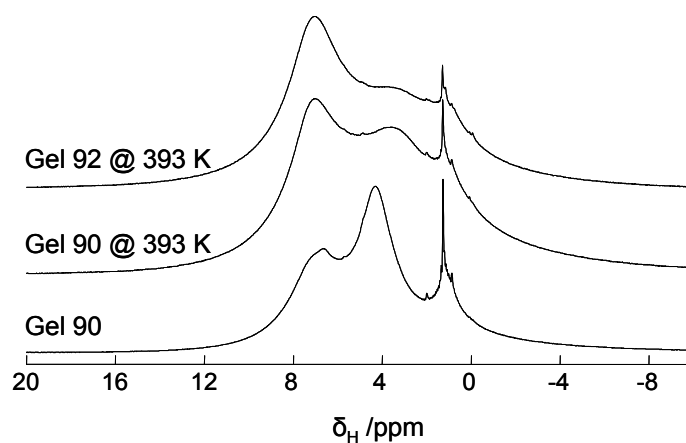


**Figure A1.16:** The  $^1\text{H}$  MAS NMR spectra of spray dried hybrid BTS Gels 90 and 92.

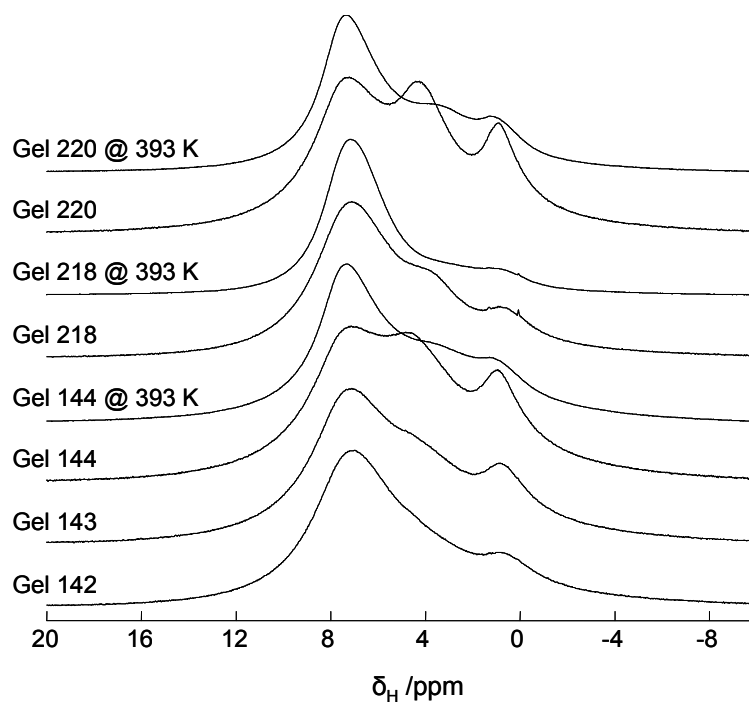


**Figure A1.17:** The  $^1\text{H}$  MAS NMR spectra of spray dried DPhDS gels.

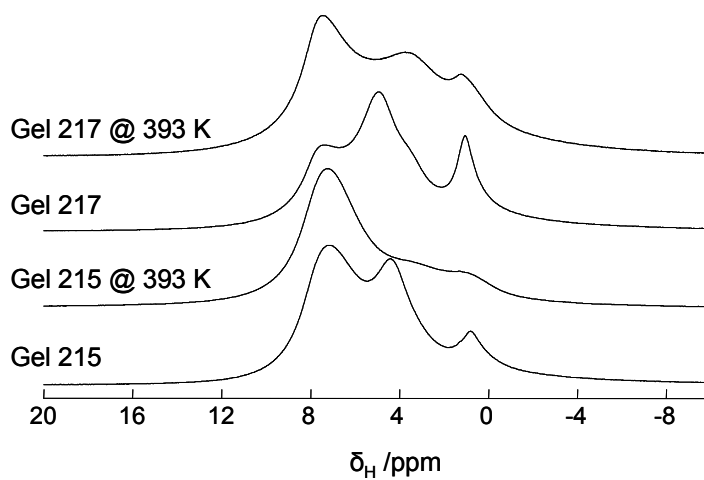


**Figure A1.18:** The  $^1\text{H}$  MAS NMR spectra of spray dried hybrid PhTS Gels 215 and 217.

## Spray dried gels with PP

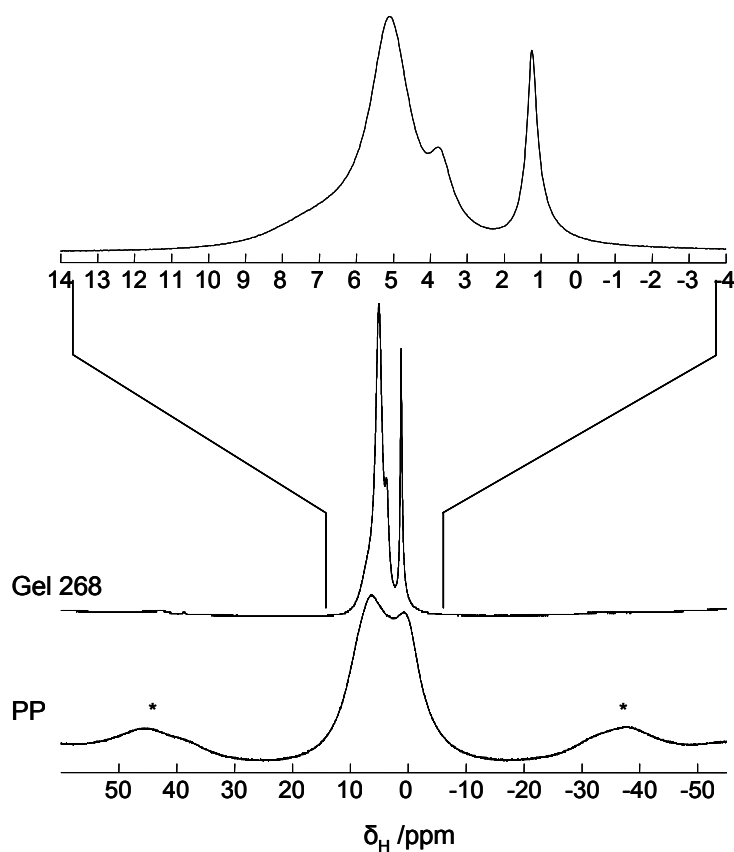


**Figure A1.19:** The  $^1\text{H}$  MAS NMR spectra of spray dried TEOS Gel 268 and pure drug at 15 kHz.

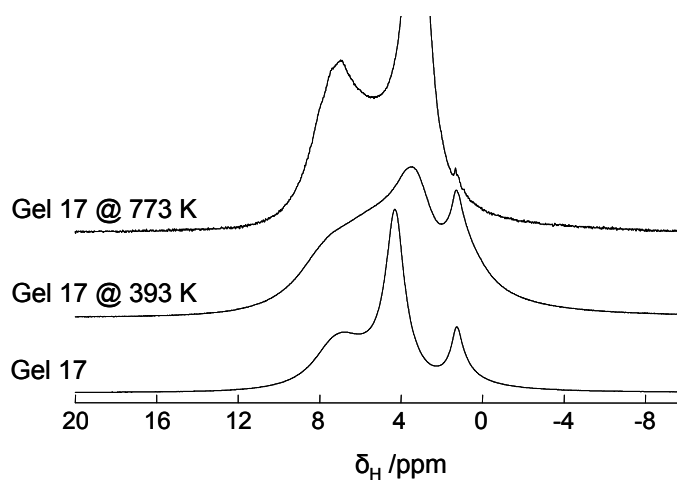


**Figure A1.20:** The  $^1\text{H}$  MAS NMR spectra of spray dried TEOS Gel 17 at 15 kHz.



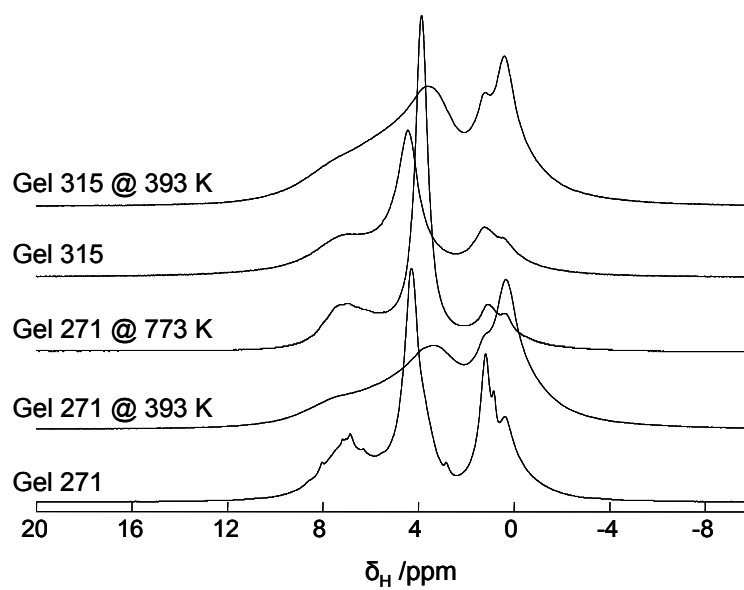


**Figure A1.21:** The  $^1\text{H}$  MAS NMR spectra of spray dried MTS Gels 271 and 315.

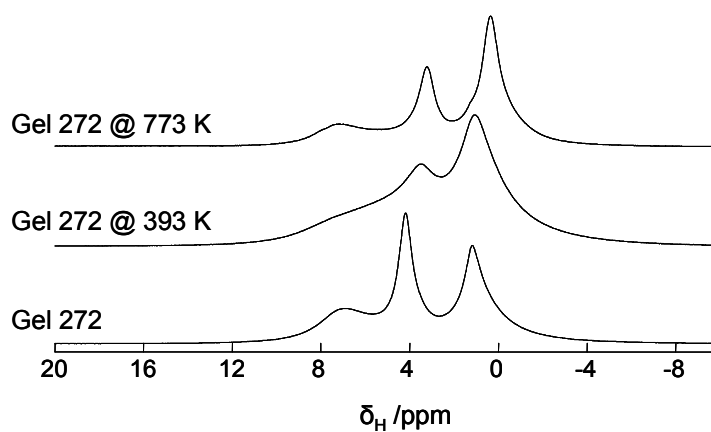


**Figure A1.22:** The  $^1\text{H}$  MAS NMR spectra of hybrid ETS Gel 272.

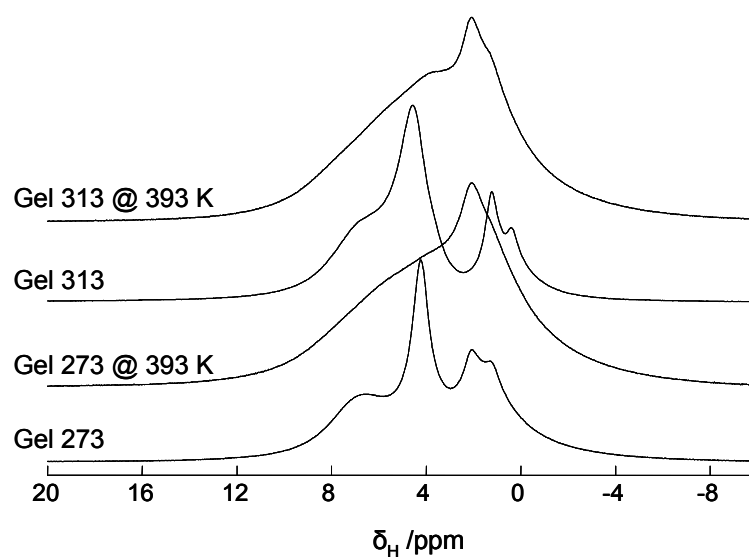


**Figure A1.23:** The  $^1\text{H}$  MAS NMR spectra of spray dried hybrid ATS Gels 272 and 313.

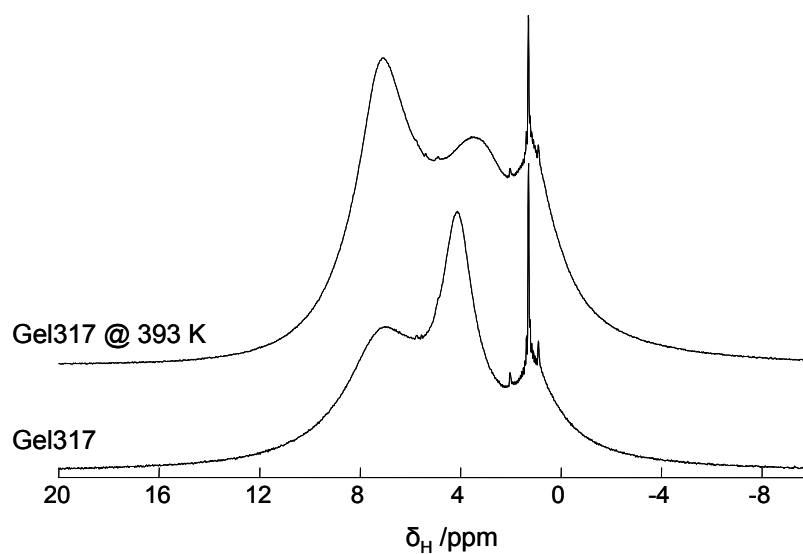


**Figure A1.24:** The  $^1\text{H}$  MAS NMR spectra of spray dried hybrid BTS Gel 317.

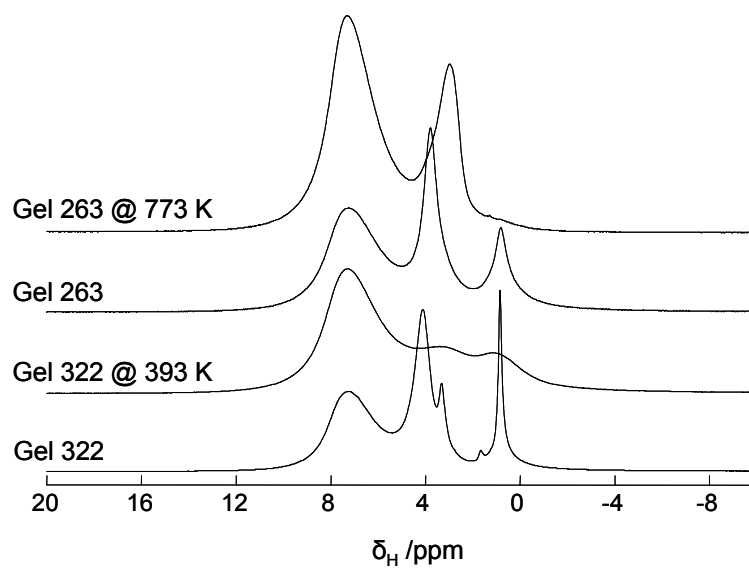


**Figure A1.25:** The  $^1\text{H}$  MAS NMR spectra of spray dried PhTS gels.

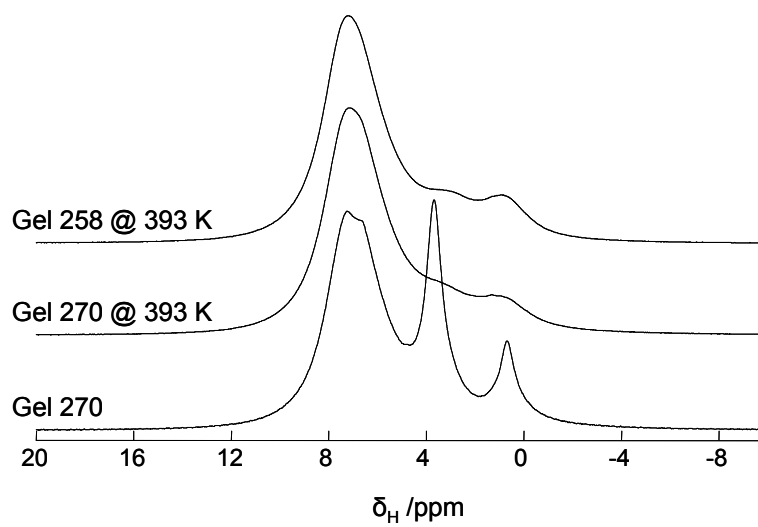


**Figure A1.26:** The  $^1\text{H}$  MAS NMR spectra of spray dried DPhDS gels.

### 9.3 $^{29}\text{Si}$ MAS NMR spectra of various EISA hybrid gels

The  $^{29}\text{Si}$  MAS spectra of various gels together with the corresponding computer simulated spectra and their individual deconvoluted contributions from each silicon site.

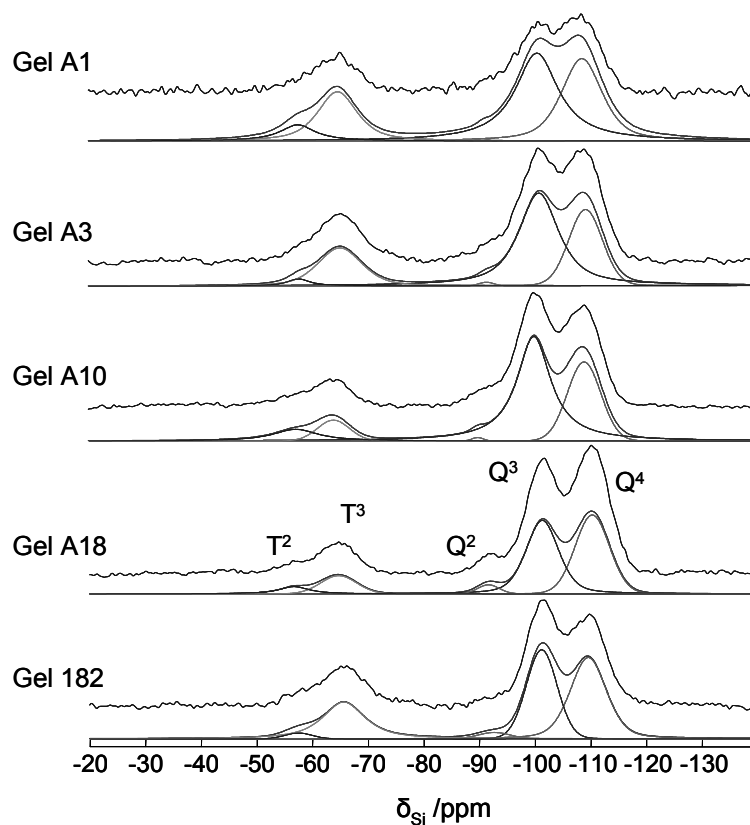


**Figure A2.1:**  $^{29}\text{Si}$  MAS NMR spectra of hybrid ATS gels.

**Table A2.1:** Peak area derived for deconvoluted peaks of the  $^{29}\text{Si}$  MAS spectra of hybrid ATS gels

Probe	T <sup>2</sup> /%	T <sup>3</sup> /%	Q <sup>2</sup> /%	Q <sup>3</sup> /%	Q <sup>4</sup> /%	Σ T /%	Σ Q /%
Gel A1	7	19	1	42	31	26	74
Gel A3	2	20	1	50	27	22	78
Gel A10	8	7	1	55	29	15	85
Gel A18	5	10	3	41	41	15	85
Gel 182	2	24	2	33	38	26	73

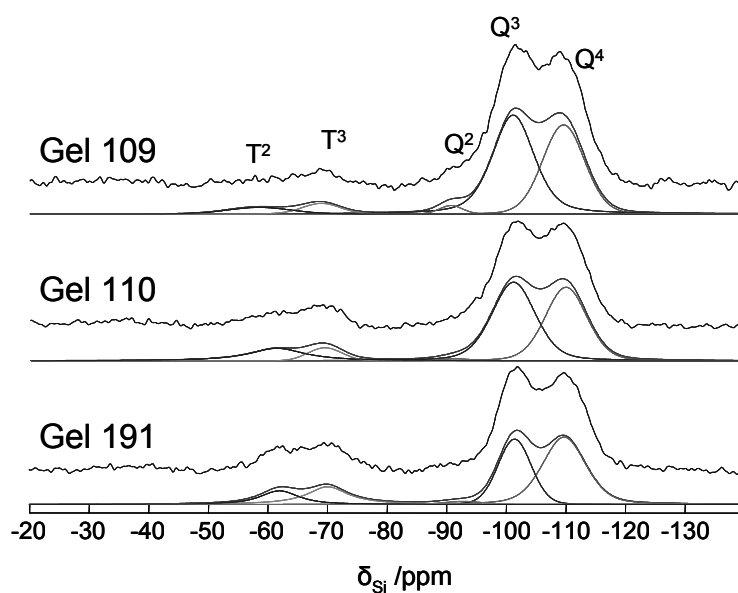


**Figure A2.2:**  $^{29}\text{Si}$  MAS NMR spectra of various BTS gels.

**Table A2.2:** Peak area derived for deconvoluted peaks of the  $^{29}\text{Si}$  MAS spectra of various BTS gels.

Probe	T <sup>2</sup> /%	T <sup>3</sup> /%	Q <sup>2</sup> /%	Q <sup>3</sup> /%	Q <sup>4</sup> /%	Σ T /%	Σ Q /%
Gel 109	5	5	2	49	39	10	90
Gel 110	11	5	1	44	39	16	84
Gel 191	10	14	2	30	44	24	76

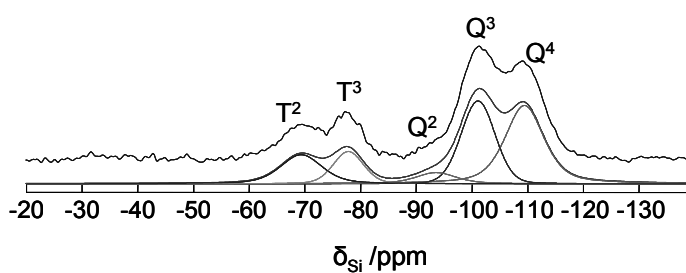


**Figure A2.3:**  $^{29}\text{Si}$  MAS NMR spectrum of hybrid PhTS Gel 185.

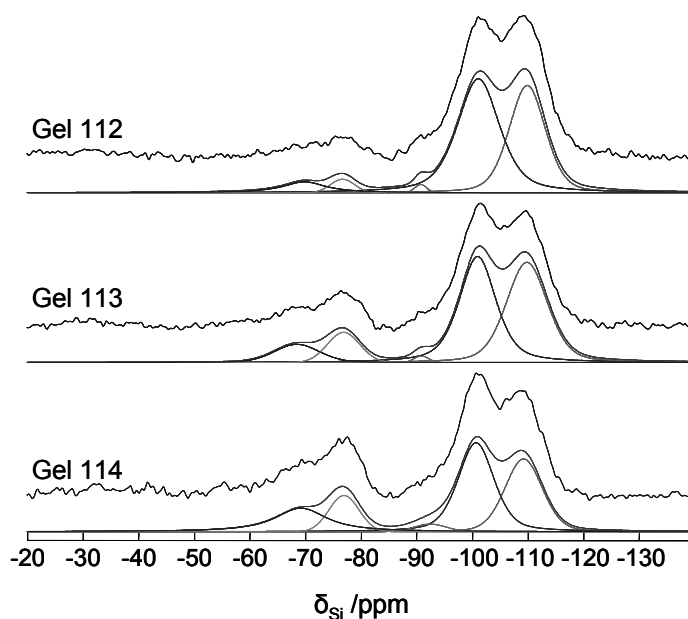


**Figure A2.4:**  $^{29}\text{Si}$  MAS NMR spectra of hybrid PhTS Gels.

**Table A2.3:** Peak area derived for deconvoluted peaks of the  $^{29}\text{Si}$  MAS spectra of various PhTS gels.

Probe	T <sup>2</sup> /%	T <sup>3</sup> /%	Q <sup>2</sup> /%	Q <sup>3</sup> /%	Q <sup>4</sup> /%	Σ T /%	Σ Q /%
Gel 112	6	3	1	51	39	9	91
Gel 113	8	9	1	41	41	17	83
Gel 114	17	11	3	38	31	28	72
Gel 185	15	11	6	30	38	26	74

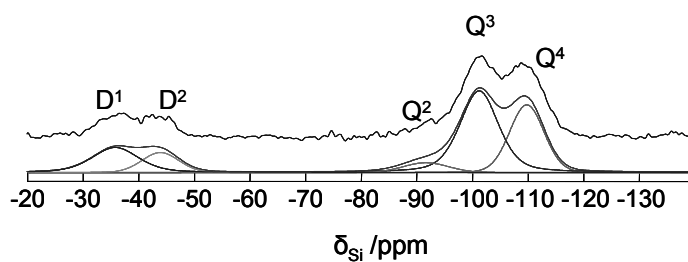


**Figure A2.5:**  $^{29}\text{Si}$  MAS NMR spectrum of hybrid DPhDS Gel 188.

**Table A2.4:** Peak area derived for deconvoluted peaks of the  $^{29}\text{Si}$  MAS spectrum of Gel 188.

Probe	D <sup>1</sup> /%	D <sup>2</sup> /%	Q <sup>2</sup> /%	Q <sup>3</sup> /%	Q <sup>4</sup> /%	Σ D /%	Σ Q /%
Gel 188	15	9	6	42	28	24	76

## 9.4 $^{29}\text{Si}$ MAS NMR spectra of various SD hybrid gels

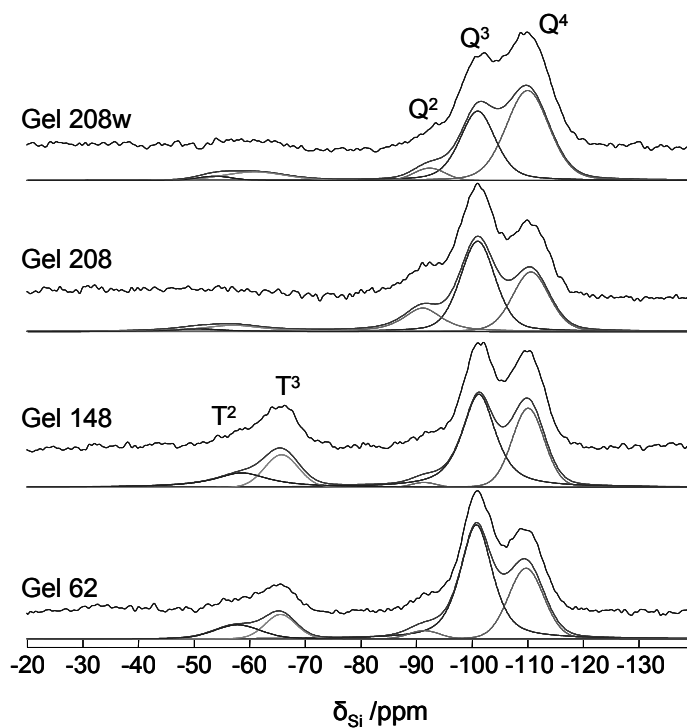


**Figure A2.6:**  $^{29}\text{Si}$  MAS NMR spectra of spray dried hybrid ATS gels.

**Table A2.5:** Peak area derived for deconvoluted peaks of the  $^{29}\text{Si}$  MAS spectra of hybrid ATS gels.

Probe	T <sup>2</sup> /%	T <sup>3</sup> /%	Q <sup>2</sup> /%	Q <sup>3</sup> /%	Q <sup>4</sup> /%	Σ T /%	Σ Q /%
Gel 208w	2	7	5	35	51	9	91
Gel 208	2	7	15	46	30	9	91
Gel 148	12	12	2	45	29	24	76
Gel 62	8	9	3	51	29	17	83

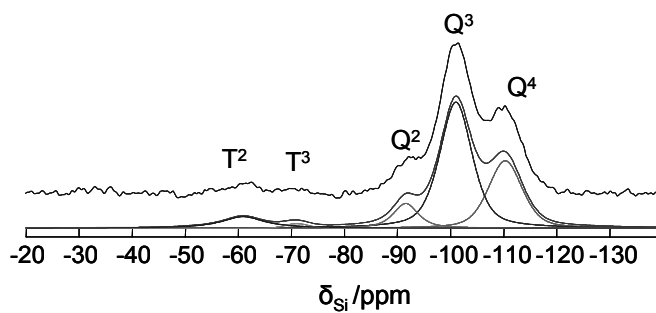


**Figure A2.7:**  $^{29}\text{Si}$  MAS NMR spectrum of spray dried hybrid BTS Gel 90.

**Table A2.6:** Peak area derived for deconvoluted peaks of the  $^{29}\text{Si}$  MAS spectrum of hybrid BTS Gel 90.

Probe	T <sup>2</sup> /%	T <sup>3</sup> /%	Q <sup>2</sup> /%	Q <sup>3</sup> /%	Q <sup>4</sup> /%	Σ T /%	Σ Q /%
Gel 90	8	1	9	53	29	9	91

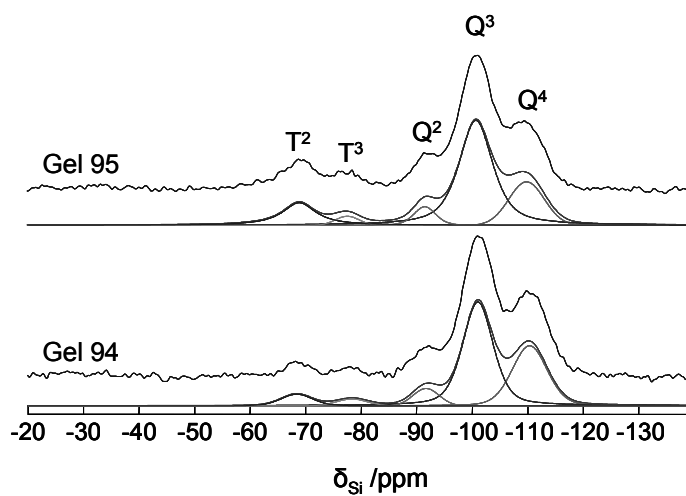


**Figure A2.8:**  $^{29}\text{Si}$  MAS NMR spectra of spray dried PhTS gels.



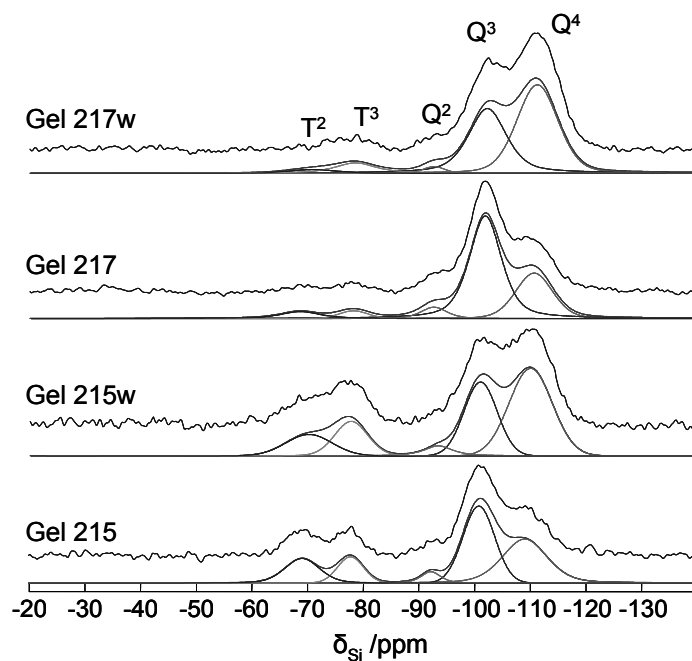


**Figure A2.9:**  $^{29}\text{Si}$  MAS NMR spectra of spray dried hybrid PhTS gels before and after drug extraction.

**Table A2.7:** Peak area derived for deconvoluted peaks of the  $^{29}\text{Si}$  MAS spectra of hybrid PhTS gels.

Probe	T <sup>2</sup> /%	T <sup>3</sup> /%	Q <sup>2</sup> /%	Q <sup>3</sup> /%	Q <sup>4</sup> /%	Σ T /%	Σ Q /%
Gel 94	6	3	6	53	32	9	91
Gel 95	14	3	6	57	20	17	83
Gel 215	14	11	4	37	34	25	75
Gel 215w	11	14	4	28	43	25	75
Gel 217	6	3	5	59	27	9	91
Gel 217w	2	7	2	38	51	9	91

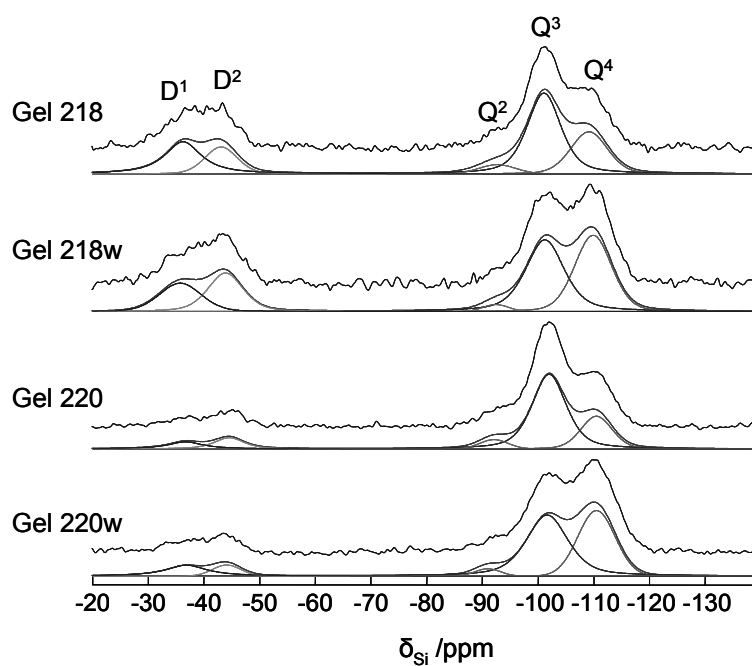


**Figure A2.10:**  $^{29}\text{Si}$  MAS NMR spectra of spray dried hybrid DPhDS gels before and after drug extraction.

**Table A2.8:** Peak area derived for deconvoluted peaks of the  $^{29}\text{Si}$  MAS spectra of hybrid DPhDS gels.

Probe	D <sup>1</sup> /%	D <sup>2</sup> /%	Q <sup>2</sup> /%	Q <sup>3</sup> /%	Q <sup>4</sup> /%	Σ D /%	Σ Q /%
Gel 218	20	12	5	42	21	32	68
Gel 218w	13	17	2	35	33	30	70
Gel 220	6	8	6	59	21	14	86
Gel 220w	9	5	3	46	37	14	86

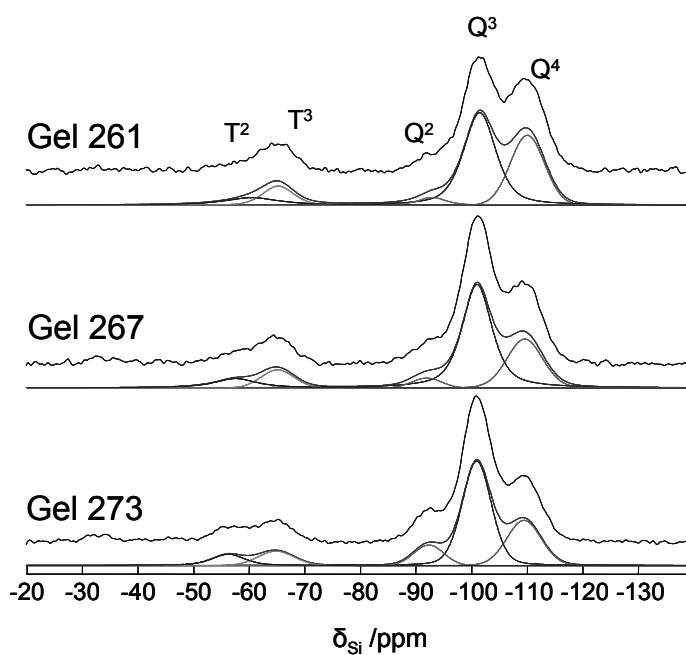


**Figure A2.11:**  $^{29}\text{Si}$  MAS NMR spectra of spray dried hybrid ATS gels synthesized with different sol stirring time.

**Table A2.9:** Peak area derived for deconvoluted peaks of the  $^{29}\text{Si}$  MAS spectra of hybrid ATS gels.

Probe	T <sup>2</sup> /%	T <sup>3</sup> /%	Q <sup>2</sup> /%	Q <sup>3</sup> /%	Q <sup>4</sup> /%	Σ T /%	Σ Q /%
Gel 261	7	9	4	48	32	16	84
Gel 267	8	8	4	54	26	16	84
Gel 273	7	8	10	50	25	15	85

## 9.5 $^{13}\text{C}\{^1\text{H}\}$ CPMAS NMR spectra of various hybrid EISA gels

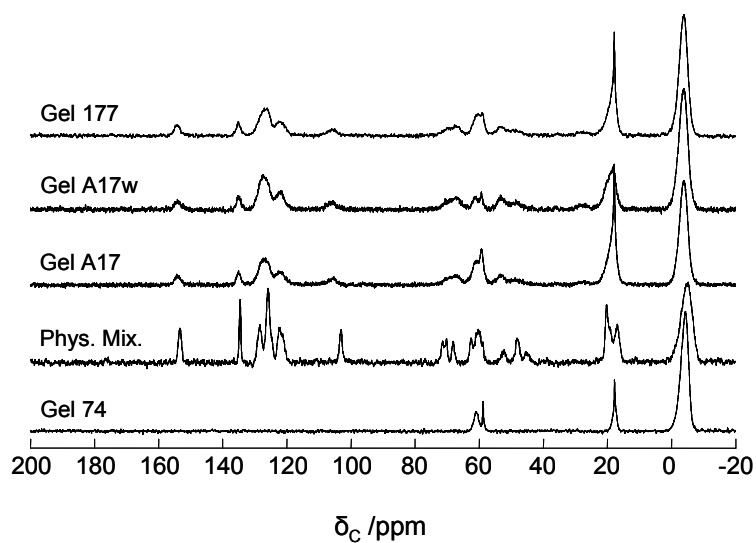


**Figure A3.1:**  $^{13}\text{C}\{^1\text{H}\}$  CPMAS NMR spectra of various hybrid MTS gels.

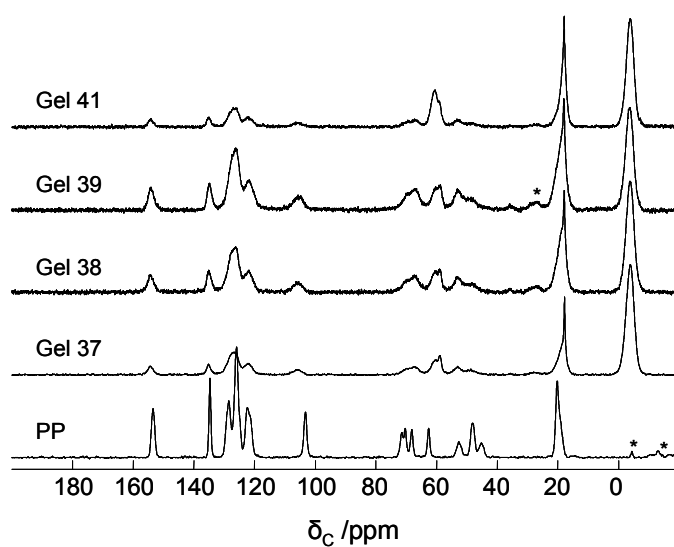


**Figure A3.2:**  $^{13}\text{C}\{^1\text{H}\}$  CPMAS NMR spectra of various hybrid MTS gels and PP.

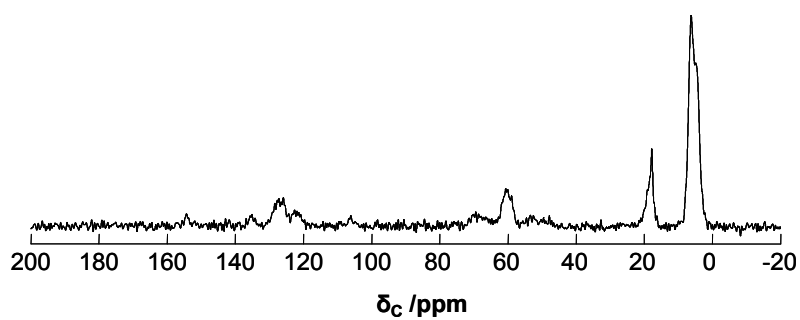


**Figure A3.3:**  $^{13}\text{C}\{^1\text{H}\}$  CPMAS NMR spectrum of ETS Gel 81.

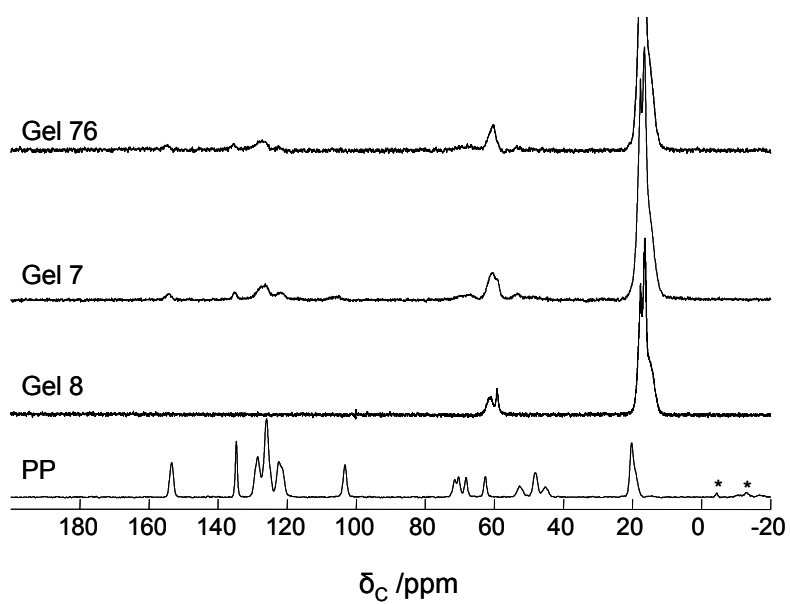


**Figure A3.4:**  $^{13}\text{C}\{^1\text{H}\}$  CPMAS NMR spectra of various hybrid PTS gels and PP.

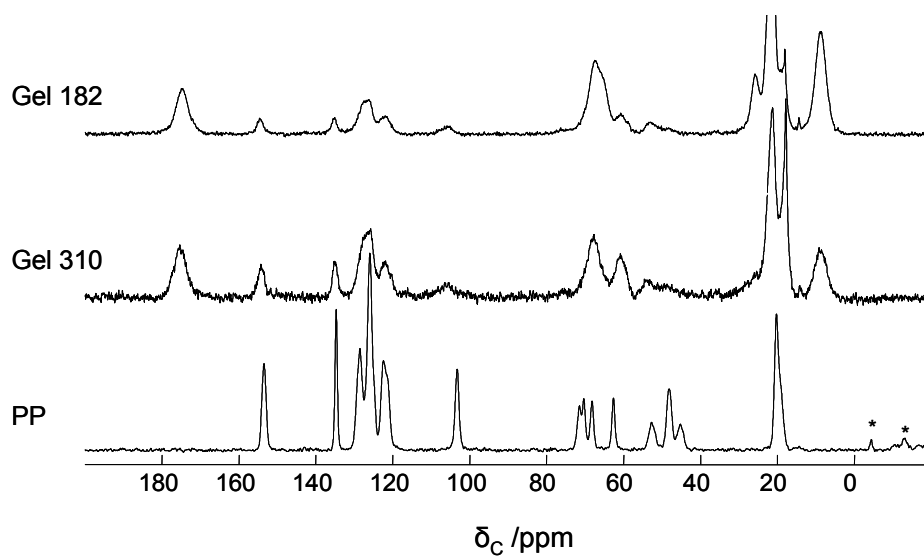


**Figure A3.5:**  $^{13}\text{C}\{^1\text{H}\}$  CPMAS NMR spectra of various hybrid ATS gels.

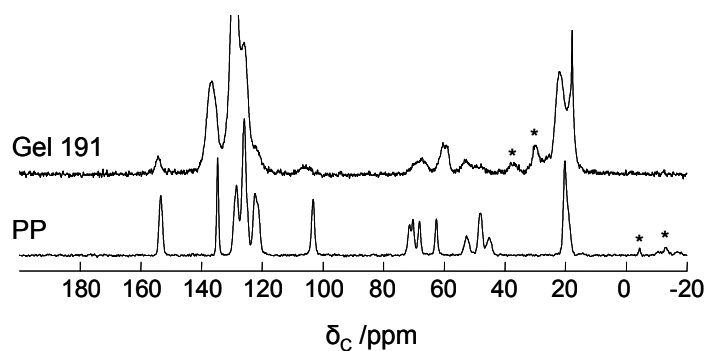


**Figure A3.6:**  $^{13}\text{C}\{^1\text{H}\}$  CPMAS NMR spectra of BTS Gel 191.

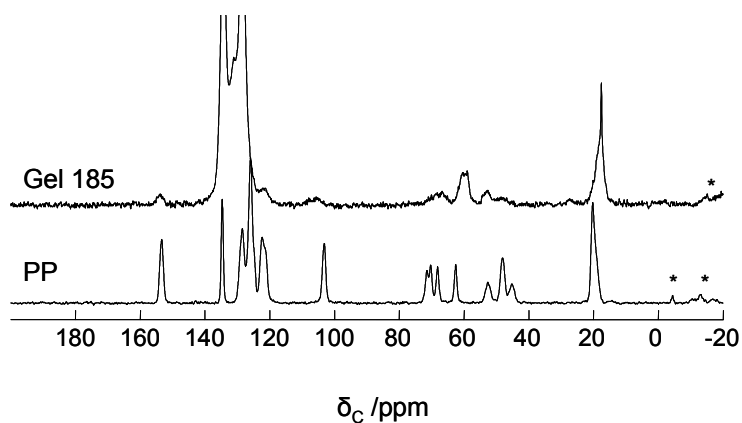


**Figure A3.7:**  $^{13}\text{C}\{^1\text{H}\}$  CPMAS NMR spectra of PhTS Gel 185.

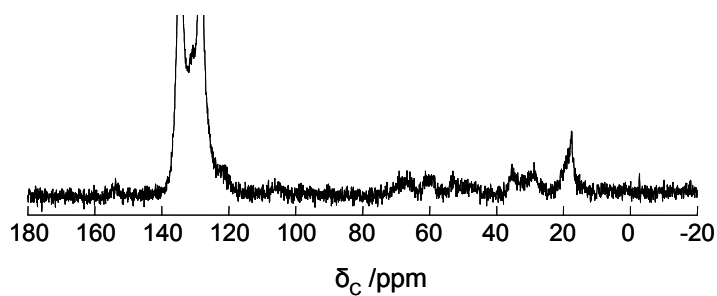


**Figure A3.8:**  $^{13}\text{C}\{^1\text{H}\}$  CPMAS NMR spectra of DPhDS Gel 188.

## 9.6 $^{13}\text{C}\{^1\text{H}\}$ CPMAS NMR spectra of various hybrid SD gels

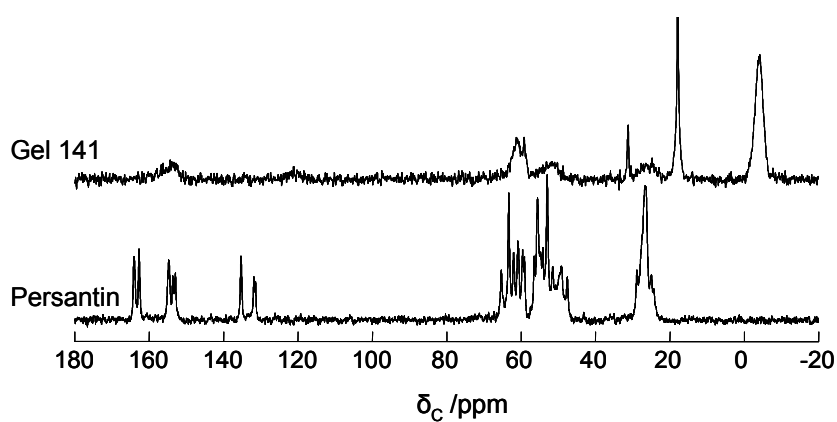


**Figure A3.9:**  $^{13}\text{C}\{^1\text{H}\}$  CPMAS NMR spectra of spray dried hybrid MTS gel 141 and PS.

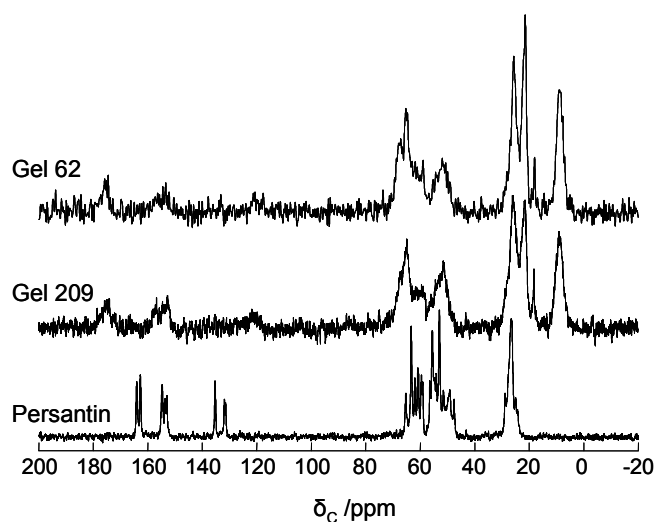


**Figure A3.10:**  $^{13}\text{C}\{^1\text{H}\}$  CPMAS NMR spectra of spray dried hybrid ATS gels 62 and 209.

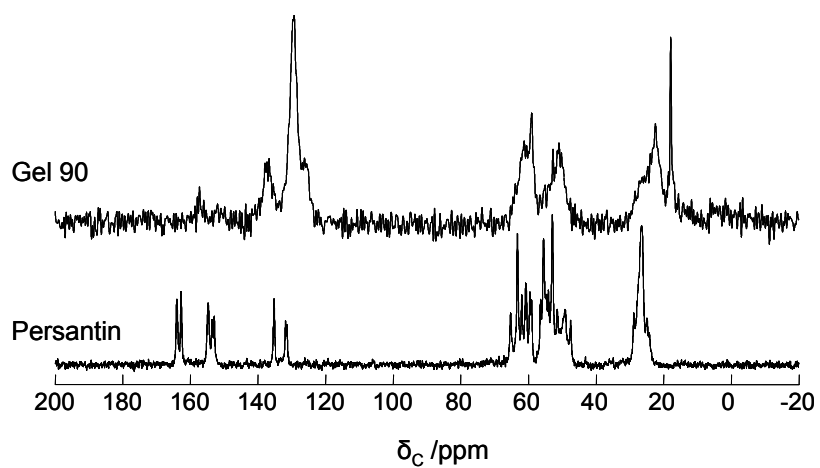


**Figure A3.11:**  $^1\text{H}-^{13}\text{C}$  CPMAS NMR spectra of BTS Gel 90.

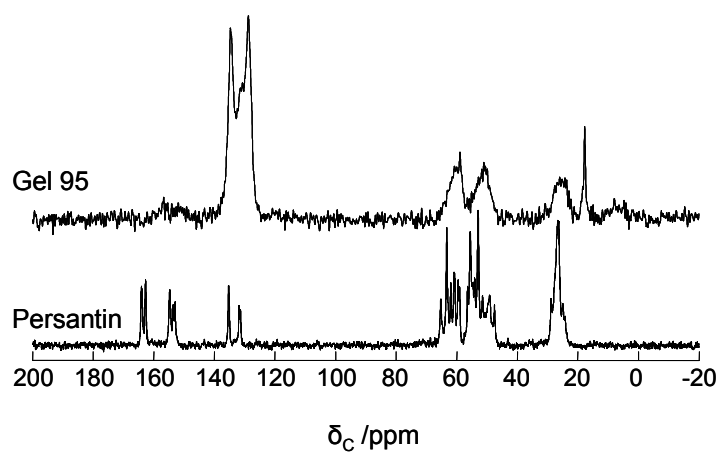


**Figure A3.12:**  $^{13}\text{C}$  CPMAS NMR spectra of PhTS Gel 95 and Persantin.



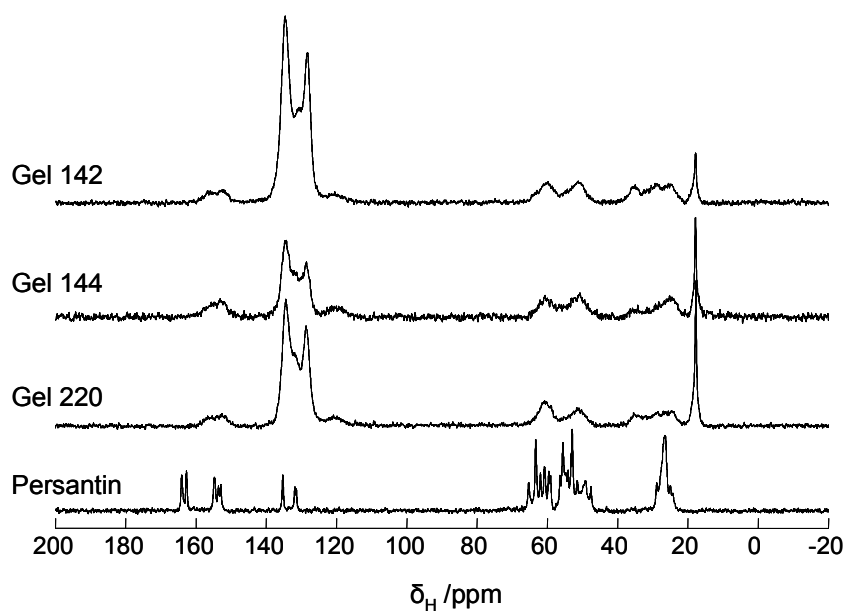


**Figure A3.13:**  $^{13}\text{C}\{^1\text{H}\}$  CPMAS NMR spectra of DPhDS gels and PS.

### Spray dried gels with PP

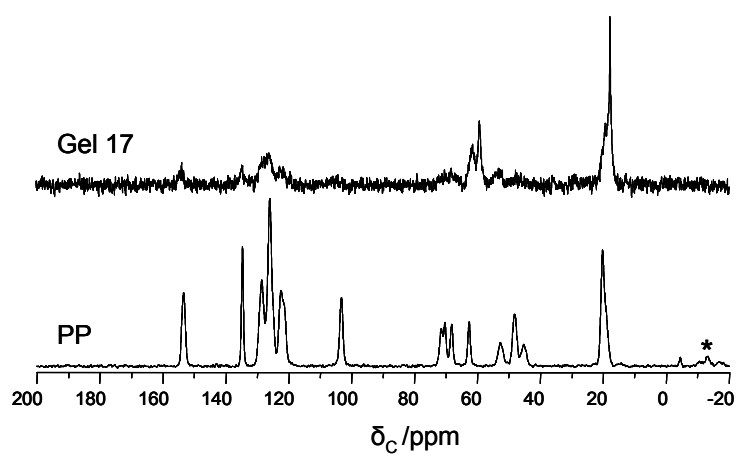


**Figure A3.14:**  $^{13}\text{C}\{^1\text{H}\}$  CPMAS NMR spectra of TEOS Gel 17.

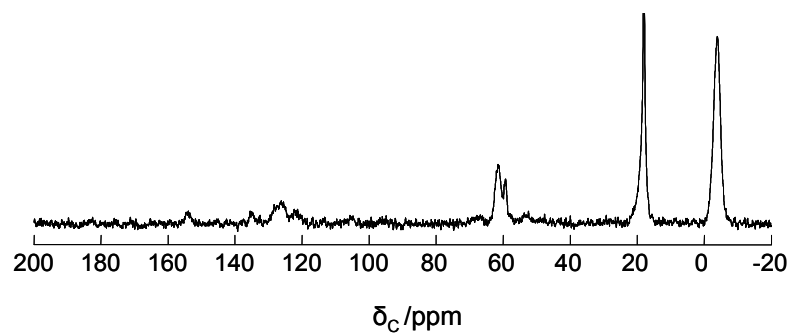


**Figure A3.15:**  $^{13}\text{C}\{^1\text{H}\}$  CPMAS NMR spectrum of spray dried hybrid MTS Gel 315.

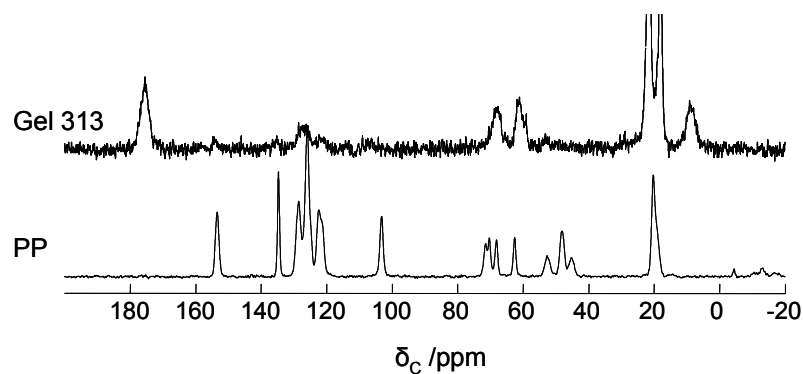


**Figure A3.16:**  $^{13}\text{C}\{^1\text{H}\}$  CPMAS NMR spectrum of spray dried hybrid ATS gel 313.

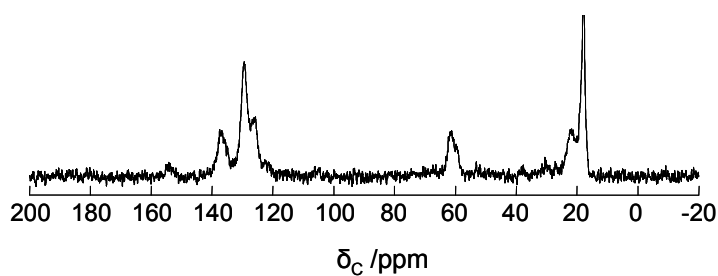


**Figure A3.17:**  $^{13}\text{C}\{^1\text{H}\}$  CPMAS NMR spectrum of BTS Gel 317.

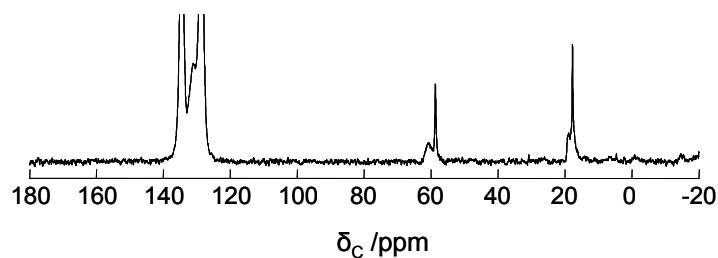


**Figure A3.18:**  $^{13}\text{C}\{^1\text{H}\}$  CPMAS NMR spectra of PhTS Gel 322.

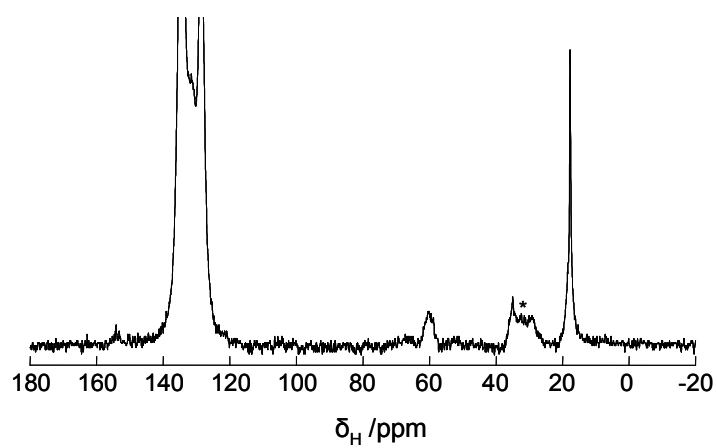


*Figure A3.19:*  $^{13}\text{C}\{^1\text{H}\}$  CPMAS NMR spectra of DPhDS Gel 258.

## 9.7 N<sub>2</sub> sorption isotherms of various aromatic hybrid EISA gels

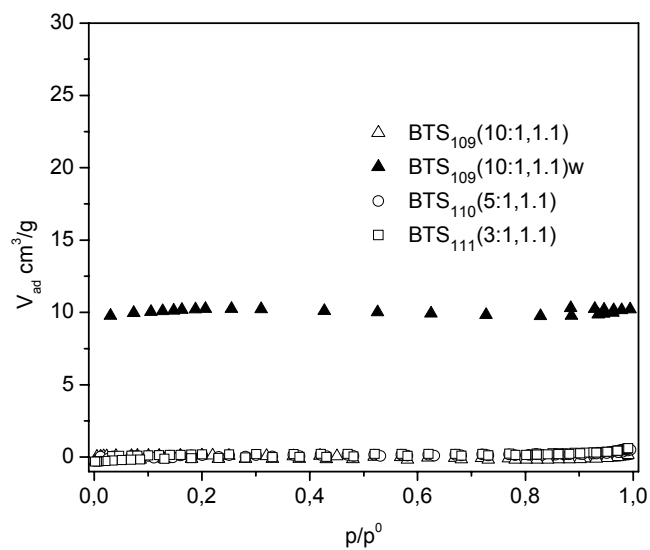


*Figure A4.1: N<sub>2</sub> sorption isotherms of various hybrid BTS gels.*

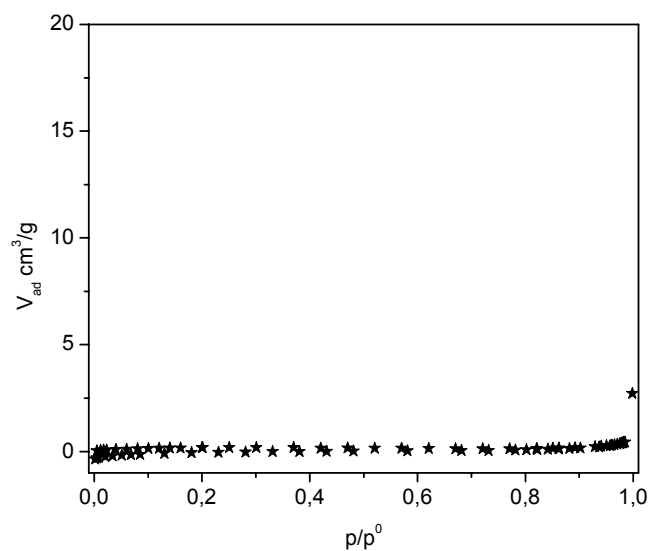


*Figure A4.2: N<sub>2</sub> sorption isotherms of hybrid PhTS Gel 112.*

---

## 10. Bibliography

---

- 1 (a) Ebelmen, M. *Ann. Chimie Phys.* **1846**, *16*, 129. (b) Ebelmen, M. C. R. *Acad. Sci.* **1847**, *25*, 854. (c) Graham, T. *J. Chem. Soc.* **1864**, *17*, 318. (d) Hench, L. L.; West, J. K. *Chem. Rev.* **1990**, *90*, 33.
- 2 (a) Roy, D.M.; Roy, R. *Am. Mineral.* **1954**, *39*, 957. (b) Roy, R. *J. Am. Ceram. Soc.* **1956**, *39*, 145. (c) Roy, R. *J. Am. Ceram. Soc.* **1969**, *52*, 344.
- 3 Iler, R. K. *The Chemistry of silica*; Wiley: New York, **1955**.
- 4 Stober, W.; Fink, A.; Bohn, E. *J. Colloid Interface Sci.* **1968**, *26*, 62.
- 5 (a) Mackenzie, J. D. *J. Non-Cryst. Solids* **1982**, *41*, 1. (b) Mackenzie, J. D. *In Ultrasonic Processing of Ceramics Glasses and Composites*; Wiley: New York; **1984**.
- 6 Kistler, S. S. *Nature* **1931**, *127*, 742.
- 7 Fricke, J., Ed. *Aerogels*; Springer Proceedings in Physics; Springer-Verlag: Heidelberg, **1986**; Vol.6.
- 8 (a) Phalippou, J.; Prassas, M.; Zarzycki, J. *J Non-Cryst. Solids* **1982**, *48*, 17. (b) Phalippou, J.; Prassas, M.; Zarzycki, J. *Int. Conf. Glasses*, 13th, Hamburg, Germany, **1985**.
- 9 Diaz-Garcia, M. E.; Laino, R. B. *Microchim. Acta* **2005**, *149*, 19.
- 10 Polyakov, M. W. *Zhur. Fiz. Khim.* **1931**, *2*, 799.
- 11 Pauling, L.; Campbell, D. H. *J Exper. Med.* **1942**, *76*, 211.
- 12 Komiyama, M.; Takeuchi, T.; Mukawa, T.; Asanuma, H. *Molecular Imprinting. From Fundamental to Applications*. Weily- VCH Verlag BmbH&Co. KGaA, Weinheim, 2002.
- 13 (a) Davis, M. E. *Nature* **2002**, *417*, 813. (b) Davis, M. E. *Nature* **1993**, *364*, 391. (c) Schaefer, D. W. *MRS Bull.* **1994**, *19*, 14. (c) Behrens, P. *Adv. Mater.* **1993**, *5*, 127.
- 14 Hoffmann, F.; Cornelius, M.; Morell, J.; Fröba, M. *Angew. Chem. Int. Ed.* **2006**, *45*, 3216.
- 15 Ozin, G. A.; Gil, C. *Chem. Rev.* **1989**, *89*, 1749.
- 16 Stucky, G. D.; MacDougall, J. E. *Science*, **1990**, *247*, 669.
- 17 Cox, S. D.; Eier, T. E.; Stucky, G. D. *Chem. Mater.* **1990**, *2*, 609.
- 18 Bein, T.; Enzel, P. *Angew. Chem. Int. Ed. Engl.* **1989**, *28*, 1692.
- 19 Raman, N. K.; Anderson, M. T; Brinker, J. C. *Chem. Mater.* **1996**, *8*, 1682.
- 20 Jokinen, M.; Györvary, E.; Rosenholm, J. B. *Coll. Surf. A: Physicochem. Engng. Asp.* **1998**, *141*, 205.
- 21 Brinker, J. C.; Lu, Y; Sellinger, A.; Fan, H. *Adv. Mater.* **1999**, *11*, 579.
- 22 Unger, K.; Rupperecht, H.; Valentin, B.; Kircher, W. *Drug Dev. Ind. Pharm.* **1983**, *9*, 69.

- 23 (a) Klein, C. P. A. T.; Li, P.; Blicek-hogervorst, J. M. A.; de Groot, K. *Biomaterials* **1995**, *16*, 715. (b) Stoor, P.; Söderling, E.; Grenman, R. *J. Biomed. Mater. Res.* **1999**, *48*, 869.
- 24 (a) Böttcher, H.; Slowik, P.; Suss, W. *J. Sol-Gel Sci. Techn.* **1998**, *13*, 277. (b) Ahola, M. E.; Sailyoja, S.; Raitavuo, M. H.; Vaahtio, M. M.; Salonen, J. I.; Yli-Urpo, A. U. O. *Biomaterials*, **2001**, *22*, 2163. (c) Falaize, S.; Radin, S.; Ducheyne, P. *J. Am. Ceram. Soc.*, **1999**, *82*, 969. (d) Jokinen, M.; Györvary, E.; Rosenholm, J. B. *Coll. Surf. A: Physicochem. Eng. Asp.* **1998**, *141*, 205. (e) Kortesuso, P. *Ph.D. Thesis*, University of Turku, Turku, Finland **2001**.
- 25 Avnir, D. *Acc. Chem. Res.* **1995**, *28*, 328 and references therein.
- 26 Kodas, T. T. *Adv. Mater.* **1989**, *6*, 180.
- 27 Kortesuso, P.; Ahola, M.; Karlson, S.; Kangasniemi, I.; Kiesvaara, J.; Yli-Urpo, A. *Biomed. Mater. Res.* **1999**, *44*, 162.
- 28 Kortesuso, P.; Ahola, M.; Kangas, M.; Yli-Urpo, A.; Kiesvaara, J.; Marvola, M. *Ind. J. Pharm.* **2001**, *221*, 107.
- 29 Kortesuso, P.; Ahola, M.; Kangas, M.; Kangasniemi, I.; Yli-Urpo, A.; Kiesvaara, J. *Ind. J. Pharm.* **2000**, *200*, 223.
- 30 Xiong, Y.; Kodas, T. T. *J. Aerosol Sci.* **1993**, *24*, 893.
- 31 Re, M-I. *Drying Technology*, **2006**, *24*, 433.
- 32 Fernandes, C. M.; Teresa, V. M.; Veiga, B. F. *Eur. J. Pharm. Sci.* **2002**, *15*, 79.
- 33 Cerchiara, T.; Luppi, B.; Bigucci, F.; Zecchi, V. *Int. J. Pharm.* **2003**, *258*, 209.
- 34 (a) Koester, L. S.; Xavier, C. R.; Mayorga, P.; Bassani, V. L. *Eur. J. Pharm. Biopharm.* **2003**, *55(1)*, 85. (b) Koester, L. S. *Int. J. Pharm.* **2004**, *22(2-3)*, 201.
- 35 Serajuddin, A. T. M. *J. Pharm. Sci.* **1999**, *88*, 1050
- 36 (a) Kortesuso, P.; Ahola, M.; Kangas, M.; Kangasniemi, I.; Yli-Urpo, A.; Kiesvaara, J. *Ind. J. Pharm.* **2000**, *200*, 223. (b) Kortesuso, P.; Ahola, M.; Kangas, M.; Jokinen, M.; Leino, T.; Vuorilehto, L.; Laakso, S.; Kiesvaara, J.; Yli-Urpo, A.; Marvola, M. *Biomaterials* **2002**, *23*, 2795.
- 37 Vanbever, R.; Mintzes, J. D.; Wang, J.; Nice, J.; Chen, D.; Batycky, R.; Langer, R.; Edwards, D. A. *Pharm. Res.* **1999**, *16*, 1735.
- 38 (a) Takeuchi, H.; Nagira, S.; Yamamoto, H.; Kawashima, Y. *Int. J. Pharm.* **2005**, *293*, 155. (b) Takeuchi, H.; Nagira, S.; Yamamoto, H.; Kawashima, Y. *Powder Technol.* **2004**, *141*, 187.
- 39 Palmieri, G. F.; Bonacucina, G.; Di Martino, P.; Martelli, S. *Drug Dev. Ind. Pharm.* **2001**, *27(3)*, 195.
- 40 Yilmaz, E.; Bengisu, M. *J. Biomed. Mater. Res. Part B: Appl. Biomater.* **2006**, *77B*, 149.

- 41 Czuryzskiewicz, T.; Areva, S.; Honkanen, M.; Linden, M. *Coll. Surf. A: Physicochem. Eng. Asp.* **2005**, *254*, 69.
- 42 (a) Hadinoto, K.; Phanapavudhikul, P.; Kewu, Z.; Tan, R. B. H. *Ind. Eng. Chem. Res.* **2006**, *45*, 3697. (b) Martinac, A.; Filipovic-Grcic, J.; Barbaric, M.; Zorc, B.; Voinovich, D.; Jalsenjak, I. *Eur. J. Pharm. Sci.* **2002**, *17*, 207.
- 43 Alonso, B.; Clinard, C.; Durand, D.; Veron, E.; Massiot, D. *Chem. Comm.* **2005**, 1746.
- 44 Lind, A.; von Hihenesche, C. F.; Smatt, J-H.; Linden, M.; Unger, K. K. *Micropor. Mesopor. Mater.* **2003**, *66*, 219.
- 45 Uhrich K. E.; Cannizzaro, S. M.; Langer, R. S.; Shakesheff, K. M. *Chem. Rev.* **1999**, *99*, 3181.
- 46 Lunt, O. R., *J. Agric. Food. Chem.* **1971**, *19*, 797.
- 47 (a) Folkman, J.; Long, D, M. *J. Surg. Res.* **1964**, *4*, 139. (b) Higuchi, T.; Desai, S. J. Simonelli, A. P.; Higuchi, W. I. *J. Pharm. Sci.* **1965**, *54*, 1459.
- 48 Langer, R.; Folkman, J. *Nature* **1976**, *263*, 797.
- 49 Park, H.; Park, K., *Pharm. Res.* **1996**, *13*, 12.
- 50 Lubach, J. W.; Padden, B. E.; Winslow, S. L.; Salsbury, J. S.; Masters, D. B.; Topp, E. M.; Munson, E. J. *Anal. Bioanal. Chem.* **2004**, *378*, 1504.
- 51 Langer, R.; Peppas, N. *JMS-Rev.Macromol. chem. phys.* **1983**, *C23(1)*, 61
- 52 Vallet-Regi, M.; Rámila, A.; del Real, R. P.; Pérez-Pariente, J. *Chem. Mater.* **2001**, *13*, 308.
- 53 Bringley, J. F.; Liebert, N. B. *J. Dispersion Sci. Technol.* **2003**, *24*, 589.
- 54 Chang, J. H.; Shim, C. H.; Kim, B. J.; Shin, Y.; Exarhos, G. J.; Kim, K. J. *Adv. Mater.* **2005**, *17*, 634.
- 55 (a) Böttcher, H.; Slowik, P.; Suss, W. *J. Sol-Gel Sci. Techn.* **1998**, *13*, 277. (b) Santos, E. M.; Radin, D.; Ducheyne, P. *Biomaterials*, **1999**, *20*, 1695. (c) Badjic, J. D.; Kostic, N. M. *J Phys. Chem. B* **2000**, *104*, 11081. (d) Kortesuso, P.; Ahola, M.; Kangas, M.; Jokinen, M.; Leino, T.; Vuorilehto, L.; Laakso, S.; Kiesvaara, J.; Yli-Urpo, A.; Kiesvaara, J.; Marvola, M. *J. Controlled release* **2001**, *76*, 227.
- 56 (a) Periera, M. M.; Hench, L. L. *J. Sol-Gel Sci. Tech.* **1996**, *7*, 59. (b) Li, P.; Ohtsuki, C.; Kokubo, T.; Nakanishi, K.; Soga, N.; Nakamura, T.; Yamamuro, T. *J. Am. Chem. Soc.* **1992**, *75*, 2094. (c) Peltola, T.; *Ph.D. Thesis*, University of Turku, Turku, Finland **2000**.
- 57 (a) Acros, D.; Ragel, C. V.; Vallet-Regi, M. *Biomaterials*, **2001**, *22*, 701. (b) Guevara-Fernandez, L.; Ragel, C. V.; Vallet-Regi, M. *Biomaterial*, **2003**, *24*, 4037.
- 58 Bögershausen, A.; Pas, S. J.; Hill, A. J.; Koller, H. *Chem. Mater.* **2006**, *18*, 664.
- 59 Kortesuso, P.; Ahola, M.; Karlsson, S.; Kangasniemi, I.; Yli-Urpo, A.; Kiesvaara, J. *Biomaterials* **2000**, *21*, 193.

- 60 (a) Sieminska, L.; Zerda, T. W. *J. Phys. Chem.* **1996**, *100*, 4591. (b) Nicoll, S. B.; Radin, S.; Santos, E. M.; Tuan, R. S.; Ducheyne, P. *Biomaterials* **1997**, *18*, 853. (c) Böttcher, H.; Slowik, P.; Suss, W. *J. Sol-Gel Sci. Techn.* **1998**, *13*, 277. (d) Falaize, S.; Radin, S.; Ducheyne, P. *J. Am. Ceram. Soc.* **1999**, *82*, 969. (e) Santos, E. M.; Radin, S.; Ducheyne, P. *Biomaterials* **1999**, *20*, 1695. (f) Ahola, M.; Korteso, P.; Kangasniemi, I.; Kiesvaara, J.; Yli-Urpo, A. *Ind. J. Pharm.* **2000**, *195*, 219. (g) Ahola, M.; Säilynoja, E.; Raitavuo, M.; Salonen, J.; Yli-Urpo, A. *Biomaterials* **2001**, *22*, 2163.
- 61 (a) Sieminska, L.; Ferguson, M.; Zerda, T. W.; Cough, E. *J. Sol-Gel Sci. Tehn.* **1997**, *8*, 1105. (b) Ahola, M.; Korteso, P.; Kangasniemi, I.; Kiesvaara, J.; Yli-Urpo, A. *Drug Dev. Ind. Pharm.* **1999a**, *25*, 955. (c) Otsuka, M.; Tokumitsu, K.; Matsuda, Y. *J. Control. Release* **2000**, *67*, 369.
- 62 Begu, S.; Girod, S.; Lerner, D. A.; Jardiller, N.; Tourne-Pereilh, C.; Devoisselle, J. M. *J. Mater. Chem.* **2004**, *14*, 1316.
- 63 Smirnova, I.; Suttiruengwong, S.; Arlt, W. *KONA*, **2005**, No.23, 86.
- 64 Shea, K. J.; Loy, D. A. *Acc. Chem. Res.* **2001**, *34*(9), 707.
- 65 (a) Ellsworth, M. W.; Gin, D. L. *Polym. News* **1999**, *24*, 331. (b) Judeinstein, P.; Sanchez, C. *J. Mater. Chem.* **1996**, *6*, 511. (c) Gomez-Romero P. *Adv. Mater.* **2001**, *13*, 163.
- 66 (a) Loy, D. A.; Shea, K. J. *Chem. Rev.* **1995**, *95*, 1431. (b) Shea, K. J.; Loy, D. A.; Webster, O. *J. Am. Chem. Soc.* **1992**, *114*, 6700.
- 67 Sanchez, C.; Lebeau, B.; Ribot, F.; In, M. *J. Sol-Gel Sci. Tech.* **2000**, *19*, 31.
- 68 Caravatti, P.; Braunschweiler, L.; Ernst, R. R. *Chem. Phys. Lett.* **1983**, *100*, 305.
- 69 Trebosc, J.; Wiench, J. W.; Huh, S.; Lin, V. S. -Y.; Pruski, M. *J. Am. Chem. Soc.* **2005**, *127*, 7587.
- 70 Vega, A. J.; *J. Am. Chem. Soc.* **1988**, *110*, 1049.
- 71 Fyfe, C. A.; Zhang, Y.; Aroca, P. *J. Am. Chem. Soc.* **1992**, *114*, 3252.
- 72 Peeters, M. P. J., Wakelkamp, W. J. J. & Kentgens, A. P. M. *J. Non-Cryst. Solids*, **1995**, *189*, 77.
- 73 Babonneau, F.; Gualandris, V.; Maquet, J.; Massiot, D.; Janicke, M. T.; Chmelka, B. F. *J. Sol-Gel Sci. Tech.* **2000**, *19*, 113.
- 74 (a) van Rossum, B. J.; Förster, H.; de Groot, H. J. M. *J. Magn. Reson.* **1997**, *124*, 516. (b) Vinogradov, E.; Madhu, P. K.; Vega, S. *Chem. phys. Lett.* **2002**, *354*, 193.
- 75 (a) Fyfe, C. A.; Aroca, P. P.; Zhang, Y. *Bull. Magn. Reson.* **1993**, *15*, 195. (b) Rataboul, F.; Baudouin, A.; Thieuleux, C.; Veyre, L.; Copéret, C.; Thivolle-Cazat, J.; Basset, J.-M.; Lesage, A.; Emsley, L. *J. Am. Chem. Soc.* **2004**, *126*, 12541.



- 
- 76 Janicke, M. T.; Landry, C. C.; Christiansen, S. C.; Kumar, D.; Stucky, G. D.; Chmelka, B. F. *J. Am. Chem. Soc.* **1998**, *120*, 6940.
- 77 (a) Hou, S. S.; Beyer, F. L.; Schmidt-Rohr, K. *Solid State Nucl. Magn. Reson.* **2002**, *22*, 110. (b) Brus, J.; Spirkova, M.; Hlavata, D.; Strachota, A. *Macromolecules*, **2004**, *37*, 1346.
- 78 (a) van Rossum, B. J.; de Groot, C. P.; Ladizhansky, V.; Vega, S.; de Groot, H. J. M. *J. Am. Chem. Soc.* **2000**, *122*, 3465. (b) Ladizhansky, V.; Vega, S. *J. Chem. Phys.* **2000**, *112*, 7158.
- 79 Luliucci, R.; Taylor, C.; Hollis, W. K. *Magn. Reson. Chem.* **2006**, *44*, 375.
- 80 Trebosc, J.; Wiench, J. W.; Huh, S.; Lin, V. S.-Y.; Pruski, M. *J. Am. Chem. Soc.* **2005**, *127*, 3057.
- 81 (a) Geppi, M.; Guccione, S.; Mollica, G.; Pignatello, R.; Veracini, C. A. *Pharm. Res.* **2005**, *22*, 1544. (b) Mollica, G.; Geppi, M.; Pignatello, R.; Veracini, C. A. *Pharm. Res.* **2006**, *23*, 2129.
- 82 Wheeler, K. E.; Nocek, J. M.; Hoffman, B. M.; *J. Am. Chem. Soc.* **2006**, *128*, 14782.
- 83 Wilhelm, M.; Feng, H.; Tracht, U.; Spiess, H. W. *J. Mag. Reson.* **1998**, *134*, 255.
- 84 Massiot, D.; Alonso, B.; Fayon, F.; Fredoueil, F.; Bujoli, B. *Solid State Sci.* **2001**, *3*, 11.
- 85 Bose, A. B.; Gangoda, M.; Jaroniec, M.; Gilpin, R. K.; Bose, R. N. *Surf. Sci.* **2006**, *600*, 143.
- 86 Baccile, N.; Maquet, J.; Bobanneau, F.; *C. R. Chimie* **2006**, *9*, 478.
- 87 Sozzani, P.; Bracco, S.; Comotti, A.; Mauri, M.; Simonutti, R.; Valsesia, P. *Chem. Comm.*, **2006**, 1921.
- 88 (a) Bielecki, A.; Burum, D. P.; Rice, D. M.; Karasz, F. E. *Macromolecules*, **1994**, *27*, 2211. (b) Mirau, P. A.; White, J. L.; *Macromolecules*, **1994**, *32*, S23. (c) Porbeni, F. E.; Shin, I. D.; Shuai, X.; Wang, X.; White, J. I.; Jia, X.; Tonelli, A. E. *J. Polym. Sci. Part B : Polym. Phys* **2005**, *43*, 2086.
- 89 Epping, J. D.; Chmelka, B. F.; *Current Opinion in Colloid & Interface Science* **2006**, *11*, 81.
- 90 Wiench, J. W.; Tricot, G.; Delevoye, L.; Trebosc, J.; Frye, J.; Mantagne, L.; Amoureux, J-P.; Pruski, M. *Phys. Chem. Chem. Phys.* **2006**, *8*, 144.
- 91 Brinker, C. J.; Scherer, G. W., *The physics and chemistry of sol-gel processing*. Academic press Inc, San Diego, CA, USA, **1990**.
- 92 Iler, R. K. *The chemistry of silica*. John Wiley & sons, New York, **1979**.
- 93 Broadhead, J.; Edmond, S. K. R.; Rhodes, C. T. *Drug Dev. Ind. Pharm.* **1992**, *18*, 1169.
- 94 (a) Wagenaar, B. W.; Müller, B. W. *Biomaterials* **1994**, *15*, 49.; (b) Clarke, N.; Connor, K.; Ramtoola, Z. *Drug Dev. Ind. Pharm.* **1998**, *24*, 703.

- 95 Ro, J. C.; Chung, I. J. *J. Non-Cryst. Solids* **1991**, *130*, 8.
- 96 Ülkü, S.; Balköse, D.; Baltacıoglu, H. *Colloid Polym. Sci.* **1993**, *271*, 709.
- 97 (a) Rouquerol, F., Rouquerol, J. & Sing, K. *Adsorption by Powders and Porous Solids* Academic Press, San Diego, **1999**. (b) Webb, P. A.; Orr, C.; *Analytical methods in fine particle technology*, Micromeritics Instrument Corporation, Norcross, GA, USA, **1997**.
- 98 Sing, K. S. W. Everett, D. H.; Haul, R. A. W.; Moscou, L.; Pierotti, R. A.; Rouquerol, J.; Siemieniewska, T. *Pure and Applied Chemistry* **1985**, *57*, 603-19. (Recommendations 1984).
- 99 Brunauer, S.; Emmett, P. H.; Teller, E. *Journal of the American Chemical Society* **1938**, *60*, 309.
- 100 Webb, P. A.; Orr, C.; *Analytical methods in fine particle technology*, Micromeritics Instrument Corporation, Norcross, GA, USA, **1997**.
- 101 (a) Ritger, P. L.; Peppas, N. A. *J. controlled release* **1987**, *5*, 37. (b) Ritger, P. L.; Peppas, N. A. *J. controlled release* **1987**, *5*, 23.
- 102 Peppas, N. A. *Pharm. Acta Helv.* **1985**, *60*, 110.
- 103 (a) Korsmeyer, R. W.; Gurny, R.; Doelker, E.; Burri, P.; Peppas, N. A. *Int. J. Pharm.* **1983**, *15*, 25. (b) Peppas, N. A. *Mathematical modelling of diffusion processes in drug delivery polymeric systems*, eds. Smolen, V. F. & Ball, L. A., Wiley, New York, **1984**. (c) Sinclair, G. W. and Peppas, N. A. *J. Membrane Sci.* **1984**, *17*, 329.
- 104 Bögershausen, A. *PhD thesis*. (Westfälische Wilhelms-Universität, Münster, **2004**).
- 105 Peppas, N. A.; *Recent Advances in Drug Delivery System*, Plenum, New York, **1984**.
- 106 (a) Ernst, R. R.; Bodenhausen, G.; Wokaun, A.; *Principles of Nuclear Magnetic Resonance in One and Two Dimensions*. Clarendon Press, Oxford. **1987**. (b) Abragam, A. *Principles of Nuclear Magnetism*. Clarendon Press, Oxford. **1983**. (c) Abraham, R. J.; Fisher, J.; Loftus, P. *Introduction to NMR Spectroscopy*. John Wiley and Sons Ltd., Great Britain. **1994**.
- 107 (a) Duer, M. J.; *Introduction to solid state NMR spectroscopy*, Blackwell publishing Ltd, Oxford, UK. **2004**. (b) Bugay, D. E.; *Pharm. Res.* **1993**, *10*, 317 and references therein.
- 108 Bruker CXP Application Note: *High resolution NMR in Solids*, **1993**.
- 109 Hafner, S; Spiess, H. W.; *Concepts Magn. Reson.* **1998**, *10*, 99.
- 110 Farrar, T. C.; Becker, E. D.; *Pulse and Fourier Transform NMR*, Academic Press, New York, **1971**.
- 111 (a) Pines, A.; Gibby, M. G.; Waugh, J. S. *J. Chem. Phys.* **1972**, *56*, 1776. (b) Pines, A.; Gibby, M. G.; Waugh, J. S. *J. Chem. Phys.* **1973**, *59*, 569.
- 112 (a) Andrew, E.; Bradbury, R. A.; Eades, R. G. *Nature*, **1959**, *183*, 1802. (b) Lowe, I.; *Phys. Rev. Lett.* **1959**, *2*, 285.

- 
- 113 Andrew, E. R.; *Prog. Nucl. Magnet. Reson. Spectrosc.* **1972**, *8*, 1.
- 114 Laws, D. D.; Bitter, H-M. L.; Jerschow, A. *Angew. Chem. Int. Ed.* **2002**, *41*, 3096.
- 115 Hartmann, S. R.; Hahn, E. L.; *Phys. Rev.* **1962**, *128*, 2042.
- 116 (a) Schmidt-Rohr, K.; Speiss, H. W.; *Multidimensional Solid State NMR and Polymers*, Academic Press, San Diego, **1994**. (b) Ernst, R. R.; Bodenhausen, G.; Wokaun, A. *Principles of Nuclear Magnetic Resonance in One and Two Dimensions*, Clarendon Press, Oxford, **1987**.
- 117 (a) Kessler, H.; Gehrke, M.; Griesinger, C. *Angew. Chem. Int. Ed. Engl.* **1988**, *27*, 490. (b) Blümich, B.; Spiess, H. W.; *Angew. Chem. Int. Ed. Engl.* **1988**, *27*, 1655.
- 118 Hafner, S.; Demco, D. E.; *Solid State Nucl. Magn. Reson.*, **2002**, *22*, 247.
- 119 Lee, M.; Goldburg, W. I.; *Phys. Rev.* **1965**, *140*, 1261.
- 120 (a) Levitt, M. H.; Kolbert, A. C.; Bielecki, A.; Ruben, D. J. *Solid State Nucl. Magn. Reson.* **1993**, *2*, 151. (b) Bielecki, A.; Kolbert, A. C.; Levitt, M. H. *Chem. Phys. Lett.* **1989**, *155*, 341. (c) Bielecki, A.; Kolbert, A. C., De Groot, H. J. M.; Griffin, R. G.; Levitt, M. H. *Adv. Magn. Reson.* **1990**, *14*, 111.
- 121 Iskandar, F.; Gradon, L.; Okuyama, K. *J. Coll. Inter. Sci.* **2003**, *265*, 296.
- 122 Xiong, Y.; Kostas, T. T. *J. Aerosol Sci.* **1993**, *24*, 893 and references therein.
- 123 Gluckert, F. A. *A. I. Ch. E. Journal* **1962**, *8*, 460.
- 124 Pauchard, L.; Couder, Y. *Europhys. Lett.* **2004**, *66*, 667.
- 125 Tsapis, N.; Dufresne, E. R.; Sinha, S. S.; Riera, C. S.; Hutchinson, J. W.; Mahadevan, L.; Weitz, D. A. *Phys. Rev. Lett.* **2005**, *94*, 018302-1 and references therein.
- 126 Hindus, W. C. *Aerosol Technology*, Wiley, New York, **1982**.
- 127 Velev, O. D.; Lenhoff, A. M.; Kaler, E. W. *Science*, **2000**, *287*, 2240.
- 128 (a) Orr, F. M.; Scriven, L. E.; Rivas, A. P. *J. Fluid Mech.* **1975**, *67*, 723. (b) Aveyard, R.; Clint, J. H.; Nees, D.; Paunov, V. N. *Colloids Surf. A* **1999**, *146*, 95. (c) Rowlinson, J. S.; Widom, B. *Molecular Theory of Capillarity*, Oxford Univ. Press, Oxford, **1989**.
- 129 (a) Joseph, D. D. *Stability of Fluid Motion*, Springer-Verlag, Berlin, **1976**. (b) Wassmuth, F.; Laidlaw, W. G.; Coombe, D. A. *Chem. Eng. Sci.* **1990**, *45*, 3483.
- 130 (a) Hadintoo, K.; Phanapavudhikul, P.; Kewu, Z.; Tan, R. B. H. *Ind. Eng. Chem. Res.* **2006**, *45*, 3697 and references therein. (b) Wang, W-N.; Lenggoro, W.; Okuyama, K. *J. Coll. Inter. Sci.* **2005**, *288*, 423.
- 131 (a) Fireman-Shoresh, S.; Avnir, D.; Marx, S. *Chem. Mater.* **2003**, *15*, 3607. (b) *Clarke's isolation and identification of drugs*, 2nd ed.; The Pharmaceutical press: London, **1986**.
- 132 Barrett, E. P. Joyner, L. G.; Halenda, P. P. *J. Am. Chem. Soc.* **1951**, *61*, 373.
- 133 Horvath, G.; Kawazoe, K.; *J. Chem. Eng. Jpn.* **1983**, *16*, 470.

- 134 (a) Storck, S. Bretinger, H.; Maier, W. F. *Appl. Catal. A: General*, **1998**, *174*, 137. (b) Groen, J. C. Peffer, L. A. A.; Perez-Ramirez, J. *Micropor. Mesopor. Mater.* **2001**, *43*, 83. (c) Jaroniec, M.; Choma, J.; Kruk, M. *Coll. Surf. A: Physicochem. Eng. Asp.* **2003**, *214*, 263.
- 135 (a) Peeters, M. P. J., Wakelkamp, W. J. J.; Kentgens, A. P. M. *J. Non-Crystalline Solids* **1995**, *189*, 77. (b) Vega, A. J. & Scherer, G. W. *J. Non-Crystalline Solids* **1989**, *111*, 153. (c) Engelhardt, G.; Koller, H. *Solid State NMR: Inorganic Matter*, Springer, Berlin, Heidelberg, **1994**. (d) Pursch, M.; Brindle, R.; Ellwanger, A.; Sander, L. C.; Bell, C. M.; Händel, H.; Albert, K. *Solid State Nuclear Magnetic Resonance* **1997**, *9*, 191.
- 136 Metz, G.; Wu, X.; Smith, S. O. *J. Magn. Reson. Ser. A* **1994**, *110*, 219.
- 137 (a) Bennett, A. E.; Rienstra, C. M.; Auger, M.; Lakshmi, K. V.; Griffin, R. G. *J. Chem. Phys.* **1995**, *103*, 6951. (b) Fung, B. M.; Khitritin, A. K.; Ermolaev, K. *J. Magn. Reson.* **2000**, *142*, 97. (c) McGeorge, G.; Alderman, D. W.; Grant, D. M. *J. Magn. Reson.* **1999**, *137*, 138.
- 138 (a) Taylor, R. E.; *Concepts Magn. Reson. Part A* **2004**, *22A*, 37. (b) Taylor, R. E.; *Concepts Magn. Reson. Part A* **2004**, *22A*, 79.
- 139 Kolodziejski, W.; Klinowski, J.; *Chem. Rev.* **2002**, *102*, 613.
- 140 van Rossum, B. J.; Förster, H.; de Groot, H. J. M. *J. Magn. Reson.* **1997**, *124*, 516.
- 141 Brown, S. P.; Spiess, H. W.; *Chem. Rev.* **2001**, *100*, 4125.
- 142 ChemDraw Ultra 8.0, Cambridge Soft corporation, Cambridge, MA, USA.
- 143 Fidalgo, A.; Nunes, T. G.; Ilharco, L. M. *J. Sol-Gel Sci. Technol.* **2000**, *19*, 403.
- 144 Dugas, V.; Chevalier, Y. *J. Coll. Inter. Sci.* **2003**, *264*, 354.
- 145 (a) Bronnimann, C. E.; Zeigler, R. C.; Maciel, G. E. *J. Am. Chem. Soc.* **1988**, *110*, 2023. (b) Liu, C. C.; Maciel, G. E.; *J. Am. Chem. Soc.* **1996**, *118*, 5103.
- 146 Shea, K.; Loy, D. A.; Webster, O. *J. Am. Chem. Soc.* **1992**, *114*, 6700.
- 147 Blümel, J. *J. Am. Chem. Soc.* **1995**, *117*, 2112.
- 148 Bögershausen, A.; Pas, S. J.; Hill, A. J.; Koller, H. *Chem. Mater.* **2006**, *18*, 664.
- 149 Müller, C. A.; Schneider, M.; Gisler, A.; Mallat, T.; Baiker, A. *Catal. Lett.* **2000**, *64*, 9.
- 150 Lu, Y.; Cao, G.; Kale, R. P.; Prabakar, S.; Lopez, G. P.; Brinker, C. J. *Chem. Mater.* **1999**, *11*, 1223.
- 151 Sefcik, J.; Rankin, S. E.; *J. Phys: Chem. B* **2003**, *107*, 52.
- 152 Marx, S.; Liron, Z.; *Chem. Mater.* **2001**, *13*, 3624.
- 153 Yang, D.; Xu, Y.; Wu, D.; Sin, Y.; Zhu, H.; Deng, F. *J. Phys. Chem. C* **2007**, *111*, 999.
- 154 Iskandar, F.; Gradon, L.; Okuyama, K. *J. Coll. Inter. Sci.* **2003**, *265*, 296.
- 155 Mathiowitz, E.; Bernstein, H.; Giannos, S.; Dor, P.; Turek, T.; Langer, R. *J. Appl. Poly. Sci.* **1992**, *45*, 125.

- 
- 156 Reichert, D.; *Anal. Bioanal. Chem.* **2003**, 376, 308.
- 157 Barrans, Y. et al. *Acta Crystallogr. Sect. B : Struct. Crastallogr. Cryst. Chem.* **1973**, 29, 1264.
- 158 Brus, J.; Jegorov, A.; *J. Phys. Chem. A* **2004**, 108, 3955.
- 159 (a) Geppi, M.; Guccione, S.; Mollica, G.; Pignatello, R.; Veracini, C. A. *Pharm. Res.* **2005**, 22, 1544.
- 160 Trebosc, J.; Wiench, J. W.; Huh, S.; Lin, V. S.-Y.; Pruski, M. *J. Am. Chem. Soc.* **2005**, 127, 7587.
- 161 van Rossum, B. J.; de Groot, C. P.; Ladizhansky, V.; Vega, S.; de Groot, H. J. M. *J. Am. Chem. Soc.* **2000**, 122, 3465.
- 162 Marx, S.; Liron, Z.; *Chem. Mater.* **2001**, 13, 3624.
- 163 van Rossum, B. J.; Boender, G. J.; de Groot, H. J. M. *J. Magn. Reson. Series A*: **1996**, 120, 274.
- 164 Van rossum, B. J.; Schulten, E. A. M.; Raap, J.; Oschkinat, H.; de Groot, H. J. M. *J. Magn. Reson.* **2002**, 155, 1.
- 165 Sozzani, P.; Bracco, S.; Comotti, A.; Ferretti, R.; Simonutti, R. *Angew. Chem. Int. Ed.* **2005**, 44, 1816.
- 166 Sozzani, P.; Comotti, A.; Bracco, S.; Simonutti, R. *Chem. Comm.*, **2004**, 768.
- 167 (a) Koller, H.; Engelhardt, G.; van Santen, R. A. *Topics in Catalysis*, **1999**, 9, 163. (b) Nakahara, M.; Wakai, C.; *Chem. Lett.* **1992**, 809. (c) Cogley, D. R.; Falk, M.; Butler, J. N.; Grunwald, E. *J. Phys. Chem.* **1972**, 76, 855.
- 168 (a) Grünberg, B.; Emmler, T.; Gedat, E.; Shenderovich, I.; Findenegg, G. H.; Limbach, H.-H.; Buntkowsky, G. *Chem. Eur. J.* **2004**, 10, 5689. (b) Chuang, I-S.; Maciel, G. E. *J. Phys. Chem. B* **1997**, 101, 3052. (c) Kinney, D. R.; Chuang, I-S.; Maciel, G. *J. Am. Chem. Soc.* **1993**, 115, 6786. (d) Chuang, I-S.; Maciel, G. E.; *J. Am. Chem. Soc.*; **1996**, 118, 401.
- 169 (a) Tsuzuki, S.; Honda, K.; Uchimaru, T.; Mikami, M.; Tanabe, K. *J. Am. Chem. Soc.* **2000**, 122, 3746. (b) Nishio, M.; *CrystEngComm* **2004**, 6, 130. (c) Sozzani, P.; Bracco, S.; Comotti, A.; Ferretti, L.; Simonutti, R. *Angew. Chem. Int. Ed.* **2005**, 44, 1816.
- 170 Kurk, M.; Antochshuk, V.; Matos, J. R.; Mercuri, L. P. Jaroniec. M. *J. Am. Chem. Soc.* **2002**, 124, 768.
- 171 (a) Badjic, J. D.; Kostic, N. M.; *J. Phys. Chem. B.* **2000**, 104, 11081. (b) Ringwald, S. C.; Pemberton, J. E.; *Environ, Sci. Technol.* **2000**, 34, 259.
- 172 (a) Sinnokrot, M. O.; Valeev, E. F.; Sherrill, C. D.; *J. Am. Chem. Soc.* **2002**, 124, 10887. (b) Grimme, S.; *J. Comput. Chem.* **2004**, 25, 1463.

- 173 (a) Hunter, C. A.; Singh, J.; Thornton, J. M. *J. Mol. Biol.* **1991**, *218*, 837. (b) Burley, S. K.; Petsko, G. A.; *Science*, **1985**, *229*, 23.
- 174 (a) Rebek, J., Jr. *Chem. Soc. Rev.* **1996**, *25*, 255. (b) Smithrud, D. B.; Diederich, F.; *J. Am. Chem. Soc.* **1990**, *112*, 339.
- 175 Fyfe, M. C.; Stoddart, J. F.; *Acc. Chem. Res.* **1997**, *10*, 3393.
- 176 Brana, M. F.; Cacho, M.; Gradillas, A.; de Pascual-, T. B.; Ramos, A. *Curr. Pharm. Des.* **2001**, *7*, 1745.

# Lebenslauf

## Geo Paul

### Persönliche Angaben

Geburtsdatum	21. Februar 1979
Geburtsort	Thrissur-Kerala, Indien
Familienstand	ledig
Eltern	Frau Regina Paul Herr Pauly Varghese

### Schulbildung

1984-1994	Govt. High School, Nadavaramba. St. Mary`s High School, Irinjalakuda. Jawahar Navodaya Vidyalaya, Mayannur, Kerala.
1994-1996	Jawahar Navodaya Vidyalaya, Karaikal, Pondicherry (UT).

### Studium

1996-1999	Bachelor of Science in Chemie. Calicut University, Kerala, Indien.
1999-2001	Master of Science in Chemie. Calicut University, Kerala, Indien.
10/2003	Beginn der Dissertation am Institut für Physikalische Chemie - International NRW Graduate School of Chemistry - Westfälische Wilhelms-Universität Münster. Betreuer: PD Dr. H. Koller

### Tätigkeiten

2001-2002	Wissenschaftlicher Angestellter, Jawaharlal Nehru Centre for Advanced Scientific Research, Bangalore, Indien.
Ab Jan. 2007	Wissenschaftliche Hilfskraft am Institut für Physikalische Chemie der Westfälischen Wilhelms-Universität Münster.

### Stipendium

2003-2006	International NRW Graduate School of Chemistry, Münster.
-----------	--